Study of surfactant-free microemulsions and microemulsions with fatty acid salts

Dissertation

zur Erlangung des Doktorgrades der Naturwissenschaften (Dr. rer. nat.)
der Fakultät für Chemie und Pharmazie
der Universität Regensburg

vorgelegt von
Julien Marcus
aus Hagondange

2015

Promotionskomitee

1. Gutachter	Prof. Dr. Werner Kunz, Institut für Physikalische und Theoretische Chemie, Universität Regensburg (Deutschland)
2. Gutachter	Prof. Dr. Thomas Zemb, Institut de Chimie Séparative de Marcoule, UMR 5257 (CEA/CNRS/UM2/ENSCM) (Frankreich)
3. Prüfer	Prof. Dr. Hubert Motschmann, Institut für Physikalische und Theoretische Chemie, Universität Regensburg (Deutschland)
Vorsitzender	Prof. Dr. Henri Brunner, Emeritus der Universität Regensburg (Deutschland)

Tag der Disputation: 16. Oktober 2015

Acknowledgment

This doctoral thesis was made out at the Institute of Physical and Theoretical Chemistry, University of Regensburg, between November 2012 and October 2015 and under the supervision of Prof. Dr. Werner Kunz. I would like to thank many people for their help and support throughout these years.

First of all, I would like to thank Prof. Dr. Werner Kunz for welcoming me and giving me the opportunity to prepare my thesis at his institute. Thank you for the numerous ideas, advices and discussions and for the time you invested to follow my work. Thank you also for this interesting topic that I had the chance to present at many conferences.
I also express my gratitude to Dr. Didier Touraud for his great help, his availability and his amazing ideas. Thank you for all the corrections and advices regarding the publications, and for taking the time to discuss any subject with me. Merci!
I deeply thank Prof. Dr. Thomas Zemb and Dr. Olivier Diat at the *Institut de Chimie Séparative de Marcoule*, France, for their help, explanations and guidance regarding the small- and wide-angle x-ray scattering and the small-angle neutron scattering techniques. Many thanks for the interest you gave to my work.
Thanks to PD Dr. Rainer Müller and Prof. Dr. Richard Buchner for letting me use their equipment.
Special thanks to Rosi and Sonja for their help, their kindness, and their good mood every day!

I would like to thank all my colleagues for all the scientific help and especially for the fantastic atmosphere at the institute. My thanks go to Auriane, Vroni, Theresa, Alex, Lydia, Andreas N., Stefan, Andreas S., Käthe, Claudia, Damian, Marcel, Tobi, Franzi, Manuel, Julian, Sebastian, and Gabriel. I really spent an amazing time with you, thank you for the fun and all the events! I thank also Michael, Vroni, Susanne and Andi for the warm welcome when I arrived at the institute.
I would like to thank the members of the Kaffeerunde, i.e. Roland, Vroni, Evi, Manuel, Georg, Richard, Julian, Andreas N., Auriane, Hellmuth and Rainer for the good moments at lunchtime and for what I learned speaking with them, especially about the German culture.

My thanks go also to the students Maximilian Pleines, Johannes Ramsauer, Johannes Mehringer, Michael Ludwig, Dea Zager, Sebastian Haumann, Alexandra Halemba, Christa Genslein, Elise Lambert, Marine Reinaud, and Erwan Le Goué for their help with some experiments of this work.

Many thanks to all my friends that I met in Germany and that made me want to stay in Bavaria. I thank Sarah, Tom, Stefan, Vroni, Helene, Christian, Beate, and Michael, Andreas, Timm, Matthias, Vroni, Jörn, Andre, Christoph, Dino, Daniel, Robert and Kevin for all the fun, holidays and adventures over the past years that made this time possible to endure.
My thanks go also to my WG, i.e. to Roxi, Ludwig, Maria and Laura, for the amazing atmosphere in the house and the best evenings.

J'aimerais également remercier mes parents, Alain and Catherine Marcus, et ma sœur, Cécile. Je vous remercie infiniment pour toute votre aide, pour vos visites et pour m'avoir soutenu dans toutes les décisions que j'ai prises depuis le début de mes études. Je n'en serais certainement pas là sans vous.

Finally, I owe my dearest thanks to my partner, Tobias Weigl, for his support and encouragement, for believing in me and making my new life in Germany so marvellous.

Abstract

This thesis deals with the study of microemulsions and is composed of two main parts. In the first part, surfactant-free microemulsions are studied, whereas in the second part microemulsions with surfactants and cosurfactants are investigated.

Over the last few years, surfactant-free microemulsions became a major topic at our institute and were thoroughly studied using the reference system water/ethanol/1-octanol. As explained later in the *Fundamentals* part (see section 1.2), fluctuating nano-structures occur in such surfactant-free microemulsions in the pre-Ouzo region, i.e. just before enough water is added to reach the multiphasic domain. They are composed of an organic-rich core surrounded by a water-rich bulk phase with a slight accumulation of ethanol at the interface.

The first work presented in this thesis concerns the influence of salts and of the surfactants sodium dodecylsulfate (SDS) and sodium diethylhexylphosphate (NaDEHP) on these nano-structures (developed in section 3.1.1). It was performed using dynamic light scattering (DLS), small-angle x-ray scattering (SAXS) and small-angle neutron scattering (SANS). It was found that electrolytes either exhibit a salting-out effect towards ethanol, more or less strongly depending on the ion, or produce charge separation via the antagonistic ion effect described by Onuki *et al.* Amphiphilic electrolytes, such as SDS or NaDEHP, induce a gradual transition toward monodisperse ionic micelles with ethanol playing the role of a cosurfactant.

Secondly, water-free and surfactant-free microemulsions were studied using DLS and SAXS (see section 3.1.2). The system glycerol/ethanol/1-octanol was studied, as well as the systems deep eutectic solvent (DES)/tetrahydrofurfuryl alcohol/diethyl adipate. Fluctuating nano-structures were also found in the pre-Ouzo region of these systems and existed in addition to molecular critical fluctuations which can appear near a critical point. This work proves that i) microemulsions can be formulated using DES instead of water, and ii) the amphiphilic character of 1-octanol is not responsible of these fluctuations.

The last two studies are examples of formulations where such nano-structures occur. Using perfumery molecules and DLS, it was shown that these aggregates can also be found in perfume tinctures (see section 3.1.3). From the model formulations, nano-droplets can be predicted in Eau de Toilette, Eau de Parfum and possibly in perfumes in presence of very hydrophobic fragrance molecules. These nano-structures may have a significant influence on the performance of the perfume and on the fragrance evaporation. Using practically all the natural and synthetic repellent molecules that are commercially used to formulate mosquito repellents, it was shown that nano-

structures can also be found in the pre-Ouzo region of hydro-alcoholic mosquito repellent formulations (developed in section 3.1.4). These structures can thus be found in products available on the market and may have an impact on the behaviour of such products on the skin.

The two studies presented in the second main part deal with a specific oil-in-water microemulsion. Its composition is 75 wt% of water, 10 wt% of sodium oleate, 9.25 wt% of ethanol, 0.75 wt% of citronellol, and 5 wt% of limonene. The microemulsion is interesting because it is highly water dilutable and can be used as perfume or aroma carriers.

The first work aims at investigating the influences of ethanol, citronellol, limonene, salts, and polyols on the temperature stability of the microemulsion and on the apparent pK_A (apK_A) of its surfactant (see section 3.2.1). Starting from the mixture water/sodium oleate, the apK_A decreases with an increase of temperature or by adding ethanol. A small amount of citronellol does not influence the apK_A, but the latter increases after the addition of limonene to form the final microemulsion, as uncharged oleic acid can be solubilised in the organic core. The anions have no specific influence on the evolution of the clearing temperature that follows electrostatic interactions, whereas the specificity of the cations is linked to their capacity to exchange with the original surfactant counterion.

The second work aims at investigating the influences of artificial and natural high intensity sweeteners and sugar alcohols on the clearing temperature of the microemulsion and its apK_A (see section 3.2.2). The high intensity sweeteners used in this study exhibit different behaviours: saccharin and acesulfame K act like electrolytes and dehydrate the interfacial film of the droplets, whereas neotame, stevia and neohesperidin DC act like (co)surfactants. Aspartame exhibits a precipitation behaviour, whereas cyclamate and sucralose interact with the interfacial film without penetrating it. Note that sucralose allows the formulation of a beverage microemulsion with a fatty acid salt as surfactant at nearly neutral pH. The sugar alcohols sucrose, sorbitol and isomalt seem to act like osmolytes and play indirectly on the interfacial film of the microemulsion nano-droplets by pushing the ethanol towards them.

To sum up, the studies of the surfactant-free microemulsions help us to better understanding their structures and behaviours in presence of different additives. It is also interesting to note that they are already used in some applications. The studies of the microemulsions with a fatty acid salt as surfactant help us understanding the influences of salts and sweeteners on such a surfactant and the important role of ethanol.

Zusammenfassung

Diese Doktorarbeit handelt über Mikroemulsionen und besteht aus zwei Hauptteilen. Im ersten Teil werden tensidfreie Mikroemulsionen untersucht, während Mikroemulsionen mit Tensiden und Cotensiden im zweiten Teil betrachtet werden.

In unserem Institut sind in den letzten Jahren tensidfreie Mikroemulsionen ein wichtiges Thema geworden und wurden eingehend mit dem Referenzsystem Wasser/Ethanol/1-Oktanol untersucht. Wie später im *Fundamentals*-Teil erklärt (siehe Absatz 1.2), befinden sich im pre-Ouzo Bereich dieser tensidfreien Mikroemulsionen fluktuierende Nanostrukturen. Dieser Bereich existiert bei einer geringen Wassermenge, bevor das mehrphasige System erreicht wird. Die Nanostrukturen bestehen aus einem von einer wasserreichen Phase umgegebenen Kern aus zum großen Teil organischen Molekülen mit einem Konzentrationspeak von Ethanolmolekülen an der Grenzfläche.

Der erste Teil dieser Doktorarbeit behandelt die Einflüsse von Salzen und den Tensiden Natriumdodecylsulfat (SDS) und Natriumdiethylhexylphosphat (NaDEHP) auf diese Nanostrukturen (siehe Absatz 3.1.1). Die Einflüsse wurden mit Hilfe von dynamischer Lichtstreuung (DLS), Kleinwinkel-Röntgenstreuung (SAXS) und Kleinwinkel-Neutronenstreuung (SANS) untersucht. Es wurde festgestellt, dass Elektrolyte entweder einen mehr oder weniger starken aussalzenden Effekt gegenüber Ethanol besitzen, oder eine Ladungstrennung gemäß dem antagonistischen Salzeffekt, der von Onuki *et al.* beschrieben wurde, fördern. Amphiphile Elektrolyte, wie SDS oder NaDEHP, induzieren einen graduellen Übergang zu monodispersen und ionischen Mizellen, in denen Ethanol als Cotensid wirkt.

Des Weiteren wurden wasserfreie und tensidfreie Mikroemulsionen mit DLS und SAXS untersucht (siehe Absatz 3.1.2). Das System Glycerin/Ethanol/1-Oktanol wurde untersucht sowie Systeme von tiefen Eutektika (DES) anstelle von Wasser mit Tetrahydrofurfurylalkohol und Diethyladipat. Fluktuierende Nanostrukturen wurden ebenfalls im pre-Ouzo Bereich dieser Systeme beobachtet und waren unabhängig von kritischen molekularen Fluktuationen, die nah eines kritischen Punktes auftauchen können. Diese Studie zeigt, dass i) Mikroemulsionen mit DES anstatt Wasser formuliert werden können und ii) der amphiphile Charakter von 1-Oktanol nicht verantwortlich für die Fluktuationen ist.

Die letzten beiden Studien sind Beispiele von praktischen Formulierungen, in denen sich solche Nanostrukturen befinden. Es wurde mit Hilfe von Duftstoffen und DLS festgestellt, dass diese Aggregate auch in Parfümtinkturen beobachtet werden können (siehe Absatz 3.1.3). Laut den Modellformulierungen können Nanostrukturen in Eau de Toilette, Eau de Parfum und

wahrscheinlich in Parfümen mit sehr hydrophoben duftenden Molekülen auftreten. Diese Nanostrukturen haben sehr wahrscheinlich einen Einfluss auf die Parfümleistung und auf die Verdunstung des duftenden Moleküls. Es wurde festgestellt, dass in fast allen im Handel erhältlichen Mückensprays, welche natürliche und synthetische Moleküle enthalten, ebenfalls fluktuierende Nanostrukturen im pre-Ouzo Bereich auftreten (siehe Absatz 3.1.4). Diese Strukturen können eine Auswirkung auf das Verhalten des Produkts auf der Haut haben.

Im zweiten Teil der Doktorarbeit wird in beiden Studien jeweils die gleiche Öl-in-Wasser Mikroemulsion verwendet. Diese besteht aus 75 Gew.% Wasser, 10 Gew.% Natriumoleat, 9,25 Gew.% Ethanol, 0,75 Gew.% Citronellol und 5 Gew.% Limonen. Die Mikroemulsion ist von Interesse, weil sie mit Wasser hochverdünnbar ist und als Duft- oder Aromaträger benutzt werden kann. Die Einflüsse von Ethanol, Citronellol, Limonen, Salzen und Polyolen auf die thermische Stabilität der Mikroemulsion und auf den scheinbaren pK_S (apK_S) ihres Tensids wurden in der ersten Studie untersucht (siehe Absatz 3.2.1). Für eine Mischung Wasser/Natriumoleat nimmt der apK_S mit steigender Temperatur oder mit dem Hinzufügen von Ethanol ab. Der apK_S ist mit einer kleinen Menge Citronellol nicht beeinflussbar. Das Hinzufügen von Limonen hat eine Erhöhung des apK_S zur Folge, weil die ungeladene Ölsäure im organischen Kern gelöst wird. Die Anionen haben keinen besonderen Einfluss auf die Temperaturabhängigkeit. Ihre Entwicklung resultiert aus elektrostatischen Wechselwirkungen. Die Wirkungsspezifität der Kationen ist mit ihrer Fähigkeit, sich mit dem Gegenion des Tensids zu tauschen, verbunden.
Die zweite Studie handelt von Temperatureinflüssen auf die Mikroemulsion von künstlichen und natürlichen hochintensiven Süßstoffen und Alditolen. Außerdem wird das Verhalten auf den apK_S untersucht (siehe Absatz 3.2.2). Die hochintensiven Süßstoffe weisen verschiedenen Verhalten auf: Saccharin und Acesulfame-K verhalten sich als Elektrolyte und trocknen den Grenzflächenfilm aus, während Neotam, Stevia und Neohesperdin DC sich als (co)Tenside verhalten. Aspartam fällt aus, während Cyclamat und Sucralose mit dem Grenzflächenfilm wechselwirken, ohne sich darin einzulagern. Außerdem ermöglicht Sucralose die Formulierung einer trinkbaren Mikroemulsion mit einem fast neutralen pH-Wert und mit einem Fettsäuresalz als Tensid. Die Alditole Saccharose, Sorbitol und Isomalt verhalten sich als Osmolyte und verschieben die Ethanolmoleküle hin zu den Tropfen.

Zusammengefasst kann gesagt werden, dass die Studien über tensidfreie Mikroemulsionen dabei helfen, mehr über ihre Strukturen und das Verhalten in Gegenwart von Zusatzstoffen zu verstehen. Bereits schon jetzt befinden sich solche tensidfreie Mikroemulsionen in Produkten. Die Studien über die Mikroemulsion mit einem Fettsäuresalz als Tensid helfen dabei, mehr über die Einflüsse von Salzen und Süßstoffen auf solche Tenside zu verstehen sowie die entscheidende Rolle des Ethanols.

Résumé

Cette thèse est divisée en deux grandes parties et traite de l'étude de microémulsions. Dans la première partie, des microémulsions sans tensioactifs sont étudiées, alors que des microémulsions avec tensioactifs et co-tensioactifs sont traitées dans la seconde partie.

Au cours de ces dernières années, les microémulsions sans tensioactifs sont devenues un sujet important dans notre institut et ont été étudiées en détail en utilisant le système de référence eau/éthanol/1-octanol. Comme il le sera expliqué plus tard dans la partie *Fundamentals* (voir le sous-chapitre 1.2), des nano-structures qui fluctuent ont été observées dans la région pré-Ouzo des microémulsions sans tensioactifs, c'est-à-dire juste avant qu'assez d'eau ne soit ajouté pour atteindre le domaine multiphasique. Ces nano-structures sont composées d'un cœur riche en phase organique, entouré d'une phase riche en eau avec une légère accumulation d'éthanol à l'interface.
La première étude de cette thèse traite de l'influence de sels et des tensioactifs dodécylsulfate de sodium (SDS) et diéthylhexylphosphate de sodium (NaDEHP) sur ces nano-structures (voir le sous-chapitre 3.1.1). Cette étude a été réalisée en utilisant la diffusion dynamique de la lumière (DLS), la diffraction des rayons X aux petits angles (SAXS) et la diffraction de neutrons aux petits angles (SANS). Il a été montré que les électrolytes peuvent soit avoir un effet salting-out, plus ou moins prononcé selon les ions, envers l'éthanol, soit produire une séparation de charge via l'effet des ions antagonistes décrit par Onuki *et al.* Les électrolytes amphiphiles, comme le SDS ou le NaDEHP, provoquent une transition graduelle vers des micelles ioniques monodisperses, dans lesquelles l'éthanol se comporte comme un co-tensioactif.
Deuxièmement, des microémulsions sans eau et sans tensioactifs ont été étudiées en DLS et en SAXS (voir le sous-chapitre 3.1.2). Le système glycérol/éthanol/1-octanol a été étudié, ainsi que les systèmes solvant eutectique profond (DES)/alcool tétrahydrofurfurylique/adipate de diéthyl. Des nano-structures ont également été observées dans les régions pré-Ouzo pour ces systèmes et étaient indépendantes de fluctuations critiques moléculaires qui peuvent apparaitre vers un point critique. Cette étude prouve que i) des microémulsions peuvent être formulées avec des DES à la place de l'eau, et ii) le caractère amphiphile de l'octanol n'est pas responsable de ces fluctuations.
Les deux dernières études sont des exemples de formulations où ce genre de nano-structures apparait. Grâce à des molécules de parfumerie et à la DLS, il a été montré que ces agrégats peuvent également être présents dans des alcoolatures utilisées en parfumerie (voir le sous-chapitre 3.1.3). D'après nos formulations modèles, des nano-gouttelettes peuvent être prédites dans les Eaux de Toilette, Eaux de Parfum et très probablement dans les parfums en présence de

molécules très hydrophobes. Ces nano-structures pourraient avoir une influence significative sur la performance du parfum et sur l'évaporation des molécules odorantes. En utilisant pratiquement toutes les molécules répulsives naturelles et synthétiques qui sont commercialement utilisées dans les formulations anti-moustiques, il a été montré que des nano-structures peuvent être présentes dans les régions pré-Ouzo des formulations d'anti-moustiques hydro-alcooliques (voir le sous-chapitre 3.1.4). Ces structures peuvent donc être trouvées dans des produits disponibles sur le marché et peuvent avoir un impact sur le comportement de tels produits sur la peau.

Les deux études présentées dans la seconde partie traitent d'une même et seule microémulsion huile-dans-eau. Sa composition est 75 %m d'eau, 1 %m d'oléate de sodium, 9,25 %m d'éthanol, 0,75 %m de citronellol, et 5 %m de limonène. Cette microémulsion est intéressante car elle est hautement diluable à l'eau et peut être utilisée comme transporteur de parfums ou d'arômes.
La première étude traite de l'influence de l'éthanol, du citronellol, du limonène, de sels et de polyols sur la stabilité thermique de la microémulsion et sur le pK_A apparent (apK_A) de son tensioactif (voir le sous-chapitre 3.2.1). A partir d'une solution eau/oléate de sodium, l'apK_A décroit par augmentation de la température ou par addition d'éthanol. Une petite quantité de citronellol n'a pas d'influence sur l'apK_A mais ce dernier augmente après l'addition de limonène pour former la microémulsion finale. L'acide oléique non chargé peut désormais être solubilisé dans le cœur organique. Les anions n'ont pas d'influence spécifique sur la température à laquelle la microémulsion se forme. Son évolution suit les interactions électrostatiques. Au contraire, la spécificité des cations est liée à leur capacité à s'échanger avec le contre-ion du tensioactif.
La seconde étude traite de l'influence d'édulcorants intenses et de polyols artificiels et naturels sur la température de formation de la microémulsion et sur son apK_A (voir le sous-chapitre 3.2.2). Les édulcorants intenses utilisés dans cette étude montrent différents comportements : la saccharine et l'acésulfame K joue le rôle d'électrolytes et déshydratent le film interfacial des gouttelettes, alors que le néotame, la stévia et la néohespéridine DC se comportent comme des (co-)tensioactifs. L'aspartame précipite, alors que le cyclamate et le sucralose interagissent avec le film interfacial sans le pénétrer. Il est à noter que le sucralose permet la formulation d'une microémulsion buvable à pH pratiquement neutre avec un sel d'acide gras comme tensioactif. Les polyols sucrose, sorbitol et isomalt se comportent comme des osmolytes et jouent indirectement sur le film interfacial des gouttelettes de la microémulsion en poussant l'éthanol en leur direction.

Pour résumer, les études des microémulsions sans tensioactifs permettent de comprendre davantage leur structure et leur comportement en présence d'additifs. Il est intéressant de noter qu'elles sont déjà employées pour certaines applications. Les études des microémulsions avec un sel d'acide gras comme tensioactif permettent de mieux comprendre l'influence de sels et d'édulcorants sur ce genre de tensioactif et le rôle primordial de l'éthanol.

Table of content

CHAPTER 1

FUNDAMENTALS

1.1. Microemulsions

1.1.1. Definition and properties

Optically transparent and thermodynamically stable mixtures were first observed by J. H. Schulman and T. P. Hoar in 1943 for the system water/alkali-metal soap/oil with the presence of an alcohol or a non-ionised amphipathic substance.[1] Schulman *et al.* were also the first to introduce the term "microemulsion" for such mixtures in 1959.[2] Microemulsions are generally described as macroscopically isotropic solutions composed of polar and non-polar liquids. They are optically translucid and thermodynamically stable mixtures obtained with a surfactant and in general a cosurfactant.[3, 4] Having commonly a shorter hydrophobic tail, the major effect of the cosurfactant is to bring the necessary flexibility to the system by taking up position between the surfactant molecules (see **Figure 1.1**).[5] Cosurfactants were pictured as "*a molecule which could create a certain disorder in the lattice*" in the work of Schulman *et al.*[6] The surfactant and cosurfactant molecules optimise the occupied area in the interfacial film in order to minimise the direct water/oil contact. As the interface is saturated by surfactant and cosurfactant molecules, the interfacial tension is nearly vanishing. Interfacial tensions in microemulsions can reach very low values and are usually of the order of magnitude of 10^{-2} to 10^{-3} mN/m. Ultra-low interfacial tensions were also observed for systems involving a surfactant and cosurfactant and were as low as 10^{-5} mN/m. In comparison, the interfacial tensions between water and hexane, decane, and hexadecane are respectively equal to 51.4, 53.2, and 55.2 mN/m at 22 °C.[7]

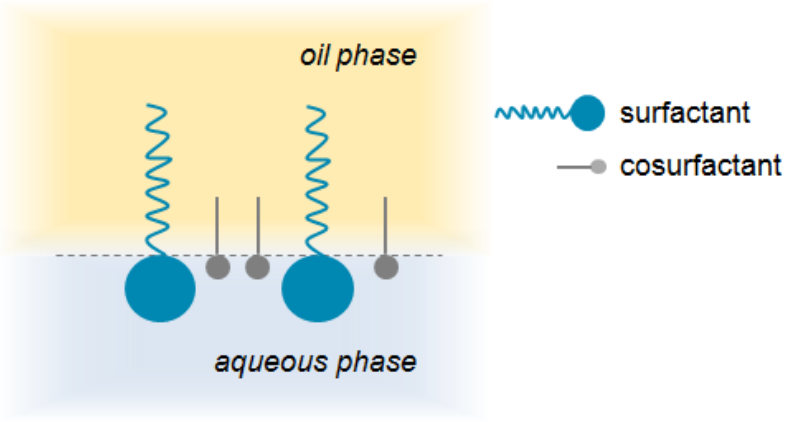

Figure 1.1. Schematic representation of the interfacial film between an aqueous and an oil phase.

For example, the systems water/sodium dodecylsulfate (SDS)/1-pentanol/n-alkane form microemulsions at defined compositions, from n-hexane to n-hexadecane.[8] The SDS molecules go onto the interface and repulse themselves being negatively charged. The interface water/n-alkane and thus the interfacial tension γ decrease. The cosurfactant 1-pentanol can then take up position between the SDS molecules and, doing so, helps decreasing the remaining water/n-alkane interface and stabilising the system. The interfacial tension becomes even smaller and the flexibility of the interfacial film increases due to the different tail lengths of both surfactant and cosurfactant. There is also less interaction between the hydrophobic tails of SDS, thus rendering the film less rigid.

1.1.2. Microemulsion formulation tools

1.1.2.1. Classification and Winsor systems

As microemulsions are composed of an aqueous and an oil phase, they are structured and can be classified in 3 different types. Oil-in-water (o/w) and water-in-oil (w/o) microemulsions consist respectively of well-defined droplets of oil dispersed in the aqueous phase, and well-defined droplets of water dispersed in oil.[1] Scriven was the first to write about bicontinuous microemulsions.[9] The latter are isotropic sponge-like structures, in which oil and water domains are distorted and interconnected.[10, 11] These networks of oil and water nano-domains are still stabilised by surfactant molecules, which form an interfacial film whose curvature is close to zero. Often, the abbreviations L1 phase, L2 phase, and L3 phase are used to respectively qualify o/w, w/o, and bicontinuous microemulsions.

Winsor also developed a classification of phase equilibrium divided into four different types.[12] The first type, called Winsor I, is a two phase system with an o/w structure and an almost pure upper oil phase. Winsor II is also a two phase system with a w/o structure and an almost pure lower aqueous phase. The third type, called Winsor III, is a three phase system with an almost pure upper oil phase, a bicontinuous middle phase containing water, oil, and surfactant molecules, and an almost pure lower water phase. The last type is the Winsor IV system, which is a single phase, clear and homogeneous microemulsion that is commonly of L3 type. They are represented in **Figure 1.2**.

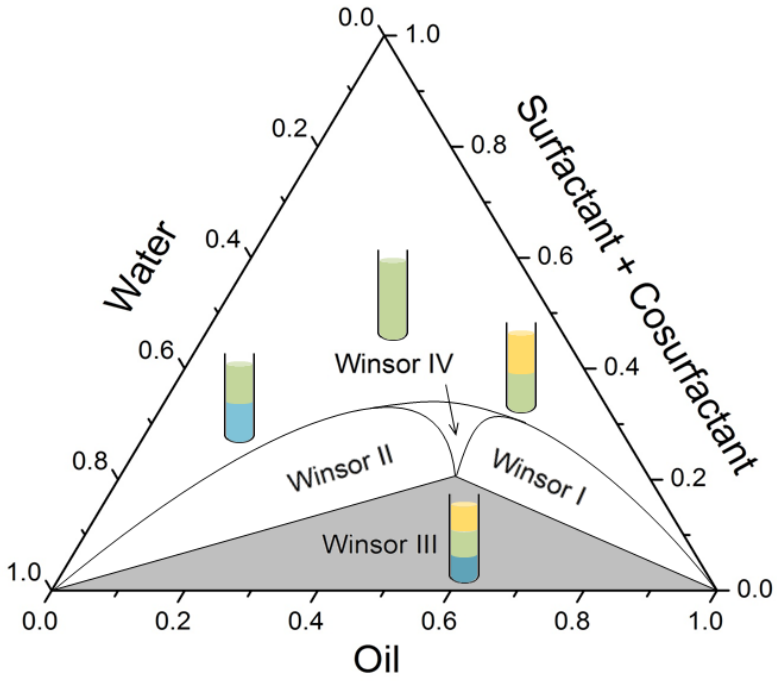

Figure 1.2. Simplified schematic representation of a phase diagram with the four Winsor systems. The colour yellow represents the oil phase, blue the aqueous phase, and green the microemulsion.

All in all, microemulsions are complex systems with different structures involving surfactants and cosurfactants as important components. Different methods were developed to optimise the formulation of microemulsions with desired properties and structures.

1.1.2.2. Addition of an alcohol

The addition of an alcohol can be very beneficial to formulate or to improve a microemulsion formulation. First of all, many alcohols such as propanol, butanol, pentanol, or hexanol can play the role of cosurfactant, an essential component in microemulsion formulations. Generally, methanol and ethanol are considered as slightly hydrophilic, while butanol and longer linear alcohols as lipophilic. Having affinities for the aqueous and oil phases, alcohols co-adsorb with

the surfactant at the interface and change the interactions of the amphiphilic film. The interfacial composition and distribution of alcohol in the oil and aqueous phases are influenced by the chain length of alcohol and oil and by the concentration of alcohol.[13-15] As described in section 1.1.1, their chain length is an important feature that can be adjusted in order to optimise the properties of the microemulsion. As Zana reviewed, alcohols exhibit multiple roles in microemulsions.[16] They delay the occurrence of liquid crystalline phases, increase the fluidity of the mixed surfactant/alcohol interfacial layers, and further decrease the interfacial tension. Alcohols can also increase the molecular disorder in these interfacial layers as well as their dynamic character. Moreover, short-chain alcohols may also act as cosolvent by increasing the hydrophobicity of the system and thus the surfactant solubility, increasing also their critical micellar concentration.[17, 18]
Several studies corroborate these observations. The importance of the alcohol chain length was for example observed by Lindman *et al*. for combinations of different surfactants and hydrocarbons.[19] They showed that the microemulsion structure varies strongly with the cosurfactant. With long-chain alcohols, closed water domains in oil were obtained, whereas a system with a considerably lower degree of organisation was observed with butanol and pentanol.
Peyrelasse *et al.* studied the systems water/potassium oleate/cosurfactant/benzene, where the cosurfactant was one of the eight isomers of pentanol.[20] They observed a strong influence of the chemical structure of the alcohol used on the electrical behaviours and phase diagrams of the systems. The more water soluble the isomeric pentanol, the more extended the microemulsion domain.
As a last example, three types of alcohol behaviours were observed in the ternary microemulsions water/dodecyl-poly[ethylene oxide-23] ether (Brij 35)/alcohols, with alcohols from ethanol to decanol.[17] These behaviours depended only on the chemical nature of the alcohols. Short-chain alcohols behaved as cosolvents, inducing a breaking effect of the structure, i.e. decreasing the size of the micelles. Medium-chain alcohols behaved as cosurfactants, enhancing the structure of the system by increasing the hydrophobicity in the interfacial film, and long-chain alcohols behaved as oil phases and were solubilised in the hydrophobic micellar core. It is worth pointing out that there is no sharp boundary between the two successive types of behaviour, but the limiting cases of very short and very long alcohols behave respectively as cosolvents and as real oil phases.

The addition of an alcohol allows the formulator to tune microemulsions. However, the formulation of such stable solutions is delicate as it depends on many parameters, i.e. the alcohol chain length, area of the polar head of the surfactant, alcohol/surfactant ratio, alkane chain length, or salinity, to name but a few.

1.1.2.3. Phase diagrams

There are many possible representations of a (pseudo-)ternary microemulsion system containing an aqueous phase, an oil phase, a surfactant and very often a cosurfactant. One of them is the well-known (pseudo-)ternary phase diagram, as represented in section 1.1.2.1 with the different Winsor systems according to the composition of the microemulsion. However, for a system based on a nonionic polyethoxylated surfactant, the temperature plays an important role and can change the affinity of the surfactant for the aqueous and oil phases, thus allowing the change from a Winsor type to another. A possible representation for that type of system is a three-dimensional triangular prism with the (pseudo-)ternary system water/surfactant + cosurfactant/oil as the basis and the temperature as the vertical axis. As it is difficult to have information from a 3-D representation, 2-D diagrams are preferred. It exists three different cuts in the prism, depending on which information is needed for the studied system.

The **Δ cut** is obtained at constant temperature. The resulting diagram is a (pseudo-)ternary phase diagram, as explained previously. This cut is useful to investigate the effects of the surfactant and cosurfactant concentrations as well as the water/oil ratio on the phase behaviours. It does not show the effect of the temperature on the system.

The **γ cut** is obtained for a constant water/oil ratio, as it can be seen in **Figure 1.3**.a. The temperature is plotted against the surfactant concentration in the solution in the 2-D diagram. The latter is sometimes called a "fish diagram" due to its particular form (see **Figure 1.3**.b). The four Winsor systems can also be directly observed and formulated considering the fish diagram. It is a useful tool to know, at a given temperature, the minimum amount of surfactant required to obtain a clear, single and homogeneous phase. The common point for the four zones is called the "critical point" CP, found at the "critical temperature". This point indicates the minimal surfactant concentration needed to solubilise the same quantities of water and oil in the system by forming a bicontinuous microemulsion.[21]

The **χ cut** is obtained for a constant surfactant and cosurfactant concentration, as it is shown in **Figure 1.3**.c. Here, the temperature is plotted against the water weight fraction, i.e. indirectly against the water/oil ratio. The diagram presented in **Figure 1.3**.d is useful to locate the boundary between the o/w and w/o microemulsions. The Winsor III system zone is the most important to locate because within phase inversion can take place due to the very low interfacial tension between the phases and the low stability of the system.[22]

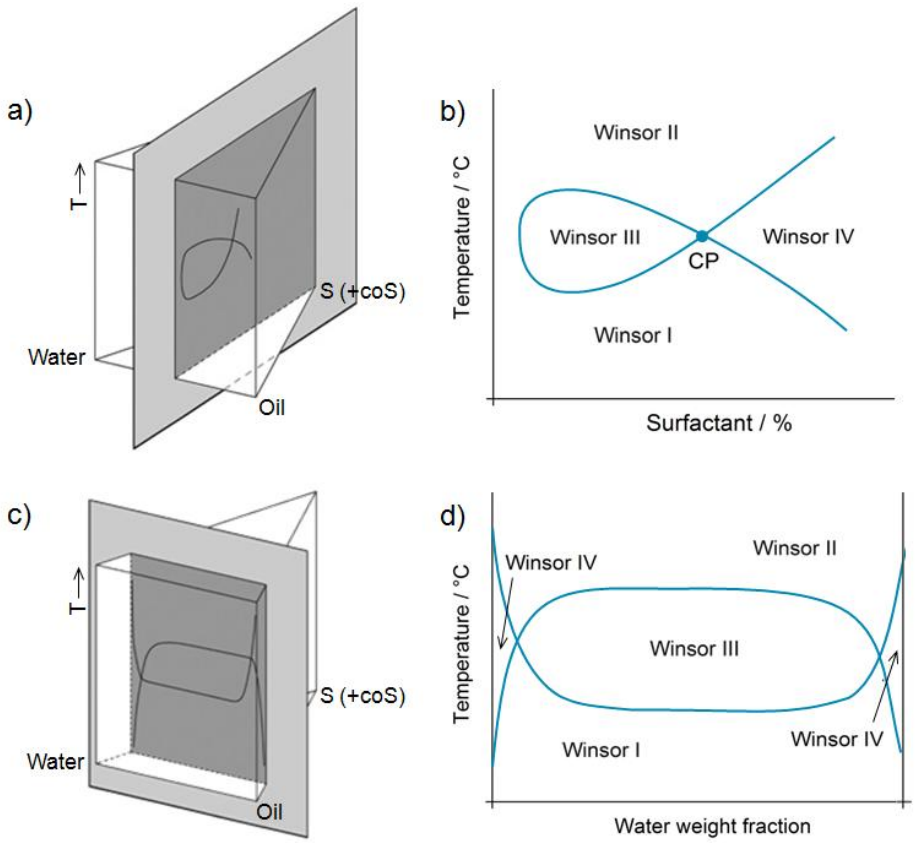

Figure 1.3. Bidimensional cuts of a water/surfactant + cosurfactant/oil-temperature prism: a) the γ cut at constant water/oil ratio with its associated 2-D diagram represented in b); c) the χ cut at constant surfactant concentration with its associated 2-D diagram represented in d). CP means "critical point". Figures a) and c) were redrawn from[22].

In the previous sections, microemulsions were presented together with their different structures and the available methods for their formulation and representation. How can their properties and behaviours be experimentally characterised?

1.1.3. Characterisation of microemulsions

1.1.3.1. Conductivity measurements

As already described in section 1.1.2.1 microemulsions can be of three different types: o/w, where micelles of oil are dispersed in an aqueous medium, w/o, where inversed micelles composed essentially of water are dispersed in an organic medium, or bicontinuous. Conductivity measurements are an adequate method to determine the nano-structure and the film rigidity of a microemulsion, especially with ionic surfactants.

Systems with a flexible interfacial film show a typically bell-shaped evolution of the conductivity with increasing amount of water, as represented in **Figure 1.4**. This well-known behaviour can be explained with a percolation model.[11, 23-25] Starting with a w/o microemulsion, the conductivity is close to zero as the outer phase is oil. A few water droplets are present but not enough for an exchange of charge. When more water is added, the conductivity rises continuously until the percolation threshold Φ_p is reached. At values below Φ_p the water droplets start to form clusters that come sufficiently close to each other so that undisturbed transport of charge carriers can take place. At Φ_p an infinite cluster of particles is formed through the system and a continuous conducting path in the microemulsion is formed.[26, 27] At higher water content the curve deviates from linearity, indicating the formation of bicontinuous structures.[28, 29] A maximum of conductivity is then reached and the slope of the conductivity curve is equal to zero. Adding more water, the conductivity starts decreasing due to dilution effects, indicating the formation of an o/w microemulsion.

Anti-percolative systems show a different evolution of the conductivity curve, as the rigid interface prevents the droplets to merge. Consequently, the conductivity values stay very low.

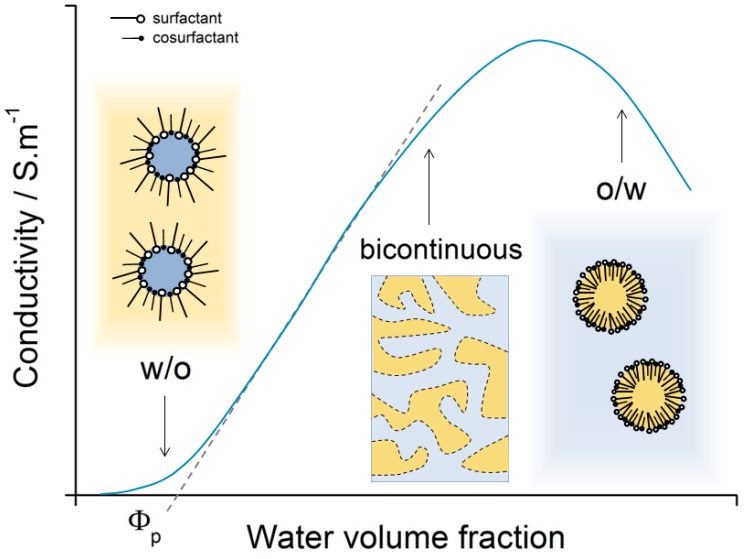

Figure 1.4. Typical conductivity curve of a microemulsion with a flexible film with schematic representations of w/o, bicontinuous, and o/w microemulsions. The color blue stands for water and yellow for oil. The dotted lines for the representation of a bicontinuous microemulsion represent the surfactant + cosurfactant film between both phases.

Conductivity measurements were used as a useful tool for the characterisation of many systems, such as water/SDS/hexylamine/heptane, water/cetyltrimethylammonium bromide (CTAB)/n-pentanol/n-hexane, and even in microemulsions stabilised by cationic/nonionic surfactant mixtures or formulated with ionic liquids instead of water.[30-33] Peyrelasse *et al.* showed for

example that the electrical behaviour of microemulsions can be correlated to phase diagram features, which are strongly influenced by the chemical structure of the alcohol used as cosurfactant.[20] In the system water/dioctyl sodium sulfosuccinate (AOT)/isooctane, Mathew *et al.* investigated the influence of additives on the percolation threshold.[34] The latter is hindered by additives stiffening the interfacial film, such as cholesterol. However, the percolation threshold is favoured by additives which make the film more flexible, such as propanol.

1.1.3.2. Dynamic light scattering (DLS)

Scattering is caused by fluctuations in the medium. For example, a colloidal particle or a microemulsion droplet scatters light because it has a different refractive index than the liquid in which it is dispersed. Dynamic light scattering is an analysis of the time dependence of fluctuations in the scattered light. It is often used to calculate the diffusion coefficient of colloidal particles suspended in solutions or the droplet size of microemulsions.

As pictured in **Figure 1.5**, the investigated solution is illuminated by a monochromatic coherent light source with a wavelength λ, such as a laser. The objects within the solution scatter some of the light in all directions as long as the diameter D of those objects are smaller than the coherent light, typically less than D = λ/10 (Rayleigh scattering). The scattered light is then collected at a defined angle θ by a detector and its intensity is measured. The scattering vector $\boldsymbol{q}$ is defined as:

$$\boldsymbol{q} \equiv \boldsymbol{k}_S - \boldsymbol{k}_I \qquad (1.1)$$

$\boldsymbol{k}_I$ is the propagation vector of the incident light, $\boldsymbol{k}_S$ the propagation vector of the scattered light (see **Figure 1.5**).[35]

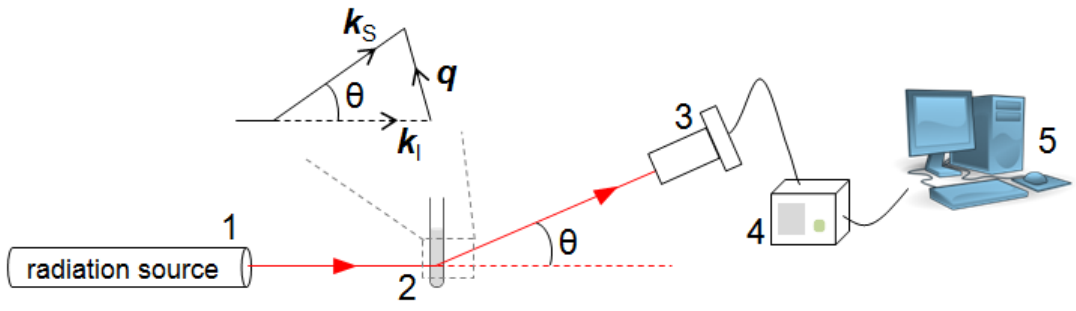

Figure 1.5. Representation of a DLS apparatus. The radiation source **1** delivers an incident light into the sample **2**. The light is scattered and is collected by the detector **3** at a given angle θ. Light intensity data are fed to the correlator **4** that computes the correlation function of the intensity fluctuations. The correlation function is then displayed and analysed on the computer **5**. The scattering vector $\boldsymbol{q}$ is defined as the difference between the propagation vectors of the scattered and incident light, respectively $\boldsymbol{k}_S$ and $\boldsymbol{k}_I$.

As the scattered objects are undergoing Brownian motion due to thermal agitation, the medium evolves in time and the distance between the scatterers is constantly changing. Constructive and destructive interferences of the scattered light occur, causing the measured intensity to fluctuate over time. Information on the motions of the particles are encoded in these fluctuations. For example, the faster the particle moves, the more rapidly the intensity fluctuates, i.e. small objects cause the intensity to fluctuate more rapidly than large ones, as it is illustrated in **Figure 1.6**.a.[35]

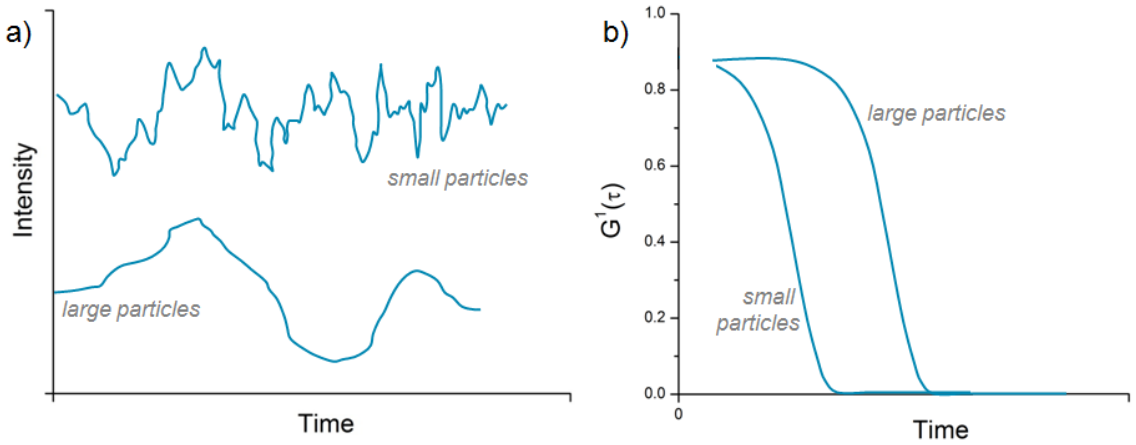

Figure 1.6. Illustrations of a) the intensity fluctuations; and b) correlation functions for small and large particles. Small particles are moving fast, so the signal is also changing fast and the correlation does not persist for a long time.

In dynamic light scattering, a digital autocorrelator is used to compare the intensities of the signals at different time intervals. An autocorrelator is a signal comparator which measures the degree of similarity between one signal with itself at varying time intervals. If the intensity of a signal at time = t is compared to the intensity a very small time later, at time = t + τ, a strong correlation between the intensities of the two signals is observed. If the signal at t is compared to the signal at t + 2τ, a reasonable correlation is observed but it is smaller than the correlation between t and t + τ. And so on, if the signals at t + 3τ, t + 4τ, t + 5τ etc. are compared with the signal at t, the correlation will decrease in time until there will be no correlation. Of course, if the objects are large and moving slowly, the signal will change slowly and the correlation will persist for a long time.

The comparison of the signals of the scattered intensity allows the construction of its time correlation function $G^1(\boldsymbol{q},\tau)$ at a particular scattering vector $\boldsymbol{q}$, defined as:

$$G^1(\boldsymbol{q},\tau) = \langle I(\boldsymbol{q},t).I(\boldsymbol{q},t+\tau)\rangle \qquad \textbf{(1.2)}$$

In equation **(1.2)** τ is the correlator delay time. For a large number of monodisperse objects undergoing Brownian motion, the time correlation function is an exponential decaying function of

the correlator delay time τ, as represented in figure **Figure 1.6**.b for small and large particles. The function is described with the following equation:

$$G^1(\boldsymbol{q},\tau) = a_0 + (a_1 * e^{-a_2 \tau})^2 \quad \textbf{(1.3)}$$

In equation **(1.3)** a_0 is the constant baseline value (usually 1), a_1 refers to the dynamic part of the amplitude, and a_2 is the decay rate, linked to the diffusion coefficient which is used to calculate the hydrodynamic radius through the Stokes-Einstein equation (see section 2.2.6.1 for more details). Regarding the time correlation function, the time when the decay starts is an indication of the mean size. That is why the decay starts at longer time for large particles compared to smaller ones.

DLS is a standard technique used in colloidal chemistry to characterise particles, nano-objects, or microemulsion droplets. DLS was used to study water-in-oil microemulsion,[36, 37] microemulsions with nonaqueous polar solvents,[38] the influence of the addition of polymers on a microemulsion,[39] or structures in fully water dilutable sustainable microemulsion with dibasic esters as oil phase.[40]

1.1.3.3. Static light scattering (SLS)

Static light scattering measurements are performed using the same apparatus previously described for DLS. As developed in the previous section, DLS measures real-time scattered intensities. On the contrary, SLS measures time-average scattered intensities as a function of the angle. It is an optical technique that measures the intensity of the scattered light in dependence of the scattering angle. Usually, it is used to determine the molecular weight of a macromolecule and its root mean square radius, called the radius of gyration R_G.

As very small molecules can be considered as isotropic scatterers, i.e. whose scattered light is independent of the scattering angle, larger macromolecules or particles scatter light from different parts of themselves and thus, their scattered intensity depends on the angle. They are anisotropic scatterers and this phenomenon is called angular dependence: as the molecular size increases, the scattered photons can constructively or destructively interfere with each other. For a solution containing a suspension of the investigated macromolecules or particles, the molecular weight and the radius of gyration of those molecules or particles can be determined by the angular dependence of the scattered light.[41]

The Rayleigh theory describes the relationship between the intensity of the light scattered by a sample and its size and molecular weight.[42, 43] The Rayleigh equation is defined as:

$$\frac{K\,C}{R(\theta)} = \left(\frac{1}{M} + 2\,A_2\,C\right)\frac{1}{P(\theta)} \quad \textbf{(1.4)}$$

In equation **(1.4)** C is the solute concentration, R(θ) the Rayleigh ratio of the solution as a function of the scattering angle θ, M the weight-averaged molecule molar mass, and A_2 the second virial coefficient. K is defined as:

$$K = \frac{4\pi^2}{\lambda^4\,N_A}\left(n_0\frac{dn}{dc}\right)^2 \quad \textbf{(1.5)}$$

where λ is the wavelength of the incident light, N_A Avogadro's number, n_0 the refractive index of the solvent, and dn/dc the refractive index increment of the solvent. P(θ) is the form factor, describes the angular dependence of the scattered light and is defined as:

$$\frac{1}{P(\theta)} = 1 + \frac{16\,\pi^2\,{n_0}^2\,{R_G}^2}{3\,\lambda^2}\left(\sin\frac{\theta}{2}\right)^2 \quad \textbf{(1.6)}$$

The angular dependence shown by the form factor is characteristic for the size and also for the form of the macromolecule or the particle.

From these equations, the molecular weight and the radius of gyration can be easily determined by plotting the Guinier plot, i.e. a plot of KC/R(θ) against $(\sin(\theta/2))^2$. By plotting the intensity of the scattered light at many different angles, a best fit line can be extrapolated back to 0° from where the molecular weight can be calculated. The initial slope of this line is related to R_G. Of course, the combination of data obtained from more angles improves the accuracy and precision of the experiment.

As DLS, SLS is often used in colloidal chemistry to study, for example, the droplet size and inter-droplet interaction[44] or the structures found in microemulsions.[45, 46]

In this thesis, SLS was performed on surfactant-free microemulsions. The theory is slightly different and presented in section 2.2.6.2.

1.1.3.4. Small- and wide-angle x-ray scattering (SWAXS)

Generally, x-rays are used to investigate the structural properties of solids, liquids, and gels. As already explained, scattering occurred in solutions due to fluctuations in the medium. Contrary to the light used for DLS that is scattered due to fluctuations of the refractive index in the solution, an x-ray beam with a wavelength λ interacts with electrons and is scattered due to fluctuations of electronic densities in a heterogeneous medium.

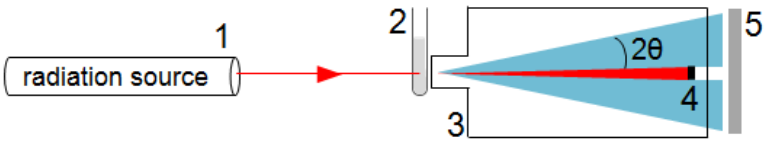

Figure 1.7. Representation of a typical SWAXS experiments. The radiation source **1** produces an x-ray beam which is scattered by the sample **2** in a vacuum flight path **3**. The main beam is stopped by a beamstop **4** which measures the transmitted intensity. The intensity of the scattered x-ray beam is collected by the detector **5**.

As represented in **Figure 1.7**, a monochromatic electromagnetic radiation, in this case x-rays, goes through the sample and is scattered. The scattered intensity is collected as a function of the scattering angle 2θ and is generally defined by:

$$I(q) = (\Delta\rho)^2 \, \Phi_V \, V \, P(q) \, S(q) \qquad \textbf{(1.7)}$$

In equation **(1.7)** $(\Delta\rho)^2$ is the electronic density difference between the scattering object and the solvent, called the contrast. The higher the contrast between objects and solvents, the greater the signal.[47] Φ_V is the volume fraction of the particles, and V the volume of one particle. P(q) is called the form factor and depends on the form of the particle, whereas S(q) is the structure factor and depends on the interactions between the particles in the solution. ***q*** is the scattering vector, the most relevant parameter to analyse the interactions happening in the sample. It has the same definition as for DLS (see equation **(1.1)**). However, the angle between the propagation vectors of the incident and scattered light is 2θ. As a part of the incident beam is absorbed in the sample, the number of photons scattered has to be normalised with respect to the number of photons transmitted through the sample to be able to measure I(q) on absolute scale. Physical quantities such as particle volume or osmotic compressibility can be determined only with an absolute intensity.[47]

Generally, the scattered intensity is plotted against the magnitude q of the scattering vector. According to Bragg's law, the distance d considered is inversely proportional to q:

$$d = \frac{\lambda}{2 \sin\theta} = \frac{2\pi}{q} \qquad \textbf{(1.8)}$$

As it can be seen in **Figure 1.8**, a measurement made at a certain q-value allows investigating the electronic density fluctuations in the sample on a certain distance scale. Three different zones are observed when the scattered intensity is plotted against q. At low q-values, i.e. at small angles and with a very large observation window, the colloidal level is considered as the interactions between the structures, particles, or droplets within the solution can be observed. At that distance scale, the

structure factor S(q) is useful to calculate the interactions between the objects in the system. At high q-values, i.e. at wide angles and with a very narrow observation window, atomic level information are obtained and interactions between the atoms of molecules are observed. Data about one particle, like its shape or its size, or interactions between molecules are harvested in the in-between zone, where the form factor P(q) can be measured.

For the sake of comprehension, SWAXS data of ethanol, octanol, and a surfactant-free microemulsion composed of 16.83 wt% 1-octanol, 39.35 wt% ethanol, 33.82 wt% water, and 10.0 wt% NaSCN are also represented in **Figure 1.8**. Considering the circle in zone 2, the distance between the alcohol groups of ethanol and 1-octanol can be compared. The peak of ethanol being at higher q-values, the distance d between –OH groups of ethanol molecules is much smaller than between –OH groups of 1-octanol molecules. Regarding the circle in zone 3, the peaks indicate the distance between carbon atoms in both molecules. As the peak for 1-octanol is at lower q-values, the distance C-C in 1-octanol molecules are greater than the distance C-C in ethanol. Both results were expected as 1-octanol has a longer carbon chain than ethanol. The high intensity for NaSCN in zone 1 indicates some interactions between the structures in the surfactant-free microemulsion.

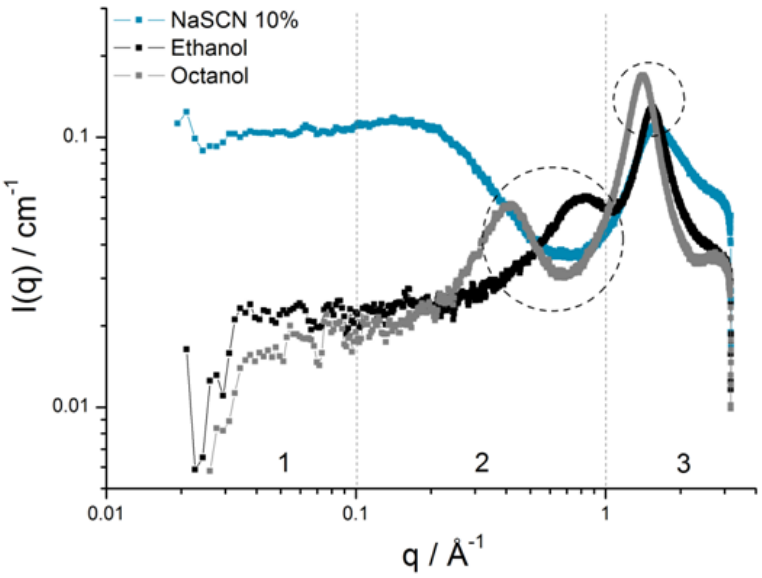

Figure 1.8. Typical SWAXS spectrum on a log-log scale for ethanol, octanol, and a formulation where 10 wt% NaSCN is added to the system water/ethanol/1-octanol. Zone 1 corresponds to low q-values, zone 2 to middle q-values (in-between zone), and zone 3 to high q-values.

As it can be seen in equation **(1.7)**, the scattering power is related to the electron density contrast (squared), so that the larger the contrast, the larger the scattering contribution. Depending on the instrument used it is possible to measure small and wide angles in a single run, as it is the case at the ICSM in Marcoule, France. SWAXS is often used for systems showing one or two phases.

When the number of phases in the system increases to three or more, the complexity increases dramatically too.[48]

Generally speaking, the slope of the scattering profile in a double logarithmic plot indicates the geometry of the particle. An initial slope of 0, -1, or -2 indicates respectively a globular, cylindrical, or lamellar shape. At higher q-values, a slope of -4 is always to be observed, more or less visible depending on the size of the scattered objects.[49]

Both Guinier's law and Porod's law are basics of x-ray scattering interpretations. Guinier approximation is a very popular and powerful method of treating data in small angle scattering. Guinier *et al.* showed that, for dilute suspension, the scattered intensity can be described as:[35, 50, 51]

$$I(q) \approx \Phi V e^{-(q R_G)^2/3} \quad \textbf{(1.9)}$$

In equation **(1.9)** Φ is the volume fraction of one given phase, V the volume of one particle and R_G the radius of gyration of an object. The Guinier approximation allows measuring a geometrical characteristic of an object, i.e. its radius of gyration, only by looking at the limit behaviour when q tends to zero. However, it works only for diluted suspension where the particles are widely separated and do not interact, i.e. when the structure factor can be neglected. It should also be noted that the equation is only valid in the so-called Guinier regime defined as $qR_G < 1$. On the whole, the Guinier formula holds surprisingly well in the majority of cases.

The Porod law applies to scattering profiles of any particle system and states that the final slope in the small-angle x-ray scattering region (end of zone 2 in **Figure 1.8**, $q \approx 0.4$ Å^{-1}) represents the interface and fractal dimension of the scattering objects. It states that the intensity is decreasing as q^{-4} at large q for a sharp interface. The Porod law in its final form is described as:[35, 50, 52]

$$\lim_{q \to \infty} I(q) = \frac{2\pi (\Delta\rho)^2}{q^4} * \frac{S}{V} \quad \textbf{(1.10)}$$

In equation **(1.10)**, S and V are respectively the surface and volume of one object. This law allows measurements of the surface of objects. As it only deals with the existence of an interface and that interactions between the structures have no effect at large angles, the same result holds for concentrated or bicontinuous systems.

1.1.4. Applications of microemulsions

Microemulsions are widely used in the field of formulation and can be found in many different products and chemistry domains. A non-exhaustive list of applications is presented.

Microemulsions are currently used in various applications related to **biotechnology** and **enzymatic reactions**. Enzymes are traditionally used in an aqueous medium but an organic solvent is more attractive when the reactants or products are lipophilic. However, proteins are poorly soluble in apolar solvents. They lose their biological activity and undergo denaturation when transferred into such solvents.[53] Thus, microemulsions can be used as a medium for enzyme-catalysed reactions and in particular reverse micelles. The latter are capable of hosting proteins and enzymes in the inner water phase. Proteins are entrapped inside the micelles, avoiding direct contact with the organic solvent. Such microemulsions have been used for the synthesis of esters or peptides, for transesterification, and for various hydrolysis reactions.[54] It was demonstrated that the catalytic activity of many enzymes confined in microemulsion water droplets varies with water content and a bell-shaped dependence of activity as a function of the water/surfactant molar ratio is observed.[55, 56] The facts that hydrophilic and hydrophobic substrates can be dissolved at high concentrations or that multienzymatic reactions are feasible are considerable advantages of w/o microemulsions.[17]

The interest of the use of microemulsions in the **pharmaceutical** field as potential drug delivery systems has grown progressively in the past decades. The thermodynamic stability of microemulsions, the fact that they act as supersolvents for drugs or that the dispersed phase can behave as a potential reservoir of lipophilic or hydrophilic drugs, the small diameter of the droplets or their low viscosity are, among others, several properties that are of particular interest in this field.[54] As an example, Kraeling *et al.* developed a peroral dosage form to deliver insulin to the colon.[57] After measuring the reduction in blood glucose concentration levels, they found that the oral pharmacological availability (PA) of insulin microemulsions as compared to intravenous insulin in beagle dogs was 2.1%. The PA increased to 6.2% with the encapsulation of gelled microemulsions and aprotinin as enzyme inhibitor in hard gelatine capsules coated with polymers for pH-dependent and time-controlled release mechanisms. Microemulsions can also be used for anticancer therapy or the solubilisation of steroids, vitamins, anti-infective, and anti-inflammatory drugs.[54]

Due to their ability to solubilise both hydrophilic and lipophilic compounds, microemulsions are also widely used in **detergency**. In the past, organic solvents were used in dry-cleaning processes for textile cleaning. Considering the health risk of chlorinated solvents and the flammability of the low-molecular-weight hydrocarbons, microemulsions came on as a substitute. Microemulsion efficiency in soil removal was investigated from textile fabrics, in raw wool scouring, and in skin degreasing processes.[54] The results from the study investigating the microemulsions water/n-undecane/$C_{12\text{-}14}$ alkyl polyglycol ether/n-pentanol as detergent can be

cited. It was observed that the microemulsion shows outstanding detergency, especially for oily soils, even at a washing temperature of 25 °C. This detergency can be attributed to the ultralow interfacial tension compared to the conventional detergent solution. Further, the composition can be tuned to suit the particular type of soil and fabric.[58]

Once again, the small droplet size and the transparency of microemulsions are advantages for **cosmetic** applications. As microemulsions are thermodynamically stable, no problems are encountered with changes or phase transitions during long-term storage. Legal restrictions on the extent of volatile organic compounds also paved the way for their use. Microemulsions are used for example in skin cleansers: in that case, the cosurfactants are chosen such that they are non-irritating. Glycerin or sorbitol may be found in hair product microemulsions,[59] as well as functionalised silicone oils to make clear conditioning shampoos.[60, 61] Fatty alcohols or sorbitan ester ethoxylates are examples of surfactants to solubilise perfume oil in water without volatile or drying solvents such as ethanol. Gels and antiperspirants can also be formulated using microemulsions.[58]

It should also be pointed out that microemulsions can be found in many other products for which the word “microemulsion” is not mentioned as it is not the main marketing argument. An ink can be cited as an example, where a colorant is dispersed in the organic vehicle phase.[62] Microemulsions are also used for metal cutting as both lubricant and coolant and in dyeing processes. One advantage for the latter application is the reduction in the amount of potentially toxic solvents required to solubilise large molecules, such as dyes, upon dispersion of the solvent in water-rich microemulsions.

To conclude, the applications and studies of microemulsions listed above are only examples of current research topics. Microemulsions are also used in paints, as decontamination media, applied in the petroleum industry for enhanced oil recovery, used for nano-particle formation, as well as in agrochemical and food industries.[17, 54] As one drawback of microemulsions may be the use of surfactants and cosurfactants, which have to be sometimes synthesised and removed from the final system, the use of surfactant-free microemulsions were considered.

1.2. Surfactant-free microemulsions

1.2.1. First studies

Already in the thirties, Washburn *et al.* unconsciously formulated surfactant-free microemulsions. In many papers, they investigated the influence of alcohols on the freezing point of oil. They formulated ternary solutions of water, alcohol, and oil which were carefully shaken. After a sufficient time, two clear and transparent layers were obtained and the refractive index of each layer was measured. The tie-lines were then determined and represented in a ternary phase diagram, along with the phase boundary between the two-phase system and the clear and transparent single phase system, i.e. the surfactant-free microemulsion area. However, as the presence of possible structures in the single phase was not investigated, no connections between microemulsions – which were not discovered at that time – or surfactant-free microemulsions were made. Examples of their work are the ternary systems water/ethanol or isopropanol/benzene, water/ethanol or methanol/cyclohexane, or water/ethanol/toluene.[63-67]

The group of Barden started to work on surfactant-free microemulsions in the late seventies in the course of adapting a microemulsion in tertiary oil recovery. They were the first to characterise such solutions with many methods and experiments. They studied the surfactant-free system water/2-propanol/hexane using conductivity and centrifugation data, as well as visual examination.[68] These data allowed them to construct the ternary phase diagram of the system and to differentiate five areas, as represented in **Figure 1.9**. They observed unstable macroemulsions, transparent and stable microemulsions, a region with small aggregates of water and 2-propanol, normal ternary solutions, and metastable microemulsions, referring respectively to areas A, B, C, D, and E in **Figure 1.9**. Oil-continuous microemulsions were observed even though a surfactant was not present. It can be noted that only 2-propanol and 1-propanol could stabilise the microemulsion. Only modest changes in the ternary phase diagram were observed after the addition of the surfactant hexadecyltrimethylammonium perchlorate. However, most short-chain alcohols containing less than eight carbons could stabilise the microemulsion containing the surfactant. Keiser *et al.* studied the influence of the addition of NaCl on the region boundaries for the same surfactant-free system using nuclear magnetic resonance (NMR) spectroscopy.[69] Significant changes in the location of the different areas were observed. The microemulsion region was stabilised, whereas the aggregates region appeared to be destabilised. They also showed that ^{1}H NMR measurements help detecting not only the same region boundaries as conductivity data but also the presence of bulk water dispersed in the microemulsion. The ternary system water/2-propanol/hexane is also suitable as a solvent for hydrolytic reactions, as it can

simultaneously dissolve both lipophilic organic molecules and hydrophilic salts, thus being a viable and less expensive alternative for reactions involving nonpolar and ionic reactants.[70]

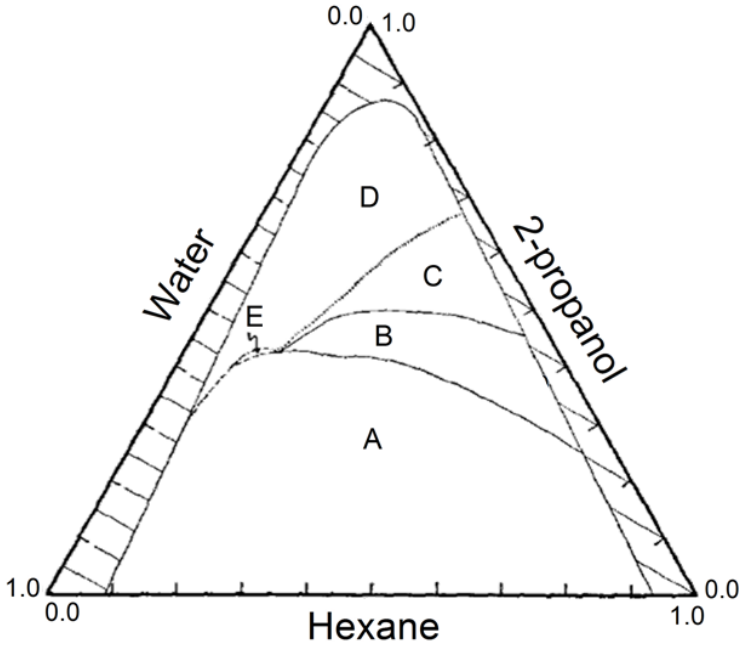

Figure 1.9. Ternary phase diagram of the system water/2-propanol/hexane in mole fractions. Area **A** corresponds to unstable macroemulsions, **B** to stable microemulsions, **C** to compositions characterised by the presence of small aggregates of water and 2-propanol, **D** to normal ternary solutions, and **E** to metastable microemulsions. The striped areas are unexplored. Redrawn from[68].

As Lund *et al.* wanted to "*expand the number of known ternary systems which produce detergentless microemulsions and to provide some insight into both statics and dynamics of microemulsification*", they investigated the system water/2-propanol/toluene using conductivity, ^{13}C NMR, and light scattering.[71] Similar results as for the system containing hexane as oil were obtained, i.e. the observation of regions with different structures. Further, light scattering measurements in the region where aggregates were observed lead to rough droplet diameters from 50 to 300 Å.

Later, surfactant-free microemulsions were investigated regarding enzyme-catalysed reactions.[72, 73] For example, Zoumpanioti *et al.* studied the catalytic activity of lipases entrapped in surfactant-free microemulsion-like ternary systems consisting of water, short chain alcohols, and hexane.[74] Both enzymes catalysed efficiently the esterification of fatty acids or natural phenolic acids. The authors showed that the stability of the entrapped enzymes at low water content in the ternary system was higher than that observed in surfactant-based w/o microemulsions.

At that time, the presence of defined droplets, nano-objects, or fluctuations in such solutions was not proven. The presence of a nano-structuring was assumed by taking indirect hints as arguments, as did Zoumpanioti *et al.* By studying the velocity of enzymatic reactions in a series of surfactant-free w/o microemulsions in which lipases were solubilised, they observed different enzyme behaviours, leading them to suggest that the structure of the systems depends on the system's composition.[75]

1.2.2. Ouzo effect

1.2.2.1. The first in-depth study

The Ouzo effect was first described in 2003 by Vitale and Katz and occurs in liquid systems involving three or more components.[76-79] In the diagram weight fraction of cosolvent against weight fraction of oil, the Ouzo region can be found between the binodal and spinodal curves. The first traces the thermodynamic minima in the Gibbs free energy of a system, and the latter the limit of thermodynamic stability. The Ouzo effect exists between those two lines in the so-called metastable region, i.e. for a state for which the Gibbs free energy is not minimised and there are large kinetic barriers to the phase separation. The necessary condition for the effect to occur is the rapid addition of a solvent A to a second solvent B, which is highly or entirely miscible with solvent A, and a third component, which is highly soluble in solvent B but not in solvent A. The authors named it Ouzo effect after the Greek alcoholic beverage in which the anise oil spontaneously nucleates into small droplets when water is added. Indeed the Ouzo effect can be observed, when water (solvent A) is added to a mixture of ethanol (solvent B), which is highly miscible with water, and *trans*-anethole, which is miscible with ethanol but not with water. This effect occurs also in beverages of the same family like Pastis (France), Raki (Turkey), or Sambuca (Italy).[80] The drink looks like a milky white emulsion, in which the formed droplets scatter light. The Ouzo effect exhibits relatively stable dispersions of very small solute droplets for certain compositions without surfactants, dispersing agents, or mechanical agitation. The droplets grow almost entirely by Ostwald ripening.

In their work, Vitale and Katz studied dispersions of oil droplets in water formed by the addition of water to a solution of divinyl benzene (DVB) and ethanol.[77] The oil supersaturates and nucleates into small droplets. They showed that the mean diameter of a droplet at constant temperature depends on the oil-to-solvent ratio. With increasing oil-to-solvent ratio, more oil is near each nucleus, so larger droplets can form. The size distribution becomes narrower with increasing temperatures because less oil is available at high temperatures since the solubility of

the oil in the aqueous phase increases with the temperature. Thus, smaller droplets are formed with addition of water. Further, the droplet number density can be controlled independently of the mean diameter as it decreases at higher water content. By varying the type of oil, the authors also showed that the bulk phase separation by creaming is slow, i.e. the solution exhibiting the Ouzo effect is more stable if the density of the droplets is close to that of the continuous phase and if the droplets are small. Finally, the effects of the solvent were investigated. It was shown that the solvent partition coefficient is an important parameter. Acetonitrile partitioning approximately evenly between the aqueous and dispersed phase, larger droplets were obtained since they likely contain some of the solvent as well as the DVB, whereas ethanol partitions nearly exclusively into the aqueous phase, leaving smaller pure DVB droplets.

As the Ouzo effect exhibits stable dispersions of hydrophilic and hydrophobic molecules and that the sizes and size distribution can be easily controlled, it was used in numerous applications. Some of them are listed in the next section.

1.2.2.2. Applications

The Ouzo effect is used for the preparation of nano-spheres, nano-capsules, or polymeric nano-particles that can be use as drug delivery devices or for cosmetic and polymerisation purposes.

For example, Aschenbrenner *et al.* used the Ouzo effect to prepare polysaccharide-based nano-particles.[81] Hydrophobic polysaccharides were synthesised by the esterification of dextran, pullulan, and starch with hydrophobic anhydrides. Acetone and THF were used as organic solvents. Immediately after the organic polymer solution was added to water, nano-particles were generated. It was shown that a fluorescent dye could be encapsulated in the nano-particles and the number of dye molecules in the particles can be adjusted by the amount of dye dissolved in the initial polymer solution. Multifunctional, oil-filled nano-capsules with controlled morphologies were also produced by Yan *et al.* using the Ouzo effect.[82] They showed that in a narrow range of polymer/water/acetone/hexadecane compositions, the polymer chains preferentially stick at the interface of the oil droplets to generate polymeric capsules in the full volume. The versatility of the Ouzo effect allowed generating more complex nano-capsules that can either be loaded with hydrophobic molecules or shell-functionalised. Finally, the Ouzo effect allows also spontaneous polymerisation or polycondensation, and the production of polymethylmethacrylate nano-particles as Aubry *et al.* showed.[83, 84]

Peng *et al.* functionalised a hydrophobic surface with polymeric lens-shaped nano-structures in a one-pot approach using the Ouzo effect.[85] The latter was used with the system water/ethanol/precursor monomer to produce a surfactant-free microemulsion of the monomer nano-droplets. As represented in **Figure 1.10**, the first step was the direct adsorption of monomer nano-droplets onto the hydrophobic substrate. The nano-droplets were then photopolymerised. Polymeric nanolenses on the substrate were obtained after sonication to clean weakly attached polymer nano-particles on the surface.

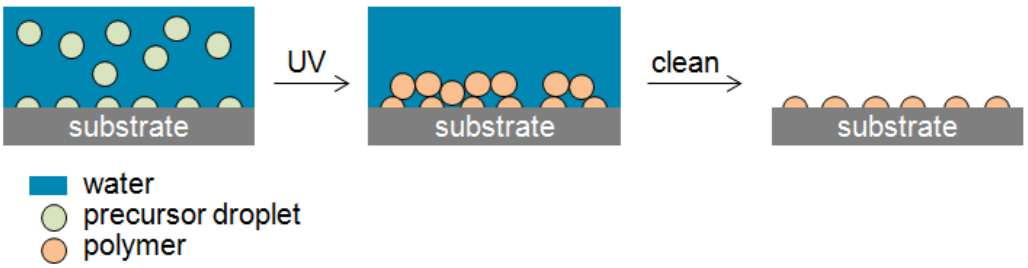

Figure 1.10. Schematic representation of the nanolenses fabrication process. Redrawn from[85].

The size of the produced nanolenses was controlled by the monomer and continuous liquid-phase content using the linear relationship with the ratio of the composition in the ternary system, as shown by Vitale and Katz. Further, this technique allowed the functionalisation of the entire surface area or just of specific area by depositing microemulsion droplets on the surface to functionalise. This work is a simple approach and may have applications as functional biomedical supporting materials or smart surface coatings.

The carotenoids are a group of natural coloured pigments that are in demand for the food industry as substitutes for artificial dyes. However, they are water-insoluble and only slightly soluble in fats and oils. They are therefore difficult to implement. In 1989, the German firm BASF used the Ouzo effect to produce water-dispersible carotenoid preparations by a solution-precipitation process.[86] First, the synthetic product is turned into a molecular dispersion in water-miscible, low-boiling, and toxicologically harmless solvents, such as ethanol or acetone. This solution is then mixed with an aqueous solution of a protective polymer, resulting in precipitation of the carotenoid. An average particle size of about 0.1 μm can be obtained by proper choice of the protective polymer. The organic solvent is then removed by distillation and a water-dispersible powder can be obtained from the hydrosol by conventional methods, such as spray-drying.

The Ouzo effect can also be applied to produce drug delivery devices such as biodegradable lipid- or polymer-based nano-particles.[79, 87]

1.2.3. Pre-Ouzo effect

1.2.3.1. First ideas

As explained in section 1.2.1, the presence of structures in surfactant-free microemulsion was suspected but not proven. By studying systems exhibiting the Ouzo effect, Klossek *et al.* also observed a nano-structuring close to the phase boundary but still within the monophasic region, before enough water is added to reach the two-phase domain. Werner Kunz coined this phenomenon the "pre-Ouzo effect".[88] Using static (SLS) and dynamic light scattering (DLS) in the ternary system water/ethanol/1-octanol, they demonstrated that well-defined domains can exist in surfactant-free microemulsions. The intensity of the correlation functions from DLS increased when more water is added to the solutions and the composition is closer to the demixing boundary, in the so-called pre-Ouzo zone. They stressed that it cannot be a critical phenomenon close to a critical point since even far from the phase separation line correlation functions occurred. SLS was also carried out to definitely validate the presence of nano-droplets. Octanol micellar aggregates swollen with ethanol of defined size exist in equilibrium with a solvent. Further, by investigating the solubilisation behaviour of such solutions with two hydrophobic dyes, it was shown that these aggregates have a less hydrophobic core than in the case of classical microemulsions.

Such a nano-structuration in the pre-Ouzo region not only exists in the water/ethanol/1-octanol ternary system, but also in other systems fulfilling the requirements for the Ouzo effect, as showed by Klossek *et al.*[89] It was demonstrated with DLS and SLS measurements that nano-structures, or rather clusters of benzyl alcohol and ethanol, also occurred in the systems water/benzyl alcohol/eco-solvent, where the eco-solvents were ethanol, ethyl lactate, and γ-valerolactone. They showed that the solubility of the benzyl alcohol was increased in presence of the eco-solvent and above all that a region of optimal solubility was observed near the demixing boundary in the monophasic domain, i.e. the pre-Ouzo region.

1.2.3.2. Investigating the nano-structures

In order to deeper investigate the pre-Ouzo region consisting of two distinct nanoscopic pseudo-phases, one oil-rich and one water-rich, Diat *et al.* combined small-angle neutron scattering (SANS) with wide- and small-angle x-ray scattering (SWAXS) for the system water/ethanol/1-octanol.[90] Both techniques unambiguously showed the existence of 1-octanol-rich domains of well defined size of the order of 2 nm radius. Further, by comparing the WAXS spectra of the surfactant-free microemulsion with those of binary mixtures, they found that the relative fractions

for the sample (34.3 v% water, 44.6 v% ethanol, and 21.1 v% octanol) are close to 40/60 of ethanol/water in the water-rich phase and close to 60/40 of 1-octanol/ethanol in the oil-rich part. The water-rich domains are structured in a similar way to binary mixtures of water and ethanol, whereas the oil-rich domains are less structured than the corresponding pure liquids. Considering ethanol vapour pressures and activity, it was affirmed that some ethanol molecules are strongly adsorbed onto interfaces of both domains.

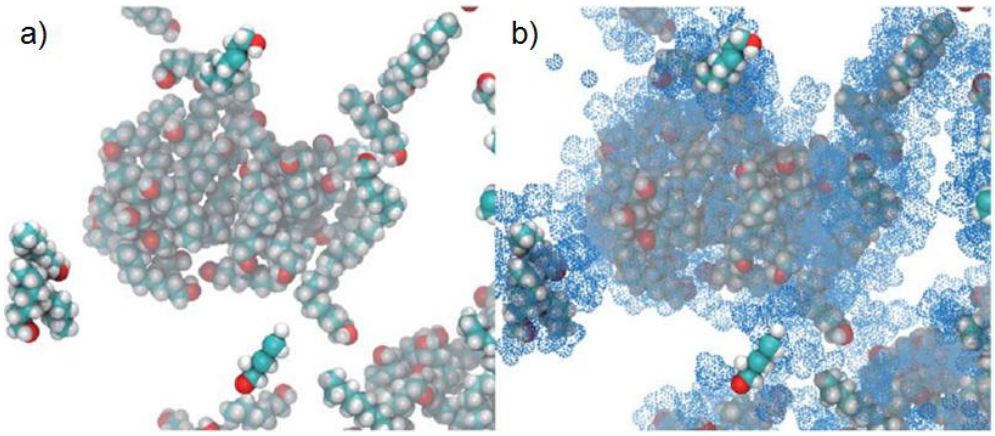

Figure 1.11. Snapshots of the simulated system in the pre-Ouzo region where a) only the 1-octanol molecules are highlighted; and b) the ethanol molecules that interact strongly with the 1-octanol molecules are shown as blue spheres. Taken from[91].

Schöttl *et al.* also studied the system water/ethanol/1-octanol with molecular dynamics simulations to better understand the shape and structure of the aggregates on a molecular-level.[91] By simulating SWAXS intensities and calculating the van der Waals interactions between an aggregate and one ethanol molecule, and then the distribution of the interaction energies, they clearly identified the structure of the micellar aggregates, as represented in **Figure 1.11**. Starting from the centre of the aggregate, the density of 1-octanol is highest in the core. A decay of the 1-octanol concentration is then observed with increasing distance from the centre. The authors found the interface at 1.5 nm from the centre of the aggregate, which is in agreement with the work of Diat *et al.* cited above. On the contrary, the water density increases with the distance from the aggregate centre. It can be noted that there is some 1-octanol in the aqueous bulk phase and some water in the aggregate. As for ethanol, it is distributed over both pseudo-phases, i.e. some of the molecules penetrate into the core and unbound ethanol molecules can be found in the aqueous phase. Further, some ethanol molecules are bound to the aggregates and tend to accumulate at the interface, after which the ethanol concentration decays slowly to the bulk value (see **Figure 1.11**). The authors also pointed out that these micelle-like aggregates are clearly distinct from simple critical density fluctuations and that the aggregates gradually disappear when adding ethanol, i.e. moving away from the pre-Ouzo region.

Subramanian *et al.* also studied the presence of a nano-structuring in the surfactant-free microemulsion water/tertiary butyl alcohol (TBA)/cyclohexane using results from molecular dynamics simulations, SANS, and DLS.[92] The presence of aggregates, called mesoscale inhomogeneities by the authors, was observed in a really narrow water-rich region of the ternary phase diagram where less than 3 mol% of cyclohexane was solubilised. Their structures were in agreement with the works of Diat *et al.* and Schöttl *et al.*, i.e. the mesoscopic droplets have a cyclohexane-rich core surrounded by a shell of water and alcohol molecules. Increasing the TBA concentration led to the disappearance of the mesoscopic droplets as the alcohol and cyclohexane prefer to remain mixed with each other rather than form droplets, in accordance with the work cited above. Subramanian *et al.* made the same observations in the systems water/TBA/propylene oxide and water/TBA/isobutyl alcohol in larger water-rich regions where mesoscale solubilisation occurs.[93]

1.2.3.3. Consequences and applications

One consequence of the pre-Ouzo effect is the impact of the nano-structures on the fragrance performance in a perfume, for example. Tchakalova *et al.* studied these effects on the ternary system water/ethanol/fragrance by simultaneous on-line gravimetric, calorimetric, and gas chromatographic monitoring.[94] They showed that the fragrance performance was affected by the transformation of the liquid and thus vapour composition from ethanol-rich to water-rich, implying also a change in the partition coefficient of ethanol molecules. A strong evaporation of ethanol in the pre-Ouzo zone was observed, as well as a noticeable auto-encapsulation of the fragrance in the Ouzo domain when the bulk water evaporates.

One application worth to be cited is the dissolution of hydrophobic compounds, such as ibuprofen, in the presence of large amount of water, carried out by Hankel *et al.*[95] The system water/acetone/CO_2 was studied. First, Raman spectroscopy was used to prove that the system is inhomogeneous on a molecular scale. Then, the non-water and non-CO_2 soluble ibuprofen was dissolved in the system to confirm the existence of acetone micellar-like aggregates swollen with CO_2. These results are promising since microemulsions with compressed CO_2 enhance the solubility of solutes.

The pre-Ouzo effect can also be found in fragrance tinctures or in mosquito repellents present on the market. Those applications are part of this thesis and will be developed respectively in sections 3.1.3 and 3.1.4.

1.2.4. Different types of fluctuations

As developed in section 1.1.3.2, DLS is a powerful technique to investigate the sizes and structures of microemulsions. However, one has to be careful with the interpretation of DLS results in ternary mixtures as different fluctuations may occur.

In the mid-seventies, kinetics of processes occurring in micellar solutions and chemical relaxation of micellar equilibrium were thoroughly investigated. Lang *et al.* studied the relaxation processes present in solutions of sodium lauryl sulphate and laurylpyridinium chloride, bromide, and iodide.[96] They showed the presence of two processes characterised by two different relaxation times, depending on concentration and ionic strength. The slow process was assigned to the micellisation-dissolution equilibrium, whereas the fast one to the exchange equilibrium of surfactant's ions between the micellar phase and the bulk solvent. Aniansson *et al.* developed that theory of micellar kinetics and were able to calculate, among others, the rate constants of the exchange of ions to/from the micelles and the enthalpy and entropy changes associated with the incorporation of one ion into the most stable micelle.[97]

Based on these results, the presence of such relaxation processes in ternary mixtures, without surfactant, starts gaining interest. By performing DLS measurements in the vicinity of the critical point of the ternary liquid mixture glycerol/acetone/water, Ivanov *et al.* observed two hydrodynamic relaxation modes with well-separated characteristic relaxation times.[98] As theoretically predicted by Anisomov *et al.*, one of these two modes can be associated with mass diffusion and the other with thermal diffusion.

Heller *et al.* studied the ternary mixtures consisting of n-dodecane and n-octacosane with dissolved hydrogen, carbon monoxide, or water.[99] Three different signals could be distinguished from the time-resolved analysis of the scattered light intensity by using photon correlation spectroscopy. The fastest mode was associated with the thermal diffusivity in the corresponding n-alkane mixture. The two further modes in the ternary mixture are comparable to the modes associated with the concentration fluctuations in the corresponding binary mixtures.

The ternary systems presented in this thesis and measured with DLS are surfactant-free microemulsions. As shown before, the interpretation of the data obtained from DLS is not always direct, as different fluctuations may occur in such mixtures. In our case, the fluctuations of the organic-rich phase in the water-rich phase and, logically, of the water-rich phase in the organic-rich phase, and the fluctuations of the ethanol distribution between both pseudo-phases can be expected. The scattered intensity in DLS in such systems is then caused by the convoluted contributions of those two fluctuations. The fluctuation of the ethanol molecules induces a distinct gradient of refractive index and thus changes the dn/dc values, as shown by Acre *et al.*[100]

1.3. Effects of salts

1.3.1. Hofmeister series

1.3.1.1. The first observations

It is well-known that ions play an important role in biology and chemistry, and are involved in a lot of physicochemical phenomena. In 1888, Hofmeister studied the precipitation of purified egg white and discovered that some salts precipitate proteins in water, and certain salts help their solubilisation.[101]

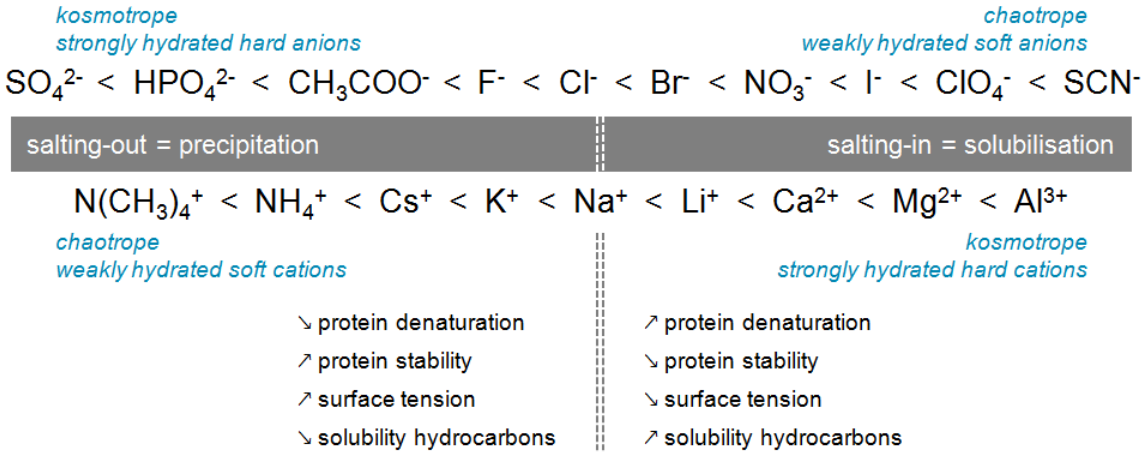

Figure 1.12. Hofmeister series of anions and cations with their most important properties and effects.

Later, an ordering of ions was made and is now known as the Hofmeister series, represented in **Figure 1.12**. Anions and cations on the left tend to precipitate proteins in water (salting-out), whereas those on the right help solubilising proteins in aqueous solution (salting-in). The borderline is usually set at the chloride ion for anions and sodium ion for cations. Salting-out ions share common properties, i.e. they tend to enhance the water structure, increase the surface tension of solvents, and decrease the solubility of hydrocarbons. On the contrary, salting-in ions tend to break the water structure, decrease the surface tension of solvents, and increase the solubility of hydrocarbons, thus adsorbing at the interface. Regarding the anions, salting-out ones are kosmotropes, in other words they are strongly hydrated and hard, i.e. strongly charged and with small polarizabilities, whereas salting-in anions are chaotropes, that is to say weakly hydrated and soft, i.e. less charged and thus more polarizable. That observation is reversed for the cation series.[102]

1.3.1.2. The contribution of Collins

In order to understand the formation of ion pairs in aqueous solutions, Collins developed in 2004 the law of matching water affinities.[103] It was shown that ion hydration depends on ion surface charge density, the latter being the ratio between the charge of the ion and its radius. Small ions of high charge density (kosmotropes, such as sulphate, phosphate, sodium, or fluoride) are strongly hydrated, whereas large monovalent ions of low charge density (chaotropes, such as ammonium, chloride, or potassium) are weakly hydrated. In his model, an ion is considered as a sphere with a point charge at its centre and the water molecule is considered as a zwitterion of medium size. As illustrated in **Figure 1.13**.a, Collins defines an ion as chaotrope when the water molecules at the surface of the sphere are so far away from the point charge at the centre of the sphere that water-ion interactions are weaker than water-water interactions (represented by the dotted line). Further, an ion is kosmotrope when the water-ion interactions are stronger than the water-water interactions.

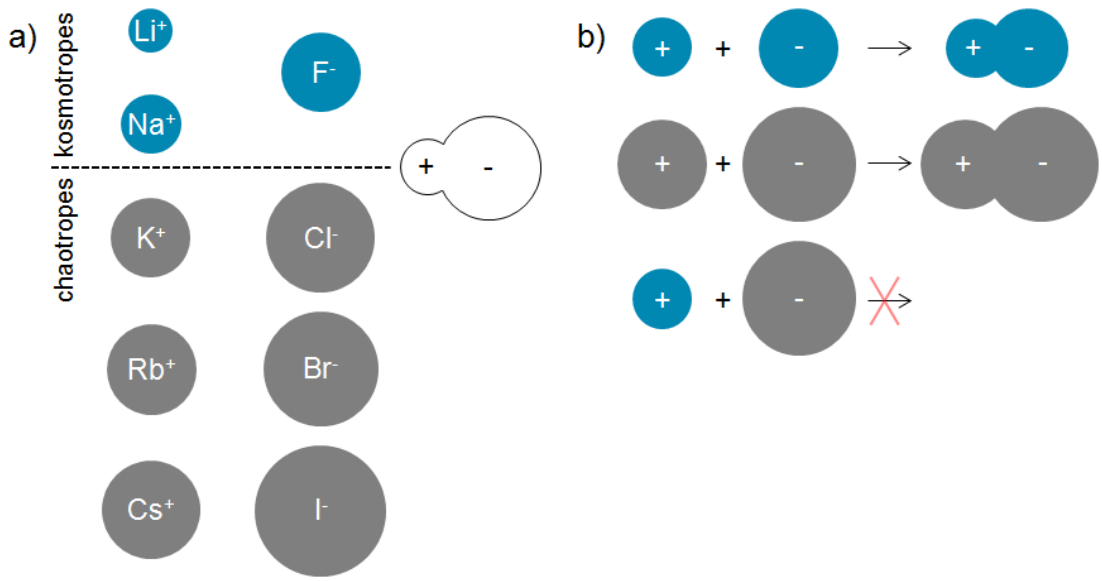

Figure 1.13. Schematic representation of a) strongly hydrated kosmotropes and weakly hydrated chaotropes, approximately to scale. Water is represented as a zwitterion next to the dotted line that represents the strength of water-water interactions; and b) inner sphere ion pair formation with ions of equal water affinities. Redrawn from[103].

According to Collins, oppositely charged ions will only form inner sphere ion pairs if they have a comparable affinity to water.[103, 104] For example, the point charge at the centre of a small kosmotropic ion can get closer to the point charge at the centre of an oppositely charged kosmotropic ion than it can to the point charge at the centre of the oppositely charged portion of a water molecule. As they experience a very strong reciprocal attraction, they can come together and form direct ion pairs by expelling the hydration spheres between them.

Accordingly, large ions of opposite charge will come together because water molecules can form stronger interactions between themselves. As the hydration spheres are loosely bound, chaotropic ions also come together by expelling the hydration water between them.
Finally, a small kosmotropic ion will not dehydrate to form an ion pair with a large chaotropic ion because the point charge at the centre of the kosmotropic ion can get closer to the point charge at the centre of the oppositely charged portion of the water molecule than to the point charge at the centre of the chaotropic ion. The small ion does not lose its hydration shell and small and large ions are always separated by water and cannot form strong ion pairs. This concept is illustrated in **Figure 1.13**.b as respectively small ions of opposite charge and large ions of opposite charge spontaneously form inner sphere ion pairs.

1.3.1.3. Ion specific effects: quite the challenge

Since Hofmeister's discovery, the interest in ion specific effects has steadily grown. Regarding the literature on the subject from the last decades, salt effects are more complicated than it appears and depend strongly on the studied system. Vlachy *et al.* studied the transition from micelles to vesicles upon addition of salts in the aqueous solution of dodecyltrimethylammonium bromide (DTAB) and an excess of sodium dodecylcarboxylate (SL).[105] They showed that the Hofmeister series for cations is reversed when the surfactant headgroup is a carboxylic group, whereas no anions specificity was found.

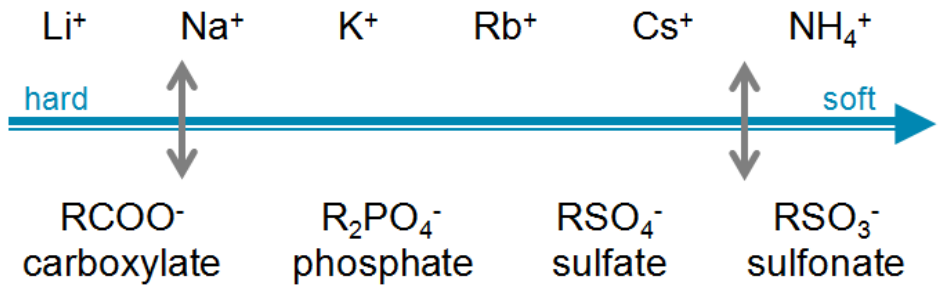

Figure 1.14. Ordering of anionic headgroups and cations regarding their capabilities of forming ion pairs. Strong interactions are represented by the grey arrows. Redrawn from[106].

The specific behaviour of cations towards carboxylic groups was explained in another study of Vlachy *et al.* in which they proposed a Hofmeister-like ordering of charged headgroups.[106] Using simulation results as well as Collins' concept, they showed that an alkyl sulphate headgroup can be classified as chaotrope and alkyl carboxylates as kosmotrope. As chaotropes can only form direct ion pairs with other chaotropes, and kosmotropes with other kosmotropes, they developed an ordering of interactions between cations and anionic headgroups represented in **Figure 1.14**.

According to **Figure 1.14**, Cs^+ will form the closest ion pair with sulfonates and sulphates, whereas Li^+ will strongly bind to carboxylic groups for which an inversed Hofmeister series is observed.

Schwierz *et al.* investigated the influences of hydrophobic and hydrophilic charged surfaces on Hofmeister series using a two-scale modelling approach.[107, 108] In a first paper, they investigated the order of the Hofmeister series regarding the anions F^-, Cl^-, and I^-. As summarized in **Figure 1.15**, the order depends on the charge and the polarity of the surface. The anionic series is direct for hydrophobic negatively charged surfaces and hydrophilic positively charged ones. The series is then indirect for both hydrophobic positively charged surfaces and hydrophilic negatively charged ones. It can also be noted that partial series reversal is to be expected for surfaces of intermediate polarity or intermediate charge, as often encountered in biology.

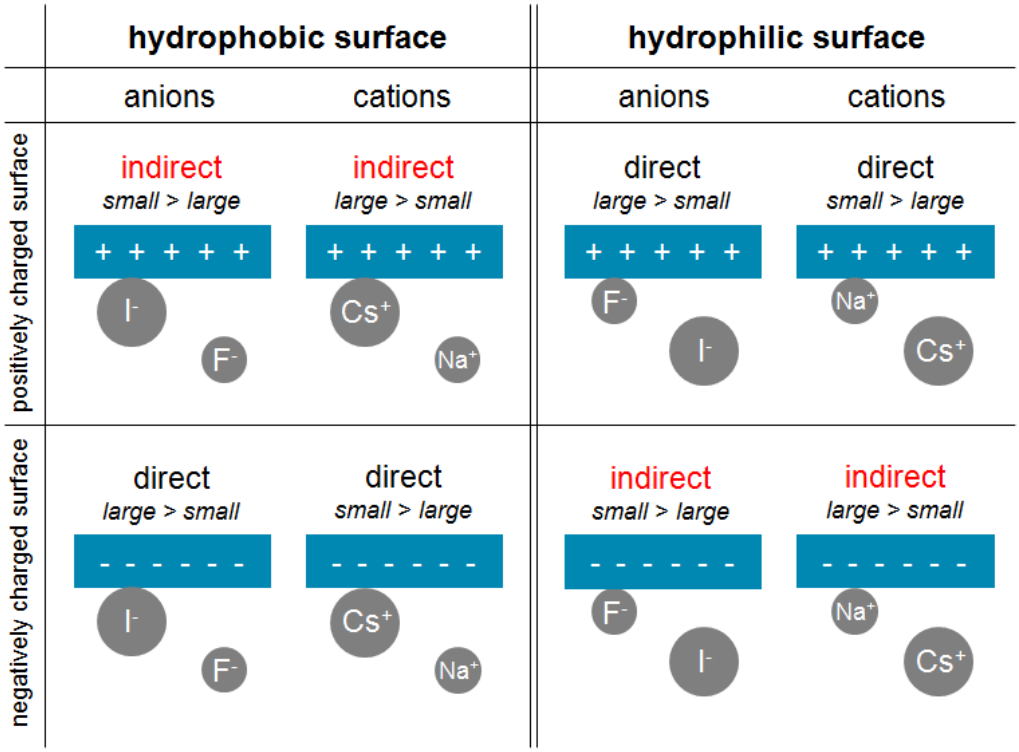

Figure 1.15. Schematic explanation of the Hofmeister series reversal when changing the polarity and the charge of the surface. The direct Hofmeister series for anions and cations are respectively $F^- < Cl^- < I^-$, and $Cs^+ < K^+ < Na^+$. Ions on the right lead to a better solubilisation. Ion sizes are arbitrary. Partially redrawn from[107, 108].

It was shown in this study that hard and small ions such as F^- are attracted by polar surfaces, contrary to soft and large ions such as I^- which are attracted by hydrophobic surfaces. Considering hydrophobic surfaces, large anions give them an effective negative charge by adsorbing on them. This leads to surface-surface repulsion and therefore stabilisation of neutral solutes. When the

surface is negatively charged, the adsorption of large anions is reduced due to electrostatic repulsions but the trend will be the same, i.e. small anions are more repelled than large anions that still give negative surfaces a more negative surface potential. This also leads to surface-surface repulsion and stabilisation. When the surface is positively charged, the trend is reversed since the surface potential is lowered by strongly adsorbing large anions such as I^-. The neutral solutes is then stabilised by the small and weakly adsorbing anions (see **Figure 1.15**).
In a second paper, the charge and the size of the ion were also investigated. It was shown that large cations such as Cs^+ have a high hydrophobic surface affinity. For the same cation-hydrophobic surface separation, K^+ is weakly repelled while Na^+ is most strongly repelled. At that distance the first hydration layer of all cations is intact. That is not the case for large anions such as I^- that partially strip off their hydration shell at the point of maximal surface attraction. For example, for negatively charged hydrophobic surfaces, large cations such as Cs^+ adsorb on the surface, thus decreasing the surface potential as well as the surface-surface repulsion. Small cations tend then to be more stabilising, which corresponds to the direct series. However, for negatively charged hydrophilic surfaces, small cations such as Na^+ tend to adsorb on the interface and screen the surface potential. The surfaces can then come closer to one another, which destabilise neutral solutes. In this case, large cations lead to stabilisation, i.e. the indirect Hofmeister series is observed.

As shown in this section, a universal Hofmeister series does not exist. Each system has its specificities and it is difficult to predict ion behaviours, even if some basic rules exist. These behaviours can also be completely different with uncommon salts.

1.3.2. Antagonistic salts

An antagonistic salt is composed of a hydrophilic and a hydrophobic ion. For example, sodium tetraphenylborate ($NaBPh_4$) is composed of the hydrophilic cation Na^+ and the large hydrophobic anion BPh_4^-, whereas the inversely antagonistic salt tetraphenylphosphonium chloride (PPh_4Cl) is composed of the hydrophobic cation PPh_4^+ and the hydrophilic anion Cl^- (see **Figure 1.16**).

Antagonistic salts are interesting in colloidal chemistry as they can induce structures in binary solutions and thus can be compared to surfactants. Sadakane *et al.* studied the binary system heavy water (D_2O) and 3-methylpyridine (3MP) in presence of $NaBPh_4$ without surfactant.[109-111] The addition of the antagonistic salt induced the shrinking of the two-phase region and an ordered phase with multilamellar structures was observed. Further, a long-range periodic structure was formed according to SANS results. First, the authors suggested that BPh_4^- ions were surrounded

by several hydrophobic 3MP molecules, whereas Na^+ had a hydration shell and was surrounded by several water molecules. In another paper, they investigated the stabilisation of the ordered structures by means of SANS and neutron spin echo (NSE) techniques.[112] The formation of different types of structures that depend on the composition and/or temperature of the mixture was confirmed. They showed that the 3MP-rich domains were separated from the bulk phase in presence of antagonistic salt in the solution. Further, the layers behaved as membranes. The explanation for such observations is that the ions of the salt are not solvated in the same solvent, i.e. Na^+ is solvated in a D_2O-rich phase and BPh_4^- in a 3MP-rich domain. This preferential solvation leads to microphase separation. The periodicity of 3MP-rich domains is stabilised by the effects of electrostatic interactions between neighbouring membranes.[112, 113] It can also be noted that a shrinking of the two-phase region and a periodic structure in a water-rich mixture were observed upon addition of the inversely antagonistic salt PPh_4Cl to a mixture of D_2O and 3MP.[114] However, the composition range of the structures was narrower than with $NaBPh_4$ and lamellar structures were not observed. The regularity of the structures may depend on the type of salt, the size difference between the ions, and interactions with the solvents.

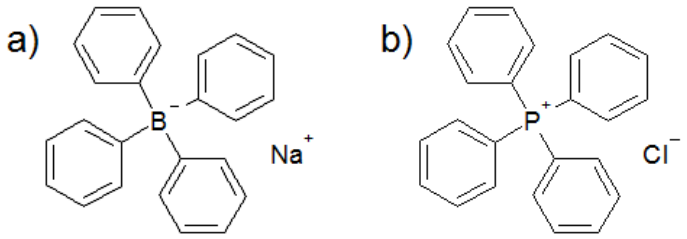

Figure 1.16. Molecular structures of a) sodium tetraphenylborate ($NaBPh_4$); and b) tetraphenylphosphonium chloride (PPh_4Cl).

Regarding the surfactant-like behaviour of $NaBPh_4$, Michler *et al.* showed that the antagonistic salt lowers both the surface tension at the water/air interface and the interfacial tension at the water/heptane interface.[115] These observations corroborate the fact that $NaBPh_4$ behaves similarly to a surfactant. However, this is not true for all antagonistic salts as guanidinium chloride only lowers the interfacial tension at the water/heptane interface, but not the surface tension. The authors supposed that a peculiar redistribution mechanism takes place for the decrease of the interfacial tension but that the same mechanism prevents a truly antagonistic salt from lowering the surface tension.

The preferential solvation of each ion of antagonistic salts and thus the appearance of structures were also numerically demonstrated by Onuki *et al.* using two-dimensional simulations and dynamic equations.[116-119] In their model, the solvation effect and critical concentration fluctuations

were coupled and a charge density wave structure was induced. Further, they showed that hydrophilic and hydrophobic ions tend to adsorb near the interface between the polar and nonpolar solvents because of the opposite preference of solvation of both ions. The electrostatic interactions between the ions lead to the formation of an electric double layer and a lowering of the interfacial tension is observed. As already explained, this segregation at liquid-liquid interfaces leads to mesophase formation.

1.3.3. Soaps: salts of fatty acids

1.3.3.1. Presentation

Soaps are alkali salts of saturated and unsaturated C_{10}–C_{20} carboxylic acids and have already been known for millennia. Regarding the number of carbon atoms, carboxylic acids are commonly named as indicated in **Table 1**. Soaps being carboxylate anions, they are named after their respective acid with the suffix *–ate*. For example, the salt of the stearic acid is sodium stearate, when sodium is the counterion. The raw materials for the manufacture of soaps are tallow, fats, and fatty oils such as animal fats, coconut oil, and palm kernel oil.[120] High proportions of unsaturated fatty acids are unwanted as they will easily become rancid. For the manufacture of soap bars, a mixture of 80 wt% of tallow and 20 wt% of coconut oil is preferred. Soaps can be produced by saponification using caustic soda, soda ash, or potash. In this process, glycerol is obtained as an important by-product. It is worth pointing out that softer potassium and ammonium soaps can also be manufactured.[120]

Table 1. Common names and melting points of the most commonly used carboxylic acids.

Carbon atoms	Common name	Melting points
-	-	°C
10	capric acid	32
12	lauric acid	43
14	myristic acid	54
16	palmitic acid	63
18	stearic acid	69
18 with 1 unsaturation	oleic acid	16
18 with 2 unsaturations	linoleic acid	-5
18 with 3 unsaturations	linolenic acid	-11
20	arachidic acid	75

Acids and soaps exhibit different physical properties.[121] For example, the acid melts to the liquid state at the same temperature as the chain-melting transition, while the soap goes through a series of liquid crystalline states before melting to an isotropic liquid. The solubility of long-chain fatty acids in water is low in contrast to the high solubility of soaps imparted by the strong interactions between the ionised groups with water.

As soaps combine good wetting ability, foaming power and a high detergency, they are widely used as surfactants. As any surfactant, soaps are composed of a hydrophilic head group $–COO^-$ and a hydrophobic hydrocarbon chain of different length regarding the carboxylic acid used for their manufacture. Further, they can organise themselves and pack at an interface between two different media. For example, different structures were observed depending on the protonation state of the oleic acid head groups by Janke *et al.* with molecular dynamics simulations.[122] The solubility of soaps depends on the length of the carbon chain and increases sharply with the temperature. Sodium laurate is already highly soluble in water at 30 °C, while 70 °C is needed to reach a comparable solubility for sodium stearate.[120] The use of soaps as surfactant or as cleaning agent suffers from two main drawbacks. It does not function well i) in acidic solutions because insoluble fatty acids form due to the protonation of the carboxylate, and ii) in hard water because of the high concentration of Mg^{2+} and Ca^{2+} ions which tend to form precipitates with carboxylates. Soft water and the addition of sequestrants or builders, i.e. complexing agents, are two solutions to overcome the second issue and to increase their detergency power. But the low solubility at neutral or acid pH still persists.

1.3.3.2. pK_A

The pK_A of a carboxylic acid-carboxylate system is defined as the pH value where 50% of the molecules are ionised and 50% of the molecules are protonated. When carboxylates and acid molecules form an interfacial film, the latter becomes largely unionised at pH values lower than pK_A. On the contrary, the film is almost completely ionised at pH values higher than pK_A. In this case, ionic repulsions occur between the polar groups that may result in an expansion of the monolayer, which may lead to a weak and unstable film. The interactions between the acid and the carboxylate are maximal at the pK_A value. The pK_A value depends of course on the studied acid-base couple.

Kanicky *et al.* investigated the effect of chain length on the pK_A of fatty acid salt solutions and found an optimum pH value where minimum evaporation of water and contact angle on PMMA surface, and maximum foamability, foam stability, and surface viscosity were observed.[123] This

optimum pH value is near the pK_A of the fatty acid salt. The authors explained these effects by the strong dipole interactions between the protonated and ionised forms at pH values near pK_A. This interaction is much stronger than ordinary hydrogen bonding, where no charge is present, and leads to a dimer formation. Further, they observed a minimum in area per molecule and intermolecular distance at pH near pK_A for sodium laurate. It was further shown that the pK_A values increased with increasing the chain length of a fatty acid. It was equal to 7.2 for a C_{10} chain and 8.7 for a C_{16} chain. When increasing chain length, the van der Waals interactions between the chains also increase, leading to the decrease of intermolecular distances. The carboxylic acid groups are then packed closer, shielding the hydrogen atom between the two oxygen atoms. Therefore, hydroxide ions have more difficulties removing the acid's proton. The closer the molecules, i.e. the longer the hydrophobic chain, the more strongly shielded the hydrogen atom and the higher the pK_A.
In another study, Kanicky *et al.* observed a decrease of the apparent pK_A when a small amount of fatty acid of a different chain length is added to a pure fatty acid solution.[124] The explanation is the same as before, i.e. the mismatch between two different adsorbed chains of unequal length results in an increase in area per molecule and in intermolecular distance, leading to a lower apparent pK_A value.

As other studies showed, pK_A values depend also on other parameters of the system. pK_A shifts were observed when the solvent was changed from water to methanol,[125] upon the addition of other components such as alcohols[126] or lecithin,[127] for acids at interfaces,[128] and in nonaqueous media.[129]

1.3.3.3. Unsaturations

Unsaturations play an important role in carboxylic acids and their respective carboxylates, for example for their melting points. It can be seen in **Table 1** that the melting points increase with the length of the hydrocarbon chain of the acid. This observation can simply be explained by the fact that as the molecular weight increases, the melting point increases. However, the melting points decrease with increasing the number of double bonds in the hydrocarbon chain. It is equal to 69 °C for stearic acid with no double bond, and -11 °C for linolenic acid in which three double bonds are present. The decrease of the melting point can be explained by the presence of unsaturation in the molecule. Saturated carboxylic acids have an almost linear geometry and consequently can organise well. This leads to important intermolecular interactions resulting in relatively high melting points. However, double bonds cause bends in the molecule as their geometry is almost always a *cis*-configuration in natural fatty acids. Thus, the molecules cannot

pack well and the intermolecular interactions are weak, leading to lower melting points. Naturally, the more double bonds in the molecule, the weaker the interactions and the lower the melting points.

Kanicky *et al.* studied the effect of degree, type, and position of unsaturations on the pK_A of fatty acids.[130] They found pK_A values equal to 10.15, 9.85, 9.24, and 8.28 for respectively stearic, oleic, linoleic, and linolenic acids. As the addition of a double bond to an alkyl chain decreases adhesion between molecules, the intermolecular distance between the molecules increases. As explained in section 1.3.3.2, the greater the intermolecular distance, i.e. the more double bonds, the lower the pK_A value of the acid.

1.3.3.4. Acid-soap crystals

As already mentioned, the physical properties of fatty acids and soaps in aqueous solutions depend on the ionisation state of the carboxyl group, but also on fatty acid concentration, temperature, counterion type, state of ionisation, and chain length. Cistola *et al.* studied the phase behaviour of medium-chain (C_{10} and C_{12}) and long-chain (C_{18}) fatty acids in water as a function of the ionisation state of the carboxyl group.[121, 131] Titrations were carried out above and below fatty acid and acid-soap chain melting temperatures Tc.

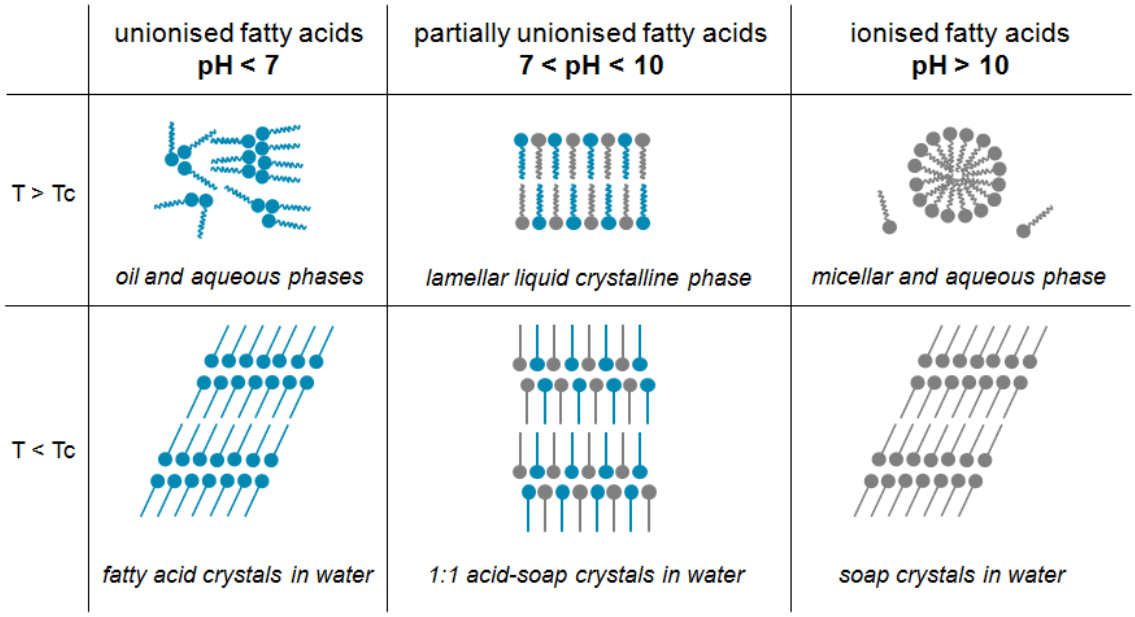

Figure 1.17. Schematic summary of the physical states formed by medium-chain and long-chain fatty acids in excess water. Tc is the hydrocarbon chain melting temperature in excess water. The blue molecules are protonated carboxyl groups, the grey ones ionised carboxylate groups. The straight lines represent ordered hydrocarbon chains, the curved lines disordered (liquid) hydrocarbon chains. Redrawn from[131].

As represented in **Figure 1.17**, three main regions were observed. At temperatures above Tc, an oil phase was observed for pH values smaller than 7, a lamellar phase corresponding to stacked multilayers or large vesicle for pH values between 7 and 10, and a micellar phase for pH values higher than 10. At temperatures below Tc, fatty acid crystals were observed for pH < 7, 1:1 soap-acid crystals for pH values between 7 and 10, and soap crystals for pH > 10. The authors pointed out that Tc vary with hydrocarbon chain length and degree of saturation, as well as the ionisation state and counterion. These results are useful to have insights of the physical state of fatty acids in biological systems. The lamellar fatty acid/soap phase is predominant at physiologic pH values. Further, no micellar phase was observed below pH 9.

Nonesterified fatty acids are known to have toxic effects on cells under certain conditions. One widely proposed mechanism is the so-called "detergent effect".[132, 133] According to this hypothesis, fatty acids are fully ionised at physiological pH, since the apK_A value for long-chain fatty acid in water is thought to be around 4.8,[134] and form micelles above a critical concentration. Those micelles solubilise membrane lipids and disrupt the physical and functional integrity of cell membranes. The fact that no micellar phase was observed below pH 9 in the study of Cistola *et al.* contradicts the suggested detergent effect.

CHAPTER 2 CHEMICALS AND METHODS

2.1. Chemicals

2.1.1. Chemicals used in section 3.1.1

Ethanol (purity ≥ 99.8%), NaSCN (purity ≥ 98%), and dietheylhexylphosphoric acid (HDEHP, purity ≥ 97%) were purchased from Sigma-Aldrich Chemie GmbH (Steinheim, Germany). 1-octanol (purity ≥ 99%), LiCl (purity ≥ 99%), KCl (purity ≥ 99.5%), NaBr (purity ≥ 99%), $NaNO_3$ (purity ≥ 99%), and NaOH (purity ≥ 99%) were purchased from Merck Schuchardt OHG (Hohenbrunn, Germany). CH_3COONa (purity ≥ 99%), $CaCl_2$ (purity ≥ 96%), and NH_4Cl (purity ≥ 99.8%) were purchased from Merck (Darmstadt, Germany). NaCl (purity ≥ 99.6%) was purchased from VWR (Leuven, Belgium). CsCl (purity ≥ 99%) and $NaBPh_4$ (purity ≥ 99.5%) were purchased from Alfa Aesar GmbH & CoKG (Karlsruhe, Germany). $NaClO_4$ (purity ≥ 88%) was from Fluka AG (Buchs, Switzerland). Sodium dodecylsulfate (SDS, ultrapure) was from AppliChem GmbH (Darmstadt, Germany). All solutions were prepared using deionised water with a resistivity of 18.2 MΩ.cm. All other chemicals were used without further purification.

2.1.2. Chemicals used in section 3.1.2

Ethanol (purity ≥ 99.8%), glycerol (purity ≥ 99.5%), ethylene glycol (anhydrous, purity ≥ 99.8%), diethyl adipate (purity ≥ 99%) were purchased from Sigma-Aldrich (Steinheim, Germany).

Octanol (purity ≥ 99%) was purchased from Merck Schuchardt OHG (Hohenbrunn, Germany). Urea p.A. was purchased from Merck KGaA (Darmstadt, Germany), choline chloride (purity ≥ 98%) from Alfa Aesar (Karlsruhe, Germany), and tetrahydrofurfuryl alcohol (purity ≥ 99.5%) from Pennakem (Memphis, USA). Prior to use, urea and choline chloride were dried under vacuum for several days. All other chemicals were used without further purification.

2.1.3. Chemicals used in section 3.1.3

R-(+)-limonene (purity ≥ 94%) and citronellol (purity ≥ 97%) were purchased from Merck Schuchardt OHG (Hohenbrunn, Germany). Geranyl acetate (purity ≥ 97%) was purchased from Acros Organics (Geel, Belgium). Citral (mixture of cis and trans, purity ≥ 96%) was purchased from Sigma Aldrich Chemie GmbH (Steinheim, Germany). Ethanol (purity ≥ 99.8%) was purchased from Carl Roth GmbH (Karlsruhe, Germany). All chemicals were used without further purification. All solutions were prepared using deionised water with a resistivity of 18.2 MΩ.cm.

2.1.4. Chemicals used in section 3.1.4

Citriodiol ((+)-cis-:(-)-trans isomers ratio equal to 66:34) was donated from Citrefine International Ltd. (Leeds, United Kingdom). PMD (purity ≥ 99%, (+)-cis-:(-)-trans isomers ratio equal to 62:38) was obtained from Takasago International Corporation (Paris, France). 2-undecanone (purity ≥ 97%), DEET (purity ≥ 97%) and ethanol (purity ≥ 99.8%) were purchased from Sigma Aldrich Chemie GmbH (Steinheim, Germany). KBR 3023 (purity ≥ 97%) was donated by Lanxess (Langenfeld, Germany). Isopropanol (purity ≥ 99.8%) was purchased and IR 3535 (purity ≥ 98%) was donated by Merck KGaA (Darmstadt, Germany). LiCl (purity ≥ 99%) was obtained from Merck Schuchardt OHG (Hohenbrunn, Germany). All chemicals were used without further purification. All solutions were prepared using deionised water with a resistivity of 18.2 MΩ.cm.

2.1.5. Chemicals used in section 3.2.1

The microemulsion was formulated with sodium oleate (purity ≥ 82%) from Sigma-Aldrich Chemie GmbH (Steinheim, Germany), ethanol (purity ≥ 99.9%) from Baker (Deventer, the Netherlands), R-(+)-limonene (purity ≥ 94%) and citronellol (purity ≥ 97%) from Merck

Schuchardt OHG (Hohenbrunn, Germany). The effects of salts on the microemulsion were investigated by using choline chloride (purity ≥ 98%) and NaSCN (purity ≥ 98%) from Sigma-Aldrich Chemie GmbH (Steinheim, Germany). LiCl (purity ≥ 99%), KCl (purity ≥ 99.5%), trimethylammonium chloride (purity ≥ 97%), NaBr (purity ≥ 99%) and $NaNO_3$ (purity ≥ 99%) were obtained from Merck Schuchardt OHG (Hohenbrunn, Germany). NaCl (purity ≥ 99.6%) was purchased from VWR (Leuven, Belgium). Na_2SO_4 was obtained from Acros Organics (Geel, Belgium). To study the effects of polyols, sorbitol (extra pure) was purchased from Merck Schuchardt OHG (Hohenbrunn, Germany) and glycerol (purity ≥ 99%) from Sigma-Aldrich Chemie GmbH (Steinheim, Germany). The titrations were done with citric acid (purity ≥ 99%) from Sigma-Aldrich Chemie GmbH (Steinheim, Germany). All chemicals were used without further purification. All solutions were prepared using deionised water with a resistivity of 18.2 MΩ.cm.

2.1.6. Chemicals used in section 3.2.2

Microemulsions: sodium oleate (purity ≥ 82%) was obtained from Sigma-Aldrich Chemie GmbH (Steinheim, Germany), R-(+)-limonene (purity ≥ 94%), and citronellol (purity ≥ 97%) from Merck Schuchardt OHG (Hohenbrunn, Germany), and ethanol (purity ≥ 99.9%) was obtained from Baker (Deventer, the Netherlands). *High intensity sweeteners*: acesulfame potassium (purity ≥ 99%), saccharin sodium salt hydrate (purity ≥ 98%), and sodium N-cyclohexylsulfamate (purity ≥ 99%) were purchased from Sigma-Aldrich Chemie GmbH (Steinheim, Germany). Aspartame (purity = 100%) was obtained from Ajinomoto Sweeteners Europe (Gravelines, France), and Truvia® stevia RA 95 (at least 95% of Rebaudioside A) from Cargill Health and Nutrition (Wayzata, United States). Sucralose was obtained from Beneo-Palatinit GmbH (Mannheim, Germany). Neohesperidine dihydrochalcone (purity ≥ 98%) was from Denk Ingredients GmbH (München, Germany). Neotame was obtained from Brenntag Food and Nutrition Europe (Mülheim an der Ruhr, Germany). Naringin dihydrochalcone (purity ≥ 98%) was obtained from Ferrer HealthTech (Barcelona, Spain). *Sugar alcohols*: sucrose (purity ≥ 99%) was purchased from Serva Electrophoresis GmbH (Heidelberg, Germany), sorbitol (extra pure) was purchased from Merck Schuchardt OHG (Hohenbrunn, Germany), and isomalt (purity ≥ 98%) was obtained from Beneo-Palatinit GmbH (Mannheim, Germany). *Salts*: NaCl (purity ≥ 99.6%) was purchased from VWR (Leuven, Belgium). *Titrations*: carried out using citric acid (food additive code E330, purity ≥ 99%) from Sigma-Aldrich Chemie GmbH (Steinheim, Germany). All chemicals were used without further purification. Deionised water has a resistivity of 18.2 MΩ.cm.

2.2. Methods

2.2.1. Ternary phase diagrams

An example of a (pseudo-)ternary phase diagram is represented in **Figure 2.1**. The determination of the domains of existence of the monophasic and clear regions was performed using a static and dynamic process described by Clausse *et al.*[135] In screw top tubes, the surfactant was mixed with the oil or water at determined weight ratios to obtain a starting weight of 3 g. Water or oil was then added dropwise with Pasteur pipettes to the resulting mixtures until a change in the phase behaviour occurred. The phase transitions were determined with the naked eye and through two cross polarised filters in order to check the presence of liquid crystals. The temperature was kept constant at 25 °C with a thermostatically controlled test tube rack.

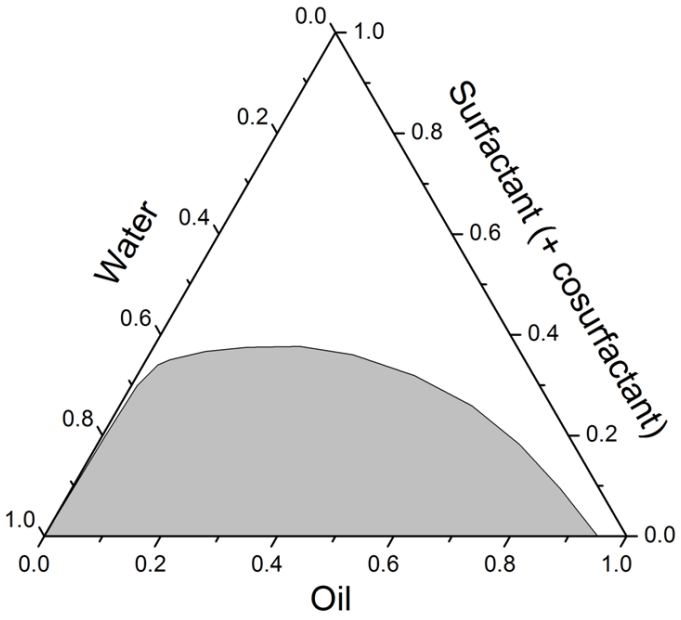

Figure 2.1. Example of a (pseudo-)ternary phase diagram in weight fractions for the system water/surfactant (+ cosurfactant)/oil. The grey region represents the multiphase domain, the white one the clear and homogeneous microemulsion.

The amount of water or oil added until the phase transition occurred was obtained with precise weight measurements. The weight ratios were then calculated for each formulations and the (pseudo-)ternary phase diagram was built.

2.2.2. Determination of the critical point

In order to determine the rough position of the critical point in the system glycerol/ethanol/1-octanol presented in section 3.1.2, different formulations in the clear and homogeneous region near the phase demixing border were prepared. The tubes were kept at a constant temperature of 25 °C in a thermostatically controlled test tube rack. A small and same amount of glycerol and 1-octanol was then added very slowly to reach the phase boundary. The formulations were then left to stand until complete phase separation. The critical point corresponds to extrapolation of the formulations, where both separated phases have equal volumes, to the phase boundary.

2.2.3. Conductivity measurements

Conductivity measurements were performed on the systems presented in section 3.1.4. The solutions were prepared in a flask by mixing the different components at the appropriate weight ratios. 0.5 wt% of the total weight of LiCl was then added to the formulations to ensure a measurable conductivity. The flask was then placed in a water bath at a controlled temperature of 25 °C and placed under agitation with a MR Hei-Standard magnetic stirrer from Heidolph (Schwabach, Germany). Water was progressively added with an Eppendorf pipette. Conductivity measurements were carried out with a pHenomenal PC 5000 L multi-parameter meter from VWR International. Conductivity values and volume of added water were recorded.

2.2.4. Refractive index

The refractive index of a solution was determined by placing a few drops on an Abbe Refractometer AR3 – AR4 from A. Krüss Optronic GmbH (Hambourg, Germany). The measurements were carried out at 25 °C with a wavelength of 589 nm.

2.2.5. Density and Viscosity

Density measurements were carried out with a vibrating tube densimeter DMA 5000 M equipped with a precision thermostat (temperature uncertainty ≥ 0.01 K) from Anton Paar (Graz, Austria), at 25 °C. Densities were used to calculate the dynamic viscosities η according to the equation:

$$\eta = K\left(\rho_B - \rho_S\right) t \quad \textbf{(2.1)}$$

K is a constant, t the measured time that the ball needs to roll the defined distance in the capillary, ρ_B the density of the ball and ρ_S the density of the solution measured as described above. The time t was obtained through measurements with an automated rolling ball viscosimeter AMVn from Anton Paar (Graz, Austria), at 25 °C. A glass capillary with the appropriate diameter (1.6 or 1.8 mm) and corresponding steel balls were used. K was obtained by calibration. The relative uncertainty of η is approximately 0.5%.

2.2.6. Light scattering techniques

2.2.6.1. Dynamic light scattering (DLS)

The solutions to be investigated were prepared by mixing the different components at the appropriate weight ratios. Each sample was then filtered with a 0.2 μm PTFE membrane filter in order to remove dust and transferred into a cylindrical light-scattering cell of 10 mm outer diameter. The latter was then placed in a temperature controlled bath of toluene of a CGS-3 goniometer system from ALV (Langen, Germany) equipped with an ALV-7004/FAST Multiple Tau digital correlator and a vertical-polarised 22-mW HeNe laser (wavelength λ = 632.8 nm). The homodyne correlation functions ⟨I(0)I(τ)⟩ (or $G^1(\tau)$, τ being the correlator delay time) were recorded at 25 °C and at an angle of 90° for 300 s. The size of the particles was determined by fitting the experimental intensity autocorrelation function using a monomodal equation with the TableCurve 2D v5.01 software. The correlation function can be described with the following equation:

$$G^1(\tau) = a_0 + (a_1 * e^{-a_2 \tau})^2 \quad \textbf{(2.2)}$$

τ is the delay time, a_0 is the constant baseline value (usually 1), a_1 refers to the dynamic part of the amplitude, and a_2 is the decay rate, linked to the diffusion coefficient D:

$$a_2 = D\,q^2 \quad \textbf{(2.3)}$$

and q is the scattering vector, which is defined as:

$$q = \frac{4\,\pi\,n}{\lambda} \sin\frac{\theta}{2} \quad \textbf{(2.4)}$$

In equation **(2.4)** λ refers to the wavelength of the irradiating light in nm, θ to the detection angle, and n to the refractive index measured as described in section 2.2.4. As the structures in the

surfactant-free microemulsions investigated in this thesis fluctuate and are not necessarily spherical, the term characteristic dynamic size is used instead of hydrodynamic radius. The characteristic dynamic size ξ_D was then deduced from D using the Stokes-Einstein equation:

$$D = \frac{k_B T}{6 \pi \eta \xi_D} \quad \textbf{(2.5)}$$

with k_B the Boltzmann constant, T the temperature in K, and η the dynamic viscosity measured as described in section 2.2.5.

2.2.6.2. Static light scattering (SLS)

The same apparatus as described in section 2.2.6.1 for DLS was used to perform SLS measurements. The samples were prepared the same way and measured at 25 °C at scattering angles of 45°, 90°, and 135°. The apparent molar mass is obtained from SLS via the Rayleigh relation:

$$M_{app} = M * S(q) = \frac{R_{solution}}{K C} \quad \textbf{(2.6)}$$

$R_{solution}$ is the Rayleigh ratio in m^{-1}, S(q) the structure factor which expresses the influence of micelle-micelle (or more general object-object) interactions on the scattering, C the concentration in $g.L^{-1}$, M the molar mass of the micelles and M_{app} the corresponding apparent mass. K is defined as:

$$K = 4 \pi^2 n^2 \left(\frac{dn}{dc}\right)^2 \lambda^{-4} {N_A}^{-1} \quad \textbf{(2.7)}$$

with n the refractive index measured as described in 2.2.4, dn/dc the refractive index increment in $L.g^{-1}$, λ the wavelength in m and N_A the Avogadro number. The Rayleigh ratio of particles in solution $R_{solution}$ was calculated with the following equation:

$$R_{solution} = \frac{{I^0}_{solution} - {I^0}_{solvent}}{{I^0}_{standard}} * R_{standard} * \left(\frac{n_{solvent}}{n_{standard}}\right)^2 \quad \textbf{(2.8)}$$

where I^0 refers to the scattered intensity of the solvent, solution, or the used standard (in our case toluene). $R_{standard}$ is the Rayleigh ratio for the standard and was taken from the work of Preu *et al.*[136] The term $(n_{solvent}/n_{standard})^2$ is used as a correction factor of the scattered volume, which is often introduced due to different diffraction effects between sample and standard. In first approximation we set this term equal to one. The spherical volume V_{sphere} can be obtained from the following equation:

$$V_{sphere} = \frac{M_{app}}{N_A * \rho_{particle}} = \frac{4}{3} \pi r^3 \quad \textbf{(2.9)}$$

In equation **(2.9)** $\rho_{particle}$ refers to the density of the micelles. The characteristic static size can be calculated assuming that the density of the micelle is equal to the density of the used oil phase.

2.2.6.3. Approximation, multiple scattering, fluctuations

Again, we stress that the approximation of a spherical structure is arbitrary and that the structure is only "apparent" because it contains the interactions between each structure. However, this approach gives us a rough idea of the characteristic dynamic and static sizes in the systems. The intention of DLS and SLS measurements is to check if there are structures or not in the investigated formulations. It is not intended to give a quantitative picture.

It has to be noted that multiple scattering do not take place in our experiments as the refractive index increment dn/dc is around 0.1 g/cm^3 for all experiments involving DLS and SLS measurements presented in this thesis.[137, 138]

It also has to be noted that in ternary systems as such presented in this thesis, dynamic light scattering is the time-convolution of two different possible fluctuations, with two dn/dc and constant chemical potential of pseudo-component 1 and of pseudo-component 2. It is the choice of the experimentalist to choose convenient pseudo-components. Here, we choose as for classical micelles the pseudo-component to be an aggregate with its typical diffusion time. According to the general theory of Aniansson *et al.*, the in-out fluctuation of the most labile component, in our case the ethanol molecules fluctuating with a short time-scale between aggregates and solvent, induces a distinct gradient of refractive index and perturbs dn/dc values.[97, 100]

2.2.7. Small- and wide-angle x-ray scattering (SWAXS)

SWAXS measurements were performed using a bench built by Xenocs and an x-ray radiation generated by a sealed molybdenum tube (wavelength λ = 0.71 Å). The large on-line detector (MAR 345, MAR Research, diameter = 345 mm) was located at 750 mm from the sample stage. Off-centre detection allowed small and wide angles to be measured simultaneously. The scattering vector q has a magnitude of:

$$q = \frac{4\pi}{\lambda} \sin\frac{\theta}{2} \quad \textbf{(2.10)}$$

In equation **(2.10)** θ refers to the scattering angle. The attainable q-region was 0.2-30 nm^{-1} with an experimental resolution of Δq/q = 0.05. Collimation was applied using a 12:∞ multilayer Xenocs mirror coupled to two sets of Forvis scatterless slits providing a 0.8*0.8 mm^2 x-ray beam at the sample position. Absolute intensities were obtained by using a 2.36 mm thick high-density polyethylene sample from Goodfellow as a calibration standard. The two-dimensional spectra were integrated with the software FIT2D. The electronic background of the detector, transmission measurements and empty cell subtraction were taken into account during the integration. The acquisition time was 3600 s per sample.

An Ornstein-Zernike (OZ) type inverse quadratic function is generally used to express the scattering by fluctuations with no define interface:

$$I(q) = (\Delta\rho)^2\, \Phi\, (1-\Phi) \frac{{\xi_X}^3}{1 + q^2\, {\xi_X}^2} \quad \textbf{(2.11)}$$

In equation **(2.11)** ξ_X refers to the correlation length in Å. We set $I(0) = (\Delta\rho)^2\, \Phi\, (1-\Phi)$, where Δρ is the difference of electronic densities between the oil-rich and water-rich domains in $Å^{-2}$, and Φ the volume fraction of the oil-rich phase including the volume fractions of ethanol and additive which may be found in that phase.

The equation **(2.12)** was developed for the work presented in section 3.1.1 for the data that cannot be fitted with the regular OZ function. This is an empirical function to fit the data showing the phenomenon known as "correlation hole" for charged polymers.

$$I(q) = (\Delta\rho)^2\, \Phi\, (1-\Phi) \frac{V_{object}}{\frac{1}{{\xi_X}^2} + (q - q_0)^2} \quad \textbf{(2.12)}$$

V_{object} is the volume of the scattered object in $Å^3$:

$$V_{object} = \frac{4}{3}\, \pi\, {R_{MV}}^3 \quad \textbf{(2.13)}$$

R_{MV} is the mean radius of an object in Å, i.e. the hypothetical radius that would have the fluctuations or nano-droplets if their geometry were a sphere. The object density in a micelle volume n_d, calculated from V_{object} and Φ and expressed in A^{-3}, is equal to:

$$n_d = \frac{\Phi}{V_{object}} \quad \textbf{(2.14)}$$

In equation **(2.12)**, (1-Φ) is introduced to account to a first-order for repulsive interactions lowering the intensity (decrease of the compressibility). The physical meaning of q_0 is the scattering vector corresponding to the most probable distance between centres of scattering objects D*. In the case of repulsive objects, the number of objects can be deduced from the position of the maximum of the structure factor S(q), that is usually very close to the maximum of the intensity:

$$D^* = \frac{2\pi}{q_0} = 1.22\ {n'_d}^{-1/3} \qquad \textbf{(2.15)}$$

It is very important to notice that n'_d and n_d, determined by two independent measurements, may differ. When both values are close, this is a proof of self-consistency.[139] If these two densities differ, this may come from anisotropy of the object or attraction of the objects instead of repulsion.

2.2.8. Small-angle neutron scattering (SANS)

SANS experiments were performed at the *Institut Laue Langevin* (ILL, France) on the D16 spectrometer. The neutron wavelength was fixed at 4.51 Å using a monochromator. A 2D gas-filled detector settled at 953 mm from the sample position (1 mm pathway quartz cell) was moved at two different angles (γ) on a goniometer arm in order to cover a q-vector range respectively between 0.025 < q ($Å^{-1}$) < 0.3 (position 1, γ = 0°) and 0.06 < q ($Å^{-1}$) < 0.6 (position 2, γ =16°) with a reasonable overlap that allows a good concatenation of the scattering data. A standard H_2O normalisation, detector noise, empty cell and incoherent scattering corrections were applied to display the scattering intensity I(q) in absolute units, the cm^{-1}.

In a first approximation, the data were also fitted using an OZ function, as described by equation **(2.11)**. The correlation length obtained from these fits is noted ξ_N.

2.2.9. Preparation of the deep eutectic solvents

The deep eutectic solvents were prepared by Veronika Fischer for the work presented in section 3.1.2. Ethylene glycol and choline chloride (DES1) and urea and choline chloride (DES2) were mixed with a molar ratio of respectively 4-1 and 2-1 under nitrogen atmosphere and stirred at 75 °C until a homogeneous colourless liquid was formed. The mixtures were stored in sealed

flasks. The water content was determined with coulometric Karl-Fischer titrations, using an Abimed MCI analyser (Model CA-02). DES1 contained 189 ppm water and DES2 66 ppm.

2.2.10. Clearing temperature

A total amount of 3 g of the studied solutions was prepared at room temperature. The tubes were immersed in a water bath and placed under agitation with a MR Hei-Standard magnetic stirrer from Heidolph (Schwabach, Germany). The temperature was controlled with an EKT Hei-Con temperature sensor from Heidolph (Schwabach, Germany). If the prepared solution was already clear and homogeneous, it was cooled down until it became cloudy, and then slowly heated until a clear solution appeared again. If the prepared solution was cloudy, it was slowly heated until a clear and homogeneous solution appeared. The temperature for which the cloudy solution turned clear is called the clearing temperature Tα and was recorded. The results were reproducible with an accuracy of ± 2 °C.

2.2.11. pK_A and apparent pK_A determination

20 g of the microemulsion to be investigated were prepared at room temperature in a flask. The latter was immersed in a water bath with a constant temperature and placed under agitation using the same apparatus as described in section 2.2.10. The formulation was then titrated with a 1 wt% citric acid solution using an Eppendorf pipette. pH measurements were performed using a pHenomenal PC 5000 L multi-parameter meter and pH electrode pHenomenal 221 from VWR International. The values were plotted against the volume of added citric acid solution and the (apparent) pK_A values were graphically determined. The results were reproducible with an accuracy of ± 0.2.

CHAPTER 3 RESULTS AND DISCUSSION

3.1. Surfactant-free microemulsions

The studies presented in this chapter led to publications which are already published, as summarized in the following table.

Subchapter	Publication
3.1.2	J. Marcus, V. Fischer, D. Touraud, O. Diat, W. Kunz, **Toward surfactant-free and water-free microemulsions**, *J. Colloid Interface Sci.*, **2015**, *453*, 186-193
3.1.3	J. Marcus, M. L. Klossek, D. Touraud, W. Kunz, **Nano-droplet formation in fragrance tinctures**, *Flav. Fragr. Journal*, **2013**, *28*, 294-299
3.1.4	J. Marcus, M. Müller, J. Nistler, D. Touraud, W. Kunz, **Nano-droplet formation in water/ethanol or isopropanol/mosquito repellent formulation**s, *Colloids Surf. A*, **2014**, *458*, 3-9

3.1.1. Influence of additives on the structure of surfactant-free microemulsions

3.1.1.1. Abstract

We study the addition of electrolytes to surfactant-free microemulsions in the domain where polydisperse pre-Ouzo aggregates are present. As in previous studies, the microemulsion is the ternary system water/ethanol/1-octanol, where ethanol acts as co-solvent. Addition of electrolytes modifies the static x-ray and neutron scattering, and dynamic light scattering patterns, as well as the position of the miscibility gap, where spontaneous emulsification occurs upon dilution with water. All observations can be rationalised considering that electrolytes are either "salting out" the ethanol, which is the main component of the interface stabilising the aggregates, or producing charge separation via the antagonistic ion effect discovered by Onuki *et al.* Amphiphilic electrolytes, such as sodium dodecylsulfate or sodium dietheylhexylphosphate, induce a gradual transition towards monodisperse ionic micelles with their characteristic broad scattering peak. In these micelles the ethanol plays then the role of a cosurfactant. Dynamic light scattering can only be understood by combination of fluctuations of aggregate concentration due to the vicinity of a critical point and in-out fluctuations of ethanol.

3.1.1.2. Introduction

The so-called Ouzo effect is characterised by the formation of remarkably fine and time-stable emulsions when water is added in appropriate amounts to a mixture of ethanol and a hydrophobic component.[76-79, 83] The name comes from the Greek drink Ouzo, in which the hydrophobic molecule *trans*-anethole is dissolved in the water-miscible solvent ethanol. The necessary condition for the Ouzo effect to occur is the addition of a solvent A (e.g. water) to a second solvent B, which is highly or entirely miscible with solvent A (e.g. ethanol), and a third component, which is highly soluble in solvent B, but not in solvent A (e.g. *trans*-anethole).[88] The Ouzo effect allows producing nano-capsules loaded with active components or to functionalise a hydrophobic surface with polymeric nano-lenses.[82, 85] Whereas the Ouzo effect had been known for a long time, the fact that well-defined aggregates of typical size similar to small surfactant-based micelles occur in the pre-Ouzo region has been demonstrated only recently, via detailed contrast-variation neutron scattering experiments.[90] All other scattering techniques may be ambiguous since there is always a critical point at compositions close to such systems and the presence of well-defined aggregates with defined size is difficult to distinguish from the occurrence of critical fluctuations. The important point is that, in a defined region close to the phase boundary, ethanol plays the role of the surfactant, an effect independent of critical

fluctuations.[91] For the sake of comprehension, we call the pre-Ouzo region this domain in the monophasic and clear phase, close to the phase separation border. In other words, the pre-Ouzo effect occurs before enough water is added to reach the Ouzo region, where the visible Ouzo effect takes place. Conductivity experiments help identifying three types of structures: pre-Ouzo aggregates, bicontinuous phases, and reverse micelles morphology. To all these structures correspond characteristic scattering patterns.[140]

The presence of a nano-ordering was also observed by Klossek *et al.* and the characterisation of the nano-structures was done by Schöttl *et al.* and Diat *et al.*, as already developed in the *Fundamentals* part. Ternary solutions in the pre-Ouzo region already showed their capability to be excellent solubilisers in the field of formulation. Zoumpanioti *et al.* showed that lipases from *Rhizomucor miehei* and *Candida antartica* could be entrapped in surfactant-free microemulsions and still have catalytic activities at 30 °C.[74] The stability of enzymes is also higher than that observed in surfactant-based microemulsions. Introducing the term "lipotrope", Bauduin *et al.* showed that polar compounds could be solubilise in dodecane by adding alcohols.[141] We also found fluctuating nano-structures in perfume tinctures and mosquito repellents using DLS. These studies are detailed respectively in sections 3.1.3 and 3.1.4. Other applications of surfactant-free microemulsions can be found in section 1.2.3.3.

The aim of this work is now to understand how additives influence the surfactant-free microemulsions. To this purpose, we study here the effect of salts and surfactants on it.

In 1888 Hofmeister described the influence of salts on protein solubility.[101, 142] As introduced in the *Fundamentals* part, section 1.3.1, the Hofmeister series for anions is, from salting-out (kosmotropes) to salting-in (chaotropes) ions, $SO_4^{2-} < CH_3COO^- < Cl^- < Br^- < NO_3^- < ClO_4^- < SCN^-$. Considering the cations, the series is reversed regarding the kosmotropic and chaotropic properties of the ions. From salting-out (chaotropes) to salting-in cations (kosmotropes) it is roughly $N(CH_3)_4^+ < NH_4^+ < Cs^+ < K^+ < Na^+ < Li^+ < Mg^{2+} < Ca^{2+}$. In both of the series the ions on the left side tend to precipitate proteins in water, whereas the ions on the right side increase the solubility of the proteins and many other colloids. The reason for the reversal of the action of chaotropes and kosmotropes when considering cations instead of anions was unclear for a long time. Today, it can be well explained using Collins' concept of matching affinities.[103, 106] In proteins, most of the charged and polar parts (carboxylates, hydroxide groups) are hard and interact preferentially with hard cations. By contrast, most of the cationic groups (e.g. ammonium) are soft, interacting much more strongly with soft anions.[106] In a recent landmark paper, Schwierz *et al.* generalised this concept of Hofmeister reversals and used molecular dynamics simulations to further quantify it. Considering polar and non-polar domains on interfaces, this work was the first to rationalise and predict the local as well as global inversions of the series that have been known for a century.[107, 108]

Beyond "simple" electrolytes, we consider in the same methodology amphiphilic molecules, i.e. sodium dodecylsulfate (SDS) and diethylhexylphosphate, as well in its acidic as sodium balanced form (HDEHP and NaDEHP, respectively). SDS and NaDEHP are water-soluble surfactants, while HDEHP is only soluble in non-polar solvents. These are the most used surfactants industrially for detergency and selective extraction. Finally, we consider also a special, so-called antagonistic salt, namely sodium tetraphenylborate ($NaBPh_4$).

Usually, the addition of a simple salt to a binary mixture of water and an organic solvent changes the phase behaviour of this mixture. Cations and anions of simple salts are sometimes labelled as hydrophilic: this means that their water hydration enthalpy as well as entropy are much larger than kT or respectively kT/K and the corresponding values are tabulated for pure water.[143] To our knowledge, these quantities are not available in water/ethanol binary mixtures. However, it is known that the solubility of salts decreases when adding ethanol, an effect used in organic synthesis.[144] By attracting water molecules for their solvation shell, some salts decrease the miscibility of water and the organic solvent when the salt concentration is high. The two-phase region is then enhanced. But this is not the case for all salts. Sadakane *et al.* observed the opposite behaviour when adding the antagonistic salt $NaBPh_4$ to the binary mixture of deuterated water (D_2O) and 3-methylpyridine (3MP).[110, 111] $NaBPh_4$ is called antagonistic, because it is composed of a chaotropic anion and a kosmotropic cation. The chaotropic ion is adsorbed to the water/oil (w/o) interface in all emulsions or micellar systems investigated so far. Is this local charge separation also true in the case of pre-Ouzo aggregates? Using SANS, Sadakane *et al.* showed even the emergence of surfactant-free lamellar lyotropic phases upon addition of $NaBPh_4$. They also observed for the first time an ordered lamellar structure as a consequence of the local charge separation due to preferential solvation of an antagonistic salt.[109] These behaviours and the preferential solvation phenomenon have been quantified and explained by Onuki *et al*.[116-119, 145] Chaotropic anions have a higher tendency to adsorb onto the interface between water and the organic solvent, thus forming an electric double layer without initial charge of the interface. Thus, electrostatic forces can drive to a minimum in free energy if a lamellar phase is formed. In other words, chaotropic ions act as "sticky" disrupting ions at soft interfaces and kosmotropic ions form a diffuse layer.[146] As a consequence, it is most interesting to test the effect of the antagonistic electrolyte $NaBPh_4$ on surfactant-free microemulsions.

Our reference system is the ternary mixture water/ethanol/1-octanol in the pre-Ouzo region, i.e. in the region where initially polydisperse pre-Ouzo aggregates of correlation length around 2 nm are observed. Further, the partition coefficient of ethanol between octanol-rich aggregates and the water-rich external medium, a water/ethanol mixture that constitutes the solvent, is close to one. Since the sample is in the single-phase region, both pseudo-phases are in dynamic equilibrium.[147]

3.1.1.3. Results

3.1.1.3.1. The investigated formulation

The ternary phase diagram water/ethanol/1-octanol was already published in another study[88] and is reproduced here for the sake of clarity, see **Figure 3.1**. The investigated formulation corresponds to point α on the phase diagrams. Its composition as well as the compositions of both octanol-rich and water-rich pseudo-phases are summed up in **Table 2** in weight and mole fractions.

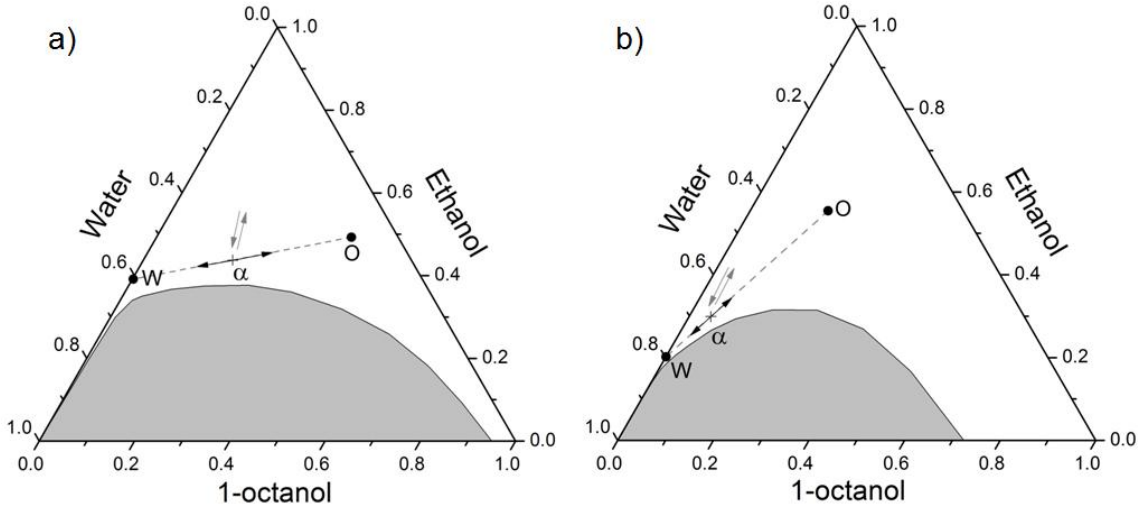

Figure 3.1. a) Ternary phase diagram in weight fractions of the system water/ethanol/1-octanol, at 25 °C; b) Ternary phase diagram in mole fractions of the same system, at 25 °C. The clear and homogeneous phase is represented in white, the multiphasic domain in grey. Positions corresponding to the octanol-rich and water-rich pseudo-phases are shown as points respectively labelled O and W. Direction of fluctuations considered in dynamic studies are shown with the arrows: the black arrows represent the local fluctuation of aggregates concentration, the gray arrows represent the in-out fluctuation of ethanol between both pseudo-phases.

As already mentioned before and explained in details in the *Fundamentals* part, the fluctuations found in that surfactant-free microemulsion can be interpreted as nano-structuring or fluctuating nano-clusters. Different amounts of salts were added to the formulation α and SAXS, SANS, and DLS were measured. In the case of NaDEHP, the same amount of sodium hydroxide was also added to the investigated formulations to ensure the ionisation of HDEHP.

Table 2. Composition of the reference formulation α and the water-rich and octanol-rich pseudo-phases in weight and mole fractions, the latter being inferred from the scattering experiments.

Point	weight fraction			mole fraction		
-	water	ethanol	1-octanol	water	ethanol	1-octanol
α	0.375	0.4375	0.1875	0.6558	0.2989	0.0453
W	0.606	0.391	0.002	0.798	0.202	0
O	0.098	0.493	0.409	0.283	0.555	0.163

3.1.1.3.2. Influence of the addition of different anions on the nano-structures of the ternary composition α

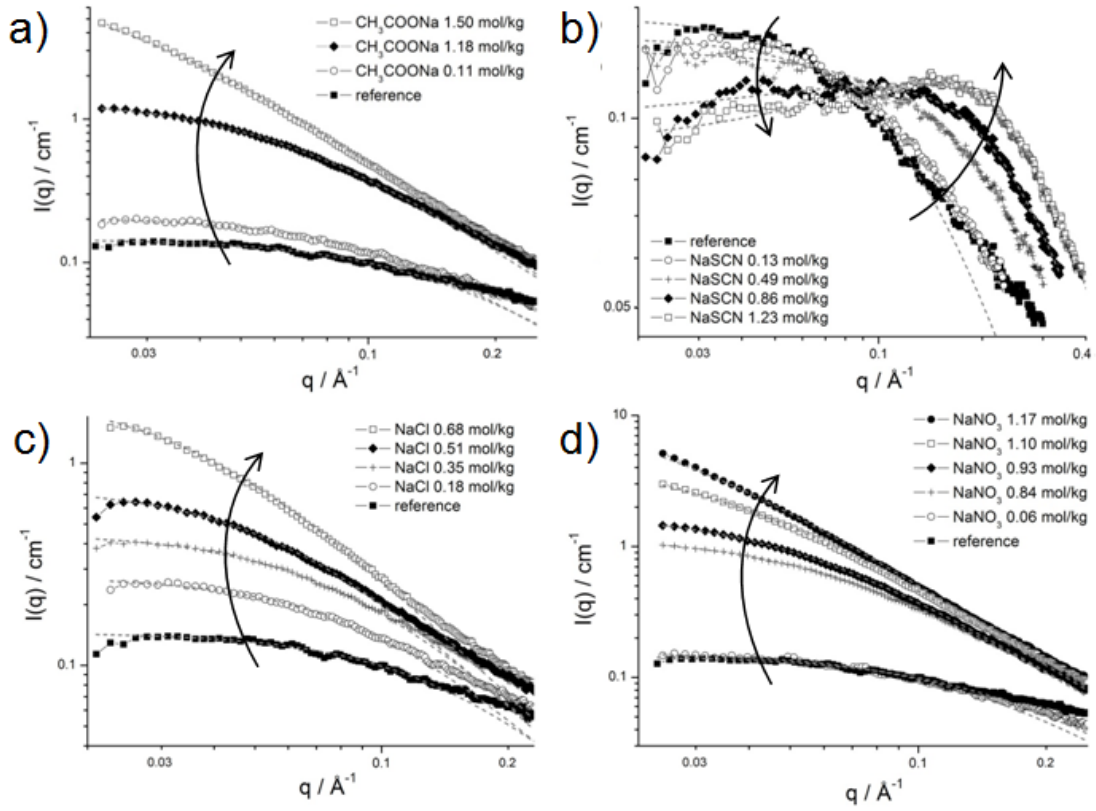

Figure 3.2. SAXS spectra on a log-log scale and in absolute units for the system water/ethanol/1-octanol in presence of a) CH_3COONa; b) NaSCN; c) NaCl; and d) $NaNO_3$. The dotted lines are the fits done with the Ornstein-Zernike equation or with equation **(2.12)** in the case of NaSCN.

In order to investigate the influence of anions on the structures of the surfactant-free microemulsion, SAXS were performed with increasing amounts of sodium salts. In the following, molarities (mol of solute per kg of solution) are used. The investigated formulation corresponded

to formulation α, whose composition can be found in **Figure 3.1**. As it can be seen in **Figure 3.2**, the curves of the absolute intensity against the scattering vector *q* obtained for the anions CH_3COO^-, Cl^-, and NO_3^- exhibit the same behaviours, i.e. the absolute intensity at low q-values increases with increasing concentration of the different salts. The increase of the intensity at $q \rightarrow 0$ is a bit more pronounced for NO_3^- than for the two other salts. The obtained curves for those three salts were all fitted using an Ornstein-Zernike function. The correlation lengths ξ_X obtained from these fits increase and are equal to 40.6 Å for 1.50 mol/kg CH_3COO^-, 27.7 Å for 0.68 mol/kg Cl^-, and 46.2 Å for 1.17 mol/kg NO_3^- (see **Figure 3.3**.a).

For SCN^-, the absolute intensity decreases at low q-values when the concentration increases from 0 to 1.23 mol/kg, see **Figure 3.2**.b. Further, a peak is observed at medium q-values, whose intensity increases with increasing SCN^- concentrations. It should be also mentioned that the peak is shifted to higher q-values with increasing concentrations. The first two concentrations, i.e. 0.13 and 0.49 mol/kg of NaSCN, were fitted using an Ornstein-Zernike function, whereas the last two ones, i.e. 0.86 and 1.23 mol/kg of NaSCN, were fitted using the model developed for this work (see section 2.2.7, equation **(2.12)**). A jump in the correlation length values is observed due to the use of two different models. However, it can be clearly seen that the correlation length tends to decrease, as shown in **Figure 3.3**.a.

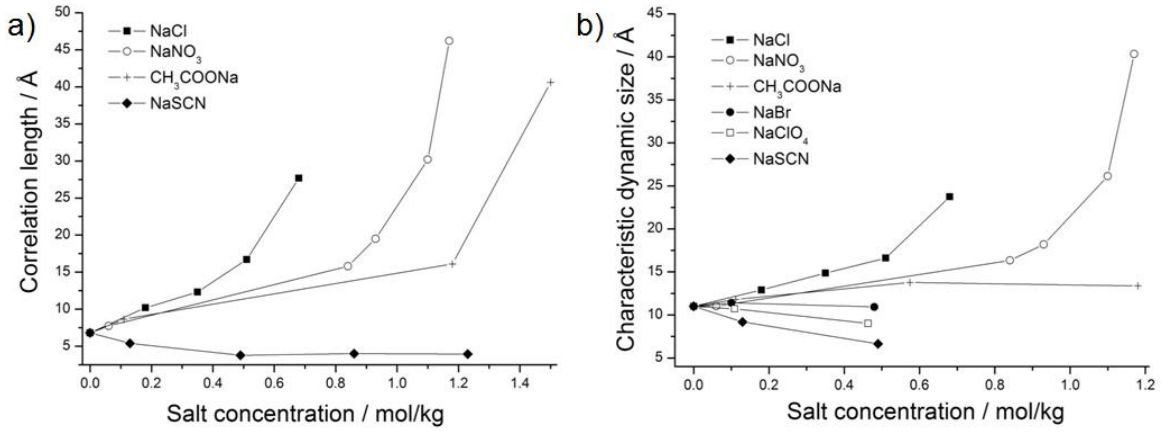

Figure 3.3. a) Correlation lengths ξ_X in Å obtained from SAXS; and b) characteristic dynamic size ξ_D in Å obtained from DLS plotted against the anion concentration in mol/kg.

SANS measurements were also carried out on the reference system without additives and with 0.35 mol/kg of NaCl and 0.46 mol/kg of $NaClO_4$, see **Figure 3.4**. Three different contrasts were measured for each sample. The octanol-rich contrast P1 allows us to visualize the octanol-rich micro-domains as emerging form an invisible "external" medium, and the water-rich contrast P3 allow us to visualize the "negative" view of this, i.e. the average size water-rich micro-domains "containing" the organic-rich aggregates. It is consistent that these values differ only slightly. On

the contrary, the ethanol-rich contrast P2 allows us to directly visualize the typical size of aggregates of the location of ethanol. This one is distributed in both phases, with an accumulation at the emerging interface. If there were no accumulation at the interface, i.e. as critical fluctuation in a ternary fluid only, the three contrasts would give the same size. Here, it is clear that the ethanol-only contrast gives a smaller apparent size: this is a direct proof of the existence of an interface, rich in co-solvent. The micro-structure in the pre-Ouzo region corresponds to two immiscible fluids separated by an interface: this corresponds to the definition of a microemulsion where the ethanol plays the role of a weak surfactant. High absolute intensities are observed for the P1 and P3 contrasts for the reference system (see **Figure 3.4**). *This observation is valid for the reference sample and remains true in the case of added salt.*[148]

In presence of Cl^-, the intensities of the curves at low q-values for the octanol-rich and water-rich contrasts P1 and P3 is higher and the curvature changes accordingly (see **Figure 3.4**.a). The correlation length values ξ_N found for the contrasts P1 and P3 are higher than ξ_N of the reference. For ClO_4^-, the absolute intensities at low q-values are smaller than the reference and a saturation of the signal is observed more rapidly, as represented in **Figure 3.4**.b. ξ_N also decreases with 0.46 mol/kg $NaClO_4$. However, no significant change is observed regarding the contrast P2 for Cl^- and ClO_4^-. All correlation lengths, sizes, and other useful data can be found in the Supplementary Materials, section 3.1.1.6, **Table 3**.

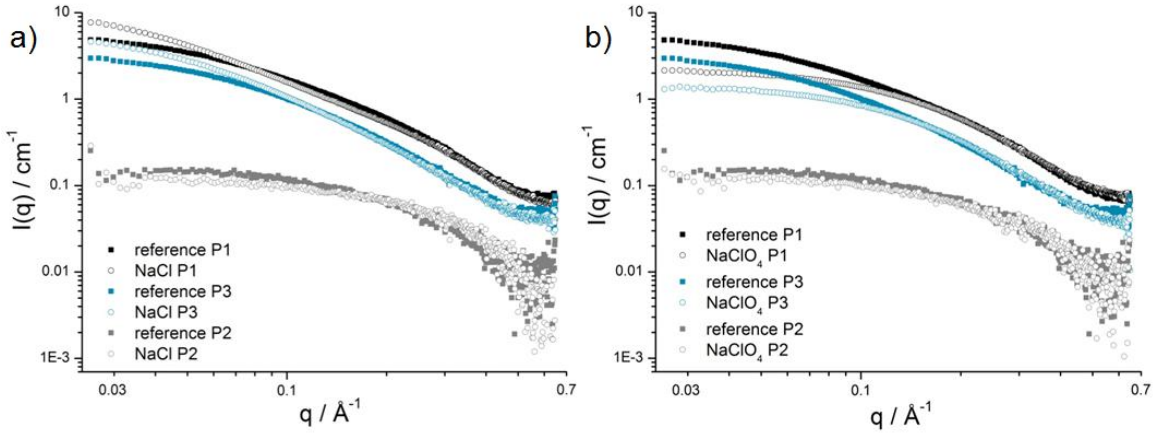

Figure 3.4. SANS curves on a log-log scale and in absolute units of the formulation corresponding to point α with a) 0.35 mol/kg NaCl, and b) 0.46 mol/kg $NaClO_4$.

DLS was also measured for the composition α with increasing salt concentrations. The autocorrelation functions for each salt can be found in the Supplementary Materials, section 3.1.1.6. The characteristic dynamic sizes ξ_D as obtained from DLS are plotted against the anion concentrations, see **Figure 3.3**.b. ξ_D increases and diverges at a given concentration for NaCl and $NaNO_3$. Regarding CH_3COONa, ξ_D is constant. It decreases for NaSCN, NaBr, and $NaClO_4$.

3.1.1.3.3. Influence of the addition of different cations on the nano-structures of the ternary composition α

SAXS measurements were also performed with increasing concentration of cations, keeping chloride as a common anion. The investigated formulation corresponded to formulation α, c.f. **Figure 3.1**.

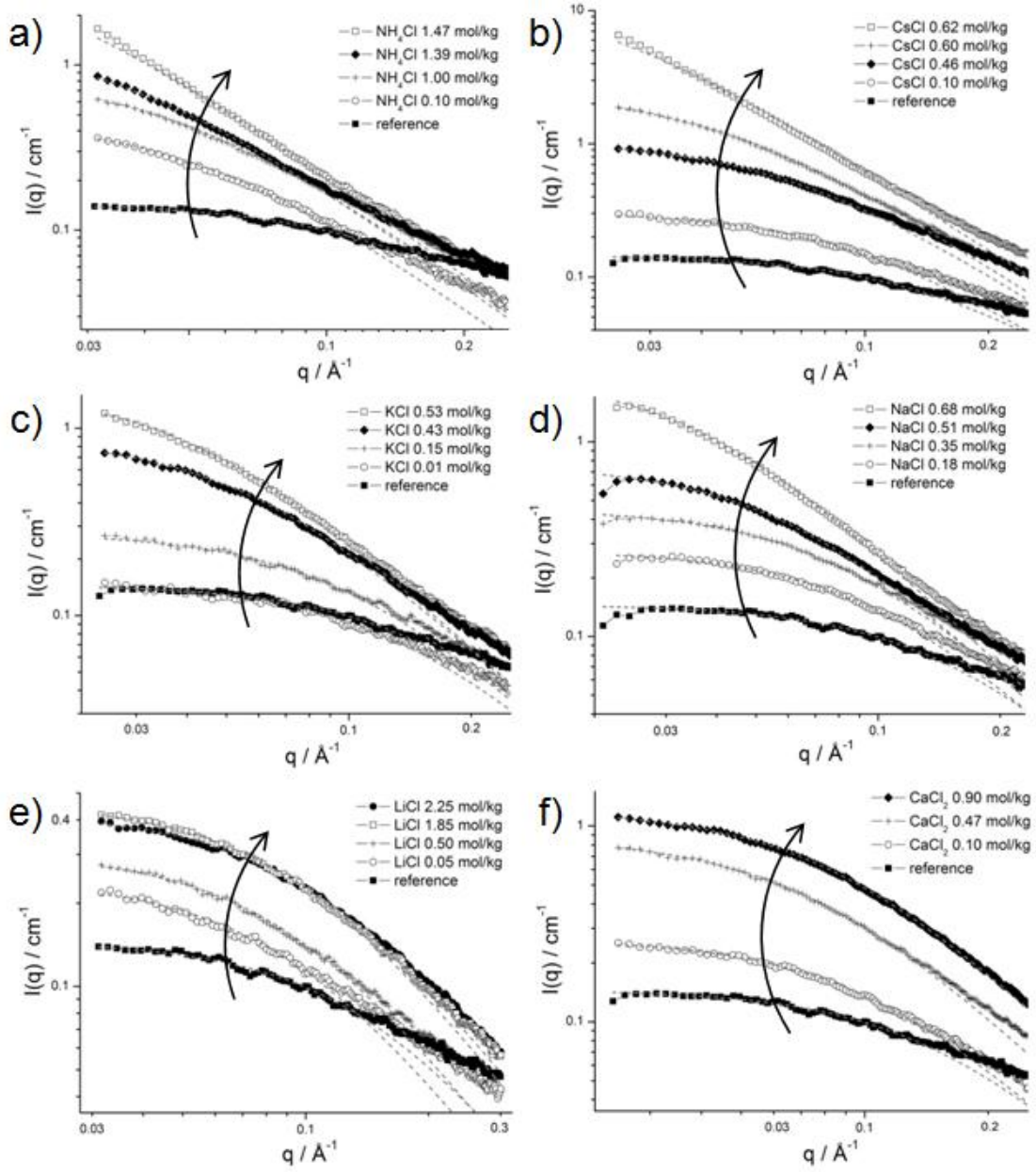

Figure 3.5. SAXS spectra on a log-log scale and in absolute units for the system water/ethanol/1-octanol in presence of a) NH_4Cl; b) CsCl; c) KCl; d) NaCl; e) LiCl; and f) $CaCl_2$. The dotted lines are the fits done with the Ornstein-Zernike equation.

The SAXS curves for all cations exhibit the same behaviour. As presented in **Figure 3.5**, the absolute intensity increases at low q-values when increasing the salt concentrations. It can be noted that the intensity at $q \rightarrow 0$ is the highest for Cs^+ and the smallest for Li^+. All the curves were fitted using an Ornstein-Zernike equation. The correlation lengths obtained from these fits increase for NH_4^+, Cs^+, K^+, and Na^+ and are equal to 45.8 Å for 1.47 mol/kg NH_4^+, 45.9 Å for 0.62 mol/kg Cs^+, 24.1 Å for 0.53 mol/kg K^+, and 27.7 Å for 0.68 mol/kg Na^+ (see **Figure 3.6**.a). The trend is less evident for Li^+ and Ca^{2+}.

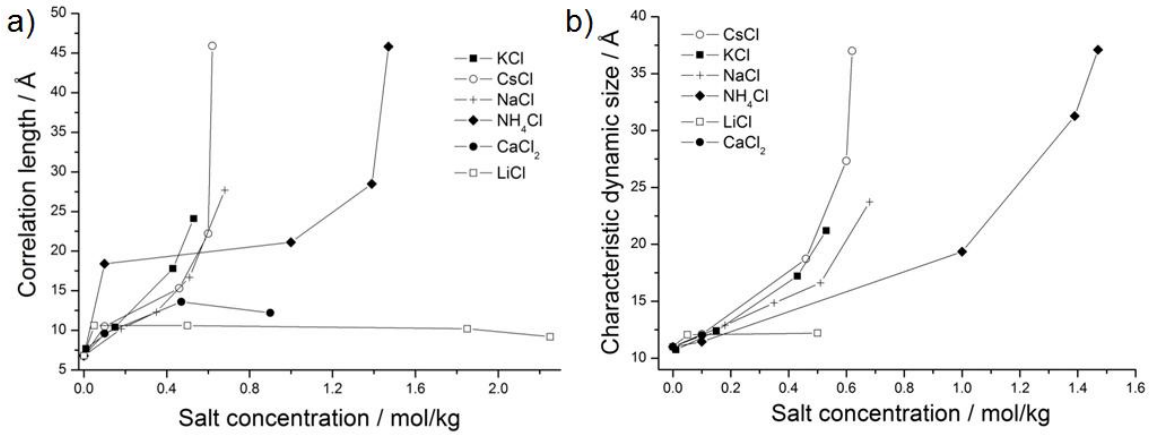

Figure 3.6. a) Correlation length ξ_X in Å obtained from SAXS; and b) Characteristic dynamic size ξ_D in Å obtained from DLS plotted against the cation concentration in mol/kg.

SANS measurements were also carried out on the reference system without additives and with 0.50 mol/kg of LiCl (see **Figure 3.7**). The same three contrasts were measured for each sample. As already described for the reference, high absolute intensities are observed for the octanol-rich and water-rich contrasts P1 and P3 contrary to the ethanol-rich contrast P2 which exhibits a lower absolute intensity. The curvature of the P1 and P3 curves is the same. In presence of Li^+, the intensities of the curves at low q-values for contrasts P1 and P3 are higher and the curvature changes accordingly. This is in agreement with the slight increase of ξ_N for P1 and P3. No significant change is observed regarding contrast P2.

As for the anions, DLS was also performed for the composition α with increasing cation concentrations. The autocorrelation functions for each salt can be found in the Supplementary Materials, section 3.1.1.6. The characteristic dynamic size ξ_D was also plotted against the cation concentration, see **Figure 3.6**.b. It increases and diverges at a given concentration of CsCl, KCl, NaCl and NH_4Cl. Note that NH_4Cl diverge at much higher concentration than the other three salts. For LiCl and $CaCl_2$, ξ_D exhibits a slight increase at low concentration and stays more or less the same at higher concentrations.

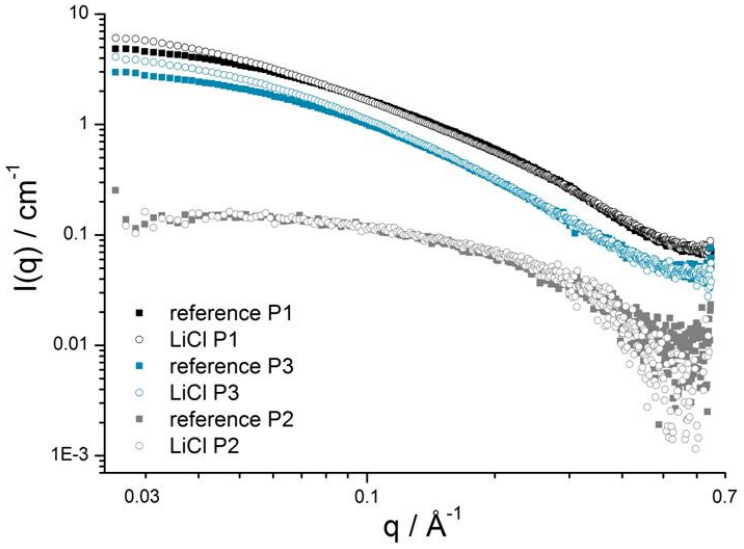

Figure 3.7. SANS curves on a log-log scale and in absolute units of the formulation corresponding to point α with 0.5 mol/kg LiCl.

3.1.1.3.4. Influence of "special" electrolytes on the nano-structures of the ternary composition α

SAXS experiments were also performed with increasing concentrations of $NaBPh_4$, SDS, HDEHP, and NaDEHP in the composition α. $NaBPh_4$ is a typical antagonistic salt since sodium is a kosmotropic ion and BPh_4^- is extremely chaotropic, hence expelled from the water-rich domains. As a consequence, it must be adsorbed on the octanol-rich domain: charge separation of antagonistic salts should produce a net electrostatic repulsion. Extreme cases are investigated with anionic surfactants, where the amphiphilic anion is expected to be mixed with the octanol-rich aggregate and stabilise them. We use HDEHP, the oil-soluble acidic form of the diethylhexylphosphoric acid, as a counter-example, since it should increase the volume of octanol-rich aggregates without inducing negative charge stabilisation.

The absolute intensity decreases for $NaBPh_4$ and SDS at low q-values when their concentrations increase respectively from 0 to 0.26 and 0.55 mol/kg (see **Figure 3.8**.a and b). The decrease of the intensity at $q \rightarrow 0$ is more significant for the surfactant SDS. Further, the emergence of the classical broad peak associated to repulsive aggregates[149] or disordered-open-connected structures[150] are observed for the two additives at medium q-values. Its intensity increases with increasing additive concentrations. The maximal intensity is observed for the highest SDS concentration. It should be also mentioned that the peak is shifted to higher q-values with increasing concentrations, a direct hint that distance between the centres of neighbouring aggregates decreases, hence there are more smaller aggregates, consistent with the general idea of charge distribution.

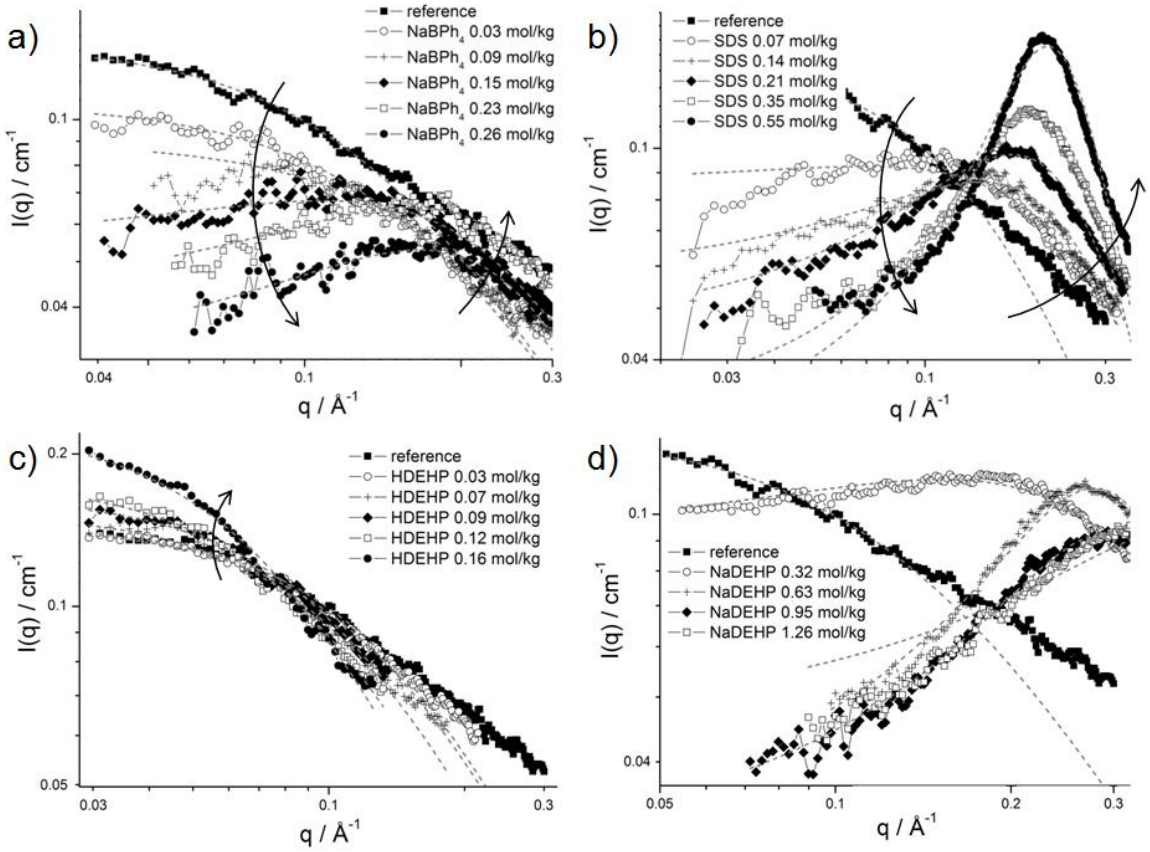

Figure 3.8. SAXS spectra on a log-log scale and in absolute units for the system water/ethanol/1-octanol in presence of a) $NaBPh_4$; b) SDS; c) HDEHP; and d) NaDEHP. The dotted lines are the fits corresponding to the Ornstein-Zernike equation or to equation **(2.12)**.

For $NaBPh_4$, the first four concentrations, i.e. from 0.03 to 0.12 mol/kg, were fitted using an Ornstein-Zernike function, whereas the last four ones, i.e. from 0.15 to 0.23 mol/kg, were fitted using the model developed for this work (see section 2.2.7, equation **(2.12)**). It can be seen that the correlation length stays more or less constant. Regarding SDS, all the curves were fitted using the model developed for this work (see section 2.2.7, equation **(2.12)**). The correlation length ξ_X obtained from these fits increases from 3.95 Å for 0.07 mol/kg SDS to 12.8 Å for 0.69 mol/kg SDS. For the uncharged HDEHP, the absolute intensity slightly increases when increasing its concentration in the surfactant-free microemulsion and no peak appears. The correlation length ξ_X obtained from these fits also increases and reaches 12.9 Å with 0.16 mol/kg HDEHP. Regarding the ionized HDEHP, called NaDEHP, the absolute intensity decreases at low q-values and a broad peak is obtained when increasing the concentration. Due to the use of two different models to fit the curves, the evolution of the correlation length ξ_X is not clear.

The measured DLS autocorrelation functions for $NaBPh_4$ and SDS can be found in the Supplementary Materials, see section 3.1.1.6.

3.1.1.4. Discussion

The surfactant-free microemulsion corresponding to composition α is in the pre-Ouzo region of the ternary system water/ethanol/1-octanol. As already described in the *Fundamentals* part, 1-octanol forms nano-clusters that are swollen by ethanol in the pre-Ouzo region. The ethanol molecules are distributed between octanol-rich nano-domains and a water pseudo-phase with a slight accumulation at the interface.

The addition of salt has two main effects:

1. A salting-out effect towards ethanol: ethanol molecules are driven to the interface or inside the octanol-rich aggregates upon addition of the electrolyte. Consequently, the size of the nano-structures increases and ξ_D, ξ_X, and ξ_N increase.
2. Charging of the interface via the antagonistic ion effect: the chaotropic ion is partly adsorbed onto the o/w interface and charges it, according to the charge regulation equilibrium.[151] As the electrostatic repulsion between the structures is enhanced, the compressibility decreases and I(0) from SAXS decreases. Further, the Ornstein-Zernike behaviour should disappear in favour of a correlation peak.

To each of these effects we can infer opposite consequences on the surfactant-free microemulsion. The consequences 1 and 2 are related respectively to the effects 1 and 2:

1. It leads to an *increase* of the dynamic scattering, with effects equivalent to a *decrease* of the initial ethanol concentration, i.e. the experimental point is getting closer to the demixing line upon addition of electrolyte.
2. It leads to a *decrease* of the dynamic scattering, with effects equivalent to an *increase* of the initial ethanol concentration, i.e. the experimental point is getting away from the demixing line upon addition of electrolyte. The pre-Ouzo aggregates are disappearing. The sample composition crosses the so-called Lifshitz line[152, 153] for which noticeable scattering at vanishing q-values disappears and the microstructure is better described as a weakly correlated ternary molecular solution and the associated transition toward a ternary unstructured fluid. If a critical point is present in the vicinity, only critical fluctuations are present. In this case, there is no pre-Ouzo region near the miscibility gap. There is no enrichment of ethanol at the interface between aggregates and there are no aggregates of a preferred size.

Regarding the SAXS measurements, the interactions between the aggregates (nano-clusters) present in the solutions can also be observed at q-values higher than 0.1 $Å^{-1}$ by the emergence of a peak, whereas the Ornstein-Zernike-like fluctuations of weakly interacting clusters can be

observed at low q-values. Concerning SANS, a saturation of the absolute intensity at low *q*-values hints at repulsive interactions between the nano-structures.

3.1.1.4.1. Static scattering: anions

NaCl, $NaNO_3$, CH_3COONa (mechanism 1). Considering the SANS spectrum of the reference formulation, the correlation length obtained from the fits for P1 and P3 is almost the same, whereas the correlation length for P2 is much smaller. As already pointed out, this result proves that the observed intensity comes from nano-structures inside the surfactant-free microemulsion and not from critical molecular fluctuations near a critical point.

Considering now the SANS spectrum of NaCl, the difference between the correlation length obtained from the fits for P1 and P3 is more important, indicating a change at the interface or in the aggregates. The apparent size increases: it can be deduced that the salt has a salting-out effect and pushes the ethanol molecules inside the aggregates, thus increasing their size, or at least the interface. This is seen by the difference in size considering the octanol and ethanol contrast. However, as the SANS curves of the reference and NaCl overlap for contrasts P1 and P3 at high q-values, the total water-rich to octanol-rich interface per unit volume remains constant.

From both these results, we suppose that the presence of salt induces a maximum stability of larger aggregates in the microemulsion. In a first order approximation of hydration force competing with entropy, the secondary hydration force comes into play, favouring larger aggregates.[154] The increase of the correlation length ξ_X and the increase of the absolute intensity in SAXS with increasing salt concentration, meaning that the compressibility increases and the repulsions between the nano-structures decrease, are in agreement with an increase of ethanol concentration in the aggregates. Further, Schöttl's and Horinek's simulations show that the ethanol concentration inside the aggregates and at the interface is enhanced upon addition of salts.[155] Consequently, this leads to an apparent decrease of ethanol concentration and the formulation is getting closer to the demixing boundary upon addition of NaCl: getting closer to the boundary increases the fluctuations that should be detected with light scattering at lower *q*-value, as will be discussed below.

$NaNO_3$ and CH_3COONa exhibit the same effect as NaCl. The same trend is indeed observed in SAXS and ξ_X also increases when increasing the salt concentration. However, the salting-out effect of CH_3COO^- is weaker than that of NO_3^-, which is weaker than Cl^- as the correlation length ξ_X starts diverging at higher concentrations, following the order Cl^-, NO_3^-, and CH_3COO^-. It is

also interesting to note that, usually, the carboxylate ion $–COO^-$ is harder than Cl^-. However, the acetate ion is less efficient than NaCl due to the presence of the hydrotropic group $–CH_3$.

NaSCN, NaBr, $NaClO_4$ (mechanism 2). The thiocyanate anion SCN^- exhibits a very different behaviour, as it is chaotropic. Thus, the sodium salt is antagonistic and easily separated. The decrease of the absolute intensity in SAXS at low q-values means that the repulsive interactions between the nano-structures increase. That increase is also confirmed by the presence of a peak at higher q-values coming from a structure factor. The Ornstein-Zernike behaviour disappears and the spectra have to be fitted using another equation, as indicated in section 2.2.7. The anion SCN^- goes onto the interface, leading to an increase of the repulsions and to a stabilisation of smaller microemulsion domains. The addition of NaSCN should also increase the monodispersity of the surfactant-free microemulsion as ξ_X tends to decrease, indicating that smaller aggregates are formed. It can be noted that both anions and ethanol participate in forming the interfacial film. The addition of NaSCN leads to an apparent increase of ethanol concentration and the formulation is moving away from the demixing boundary.

Considering the SANS spectrum of $NaClO_4$, the intensity shows no divergence at low q-values compared with the intensity of the reference. This is due to low osmotic compressibility, indicating the presence of repulsive interactions. Like in the case of SCN^-, the anion ClO_4^- goes onto the interface and charges it, leading also to repulsive interactions. The size of the aggregates is also smaller, as the correlation length ξ_N decreases for the three contrasts with 0.46 mol/kg $NaClO_4$. Further, as the P1 and P3 curves of the reference and $NaClO_4$ overlap at high q-values, the interface per unit volume remains the same. This means that the presence of antagonistic salt induces smaller and a larger number of aggregates inside the surfactant-free microemulsion. We are here in a situation very similar to the case first described by Onuki *et al.* when concentrated antagonistic salts, by themselves and without even a co-solute, induce stability of spontaneous emulsions. Instead of two macroscopically separated phases, droplets of 100 nm are observed in the system water/3-methylpentane and NaBr, used as antagonistic salt.[156]

It is worth stressing the main result here: *an antagonistic salt, such as NaSCN, $NaClO_4$, and probably NaBr (as its behaviour is the same as the perchlorate and thiocyanate ion in DLS) behaves like a surfactant in presence of ethanol.*

3.1.1.4.2. Static scattering: cations

NaCl, KCl, CsCl, NH_4Cl, LiCl, $CaCl_2$ (mechanism 1). Regarding the SANS spectrum of LiCl and the correlation lengths obtained from the fits for P1, P2, and P3, it is again confirmed that the obtained intensities originate from nano-structures inside the solution and not from critical fluctuations. Like in the case of NaCl, the facts that i) the difference between the sizes of contrasts P1 and P3 is more important than the one for the reference and ii) the absolute intensity in SAXS increases, indicate that LiCl "pushes" the ethanol molecules inside the octanol-rich aggregates. However, as the correlation length ξ_X stays almost the same and the increase of ξ_N is smaller than the increase for NaCl, the salting-out effect of Li^+ is much weaker that the one of Na^+. This is also in agreement with the work of Schöttl and Horinek who showed that the increase of the concentration of ethanol inside the organic-rich phase and at the interface upon addition of LiCl in smaller compared to CsCl (which behaves like NaCl, see next paragraph).[155] Further, they also showed that the aggregates with LiCl are a bit broader. Ca^{2+} should behave like Li^+ as they exhibit the same behaviour in DLS.

K^+, Cs^+, and NH_4^+ exhibit a behaviour similar to the one of NaCl in SAXS and thus have a salting-out effect towards ethanol. The free energy of transfer of the ethanol molecules inside the aggregates changes from 0.25 kT/mole to 1 kT/mole (2.5 kJ). This induces a size increase as shown by the measured correlation lengths ξ_X. Na^+, K^+, and Cs^+ behave approximately alike, whereas NH_4^+ has a much weaker salting-out effect when considering the divergence of the correlation length with increasing salt concentration. The addition of those salts leads to an apparent decrease of the ethanol concentration, i.e. the studied formulation comes closer to the demixing line.

3.1.1.4.3.Static scattering: "special" electrolytes

$NaBPh_4$ (mechanism 2). The strong decrease of the SAXS absolute intensity of BPh_4^- at low q-values shows that the electrostatic repulsions between the nano-structures increase. Further, the emergence of a slight peak at around 0.2 $Å^{-1}$ corroborates the increased interactions between the clusters. That can be explained by the strong propensity of the bulky organic and hydrophobic anion to the interface. The small sodium ion must follow to ensure local electro-neutrality. Since the structures are charged and repulsive, the Ornstein-Zernike fluctuations vanish and a correlation peak appears. As explained by Sadanake *et al.* and Onuki *et al.* (see introduction), the antagonistic salt acts as a significant surface active agent, but due to its bulky structure, it cannot form a well-ordered film or a sharp interface, as observed by the presence of a small broad peak in the SAXS spectra. Another type of microemulsions is observed here. It is neither stabilised by

surfactants nor by any hydration forces due to the ordering of alcohol groups at the interface. The structuring is mainly (or even purely) due to electrostatic interactions. Like NaSCN or $NaClO_4$, $NaBPh_4$ can play the role of a surfactant in presence of ethanol. Further, as ξ_X stays constant, there is no strong variation of the free energy of transfer of ethanol from water-rich to oil-rich domains and no changes in the size of aggregates is induced. The latter are now simply stabilised by the antagonistic salt and ethanol molecules, which render the interface more "visible".

SDS. The decrease of the absolute intensity observed upon addition of SDS at low q-values coupled with the apparition of a peak at medium *q*-values with increasing SDS concentrations are proofs that true surfactant micelles appear progressively. It cannot be excluded that the addition of SDS destroys first (meaning upon addition of very small amounts of SDS) the surfactant-free clusters. Qualitatively, this would lead to a decrease of intensity at low *q*-values similar to the measured one and cannot be distinguished from the intensity decrease because of increasing repulsions between charged micelles. But at least at low SDS concentrations, ethanol might prevent the formation of classical micelles, whereas at higher SDS concentrations, SDS micelles stabilised by octanol acting as cosurfactant can be expected.[16] At such high SDS concentrations, the characteristic peak of classical surfactant micelles is observed. The latter becomes narrower, its intensity higher with increasing concentrations of SDS, and polydispersity decreases. The correlation length ξ_X increases, meaning the size of the micelles also increases. We suppose that ethanol molecules are partitioned between both pseudo-phases and also participate in the interface, together with the surfactant.[28, 157]

HDEHP, NaDEHP. HDEHP can be considered as an oil. As such, the HDEHP molecules go inside the micelles and swell them, which is in agreement with the increase of the correlation length ξ_X from 6.8 Å without additive to 12.9 Å with 0.16 mol/kg HDEHP.
The behaviour of NaDEHP is comparable with the one of SDS, as the absolute intensity at low q-values decreases and the emergence of a broad peak is observed, both results leading to an increase of the electrostatic repulsions. In that case, a surfactant is formed *in situ* by deprotonating the HDEHP oil with sodium hydroxide.

To sum up, anions have either a salting-out effect where the ethanol molecules are pushed inside the nano-structures (the formulation is closer to the demixing boundary), or behave like a surfactant by stabilising the interface with electrostatic effects (the formulation is farther away from the boundary). Cations mainly induce an increase of the size by salting-out. All antagonistic salts produce a transformation from pre-Ouzo aggregates into smaller charged repulsive micelles. We now examine if this global unified picture is consistent with what is observed by dynamic light scattering at lower-*q*.

3.1.1.4.4. Dynamic scattering

We consider here the Rayleigh ratios obtained from DLS to see if the results obtained with this method are in agreement with the static methods previously explained.

As it can be seen in **Figure 3.3**.b, **Figure 3.6**.b, and **Figure 3.9**.a and b, the characteristic dynamic size ξ_D and the Rayleigh ratios of NaCl, $NaNO_3$, KCl, CsCl, and NH_4Cl increase with increasing salt concentration. This, together with the increase of the characteristic time obtained from DLS (see **Table 3** in the Supplementary Materials, section 3.1.1.6), is in agreement with the SAXS and SANS results and confirms that the formulation comes closer to the demixing line. Likewise, the fact that ξ_D, the characteristic time, and the Rayleigh ratios decrease for $NaClO_4$, NaBr, and NaSCN upon increasing the salt concentration is in agreement with the Onuki's behaviour previously explained: the line of the phase boundary moves away from the position of the sample, meaning that critical fluctuations of local density of octanol-rich pre-Ouzo aggregate (as shown by the black arrows in **Figure 3.1**) and/or the fluctuations of local ethanol concentrations (as shown by the grey arrows in **Figure 3.1**) decrease. Thus, the amplitude of the correlation functions obtained by DLS and the Rayleigh ratios decrease.

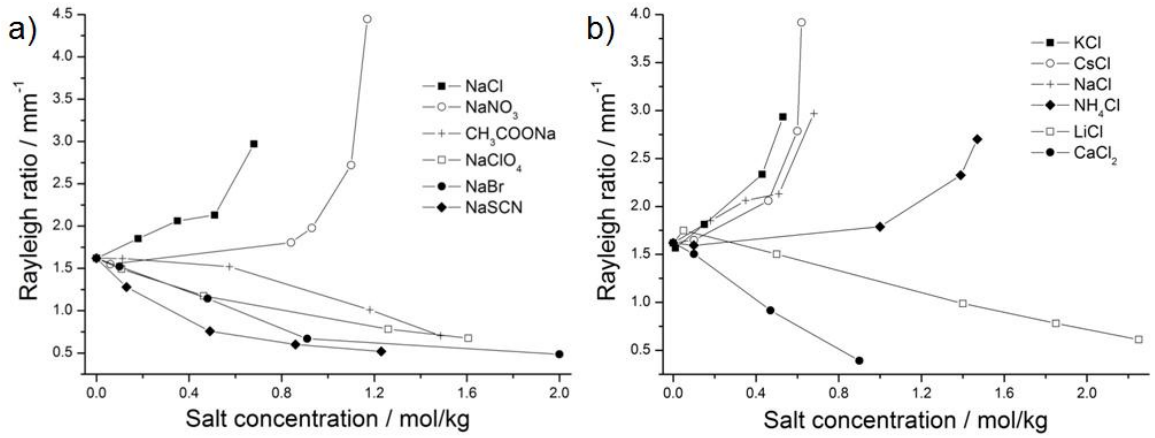

Figure 3.9. a) Rayleigh ratio in mm^{-1} obtained from DLS plotted against the anion concentration in mol/kg; and b) Rayleigh ratio in mm^{-1} obtained from DLS plotted against the cation concentration in mol/kg.

However, the Rayleigh ratios of CH_3COONa, LiCl, and $CaCl_2$ exhibit an opposite behaviour and decrease, although the formulation gets closer to demixing boundary upon addition of salt (**Figure 3.9**.a and b).

In surfactant-free systems, two different types of fluctuations occur: i) the fluctuations of the organic-rich phase in the water-rich phase and vice-versa, and ii) the fluctuations of the ethanol distribution between those pseudo-phases; these are represented in the ternary phase diagram on **Figure 3.1** by respectively the black and grey arrows. The scattered intensity in DLS in such

system is caused by the convoluted contributions of those two fluctuations. In the case of those three salts made of kosmotropic ions, we may suppose that the ethanol fluctuation is perturbed and that the exchange dynamics of ethanol between both pseudo-phases is slowed down upon addition of salts. This would lead to a decrease of the Rayleigh ratios. The interactions acetate-ethanol, lithium-ethanol, and calcium-ethanol may be stronger than the corresponding interactions for the other salts.

3.1.1.5. Conclusion

Pre-Ouzo aggregates are a general type of weak aggregation that is very sensitive to addition of electrolytes. The pre-Ouzo domain sizes increase as soon as the presence of salt in the water-rich pseudo-phase induces a salting-out of the ethanol. In the case of antagonistic ion containing one chaotropic ions, the charge separation at the interface produces an electrostatic stabilisation of the aggregates, which gradually transform to micelles similar to classical surfactant-cosurfactant micelles with an excess of anionic surfactant. This means that ethanol/chaotropic ion combinations may serve as an alternative to surfactants for the formulation of microemulsions.

When true surfactants are added to surfactant-free microemulsions, the main constituent at the interface is ethanol at low concentrations of additives, moving towards octanol-surfactant interfaces at higher additive concentration, where, as expected, classical mixed micelles are formed. The variations of these molecular interactions are also at the origin of the variation of the phase boundary line. The light scattering is more sensitive to fluctuations, while SAXS/SANS patterns transform from pure Ornstein-Zernike behaviour to a structured pattern with a broad peak. For the latter, we propose in this work a general formula for a convenient fitting of the data, introducing two quantities: the correlation size and the distance between centres at $2\pi/q_0$ (equation **(2.15)**).

3.1.1.6. Supplementary Materials

3.1.1.6.1. DLS of composition α with increasing the anion concentration

As observed in **Figure A**, two different behaviours are observed with DLS when increasing the concentration of the sodium salts. For CH_3COO^-, Br^-, ClO_4^-, and SCN^- the intensity of the correlation functions decreases from 0 to respectively 1.50, 2.00, 1.60, and 1.30 mol/kg of the respective salt. The intensity of the correlation functions increases for Cl^- and NO_3^- from 0 to respectively 0.67 and 1.17 mol/kg.

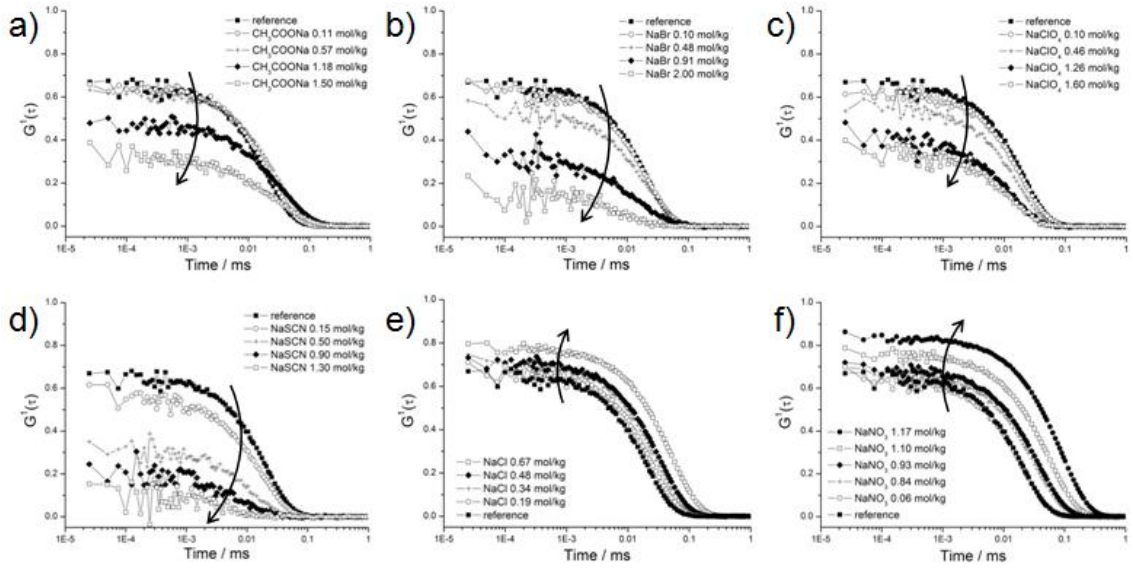

Figure A. Time-dependent self-correlation functions as obtained by DLS for the system water/ethanol/1-octanol in presence of different sodium salts: a) CH_3COONa; b) NaBr; c) $NaClO_4$; d) NaSCN; e) NaCl; f) $NaNO_3$, at 25 °C.

3.1.1.6.2. DLS of composition α with increasing the cation concentration

Regarding the DLS measurements performed with chloride salts and presented in **Figure B**, following observations can be made: the intensity of the correlations functions decreases with Li^+ and Ca^{2+} as cations, from 0 to 2.25 and 0.90 mol/kg of the respective salts. For NH_4^+, Cs^+, K^+, and Na^+ the intensity of the correlation functions increases from 0 to respectively 1.47, 0.62, 0.53, and 0.67 mol/kg.

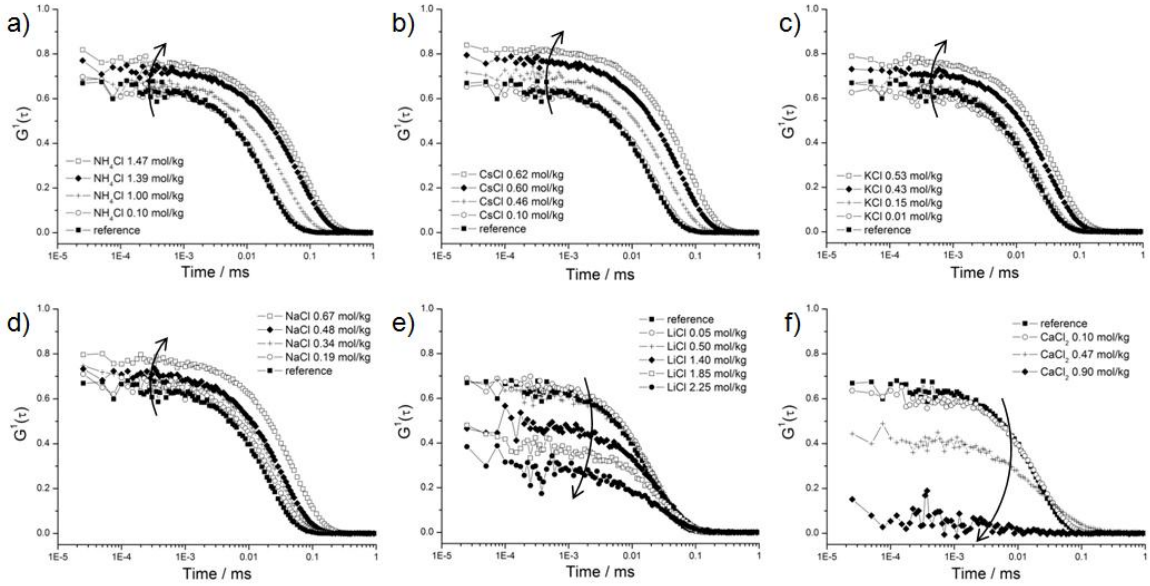

Figure B. Time-dependent self-correlation functions as obtained by DLS for the systems water/ethanol/1-octanol in presence of different chloride salts: a) NH_4Cl; b) CsCl; c) KCl; d) NaCl; e) LiCl; and f) $CaCl_2$, at 25 °C.

3.1.1.6.3. DLS of composition α with increasing concentration of $NaBPh_4$ and SDS

As can be seen in **Figure C**.a, the time-correlation becomes less and less pronounced when the concentration of $NaBPh_4$ increases from 0 to 0.27 mol/kg. The same trend was observed with increasing concentration of SDS from 0 to 0.70 mol/kg (see **Figure C**.b).

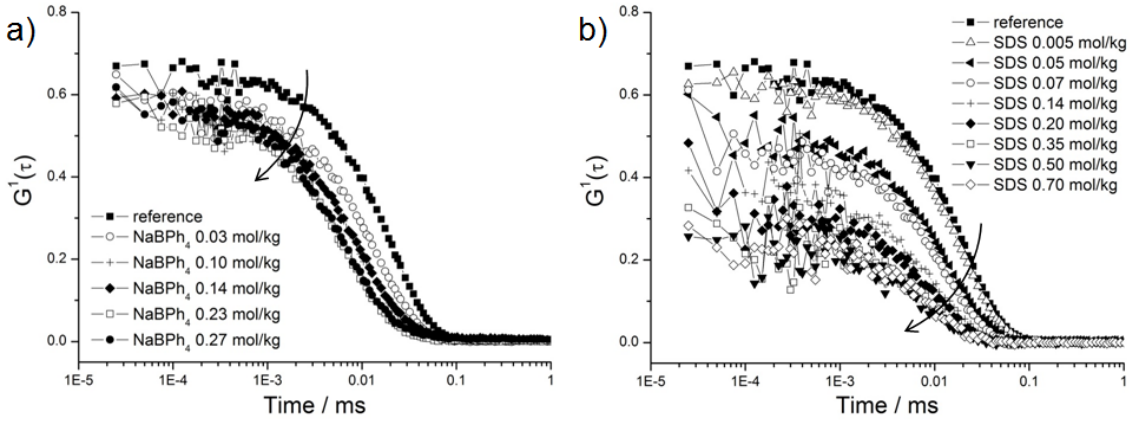

Figure C. Time-dependent self-correlation functions as obtained by DLS for the systems water/ethanol/1-octanol/additive, where the additive is a) $NaBPh_4$; and b) SDS, at 25 °C.

3.1.1.6.4. Table summing up the important results

Table 3. Data for the investigated salts and surfactants. Concentrations of anions or cations in the surfactant-free microemulsion in mol/kg and wt%. From **SAXS**: correlation length ξ_X in Å, absolute intensity at q→0 I(0) in cm^{-1}, mean radius R_{MV} in Å, distance D* in Å; from **SANS**: correlation length ξ_N in Å for the three contrasts; and from **DLS**: characteristic time τ (inverse of the decay rate) in µs.

			SAXS				SANS			DLS
Ions	**Concentration**		ξ_X	I(0)	R_{MV}	D*	ξ_N			τ
-	*mol/kg*	*wt%*	*Å*	*cm^{-1}*	*Å*	*Å*	P1 *(Å)*	P2 *(Å)*	P3 *(Å)*	*µs*
reference	0	0	6.8	0.145	15.23		16.3	6.35	16.0	40.2
Cl^-	0.18	1	10.2	0.275	22.85	∞	-	-	-	48.6
	0.35	2	12.3	0.45	27.55	∞	18.8	5.1	22.0	57.1
	0.51	3	16.7	0.76	37.41	∞	-	-	-	66.4
	0.68	4	27.7	2.25	62.05	∞	-	-	-	100.0
NO_3^-	0.06	0.5	7.75	0.155	17.36	∞	-	-	-	40.6
	0.84	7	15.8	1.18	35.39	∞	-	-	-	63.9
	0.93	8	19.5	1.79	43.79	∞	-	-	-	72.1
	1.10	9	30.2	4.62	67.65	∞	-	-	-	107.4
	1.17	10	46.2	11.25	103.49	∞	-	-	-	170.6
CH_3COO^-	0.11	1	8.65	0.207	19.38	∞	-	-	-	44.5
	1.18	10	16.1	1.35	36.06	∞	-	-	-	69.7
	1.50	12	40.6	8.6	90.94	∞	-	-	-	-
SCN^-	0.13	1	5.39	0.13	12.07	∞	-	-	-	33.8
	0.49	4	3.78	0.13	8.47	∞	-	-	-	24.2
	0.86	7	4.01 (3)	-	29.39	85.98	-	-	-	↘
	1.23	10	3.94 (3)	-	20.00	57.57	-	-	-	↘
Br^-	0.10	1	-	-	-	-	-	-	-	41.5
	0.48	5	-	-	-	-	-	-	-	40.8
	0.91	9	-	-	-	-	-	-	-	↘
	2.00	20	-	-	-	-	-	-	-	↘
ClO_4^-	0.10	1	-	-	-	-	-	-	-	39.1
	0.46	6	-	-	-	-	8.6	5.8	9.4	32.6
	1.26	15	-	-	-	-	-	-	-	↘
	1.60	20	-	-	-	-	-	-	-	↘
NH_4^+	0.10	0.5	18.4	0.48	41.22	∞	-	-	-	42.5
	1.00	5	21.1	0.9	47.26	∞	-	-	-	74.7
	1.39	7	28.5	1.51	63.84	∞	-	-	-	125.8
	1.47	8	45.8	4.5	102.59	∞	-	-	-	150.0
Cs^+	0.10	2	10.5	0.308	23.52	∞	-	-	-	44.7
	0.46	8	15.3	2.43	34.27	∞	-	-	-	70.0
	0.60	10	22.2	1.05	49.73	∞	-	-	-	106.0
	0.62	10.5	45.9	13.5	102.82	∞	-	-	-	146.3
Na^+	0.18	1	10.2	0.275	22.85	∞	-	-	-	48.6
	0.35	2	12.3	0.45	27.55	∞	18.8	5.1	22.0	57.1
	0.51	3	16.7	0.76	37.41	∞	-	-	-	66.4
	0.68	4	27.7	2.25	62.05	∞	-	-	-	100.0
K^+	0.01	0.1	7.7	0.147	17.25	∞	-	-	-	39.7
	0.15	1	10.4	0.275	23.30	∞	-	-	-	46.4
	0.43	3	17.8	0.89	39.87	∞	-	-	-	65.6
	0.53	4	24.1	1.62	53.98	∞	-	-	-	82.0

Li^+	0.05	0.2	10.6	0.24	23.74	∞	-	-	-	44.8
	0.50	2	10.6	0.302	23.86	∞	16.4	6.55	19.0	49.5
	1.85	8	10.2	0.46	22.85	∞	-	-	-	↗
	2.25	10	9.2	0.42	20.61	∞	-	-	-	↗
Ca^{2+}	0.10	1	9.6	0.262	21.62	∞	-	-	-	46.3
	0.47	5	13.6	0.86	30.46	∞	-	-	-	↗
	0.90	10	12.2	1.2	27.33	∞	-	-	-	-
BPh_4^-	0.03	1	5.7	0.108	12.77	∞	-	-	-	28.6
	0.06	2	4.73	0.1	10.59	∞	-	-	-	-
	0.10	3	4.42	0.09	9.90	∞	-	-	-	21.0
	0.12	4	3.55	0.08	7.95	∞	-	-	-	-
	0.14	5	4.73 (3)	-	22.63	70.47	-	-	-	20.3
	0.17	6	6.27 (3)	-	19.85	59.22	-	-	-	-
	0.20	7	6.12 (3)	-	18.47	53.85	-	-	-	-
	0.23	8	4.91 (3)	-	16.80	47.56	-	-	-	15.5
	0.27	9	5.38 (3)	-	16.29	45.96	-	-	-	15.2
SDS	0.005	0.1	-	-	-	-	-	-	-	37.8
	0.05	1	-	-	-	-	-	-	-	28.5
	0.07	2	3.95 (3)	-	36.47	110.21	-	-	-	25.9
	0.14	4	5.06 (3)	-	21.20	55.00	-	-	-	19.8
	0.20	6	6.20 (3)	-	17.95	45.13	-	-	-	↘
	0.35	10	8.40 (3)	-	15.44	38.87	-	-	-	↘
	0.42	12	8.52 (3)	-	14.77	37.03	-	-	-	-
	0.50	14	9.55 (3)	-	14.42	36.33	-	-	-	↘
	0.55	16	10.5 (3)	-	14.51	36.31	-	-	-	-
	0.70	20	12.8 (3)	-	13.82	35.19	-	-	-	↘
HDEHP	0.03	1	6.95	0.144	15.59	∞	-	-	-	-
	0.07	2	8.2	0.153	18.37	∞	-	-	-	-
	0.09	3	8.65	0.165	19.38	∞	-	-	-	-
	0.12	4	10.15	0.177	22.74	∞	-	-	-	-
	0.16	5	12.9	0.227	28.90	∞	-	-	-	-
NaDEHP	0.32	10	3.75 (3)	-	20.42	50.32	-	-	-	-
	0.63	20	7.18 (3)	-	10.96	27.56	-	-	-	-
	0.95	30	6.14 (3)	-	10.81	26.18	-	-	-	-
	1.26	40	2.88 (3)	-	7.37	18.33	-	-	-	-

3.1.2.Towards surfactant-free and water-free micro-emulsions

3.1.2.1. Abstract

It was recently demonstrated that a nano-clustering was present in the monophasic "pre-Ouzo" region of ternary liquid mixtures without surfactants. The goal of this work is to check if this nano-clustering is also present in the surfactant-free and water-free "green" microemulsions glycerol/ethanol/1-octanol and deep eutectic solvent/tetrahydrofurfuryl alcohol/diethyl adipate. The deep eutectic solvents used instead of water were ethylene glycol-choline chloride (molar ratio 4-1) and urea-choline chloride (molar ratio 2-1). To our knowledge this is the first time that deep eutectic solvents were used to formulate microemulsions. The surfactant-free and water-free microemulsions were studied using phase diagrams, dynamic light scattering, and small-angle x-ray scattering. The presence of aggregate fluctuations was demonstrated and they were found to be independent of molecular critical fluctuations, except when approaching the critical point where the critical phenomenon is superimposed to the signal. These structures have similarities to classical microemulsions but, in contrast to them, without having a sharp interface between the non-miscible phases, much as it is the case for the system previously investigated water/ethanol/1-octanol.

3.1.2.2. Introduction

Microemulsions are macroscopically homogeneous liquids composed of polar and non-polar constituents. A surfactant and, usually, a cosurfactant are necessary to obtain these translucid and thermodynamically stable solutions.[3, 29, 158] According to Winsor, microemulsions can be either a one-phase system (Winsor IV) or part of a multi-phase system as Winsor I, II, or III when it is in equilibrium with the oil phase, the aqueous phase or both phases, respectively.[12] Depending on the composition, a microemulsion can be of three different types: water-in-oil, bicontinuous or oil-in-water. Microemulsions have been proven useful, particularly in the area of enhanced oil recovery[159] but also in the cosmetic,[160-162] food,[163, 164] and pharmaceutical industries[165-167] or as cleaning agents.[168, 169]

Most examples concerning microemulsions are given by considering the polar constituent as aqueous phase. An aqueous phase is of course the most common one, but it is not essential for the formulation of a microemulsion. In literature many papers deal with water-free microemulsions and their interesting properties. The pioneers in this field were Lattes *et al.* They replaced water by formamide in a system containing cyclohexane as oil and butanol as cosurfactant and studied the influence of two different surfactants.[170] They published several papers using formamide as a

highly structured solvent and used the resulting non-aqueous microemulsion for example as reaction medium to perform Diels-Alder reactions.[171-173] Harrar *et al.* have studied a non-aqueous microemulsion containing the ionic liquid [emim][$etSO_4$], the oil limonene and the surfactant Triton X-114.[174] They observed that large temperature stability down to -35 °C can be achieved using high amounts of ionic liquid, which traces the way for applications in extraction processes or as reaction media for water-sensible reactions. Concerning perfumes, the effect of humidity on evaporation from aqueous and non-aqueous microemulsions containing perfume was investigated by Hamdan *et al.*[175] They observed that the weight loss is greater at lower humidity for both systems, but is higher for the aqueous system. Further, other water-free microemulsions were studied like the system ethylene glycol/sodium dodecyl sulfate (SDS)/decanol/toluene by Friberg *et al.*, who found a critical point in the system[176] or the system N,N-dimethylacetamide (DMA)/sodium di-(2-ethylhexyl) sulfosuccinate (AOT)/octane by Cai *et al.*, who examined the critical behaviour of the non-aqueous microemulsion.[177] A quantitative determination of the percolation threshold in water-free microemulsions was also described by Peyrelasse *et al.*[178] They showed that a model for microemulsion could be successfully applied for non-aqueous ones. The self-assembly of amphiphiles in the absence of water, the capability of reverse micelles to encapsulate non-aqueous polar organic solvents, the use of ionic liquids, or the possibility to employ non-aqueous reverse micelles as nano-reactors are examples of current research topics on water-free microemulsions.[179]

Further to water-free microemulsions, surfactant-free microemulsions are currently investigated at our institute. For more information, please refer to the *Fundamentals* part, section 1.2. We just remind that octanol-rich aggregates were observed in the pre-Ouzo region and that the ethanol molecules were distributed between both pseudo-phases with a slight accumulation at the interface.

Concerning the possible existence of surfactant-free and water-free microemulsions, we can also mention organic blends of biodiesel and diesel with ethanol and various additives, used as fuel. Biodiesel, a blend of fatty acid alkyl esters, is industrially produced by transesterification. The latter is a reaction of vegetable oils or a fat with an alcohol and yields fatty acid esters and glycerol. The exact knowledge of the phase equilibrium is essential for the optimisation of the biodiesel production and purification. Liquid-liquid equilibriums for the glycerol/ethanol/biodiesels systems were therefore studied, where biodiesels came from canola oil, cottonseed oil, soybean oil, coconut oil, and sunflower oil.[180-184] The term “microemulsion” is never used in the related papers, as no connection between these solutions and surfactant-free water-free microemulsions was made. Recently, Arpornpong *et al*. reported the possible existence of nano-droplets in such blends by investigating the effects of co-solvent saturation and unsaturation on the phase behaviour and on the viscosity of a biofuel.[185] The question of the

existence of nano-droplets in water-free and surfactant-free microemulsion is set. It can be noted that Silva *et al.* also observed nano-structures in mixtures of ethanol and diesel oil (or synthetic diesel) in presence of additives, also inferred from dynamic light scattering data.[186] However, the technique used in these two last studies is not enough to postulate the presence of a microemulsion, as critical molecular fluctuations may occur and give a signal in dynamic light scattering similar to those arising from fluctuating nano-droplets.

The goal of this paper is to formulate and characterise unambiguously green surfactant-free and water-free microemulsions. First, water was replaced with glycerol and the system glycerol/ethanol/octanol was studied. Second, water was replaced with two different deep eutectic solvents (DESs), i.e. the deep eutectic ethylene glycol-choline chloride (4-1) and the deep eutectic urea-choline chloride (2-1). In particular, the system DES/tetrahydrofurfuryl alcohol (THFA)/diethyl adipate was investigated. DESs, which were discovered by Abbott *et al.*,[187] have considerable advantages compared to classical ionic liquids, for example their easy production, low costs, and biodegradability.[188, 189] THFA stems from wood chemistry and is biodegradable,[190] and the diethyl adipate is of very low toxicity. The chemical formulae are sketched in **Figure 3.10** for information.

The domains of existence of the single clear and homogeneous phase were established for each system using ternary phase diagrams. Dynamic light scattering (DLS), as well as small-angle x-ray scattering (SAXS) were carried out to characterise the nano-domains. To our knowledge this is the first time that the formation of surfactant-free and water-free microemulsions was really characterised.

3.1.2.3. Results and discussion

3.1.2.3.1. Ternary phase diagrams

Figure 3.10 presents the phase diagrams obtained for the three investigated systems. A common trend can be observed, as a single, clear, homogeneous, and thermodynamically stable phase with no opalescence (white regions) and a multiphasic domain (grey parts) is obtained in each case.

The largest single translucid phase is found for the system glycerol/ethanol/1-octanol (**Figure 3.10**.a), the smallest one for the system DES2/THFA/diethyl adipate (**Figure 3.10**.c).

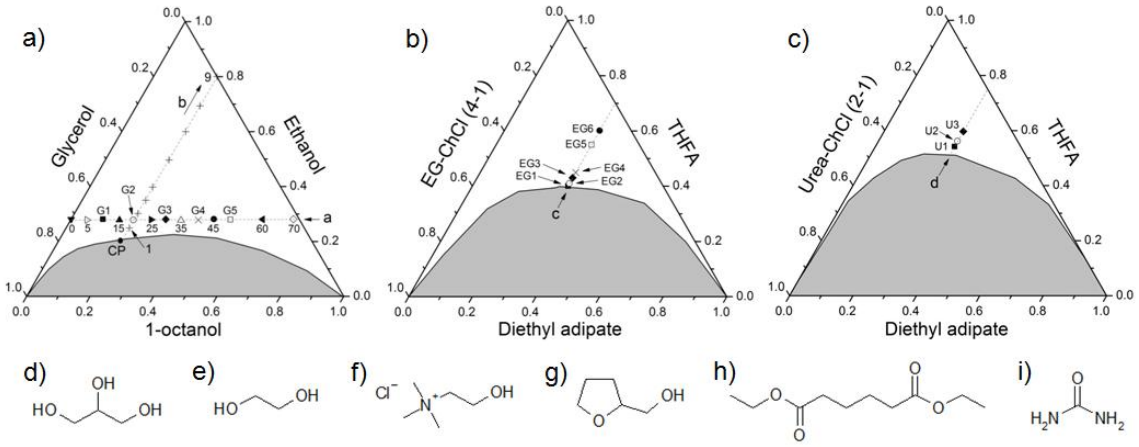

Figure 3.10. Ternary and pseudo-ternary phase diagrams of surfactant-free and water-free systems in weight fractions. a) Ternary diagram glycerol/ethanol/1-octanol; b) Pseudo-ternary diagram DES1/THFA/diethyl adipate; and c) Pseudo-ternary diagram DES2/THFA/diethyl adipate, at 25 °C. The white area corresponds to the single and homogeneous domain, the grey one to the multiphasic (diphasic) region. CP means "critical point". DLS measurements were carried out along paths a, b, c, and d. SAXS measurements were carried out along paths a, c, and d. The chemical structures of d) glycerol; e) ethylene glycol (EG); f) choline chloride (ChCl); g) tetrahydrofurfuryl alcohol (THFA); h) diethyl adipate; and i) urea are represented below these phase diagrams.

It can be noted that these systems fulfil the conditions needed to observe the Ouzo effect: a solvent A (i.e. glycerol or the DES) is added to a second solvent B, which is highly soluble or entirely miscible with solvent A (i.e. ethanol or THFA), and a third component, which is highly soluble in solvent B, but not in solvent A (i.e. 1-octanol or diethyl adipate). The critical point for the demixion was determined only for the system glycerol/ethanol/1-octanol and is located approximately at the beginning of path b (**Figure 3.10**.a). DLS measurements were carried out along paths at octanol or diethyl adipate constant mass fractions and also at ethanol constant mass fraction for the first ternary system. The objective was to investigate the presence of possible nano-clustering in these surfactant-free and water-free systems in analogy to the water containing solutions.

3.1.2.3.2. Dynamic light scattering

Glycerol containing mixture. DLS measurements were carried out in the system glycerol/ethanol/1-octanol on two different paths. Along line a (see **Figure 3.10**.a) the amount of ethanol was kept constant and equal to 28 wt%. Different samples with an increasing amount of 1-octanol were prepared and measured. Well-defined correlation functions (see **Figure 3.11**) are first hints of the presence of density fluctuations inside the solutions and are recorded in a large domain around the critical point. The correlation functions progressively became less and less

pronounced when moving away from the critical point by either decreasing or increasing the amount of 1-octanol along path a, from 20 down to 0 or from 20 up to 70 wt% of 1-octanol (see **Figure 3.11**.a and **Figure 3.11**.b). The same is also observed along path b (see **Figure 3.11**.c), increasing the amount of ethanol (from sample 1 to sample 9). This indicates that the corresponding fluctuations vanish or exist at higher frequencies.

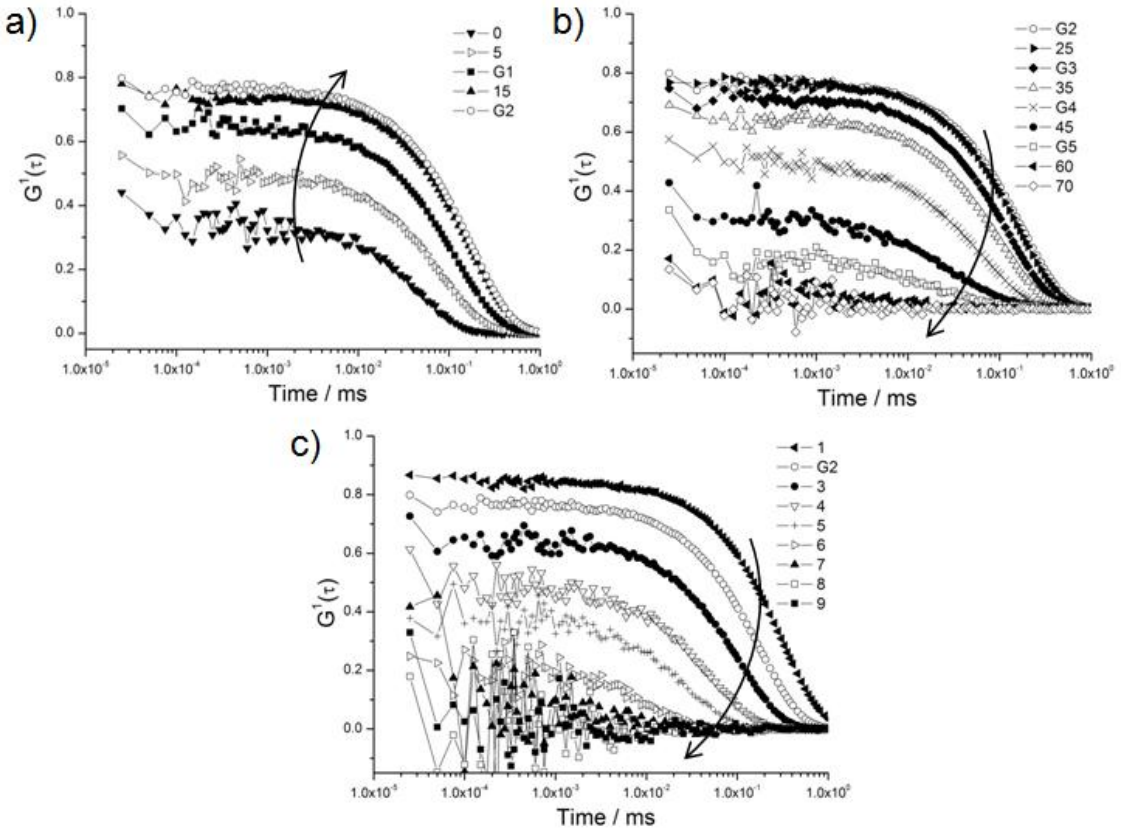

Figure 3.11. Time-dependent self-correlation functions as obtained from DLS for the system glycerol/ethanol/1-octanol along a) beginning of path a until 20 wt% of 1-octanol: b) end of path a from 20 wt% of 1-octanol; and c) path b, at 25 °C. For a) and b) the symbols correspond to those on the phase diagram for the corresponding system (see **Figure 3.10**.a).

The decay of these correlation functions are quasi mono-exponential and the characteristic times of the order of tens or hundreds milliseconds vary as the inverse of the q^2 when the spatial coherence factor is larger than 0.4 (data not shown here). A rough estimation of the fluctuation sizes using a Stokes-Einstein's relationship gives a size from 1 to few nanometres, depending on how far the formulation is from the demixing line, and cannot be due to molecular fluctuations. It is supposed that the presence of a nano-organisation is due to density fluctuations that are not critical, except when approaching the critical point where the critical phenomenon is superimposed to the signal. Further, static information I(t=0, θ=90°) were plotted for each sample in the respective series for comparison (see **Figure 3.12**). I(0) increases when approaching the

critical point but without showing a real singularity. However, to get an insight at a more suitable spatial scale, small-angle x-ray scattering is performed and will be further discussed in section 3.1.2.3.3.

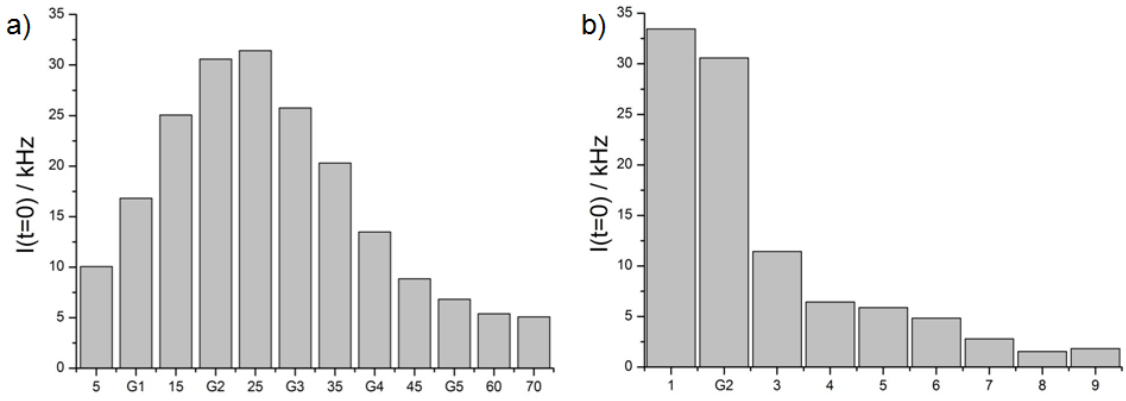

Figure 3.12. I(t=0) and at θ = 90° plotted for each sample for the system glycerol/ethanol/1-octanol along a) path a; and b) path b.

DESs containing systems. DLS measurements were also carried out following path c for the system DES1/THFA/diethyl adipate (see **Figure 3.10**.b), and path d for the system DES2/THFA/diethyl adipate (see **Figure 3.10**.c). The amount of diethyl adipate was kept constant on both paths and the amount of THFA was progressively increased. As it was the case for the system with glycerol, the correlation functions are well-defined near the demixing boundary and decreased progressively with an increasing amount of THFA (see **Figure 3.13**.a and **Figure 3.13**.b, respectively for the system containing DES1 and DES2).

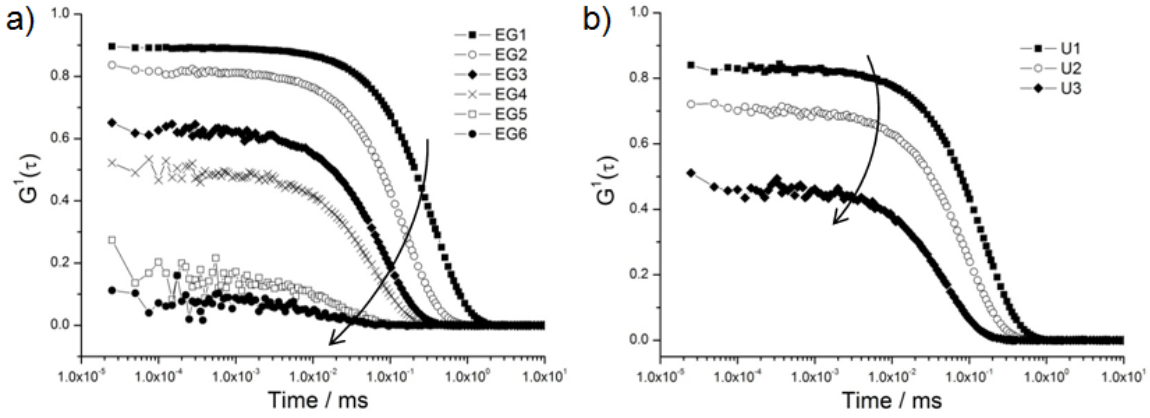

Figure 3.13. Time-dependent self-correlation functions as obtained from DLS for the system a) DES1/THFA/diethyl adipate along path c; and b) DES2/THFA/diethyl adipate along path d, at 25 °C. For a) and b) the symbols correspond to those on the phase diagram for the corresponding system (see **Figure 3.10**.b and **Figure 3.10**.c).

Comparison. As mentioned previously, the correlation size of the density fluctuations observed in these three ternary mixtures are of the order of few nanometres. Static light scattering can also be used to determine the volume of the "equivalent" particle but we cannot consider here isolated structures. Much incertitude also exists on the determination of the density of the fluctuating aggregates. Moreover, these aggregates are certainly not spherical in average.

Nevertheless, the variation of the obtained correlation functions is similar for all systems. The results found along paths b, c, and d are the same than those found on a comparable path in the system water/ethanol/1-octanol.[88] It is worth pointing now out that comparable results were found in surfactant-free ternary systems with perfumery molecules and mosquito repellents and will be respectively presented in sections 3.1.3 and 3.1.4. This shows the universality of this "pre-Ouzo" effect, with or without water, and at low or high viscosity values of the solutions, as the formulations with glycerol and both deep eutectics were very viscous. As examples, the viscosities for EG1, U1, and G1 (formulations near the demixing boundary and near the CP for G1) were respectively 9.9, 16.2, and 39.5 mPa s. Those of the formulations EG6, U3, and G5 (formulations away from the demixing boundary and away from the CP for G5) were respectively 6.4, 10.6, and 7.5 mPa s. One point to notice is that the pre-Ouzo domain is narrower when the miscibility gap is higher in ethanol fraction.

3.1.2.3.3. Small-angle x-ray scattering

SAXS measurements were carried out along path a (points G1 to G5) for the system with glycerol, path c for the system involving DES1 and path d for the system with DES2 (see respectively **Figure 3.10**.a, **Figure 3.10**.b, and **Figure 3.10**.c). The absolute intensity of the sample is directly proportional to the square of the electron density difference between both pseudo-phases (the water-rich and the oil-rich ones), called the scattering contrast. The latter can be assessed when structures composed of two phases with different electron densities are present in the solution. Logically, the scattering contrast cannot be characterised if there are no structures in the solution.

As can be seen in **Figure 3.14**, the behaviour in the variation of excess of scattering at low *q*-value in the SAXS spectra are in good accordance with those observed using DLS. For the system glycerol/ethanol/1-octanol, the absolute scattered intensity increases along path a from G1 to G2 and then decreases from G2 to G5 (see **Figure 3.14**.a). These results show that nano-structures developed along path a and progressively disappeared, as observed with light scattering. The correlation length ξ_X of the nano-clustering was extracted from the data adjustment using an Ornstein-Zernike function. Along path a the correlation length increased from 0.8 nm for G1 to 1.3 nm for G2 and then decreased to 0.3 nm for G5 (see **Figure 3.14**.d, curve with black squares). The size of point G5 is very small and may correspond to the size of octanol-octanol or octanol-

glycerol dimers, as the formulation is far away from the boundary and no well-defined structures occur.

High intensities upturn at low q-values were also observed for samples EG1 and U1 (see respectively **Figure 3.14**.b and **Figure 3.14**.c), which indicates that nano-structures are also present at the beginning of path c and d, near the demixing boundary. With increasing distances from the demixing boundary, these nano-droplets became smaller and finally disappeared in favour of true molecular solutions. The characteristic length decreased from 4.5 nm for EG1 to 1.2 nm for EG4, and from 1.9 nm for U1 to 0.5 nm for U3 (see **Figure 3.14**.d, respectively the curves with crosses and black circles). Along paths c and d for the systems with DES1 and DES2, the characteristic length is more important for DES1 near the demixing boundary. This may be explained by the size of the EG molecule which is larger than urea molecules. EG may form larger clusters.

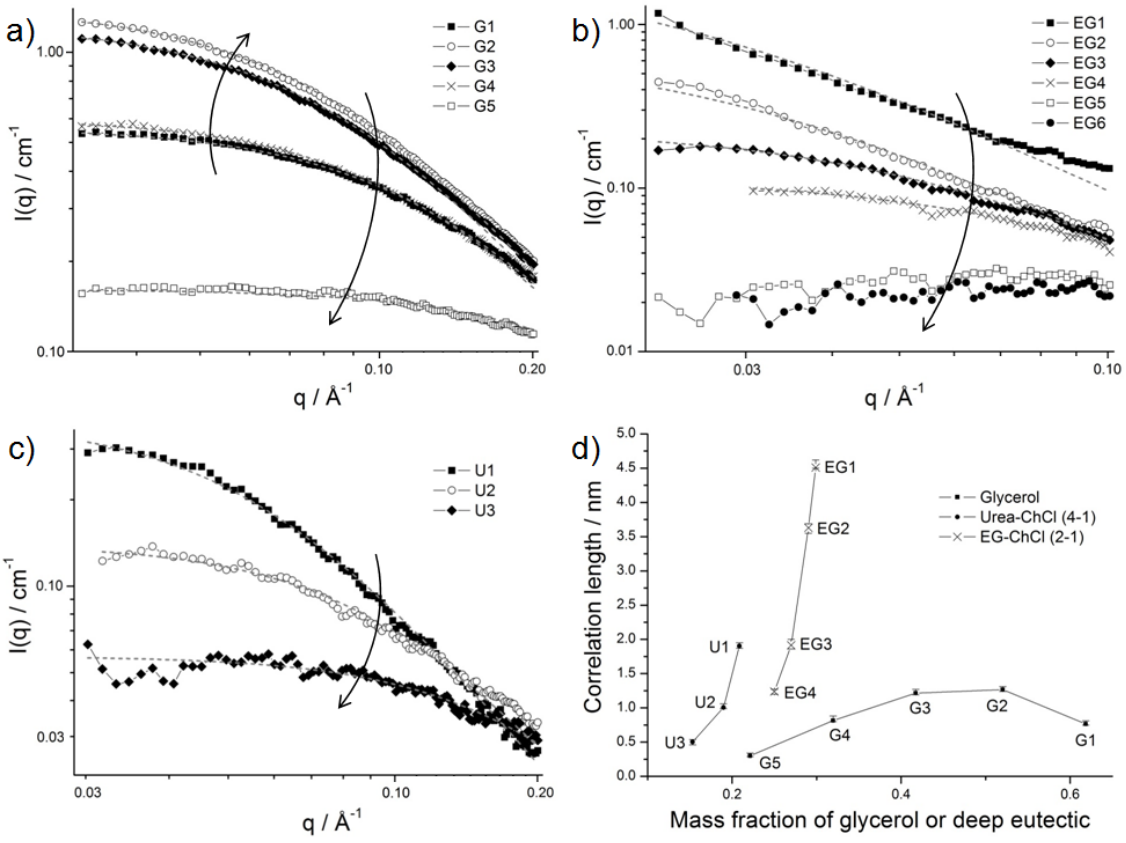

Figure 3.14. SAXS spectra on a log-log scale and in absolute units for the system a) glycerol/ethanol/1-octanol; b) DES1/THFA/diethyl adipate; c) DES2/THFA/diethyl adipate. The different symbols correspond to the ones on the phase diagrams (see **Figure 3.10**). The grey dotted lines on the SAXS data are the corresponding Ornstein-Zernike fits. d) Correlation lengths ξ_X in nm obtained from Ornstein-Zernike fits versus the mass fraction of glycerol or the DES for the three systems (black squares for the system with glycerol, crosses for DES1, and black circles for DES2).

For comparison, correlation lengths of typical microemulsion systems are of the same order of magnitude, i.e. ranging from one to few nanometers. However, typical microemulsions are characterised by a liquid order peak due to the presence of a sharp interface and repulsions between the water or oil droplets. This peak is lacking here.

SAXS experiments prove and confirm the existence of a nano-clustering near the demixing boundary for these types of system, in the pre-Ouzo zone. This nano-structuring is less and less pronounced when the composition is farther away from the demixing boundary. However, it is important to show that nano-structures can be present in a deep-eutectic system without using a surfactant.

3.1.2.4. Conclusion

In this paper we investigated the presence of a nano-structuring in the pre-Ouzo zone for water-free and surfactant-free green microemulsions. The three investigated systems, one containing glycerol, and two others using DESs, meet the requirements of the Ouzo effect in the biphasic zone and present similar phase diagrams. DLS as well as SAXS experiments were carried out in the pre-Ouzo region. Well-defined time-correlation functions appeared in the pre-Ouzo region and even far from the demixing boundary. These results combined with the SAXS measurements show the presence of spatial fluctuations. These aggregate fluctuations are independent of molecular critical fluctuations which can appear near a critical point. It should be pointed out that this is also the first time that microemulsions were formulated using DES instead of water.

The obtained results confirm previous studies from our group where such fluctuations were observed in aqueous system also fulfilling all the required conditions for the Ouzo effect.[88, 191, 192]

This paper aims at proving that the pre-Ouzo effect is general and independent of the presence of water. The lack of 1-octanol in the systems containing DESs also demonstrates that the amphiphilic character of 1-octanol is not responsible of these fluctuations, and thus, a general behaviour can be postulated. However, we cannot exclude that this general behaviour, i.e. the presence of a nano-clustering in the pre-Ouzo region, may depend on the presence of hydrogen bonds between the molecules. These bonds were present in all the investigated systems and hence, further studies are now necessary to check this point.

It exists also an interest for studying such a structured non-aqueous solvent in a ternary system as a medium for nanoparticles synthesis when these nanoparticles are sensitive to water hydrolysis or oxidation.[193] However, this research belongs to another approach.

3.1.3. Nano-droplet formation in fragrance tinctures

Please note that this work was carried out before the studies investigating the nano-structures of surfactant-free microemulsions. At this time, the fact that there was a slight accumulation of ethanol at the interface or that the structures were fluctuating and were not spherical was still unknown. However, this does not change the conclusions of this work.

3.1.3.1. Abstract

As explained in the *Fundamentals* part and in section 3.1.2, it was recently shown that water/ethanol/long-chain alcohol mixtures and surfactant-free and water-free microemulsions can be significantly structured in a wide range of compositions. This work is an extension of these studies and suggests that some formulated products on the market correspond to these mixtures. We consider the domains of existence of the clear and homogeneous phase of four water/ethanol/perfumery molecule systems, the perfumery molecules being citronellol, citral, geranyl acetate and limonene, as they can be found in perfumery formulations. Dynamic and static light scattering experiments reveal also the presence of nano-droplets in these ternary tincture systems. Based on these results the presence of nano-droplets can be expected in Eau de Toilette, Eau de Parfum, and possibly in perfumes.

3.1.3.2. Introduction

A tincture is a solution in which the solvent is an alcohol, most of the time, ethanol. Alcoholic tinctures have an ethanol percentage of at least 40-60 wt%. They are advantageous because ethanol can dissolve compounds which are only slightly soluble in water, such fragrance molecules. Tinctures are widely used and form the base of hydroalcoholic formulations produced in perfume industry. Different types of tinctures exist regarding their compositions. As shown in **Figure 3.15**, perfumes contain usually between 15 and 40 wt% of perfumery compounds for an amount of ethanol (96% in concentration) between 60 and 85 wt%. Eau de Parfum is composed of 10-20 wt% of fragrances dissolved in a mixture of ethanol/water, where the amount of ethanol is generally higher than the amount of water. Eau de Toilette contains 5-15 wt% of perfumery compounds, but in this case the amount of water is higher than the amount of ethanol. Thus, the fragrance of Eau de Parfum lasts longer than Eau de Toilette. Between 3 and 8 wt% of perfumes are present in Eau de Cologne, a registered trademark using 70-80 wt% of ethanol in the formulation. Finally, aftershaves contain 1-3 wt% of fragrances for around 40 wt% of ethanol. It should be mentioned that these compositions may vary from product to product.

In industry, tinctures can find other applications. As an example, Arce *et al.* showed that the formulation of essential oil tinctures can be also used for deterpenation.[194] They explained that for deterpenation of a citrus essential oil with ethanol/water mixtures as solvent, high proportion of ethanol in solvent and low essential oil:solvents ratio should be used.

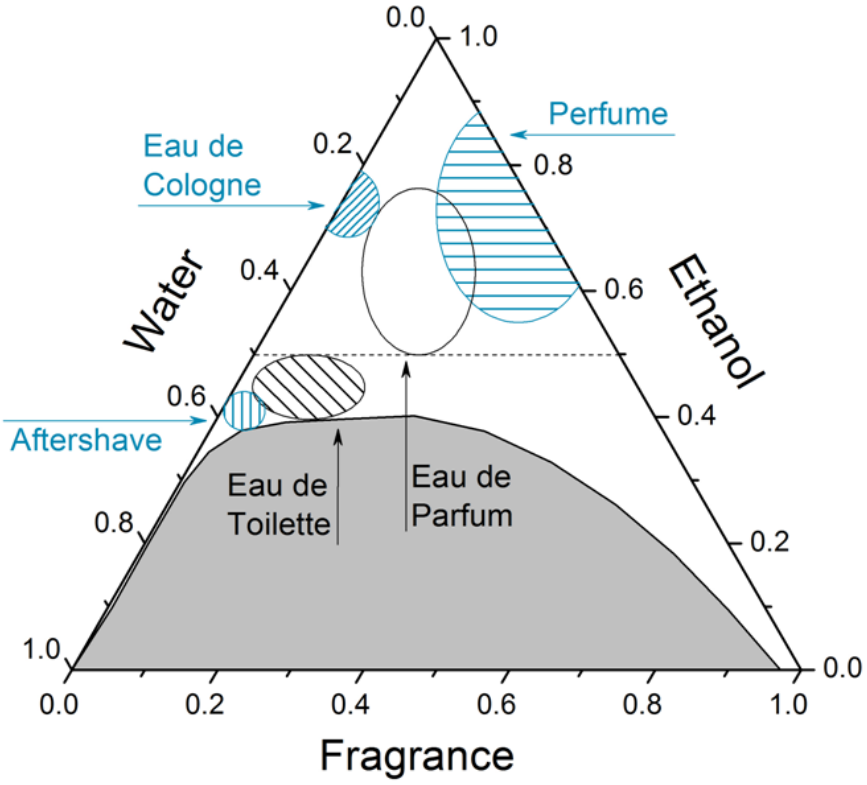

Figure 3.15. Ternary phase diagram showing the different types of fragrance tinctures and their locations on the diagram. The grey area is a multiphasic domain, the white area is a monophasic domain and hatched areas are compositions of different perfume formulations.

Recently we showed that nano-structures exist in monophasic water/ethanol/1-octanol mixtures.[88] As a consequence, the question of the existence of such nano-structures in perfume tinctures is raised. To answer this question we formulate tinctures with four different molecules: citronellol, citral, geranyl acetate and limonene, respectively an alcohol, aldehyde, ester, and terpene. These four compounds are representative of the main types of functionalised molecules present in essential oils and perfumes.[195-198] First, the influence of these compounds on the domains of existence of the clear single phase area (tincture) for the water/ethanol/perfumery molecule systems is studied using ternary phase diagrams. And second, DLS and SLS experiments are performed in these single phase regions to investigate the presence of a nano-ordering.

3.1.3.3. Results and discussion

3.1.3.3.1. Ternary phase diagrams

The four ternary phase diagrams water/ethanol/perfumery molecule are represented in **Figure 3.16**. A common trend can be observed, and two different areas can be found in each diagram. On the one hand, a clear translucid single phase is obtained in the upper part of the diagram. On the other hand, a turbid two-phase zone, represented in grey, is observed in the lower part. The largest single phase area is obtained with citronellol, followed by citral and geranyl acetate (see **Figure 3.16**.1 – 3).

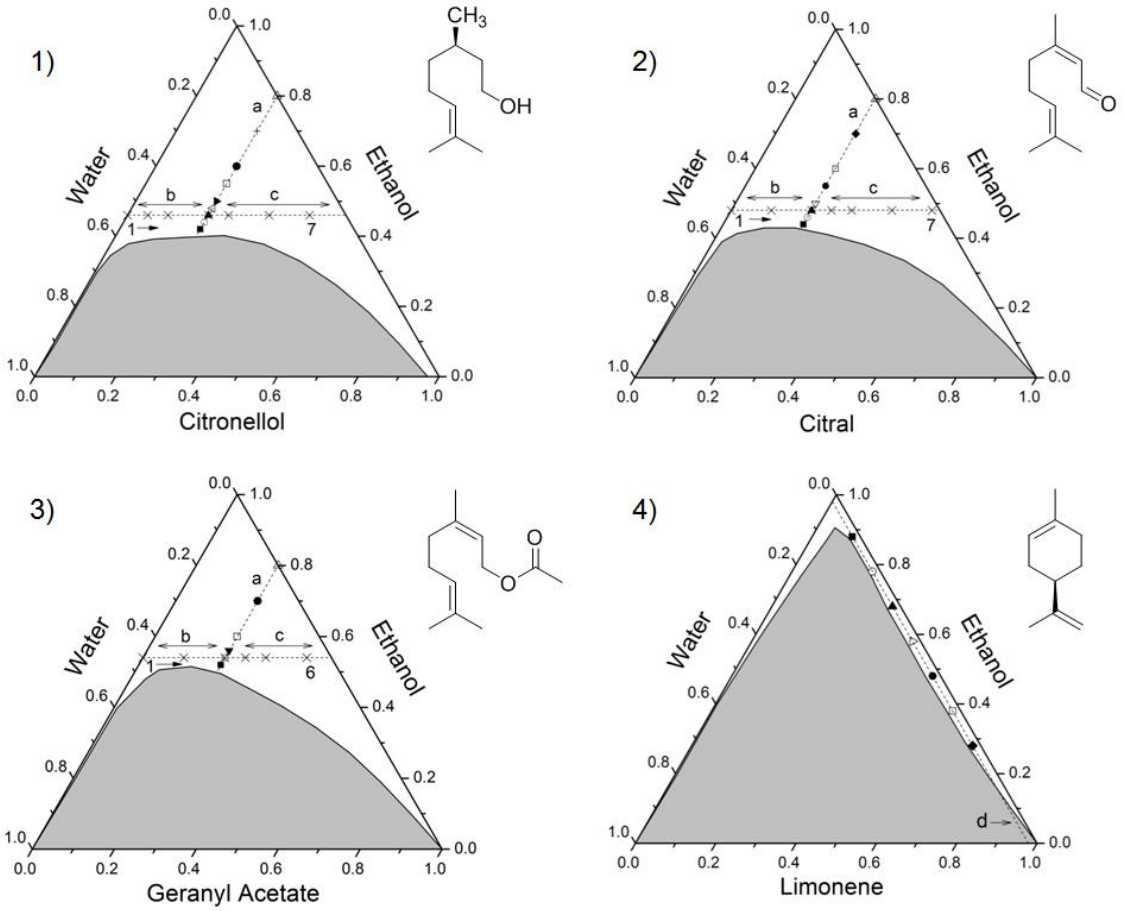

Figure 3.16. Ternary phase diagrams in weight fraction of the systems water/ethanol/perfumery compound where perfumery compounds are 1) citronellol; 2) citral; 3) geranyl acetate; 4) limonene, at 25 °C. The grey area corresponds to the bi- or multiphasic domain, the white area to the monophasic region. DLS experiments were carried out along paths a, b, c, and d and SLS experiments were performed along paths b, c, and d.

Above a certain quantity of ethanol (41 wt% for citronellol, 45 wt% for citral and 53 wt% for geranyl acetate), a monophasic area is obtained for every water/ethanol ratio. However, 90 wt% of ethanol is necessary to obtain this single phase area when limonene is used as the oil phase (see

Figure 3.16.4). It can be noted that the system water/ethanol/citronellol is very similar to the one with octanol, previously studied by our group.[88] The domain of the clear and homogeneous phase is however slightly larger for octanol.

3.1.3.3.2. Light scattering experiments

DLS measurements were performed following two different paths for the systems containing citronellol, citral and geranyl acetate. As shown in **Figure 3.16**, the mass percentage of the perfumery compound is constant on path a, and the mass percentage of ethanol is constant along paths b and c (c being a prolongation of path b). First of all, a common trend can be observed on path a for these three systems. The correlation becomes more and more pronounced the closer the formulation is to the demixing boundary (see **Figure 3.17**.1a – 2a – 3a). A pronounced and well defined correlation function is a first hint at the presence of nano-droplets. The characteristic dynamic sizes ξ_D were calculated from DLS measurements assuming a spherical geometry. The size of particles, calculated from only well-defined correlation functions, increased along path a to end up at 2.5 nm for citronellol, 2.62 nm for citral and 1.50 nm for geranyl acetate. Another common trend can be observed along paths b and c, see respectively **Figure 3.17**.1b – 2b – 3b and **Figure 3.17**.1c – 2c – 3c. Measurements were carried out every 5 wt% of perfumery compound, but only certain points are plotted for clear visual representation. No structures were found in the starting water/ethanol formulations for any of the three systems, but correlation functions progressively developed along the composition line (path b). Then, the correlation became less pronounced, which indicates a loss of nano-organisation in the tinctures (path c). It should be stressed that this is not a critical phenomenon with large fluctuations close to a critical point, because even far from the phase separation nano-droplets clearly occurred. This fact was checked in section 3.1.2 for surfactant-free and water-free microemulsions.

In the case of limonene, DLS measurements were carried out along path d (see **Figure 3.16**.4), where the mass percentage of water is constant. As shown in **Figure 3.17**.4, the correlation became more and more pronounced with increasing amount of limonene in the solution. The characteristic dynamic aggregate size ξ_D also increased along path d to end up at 2.24 nm with 70 wt% of limonene in the solution. As the scan is made much closer to the demixing boundary, critical fluctuations may occur.

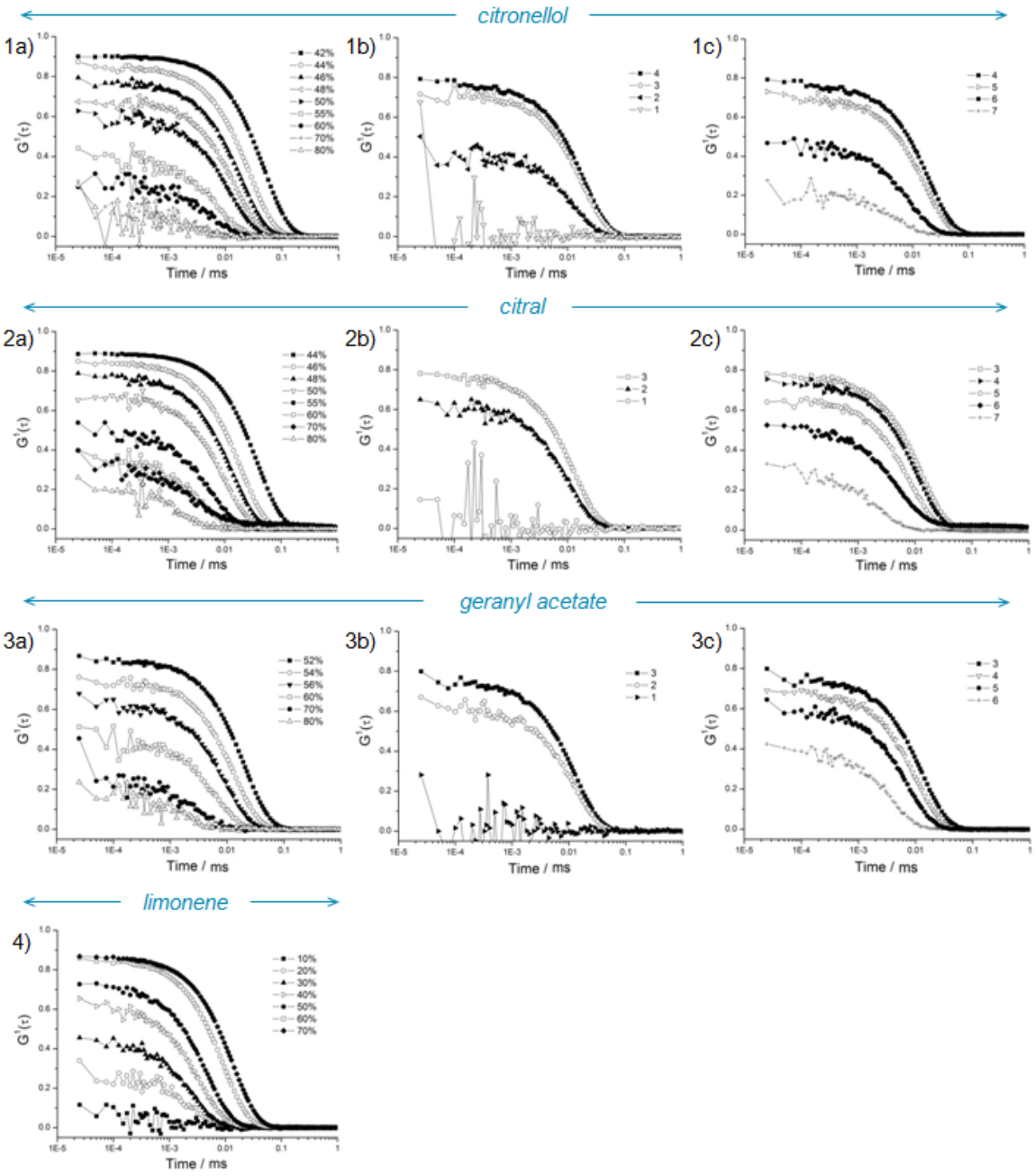

Figure 3.17. Time-dependent self-correlation functions as obtained by DLS for the systems water/ethanol/perfumery compounds, where the perfumery compounds are 1a) – 1c) citronellol; 2a) – 2c) citral; 3a) – 3c) geranyl acetate; 4) limonene, at 25 °C. For 1a, 2a and 3a the mass percentage of perfumery compound is constant (path a), the legend corresponds to the mass percentages of ethanol in the formulations. The symbols correspond to the ones on the phase diagrams for the corresponding systems. For 1b, 2b and 3b the mass percentage of ethanol is constant (path b). For 1c, 2c and 3c the mass percentage of ethanol is constant (path c). For 4) the mass percentage of water is constant (path d) and the legend corresponds to the mass percentage of limonene in the formulations. The symbols are the same as in **Figure 3.16**.4.

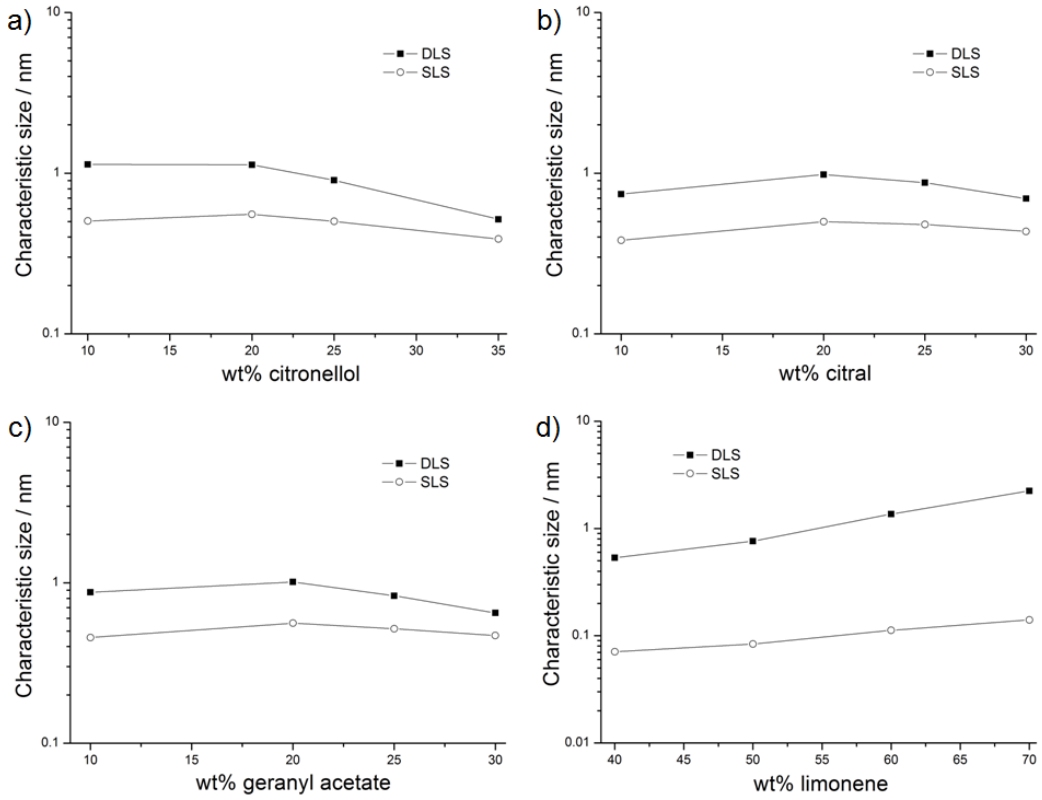

Figure 3.18. Estimated characteristic dynamic (from DLS) and static (inferred from the apparent masses from SLS) size of scattered objects in nm versus the weight percentage of a) citronellol; b) citral; c) geranyl acetate and d) limonene, assuming spherical geometry. Measurements were carried out on paths b and c for citronellol, citral and geranyl acetate and path d for limonene (see **Figure 3.16**). DLS is represented with black squares, SLS with open circles.

However, DLS is not enough to validate the spherical geometry. Thus, SLS measurements were performed along paths b and c for citronellol, citral and geranyl acetate, and on path d for limonene. **Figure 3.18** shows the characteristic dynamic sizes calculated from DLS and the static sizes inferred from the apparent masses as determined with SLS, only for well-defined correlation functions. The difference between the sizes calculated at three different angles with SLS is around 1% for the four systems. This result shows that there is no angle dependence and confirms that the measured sizes come from the objects present in the tincture and not from critical fluctuations. Almost all object sizes are smaller than 1 nm for both methods for the systems with citronellol, citral, and geranyl acetate. We would not call these objects micelles as in the presence of surfactants, but rather small nano-droplets. The object sizes calculated with DLS and SLS experiments are close for citronellol, citral and geranyl acetate, a result that suggests a low polydispersity, while the relatively different sizes resulting from the two scattering techniques for limonene suggest a higher polydispersity. The low polydispersity is confirmed with the DLS curves as the polydispersion index is smaller than 0.1 for all formulations.

From the correlation functions of citronellol and citral along path b (**Figure 3.17**.1b – 2b) and **Figure 3.15**, it can be inferred that nano-droplets are probably present in Eau de Toilette. The correlation functions of citronellol, citral, and geranyl acetate on path a show that nano-droplets start appearing at the beginning of the Eau de Parfum area, i.e. at 60-65 wt% of ethanol. The correlation becomes more and more pronounced in this zone when the percentage of ethanol decreases. At the bottom of the Eau de Parfum area, i.e. at 50-55 wt% of ethanol, defined correlation functions are found. Almost no structures are present in the perfume area, at the beginning of path a for the systems with citronellol, citral, and geranyl acetate. However, nano-droplets appear along path d when the mass percentage of limonene increases. Nano-droplets can then form when the perfume becomes more hydrophobic.

Of course, from light scattering alone it is difficult to say more about structuring. However, these systems are conceptually similar to the ones described by Diat *et al.*[90] and Schöttl *et al*.[91] and to others for which more detailed information is available.[70, 71, 75] The composition of these nano-droplets should be the same as those described in these works, i.e. an inner organic-rich phase (composed essentially of ethanol and perfumery molecules) in a water-rich bulk phase with a slight accumulation of ethanol at the interface.

3.1.3.4. Conclusion

In this paper we investigated the presence of nano-droplets in perfume tinctures, where four different perfumery molecules were solubilised. The clear and homogeneous single phase was found to be large for citronellol, citral and geranyl acetate solutions, but very small for limonene mixtures. DLS and SLS showed that well-defined correlation functions were found even far away from the demixing boundary, which is a hint at the appearance of nano-droplets that are independent of critical fluctuations. They appear to be too small to be comparable to surfactant micelles. From our model formulations nano-droplets can be predicted in Eau de Toilette and Eau de Parfum. Further, they can possibly appear in perfumes in presence of very hydrophobic fragrance molecules. Their presence may affect the chemical and biological stability of fragrance molecules in such hydroalcoholic solutions and could be used as micro-reactors for transformation of one fragrance molecule into another one. The nano-droplets may also have a significant influence on the vapour pressures of the different components and on the performance of the tincture. These aspects were investigated by Tchakalova *et al.*[94] and are discussed in more details in the *Fundamentals* part of this thesis, see section 1.2.3.3.

3.1.4. Nano-droplet formation in water/ethanol or isopropanol/mosquito repellent formulations

Please note that this work was carried out before the studies investigating the nano-structures of surfactant-free microemulsions. At this time, the fact that there was a slight accumulation of ethanol at the interface or that the structures were fluctuating and were not spherical was still unknown. However, this does not change the conclusions of this work.

3.1.4.1. Abstract

It was recently demonstrated that nano-structures were present in water/ethanol/oil systems, where the oil was either octanol (see the *Fundamentals* part) or fragrance molecules (see section 3.1.3). Such nano-structures also exist in more complicated systems, involving for example glycerol or deep eutectic solvents (see section 3.1.2). The goal of the present work is to check if such structures exist also in other, related systems and if a general concept can be deduced from these observations. To this purpose, natural and synthetic mosquito repellent molecules were investigated, which represent nearly all repellents used on the market. For the ternary water/alcohol (ethanol or isopropanol)/repellent systems ternary phase diagrams were established. The presence and the ordering of the nano-droplets were checked and characterised with dynamic and static light scattering and conductivity measurements. Based on these results it can be concluded that a nano-ordering with generally an organic continuum exists in hydro-alcoholic commercial mosquito repellents, and thus that these systems are not simply molecular solutions. This might have a consequence for diffusion processes in the skin.

3.1.4.2. Introduction

All around the world mosquitoes are the carriers of serious and lethal diseases, such as malaria, dengue, West Nile virus, yellow fever, and chikungunya.[199, 200] According to the World Health Organisation, 247 million malaria infections occurred in 2008 causing the death of 863,000 people, mainly children under the age of 5.[201] Further, due to global warming, more and more species of mosquitoes carry such diseases.[202] Since the different pathogens are transmitted by injection of saliva into humans,[203] the main protection is to prevent bites by minimizing contacts between the mosquitoes and their targets. In order to reach this goal, mosquito repellents are investigated and used worldwide, because they prevent mosquitoes from landing on humans and biting them.

Before the discovery of synthetic insecticides, natural products, for example nicotine from tobacco leaves, proved their efficiency against mosquitoes.[204] Nowadays, natural repellents are still used, such as citriodiol, *para*-menthane-3,8-diol (PMD), and 2-undecanone. Citriodiol is obtained by cyclisation of the citronellal from *Eucalyptus citriodora* oil (oil of lemon eucalyptus) in acid medium. This oil is obtained by hydrodistillation and can be then considered as an essential oil where citronellal is present at about 80 wt%. The tree was originally found in Australia and is now cultivated in warm places around the world, like Malawi by the firm *Citrefine International Ltd.*, which produces a melt of 60-70 wt% of *cis*- and *trans*-PMD, acetals from PMD, and residual non-reactive terpene and terpenoid molecules.[205]
Mosquito repellents can be formulated either by using directly the citriodiol or the pure PMD (cis and trans isomers) synthesised by the firm *Takasago International Corporation*.
2-undecanone is obtained from a selective separation of rue (*ruta graveolens*) essential oil, its proportion being around 50 wt%.[206] Rue is a very common plant, which is native to the Balkan Peninsula and southeastern Europe.

Synthetic mosquito repellents, not found in nature, are also used, such as *N*,*N*-diethyl-*m*-methylbenzamide (DEET), 1-methylpropyl 2-(2-hydroxyethyl)piperidine-1-carboxylate (KBR 3023) and ethyl 3-[(acetyl)(butyl)amino]propanoate (IR 3535). DEET was first used in 1946 by the United State Army and entered civilian use in 1957. It is now the most widely used insect repellent. Its effectiveness was proven against a lot of insects, including mosquitoes, black flies, ticks and bedbugs.[201]

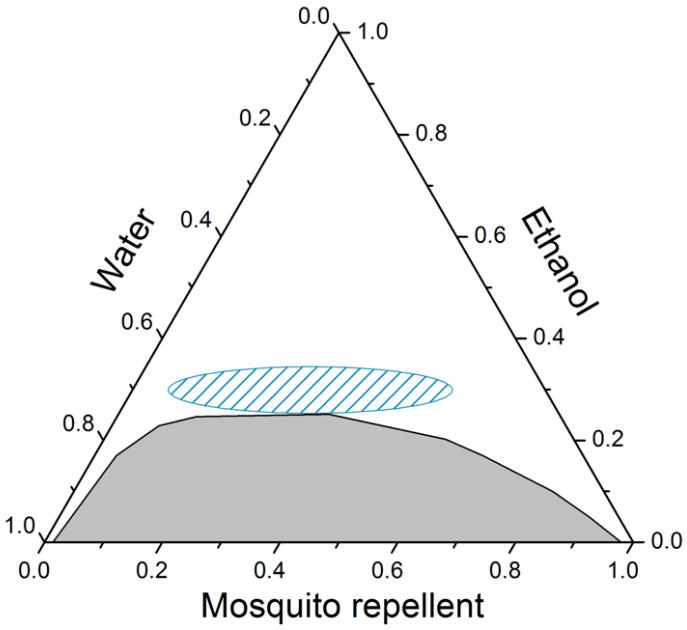

Figure 3.19. Ternary phase diagram showing the solubilisation area of mosquito repellents as it is commonly formulated (hatched area). The grey area is a multiphasic domain, the white area is a monophasic domain.

The only mosquito repellent more effective than DEET is KBR 3023, which was developed in the mid-1990s by Bayer and first used in Europe in 2001 with a 7 wt% solution or with a 20 wt% solution by the Australian Army.[207]

IR 3535 was developed by the firm Merck KGaA and is classified by the Environmental Protection Agency as a biopesticide. It has been used in Europe for more than 20 years and was approved for use in the United States in 1999.[208]

Almost all mosquito repellent products available on the market are hydro-alcoholic formulations, incorporating water, ethanol and/or isopropanol, and a repellent or a melt of them. As shown in **Figure 3.19**, mosquito repellents contain generally between 10 and 50 wt% of repellent and the minimum quantity of ethanol or isopropanol necessary to solubilise this molecule.

Drapeau *et al*. showed the possibility to obtain a surfactant-free microemulsion in the water (42 wt%)/isopropanol (38 wt%)/PMD (20 wt%) system,[200] Klossek *et al.* found the presence of nano-structures in the system water/ethanol/1-octanol by DLS,[88] and we extended these studies and found these nano-structures in systems containing fragrance molecules (see section 3.1.3).[192] Therefore, the presence of similar nano-structures in the system water/ethanol/repellent appears very probable. The aim of the present work is to check this point.

First, the influence of the mosquito repellent molecules on the domains of existence of the clear and single phase area of the water/ethanol or isopropanol/repellent systems is studied by establishing ternary phase diagrams. And second, DLS and SLS are performed in these single phase regions to investigate the presence of a nano-ordering.

3.1.4.3. Results and discussion

3.1.4.3.1. Ternary phase diagrams

The repellents used in this study represent nearly all the used insecticides available on the market, i.e. natural repellent molecules, such as citriodiol, PMD and 2-undecanone, and synthetic molecules, such as DEET, KBR 3023, IR 3535 (for molecular structures, see respectively **Figure 3.20**.1a, 2a and 3a, and **Figure 3.21**.1a, 2a and 3a). The ternary phase diagrams water/alcohol (ethanol or isopropanol)/repellent are represented in **Figure 3.20** (1b, 2b and 3b) for natural mosquito repellents. Note that the alcohol used to solubilise citriodiol was isopropanol. A common trend can be noted for all the diagrams. In the upper part of the phase diagrams a clear and homogeneous monophase is observed. On the contrary, a cloudy multi-phase area is obtained in the lower part of the diagrams. The phase diagrams for citriodiol and PMD look very similar, even if isopropanol is used instead of ethanol to solubilise the repellent. As citriodiol is composed of 73 wt% of *cis*- and *trans*-PMD the phase behaviours are nearly the same and the residual molecules do not play an important role. It can be pointed out that the alcohol does not

considerably change the phase behaviours. The one-phase region for 2-undecanone is smaller than the corresponding ones for citriodiol and PMD.
The ternary phase diagrams water/ethanol/repellent are represented in **Figure 3.21** (1b, 2b and 3b) for synthetic mosquito repellents. First, the same trend as for natural repellents can be observed for synthetic insecticides, i.e. a clear and homogeneous one-phase domain in the upper part of the diagram and a turbid multi-phase region in the lower part of the diagram. The largest translucid area is obtained for IR 3535. The translucid domains are practically the same for DEET and KBR 3023.

3.1.4.3.2. Light scattering experiments

DLS measurements were carried out with constant ethanol or isopropanol contents for the systems with citriodiol, PMD, DEET, KBR 3023 and IR 3535, respectively 45, 35, 30, 30 and 15 wt%.

Measurements were performed every 10 wt% of PMD, DEET, KBR 3023 and IR 3535 and every 5 wt% of citriodiol to show a more accurate evolution of the correlation function (see **Figure 3.20**.1c, 1d; 2c, 2d; and **Figure 3.21**.1c, 1d; 2c, 2d; and 3c, 3d). As shown in **Figure 3.19**, the measurements were performed in the area where mosquito repellents are formulated.
Common observations can be made for all the systems. Pronounced correlation functions are already obtained with low repellent content, i.e. around 10 wt%, which is a first hint at the presence of nano-droplets. The correlation functions progressively develop with increasing repellent molecule content until those functions reach a maximum around 20-30 wt% of oil, the percentage where the nano-structures are the biggest (see **Figure 3.20**.1c, 2c; and **Figure 3.21**.1c, 2c and 3c). The characteristic dynamic sizes ξ_D are calculated from DLS measurements assuming spherical geometry. With 20 wt% of oil in the formulations, the calculated sizes are 1.17 nm for citriodiol, 2.16 nm for PMD, 1.54 nm for DEET, and 2.01 nm for KBR 3023. The biggest size is obtained with 30 wt% of IR 3535 in the solution and is equal to 2.37 nm. Then, the correlation becomes less pronounced, which indicates a loss of nano-organisation in the solution (see **Figure 3.20**.1d, 2d; and **Figure 3.21**.1d, 2d and 3d). The sizes are equal to 0.79 nm with 30 wt% of citriodiol, 0.81 nm with 40 wt% of PMD, 0.54, 0.39, and 0.75 nm with 50 wt% of respectively DEET, KBR 3023, and IR 3535. Nearly no structures are found when 45 wt% of citriodiol, 60 wt% of PMD or 70 wt% of IR 3535 are involved in the formulations. As it can be seen in **Figure 3.21** (1d and 2d), no structures are obtained in pure ethanol/DEET or ethanol/KBR 3023 formulations.

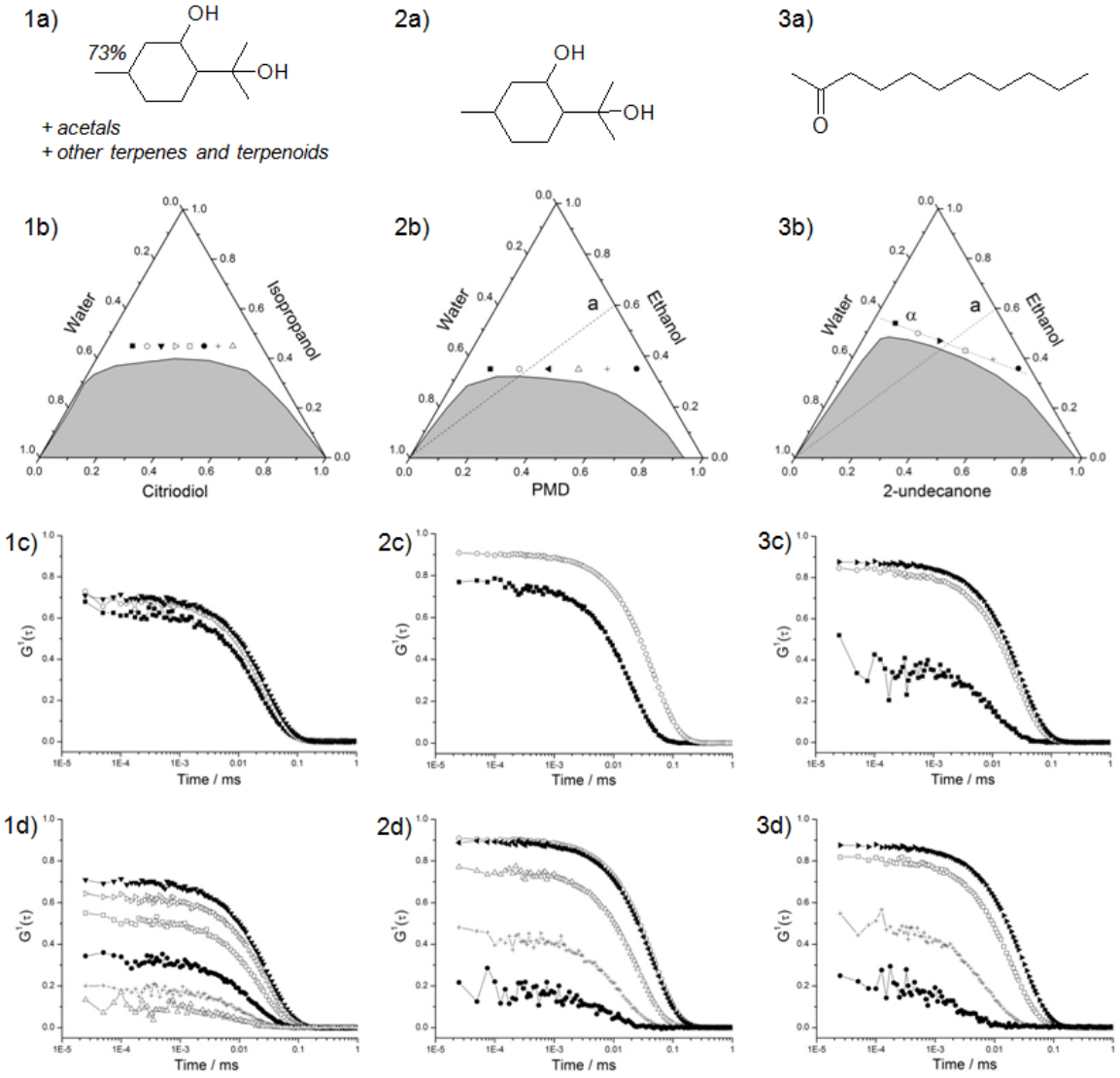

Figure 3.20. Molecular structures, phase diagrams in weight fraction and time-dependent self-correlation functions as obtained by DLS for the *natural* mosquito repellent systems water/ethanol or isopropanol/repellent, where the repellent is 1a)-1d) citriodiol with isopropanol; 2a)-2d) PMD with ethanol; and 3a)-3d) 2-undecanone with ethanol, at 25 °C. The grey area corresponds to the bi- or multiphasic domain, the white area to the monophasic region. The symbols on the DLS curves correspond to the ones on the phase diagrams for the corresponding systems. DLS measurements were carried out on path α for 2-undecanone. Pictures 1c, 2c, 3c correspond to the area where correlation functions become more and more pronounced with increasing oil content, whereas figures 1d, 2d, 3d show the auto-correlation functions along the points in figures b in the region where they become less and less pronounced with still increasing oil content. Conductivity measurements were carried out along path a for the PMD and 2-undecanone systems.

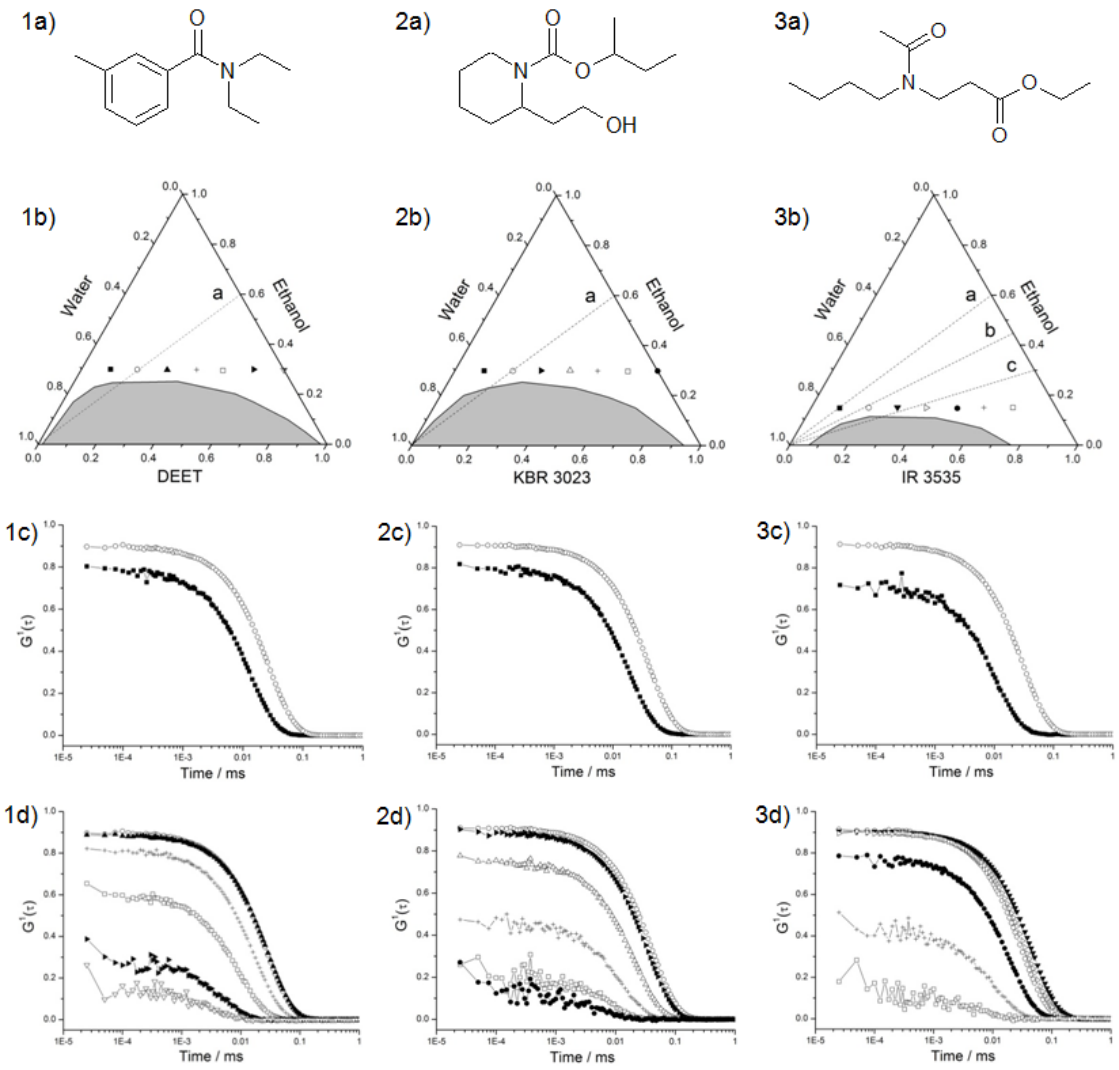

Figure 3.21. Molecular structures, phase diagrams in weight fraction and time-dependent self-correlation functions as obtained by DLS for the *synthetic* mosquito repellent systems water/ethanol/repellent, where the repellent is 1a) – 1d) DEET; 2a) – 2d) KBR 3023; and 3a) – 3d) IR 3535, at 25 °C. The grey area corresponds to the bi- or multiphasic domain, the white area to the monophasic region. The symbols on the DLS curves correspond to the ones on the phase diagrams for the corresponding systems. Pictures 1c, 2c, 3c correspond to the area where correlation functions become more and more pronounced with increasing oil content, whereas figures 1d, 2d, 3d show the auto-correlation functions along the points in figures b in the region where they become less and less pronounced with still increasing oil content. Conductivity measurements were carried out along path a for the DEET and KBR 3023 systems, and along paths a, b, and c for the IR 3535 system.

For 2-undecanone, DLS measurements are carried out along path α (see **Figure 3.20**.3b) in order to stay close to the phase boundary. However, the same observations are made. A nano-ordering starts to appear at the beginning of path α and the correlation becomes more and more pronounced with increasing amount of 2-undecanone in the solution (see **Figure 3.20**.3c). The biggest size is then equal to 2.21 nm in radius with 27 wt% of 2-undecanone. Then, as it can be seen in **Figure 3.20**.3d and already observed for the other molecules, the correlation becomes less developed and nearly no structures can be observed at the end of path α.
The presence of these nano-structures is not a critical phenomenon with large fluctuations close to a critical point, because even far from the phase boundary nano-droplets are clearly observed, for example with 60 wt% of IR 3535. This fact was checked in section 3.1.2 for surfactant-free and water-free systems.

However, as only fluctuations in local concentrations are detected with DLS, the interpretation of spherical un-connected domains is arbitrary and DLS results taken alone are not a definitive argument.[88] Thus, in order to validate the spherical geometry, SLS measurements were carried out with the same ethanol or isopropanol contents as DLS and along path α for 2-undecanone. The presence of well-defined droplets was confirmed with the characteristic static sizes calculated from SLS which are in rough agreement with those found from DLS.[88] **Figure 3.22** shows the characteristic dynamic sizes calculated from DLS and the static sizes inferred from the apparent masses as determined with SLS as a function of the repellent molecule weight percentage. The sizes are calculated only for the well-defined correlation functions. The difference between the sizes calculated for the SLS results at 45°, 90°, and 135° is around 1% only, which confirms the fact that the measured sizes come from objects present in the formulations, and not from critical fluctuations, because there is no angle dependence.

From both types of experiments it can be concluded that the sizes of the nano-structures increase to reach a maximal size, generally bigger than 1 nm, and then decrease with increasing oil concentration. It can be noted that the object sizes measured with DLS and SLS are close for the six systems, which suggests a low polydispersity.
From these results and **Figure 3.19** it can be inferred that nano-structures can be found in mosquito repellent formulations available on the market.

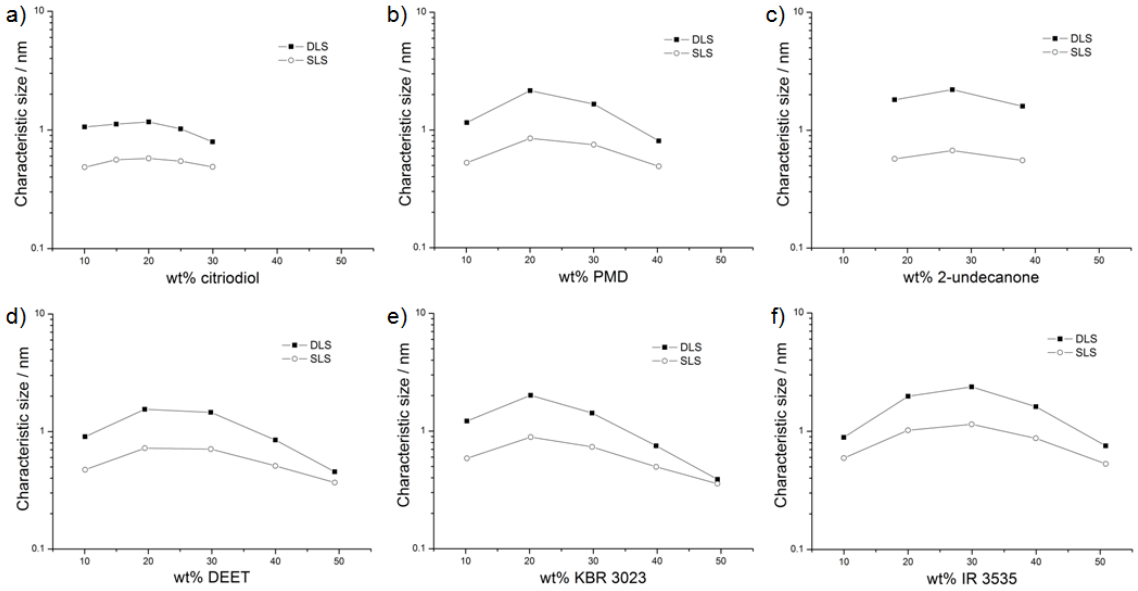

Figure 3.22. Estimated characteristic dynamic (from DLS) and static (inferred from the apparent masses from SLS) size of scattered objects in nm versus the weight percentage of the repellent in the formulation for the water/ethanol or isopropanol/repellent systems, where the repellent is a) citriodiol; b) PMD; c) 2-undecanone; d) DEET; e) KBR 3023; f) IR 3535, at 25 °C and assuming spherical geometry. DLS is represented with black squares, SLS with open circles.

3.1.4.3.3. Conductivity measurements

Conductivity measurements were carried out on path a for the systems with PMD, 2-undecanone, DEET, KBR 3023 (see **Figure 3.20** and **Figure 3.21**) and on paths a, b, and c for the system with IR 3535 as oil (see **Figure 3.21**.3b). The aim was to observe the pseudo-phase inversion from an organic to an aqueous continuum for the formulations studied in DLS and SLS.

The conductivity curves plotted in **Figure 3.23** exhibit the same behaviour for all the systems. The conductivity values start between 500 and 900 $\mu S.cm^{-1}$, respectively for PMD and IR 3535, with no water in the system. Then, the conductivity increases until a maximum when water is added. The high initial conductivity is due to the fact that LiCl is highly soluble in organic phases. The increase of the conductivity is due to an even better solubility and a pronounced ion dissociation in presence of water. The constantly increasing conductivity demonstrates the presence of an organic continuum without dilution of the charge. A water continuum would lead to a decrease of the conductivity. That means that DLS and SLS were measured for formulations having an internal aqueous phase.

However, the conductivity starts to decrease for IR 3535 when 60 wt% of water is involved in the system and reaches 200 $\mu S.cm^{-1}$ when more than 97 wt% of water are added (see **Figure 3.23**.a and b). According to the results it can be said for the IR 3535 system that the continuum is organic, as previously explained, until the curve slope becomes equal to zero. Then, the decrease of the conductivity is due to the dilution of charges, which indicates that the continuous medium

is water from 60 wt% of water on path a. As shown in **Figure 3.23**.b, the conductivity behaviour and thus the continua are different along the three different paths. The same conclusions as for path a can be drawn for path b, whereas the continuum is still organic at the end of path c. DLS and SLS measurements were then carried out with an external phase composed of either water (paths a and b) or oil (path c). Mosquito repellents formulated with IR 3535 in defined proportions are then the only ones with an aqueous external phase.

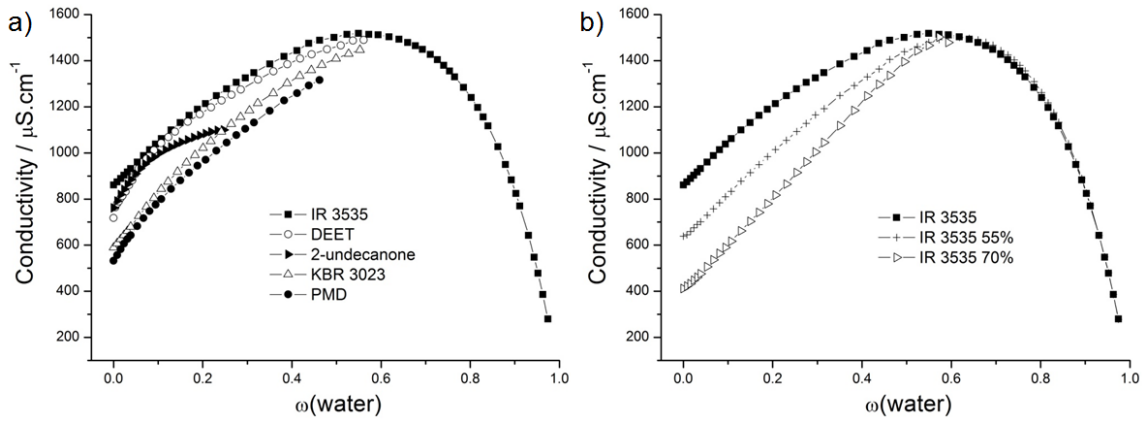

Figure 3.23. a) Conductivity in $\mu S.cm^{-1}$ as function of the mass fraction of water in the water/ethanol/repellent systems, where the repellent is IR 3535 (black squares), DEET (open circles), KBR 3023 (open triangles), PMD (black circles), or 2-undecanone (black triangles), along path a at 25 °C; b) Conductivity in $\mu S.cm^{-1}$ as function of the mass fraction of water in the water/ethanol/IR 3535 system, along path a (black squares), path b (crosses), or path c (open triangles) at 25 °C.

3.1.4.3.4. Influence of chemical groups

The presence of nano-structures in water/ethanol or isopropanol/oil systems was investigated with different oils containing different chemical groups. Nano-structures have been found before for systems where the oil phase was a primary alcohol (citronellol), a conjugated aldehyde (citral), an ester (geranyl acetate), and a terpene (limonene), see section 3.1.3.[192] Such structures were also observed in water-free and surfactant-free microemulsions with diethyl adipate as oil phase and with glycerol and deep eutectic solvents (see section 3.1.2). More systems and more chemical groups were investigated in the present work. The presence of nano-structures can now be extended to systems where a diol (citriodiol and PMD), a ketone (2-undecanone), an amide (DEET), and oils containing different nitrogen groups (KBR 3023 and IR 3535) are used as oil phase. It can be pointed out that nano-structures are present in all these systems, independently of the used oil and of the chemical groups present in the fragrance molecules or mosquito repellents. The presence of nano-structures in such systems can be generalised as it does not depend on the oil type or on the chemical groups present. A nano-structuring can be observed even with molecules having a complex chemical structure, such as KBR 3023 or DEET.

3.1.4.4. Conclusion

In this work the presence of nano-structures in various hydro-alcoholic mosquito repellent formulations was investigated. The natural repellents were citriodiol, a mixture of *cis*- and *trans*-PMD with acetals, terpenes, and terpenoids, PMD, and 2-undecanone, whereas the synthetic insecticides were DEET, KBR 3023, and IR 3535. The clear and homogeneous one-phase domains have a similar extension for the six systems. The largest area was found for IR 3535, the smallest one for 2-undecanone. DLS and SLS measurements showed that correlation functions developed near the phase separation to reach a maximum and then decreased when more repellent is added in the formulation. As already explained, these nano-droplet formations are not due to critical molecular fluctuations. Conductivity measurements showed that the inner phase of these nano-droplets is composed of water, except for the lowest concentrations of IR 3535 where an aqueous external pseudo-phase exists. The composition of the pseudo-phases have to be investigated but might be the same as in the works of Diat *et al.*[90] and Schöttl *et al.*[91] even if the inner phase is aqueous. The inner aqueous phase is surrounded by the organic-rich pseudo-phase with a slight accumulation of ethanol at the interface.

The used repellents represent practically all the ones that are commercially used to formulate mosquito repellents. So we can conclude that nano-droplets can also be found in such products available on the market. Note that such a nano-structuring may have an impact on the behaviour of such products on the skin. For example, the real concentration of the active substance on the skin may be different as well as its diffusion into the upper skin layers. Also the influence of the outer pseudo-phase and of the repellent on the mosquito receptors may depend on this structuring.

This work was an extension of previous papers of our group aiming at generalizing the concept of finding nano-structures in hydro-alcoholic solutions when the solubilised molecule is co-soluble with ethanol or isopropanol and slightly soluble with water.[88, 192] We showed that concept with and without octanol (see section 3.1.2) and fragrance molecules (see section 3.1.3), and now with other chemical groups with more complex chemical structures. It seems as if the appearance of nano-structures is independent of the oil type. The main and perhaps only criterion is that oil and water are rendered mutually soluble by a third solvent (here alcohol).

3.2. Microemulsions with surfactants

The studies presented in this chapter led to publications which are already published or accepted, as summarized in the following table.

Subchapter	Publication
3.2.1	J. Marcus, D. Touraud, W. Kunz, **Formulation and stability of a soap microemulsion and the apparent pK_A herein**, *J. Colloid Interface Sci.*, **2013**, *407*, 382-389
3.2.2	J. Marcus, S. Wolfrum, D. Touraud, W. Kunz, **Influence of high intensity sweeteners and sugar alcohols on a beverage microemulsion**, *J. Colloid Interface Sci.*, **2015**, doi:10.1016/j.jcis.2015.08.036

3.2.1. Formulation and stability of a soap microemulsion and the apparent pK_A herein

3.2.1.1. Abstract

The influence of composition and added salts and polyols on the stability of an oil-in-water microemulsion formulation and on the apparent pK_A (apK_A) of the used oleate surfactant is investigated.

High temperature favours a decrease of the apK_A and leads to the formation of more hydrated micelles. The apK_A decreases also when the percentage of ethanol increases. Citronellol molecules do not significantly influence the apK_A at concentrations between 0 and 2 wt%. By contrast, with increasing limonene concentration, the apK_A increases.

It was observed that anions of sodium salts destabilise the microemulsion and high temperatures are needed to recover it. By increasing the concentration of NaCl, a slight increase of the apK_A is observed, which can be associated with a non-specific, electrostatic (Debye-Hückel) effect. Cations of chloride salts have different effects depending on their ability to exchange with Na^+ near the carboxylate group. Li^+, Na^+, and K^+ have apparently a salting-out effect. Tetramethylammonium chloride and choline chloride have salting-in effects until respectively 0.6 and 0.4 $mol.kg^{-1}$.

The associations of sorbitol or glycerol with ethanol lead to a salting-in effect and to a decrease of the apK_A of Na-Oleate.

3.2.1.2. Introduction

More than a century ago Hofmeister considered the influence of salts on protein solubility.[101, 142] He made a classification of salts according to their ability to salt-in or salt-out proteins. Salting-in anions enhance their solubilisation in water. They are also known as chaotropes, are weakly hydrated and strongly polarizable. On the contrary, a salting-out anion lowers the solubilisation of proteins in water. These kosmotropes are strongly hydrated and weakly polarizable.[209] The Hofmeister series for anions is, from salting-out to salting-in ions, $SO_4^{2-} < HPO_4^{2-} < CH_3COO^- < F^- < Cl^- < Br^- < NO_3^- < I^- < ClO_4^- < SCN^-$. The series for cations is reversed. From salting-out (chaotropic) to salting-in ions (kosmotropic) it is roughly $N(CH_3)_4^+ < NH_4^+ < Cs^+ < K^+ < Na^+ < Li^+ < Ca^{2+} < Mg^{2+}$. In both of the series the ions on the left side tend to precipitate proteins in water, whereas the ions on the right side solubilise the proteins.

Microemulsions are optically homogeneous mixtures of non-polar solvents and polar liquids. These are translucid and thermodynamically stable solutions obtained with a surfactant and generally a cosurfactant.[3, 4, 157] They can be the only phase (Winsor IV) of the studied system or in equilibrium with another phase (Winsor I, II and III).[12, 88, 158] According to the composition, a microemulsion can be of three types: water-in-oil, bicontinuous, or oil-in-water. Even though they are macroscopically homogeneous solutions, ordered structures can be found on the nanoscopic scale, such as dynamic spherical, non-spherical or polymer-like structures.[1, 29, 210] The surfactant and cosurfactant form always an interfacial film between the non-polar solvent and the polar liquid.

In literature only a few papers deal with the influence of Hofmeister series on microemulsions. Kabalnov *et al.* investigated the effects of inorganic salts on the phase equilibrium of the water/$C_{12}E_5$/decane system.[211] They found a regular Hofmeister series trend and explained that the salt effects on the phase equilibrium have an interfacial origin. They come from the salt depletion/adsorption at the surfactant monolayer. This is in agreement with Kunz *et al.*, who reported that each salt either adsorb at the interface between the micelles and water (salting-in) or remain strongly hydrated in the bulk (salting-out).[142] L. Romsted studied the competitive trapping of arenediazonium ions by weakly basic nucleophiles such as alcohols, urea, anionic headgroups, halide counterions, and water.[212] Their concentrations in the interfacial regions of association colloids were estimated with the chemical trapping method. In this method, product yields are proportional to the concentrations of water and other nucleophiles within the interfacial region. It was found that significant changes in interfacial water and counterion concentrations are obtained during structural transitions. They interpreted the specific ion effects on sphere-to-rod transitions of cationic amphiphiles in terms of the strengths of headgroup-counterion pairing and ion hydration interactions. Bauer *et al.* investigated the system water/dodecane/tributylphosphate (TBP)/n-octyl-β-glucoside, a sugar surfactant.[213] They observed that by replacing hexanol by

TBP, a subtle change occurred in the microemulsion structure depending on the type of added salt. Their study shows that LiCl has a kosmotropic effect and consequently that this salt is depleted from the water/oil interface. That depletion induces the transition from connected cylinders to local lamellar structure by decreasing the curvature. $LiNO_3$ is composed of a chaotropic anion and a kosmotropic cation and has a neutral Hofmeister effect and does not influence the microemulsion structure. In the ternary dimethyl-dioctadecyl-ammonium-bromide (DOAB)/n-decane/water system Murgia *et al.* found that for a microemulsion with a water/oil interface stabilised by a cationic DOAB surfactant, a small change in ionic composition of the aqueous phase changes the microstructure.[214] Nydén *et al.* studied the didodecyldimethylammonium sulfate (DDAS) and bromide (DDAB)/hydrocarbon/water systems with NMR self-diffusion.[215] For a microemulsion containing a mixture of divalent and monovalent counterions, i.e. respectively DDAS and DDAB, they found that the system changed curvature from being of the normal type in the sulfate-rich samples to the reversed type when bromide is present in excess. The ratio of the two counterions can be used to tune the curvature of the surfactant film.

The Hofmeister series concept can be transferred to microemulsions by assimilating micelles to proteins. To simplify, a salting-in salt would help hydrating the interfacial film and thus stabilise the microemulsion. A salting-out salt would dehydrate the film, making it more hydrophobic and consequently break the microemulsion. In this work, a microemulsion formulated with 10 wt% of soap as surfactant, i.e. sodium oleate (Na-Oleate), 9.25 wt% of ethanol and 0.75 wt% of citronellol as cosurfactants, 5 wt% of limonene as oil and 75 wt% of water was chosen as the basic system. The oil-in-water microemulsion region of this composition, first investigated by Klossek *et al.*,[157] exists between 23 °C and 100 °C. Below this temperature the solution is cloudy. Many papers deal with the use of soap to formulate microemulsions,[28, 216-224] but few report the use of two cosurfactants[28, 157] and there are no published studies of the effect of different salts on the existence of a soap microemulsion as a function of their concentrations and temperature.

First, the influence of the temperature on the micellar system water/Na-Oleate is investigated. Second, the effects of the addition of ethanol, citronellol, and limonene on the apK_A are studied. Third, the stability of the microemulsion as a function of the temperature is studied for increasing amounts of added sodium and chloride salts. Finally, the effects of two polyols, at first sight salting-out, are investigated. The results will be discussed in terms of electrostatic and Hofmeister effects, taking into account the oleic acid/sodium oleate equilibrium and the probable geometrical localisation of the different components in the microemulsion. A titration method is used to determine the apK_A.

A schematic representation of the structure of the basic microemulsion is given in **Figure 3.24**.

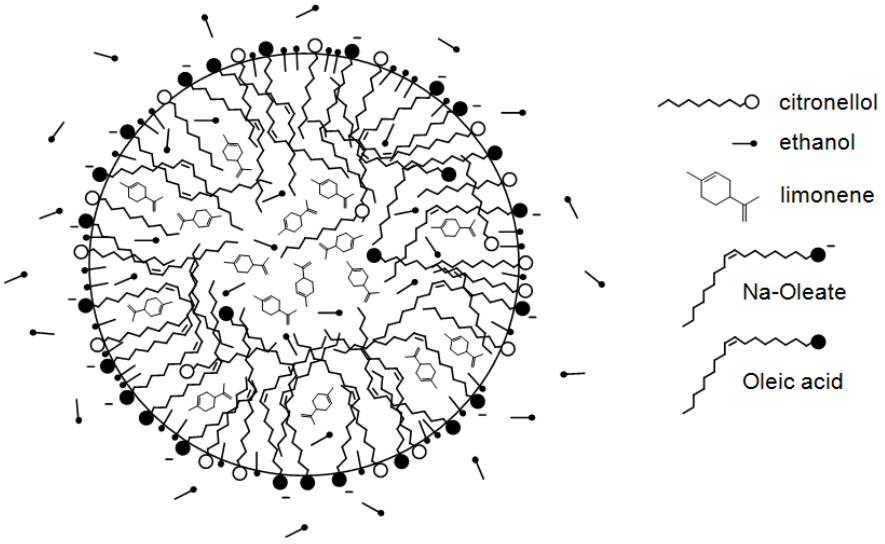

Figure 3.24. Schematic representation of the structure of the basic microemulsion

3.2.1.3. The studied microemulsion

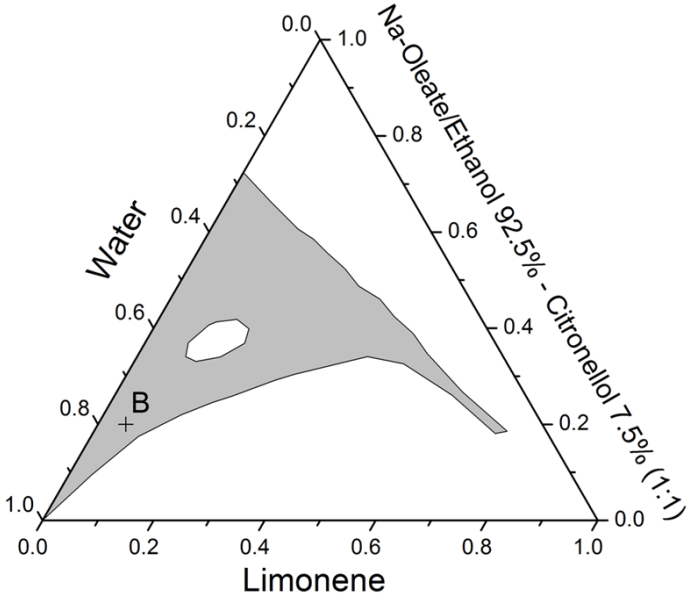

Figure 3.25. Partial pseudo-ternary phase diagram in weight fraction of the system water/Na-Oleate/ethanol (92.5 wt%) – citronellol (7.5 wt%)/limonene, with a surfactant-to-cosurfactant ratio equal to one, at 25 °C. The microemulsion area is in grey. Composition of point B is 75 wt% of water, 5 wt% of limonene and 20 wt% of surfactant/cosurfactant mixture.

The composition of the studied microemulsion corresponds to a particular point in the pseudo-ternary phase diagram of the system water/Na-Oleate/ethanol (92.5 wt%) – citronellol (7.5 wt%)/limonene with a Na-Oleate:mixture ethanol/citronellol mass ratio equal to one, see point B in **Figure 3.25**. This system has already been considered in a previous work by Klossek *et al.*[157] We have chosen to study the effect of additives at this point, because this composition is a highly water dilutable microemulsion.

3.2.1.4. Results and discussion

3.2.1.4.1. Influence of the temperature on the apparent pK_A in micellar solution of Na-Oleate

The apK_A of the micellar system water/Na-Oleate (10 wt%) is determined at 25 °C and 50 °C. The started solutions are homogeneous and clear, the Krafft temperature of Na-Oleate in water being lower than 25 °C.[225] As shown in **Figure 3.26**, the temperature has an influence on the apK_A and on the volume of citric acid needed to reach the equivalence point. The values are respectively equal to 9.7 and 6.7 ml at 25 °C and 9.14 and 12.6 ml at 50 °C. A high temperature furthers the formation of ionised carboxylate groups, which results in a stronger headgroup hydration. As more headgroups are charged, more citric acid is necessary to reach the equivalence point of the surfactant at 50 °C and consequently the apK_A decreases. Note that the minimum ionisation to solubilise ionic surfactants is obtained at the Krafft temperature and higher temperatures progressively favour higher ionisation degrees.

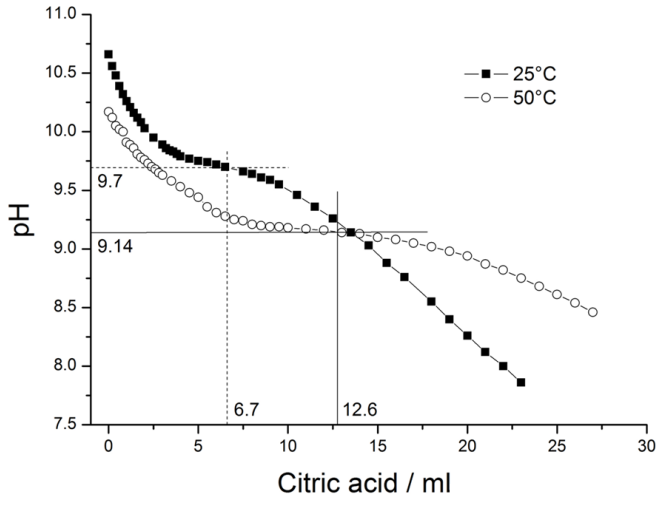

Figure 3.26. pH of the system water/Na-Oleate (10 wt%) plotted against the added volume of 1 wt% citric acid aqueous solution at 25 °C (black squares) and 50 °C (open circles). Apparent pK_A and volumes of citric acid necessary to reach the equivalence point are reported.

Equation **(3.1)** shows the equilibrium shift of the ionisation reaction, when the temperature increases in the previously described system.

$$R\text{-}COOH \rightleftharpoons R\text{-}COO^- + H^+ \qquad (3.1)$$

3.2.1.4.2. Influence of the microemulsion constituents on the apparent pK_A

Influence of ethanol. For the micellar system water/Na-Oleate/ethanol, 10 wt% of Na-Oleate was used in the solution and the percentage of ethanol was varied from 0 to 20 wt% (see **Figure 3.27**). The apK_A decreases by more than one unit when 10 wt% of ethanol is used in the system and drops to 8.16 in presence of 20 wt% of ethanol. Ethanol molecules have a major influence on the apK_A of the fatty acid. This can be explained by the fact that ethanol molecules are integrated in the interfacial film and separate the Na-Oleate headgroups. The unfavourable interactions between the charged headgroups decrease and thus a decrease of the apK_A is observed. As a consequence, the volume of citric acid necessary to reach the equivalence point increases with the percentage of ethanol added in the solution. Ethanol furthers then the hydration of the micelles.

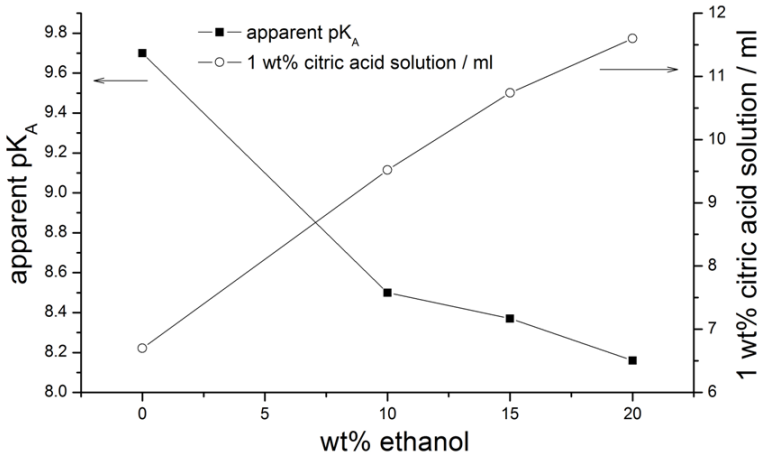

Figure 3.27. Apparent pK_A (left scale and black squares) and volume of 1 wt% citric acid added to the formulation (right scale and open circles) plotted against the mass percentage of ethanol involved in the mixture water/Na-Oleate (10 wt%)/ethanol, at 25 °C.

Influence of citronellol. In order to investigate the influence of citronellol, the system water/Na-Oleate (10 wt%)/cosurfactant (10 wt%) was also studied. The cosurfactant was either ethanol or a mixture of ethanol and citronellol. In the case of the mixture, 9.25 wt% of ethanol and 0.75 wt% of citronellol were used. The apK_A of the surfactant and the volume of citric acid necessary to reach the equivalence point were determined. As shown in **Figure 3.28**.a no changes

in the apK_A or the volume of citric acid were observed. Both apK_A are equal to 8.5 for 10 ml of citric acid.

In **Figure 3.28**.b the stability of the system water/Na-Oleate (10 wt%)/ethanol (10 wt%)/citronellol regarding the temperature is illustrated. The percentage of citronellol was varied from 0 to 10 wt% of the total weight of the sample. A very weak temperature dependence is observed between 0 and 2 wt% of citronellol. Above 2 wt% of citronellol, the solution has to be warmed up to obtain the clear and homogeneous phase. In the formulation corresponding to point B, 0.75 wt% of citronellol was used. Therefore, in the reference composition, the citronellol molecules are not supposed to significantly influence the studied properties of our formulation, although the addition of this small amount of citronellol is necessary to ensure that the microemulsion with oil is fully water dilutable.[157] By increasing the percentage of citronellol, the latter starts to decrease the thermostability of the micellar system.

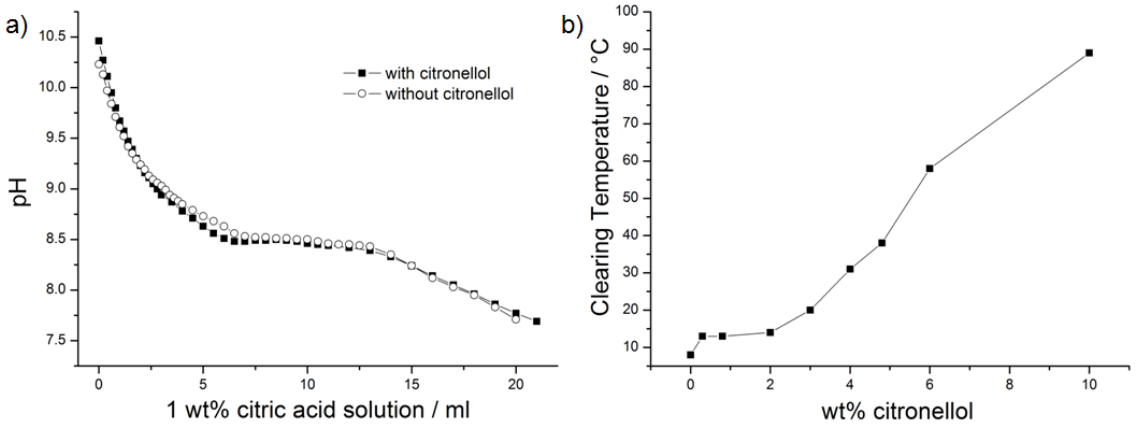

Figure 3.28. a) pH versus the volume of 1 wt% citric acid solution added to the system water/Na-Oleate (10 wt%)/cosurfactant (10 wt%), where the cosurfactant is ethanol 9.25 wt% + citronellol 0.75 wt% (black squares) or ethanol only (open circles), at 25 °C; b) Clearing temperature of the system water/Na-Oleate (10 wt%)/ethanol (10 wt%)/citronellol plotted against the mass percentage of citronellol in the solution.

Influence of limonene. Limonene is then added to the other compounds to form the microemulsion described in the experimental section. Now, the studied system is water/Na-Oleate (10 wt%)/ethanol (9.25 wt%)/citronellol (0.75 wt%)/limonene, in which the percentage of limonene is varied from 0 to 5 wt%. As shown in **Figure 3.29**.a, the apK_A is equal to 8.52 with no limonene in the formulation and increases to 9.02 when 5 wt% of limonene is involved in the solution. A strong variation of the apK_A is observed with limonene between 0 and 3 wt%. Above 3 wt% the apK_A remains constant until 5 wt%. The volume of citric acid needed to reach the equivalence point also decreases when limonene is added to the formulation, and drops from 8.81 to 3.68 ml with respectively 0 and 5 wt% of limonene. The significant increase of the apK_A observed between 0 and 3 wt% is correlated with the significant decrease of the citric acid volume

needed. This observation can be explained as follows: limonene is dissolved in the micellar core[226] and solubilises the protonated form of the surfactant (oleic acid). As a consequence, there is less ionised surfactant which is reflected by an increased apK_A.

In **Figure 3.29**.b the clearing temperature of the formulation is plotted against the percentage of limonene in it. This temperature increases when limonene is added to the solution. The microemulsion forms at 8 °C with no limonene and only at 23 °C with 5 wt% of limonene. These observations confirm the decrease of ionic forms in the formulation when limonene is added. The interfacial film of the microemulsion is less soluble and the temperature has to be increased to form the stable microemulsion by an increase of the surfactant ionisation (see section 3.2.1.4.1.). The apK_A and the volume of citric acid are reported only until 5 wt% of limonene. For higher limonene concentrations and at 25 °C, phase transition occurs during titration before half neutralisation is achieved.

The loss of thermostability observed by increasing the concentration of citronellol above 2 wt% (see **Figure 3.28**.b) could be due to the fact that citronellol acts like limonene at high concentrations, which means that citronellol is progressively solubilised in the core of the micelles.

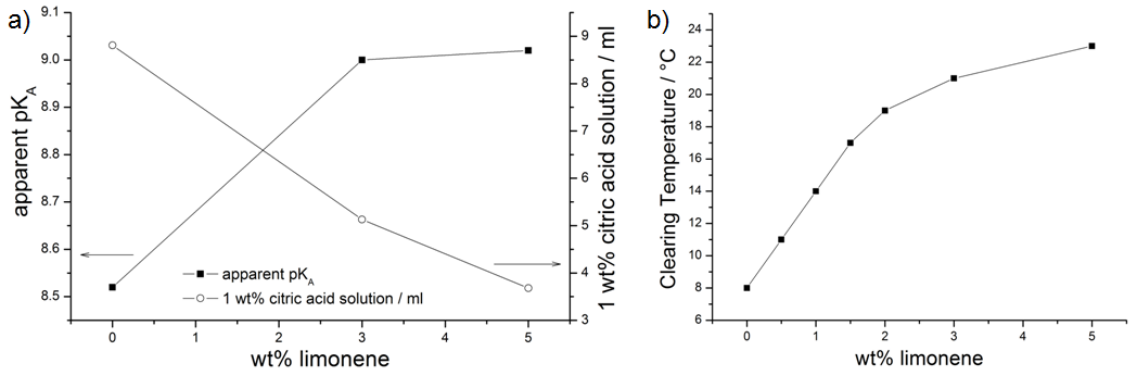

Figure 3.29. a) apparent pK_A (left scale and full squares) and volume of 1 wt% citric acid added to the formulation (right scale and open circles) plotted against the mass percentage of limonene in formulations having same quantities of sodium oleate, citronellol and ethanol as point B, at 25 °C. b) Clearing temperature of formulations having same quantities of sodium oleate, citronellol and ethanol as point B plotted against the mass percentage of limonene in the solution.

3.2.1.4.3. Effect of salts on the formulation

Effect of the anions. The effect of different anions was studied by varying the concentration of different sodium salts in the formulation corresponding to point B (see **Figure 3.25**). The sodium salts used were NaSCN, $NaNO_3$, NaCl, NaBr and Na_2SO_4. In **Figure 3.30**.a the clearing temperature Tα is plotted against the salt concentration. Without any salt the microemulsion

forms at 23 °C. Then, a common trend can be observed, i.e. the higher the salt concentration, the higher the clearing temperature. For example, the microemulsion forms at 76 °C, 70 °C and 64 °C for respectively 0.3 mol.kg^{-1} of NaBr, NaCl and NaSCN. It can be noted that the differences between the different salts is detectable, though not very pronounced. This can be explained by the anionic nature of the surfactant. By being negatively charged the anions do not come close to the carboxylate group and cannot change significantly its properties. However, sodium sulfate exhibits a different behaviour when at least 0.3 mol.kg^{-1} are present in the microemulsion. The special behaviour of Na_2SO_4 with its divalent anion is not the topic of this work and will not be discussed in details.

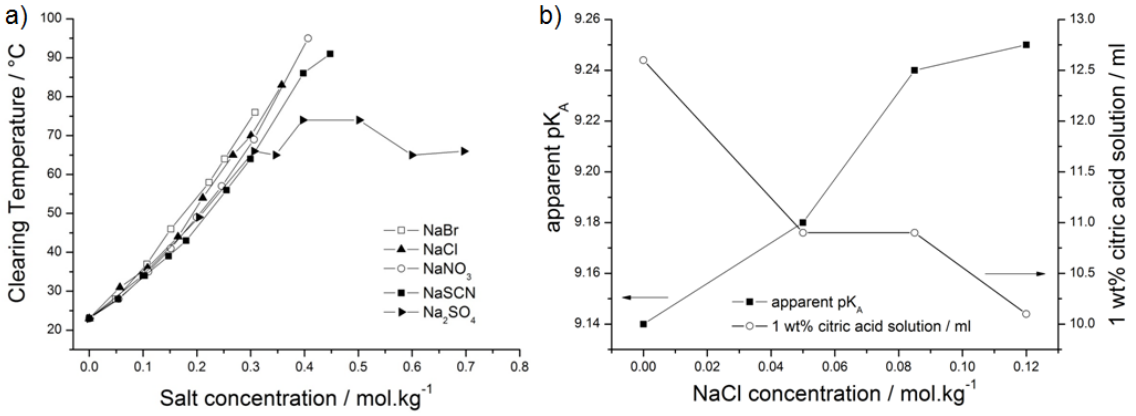

Figure 3.30. a) Clearing temperature of the formulation B as function of the anion concentrations in the solution. The microemulsion areas are above the curves; b) apparent pK_A (left scale and full squares) and volume of 1 wt% citric acid added to the formulation (right scale and open circles) plotted against the NaCl concentration in the system water/Na-Oleate (10 wt%)/NaCl, at 50 °C.

These salts have also influences on the apK_A of the fatty acid. The system water/Na-Oleate (10 wt%)/NaCl was investigated to observe the influence of sodium chloride on the surfactant. The different formulations were warmed up to 50 °C to allow the solutions to become clear and homogeneous when the titration started. As shown in **Figure 3.30**.b, the apK_A increases from 9.14 with 0 mol.kg^{-1} of NaCl to 9.25 with 0.12 mol.kg^{-1} of NaCl. On the contrary, the volume of citric acid needed to reach the equivalence point decreases. It falls from 12.6 ml for 0 mol.kg^{-1} of NaCl to 10.1 ml for 0.12 mol.kg^{-1} of NaCl. This observation leads to the conclusion that the higher the salt concentration is, the less carboxylate groups are present at the beginning of the titration. So the addition of salts furthers the formation of the acidic form –COOH. Obviously, NaCl and temperature have opposing effects on the equilibrium of the fatty acid. NaCl furthers the formation of the protonated form, whereas the increase of the temperature furthers the formation of the carboxylate group. These observations can also explain what is shown in **Figure 3.30**.a. The salt decreases the solubilisation of the structures by furthering the acidic form. Then, the

transparent microemulsion is found again by warming up the solution and forming the carboxylate groups.

The effect of the anions of sodium salts, except Na_2SO_4 at concentration above 0.3 mol.kg^{-1}, can be considered as almost non-specific and is similar to what was found by Bauduin *et al.*[227] and explained with an extended Debye-Hückel equation.[228] Bauduin *et al.* showed also that the change of pH of a citrate buffer when adding sodium salts was the same for all the studied anions, except for SO_4^{2-} at high salt concentrations.

Effect of the cations. The effect of cations on the clearing temperature of the microemulsion is now studied by using different chloride salts (see **Figure 3.31**). Differences between the salt can be noted. For LiCl, NaCl, and KCl the higher the concentration, the higher the clearing temperature. However, significant differences can be observed. For example, the microemulsion forms at 41 °C, 54 °C, and 75 °C for 0.2 mol.kg^{-1} of respectively KCl, NaCl, and LiCl in the formulation. In this case, by describing the curves with straight lines, the slopes are different and equal to 153.64, 198.47 and 357.53 °C kg.mol^{-1} for respectively KCl, NaCl, and LiCl. The microemulsion is destabilised and these salts are considered as salting-out. According to the curves, LiCl is more salting-out than NaCl, which is more salting-out than KCl. By warming up the cloudy solution, the cations are less strongly bound to the carboxylate groups, which enables the microemulsion to form.

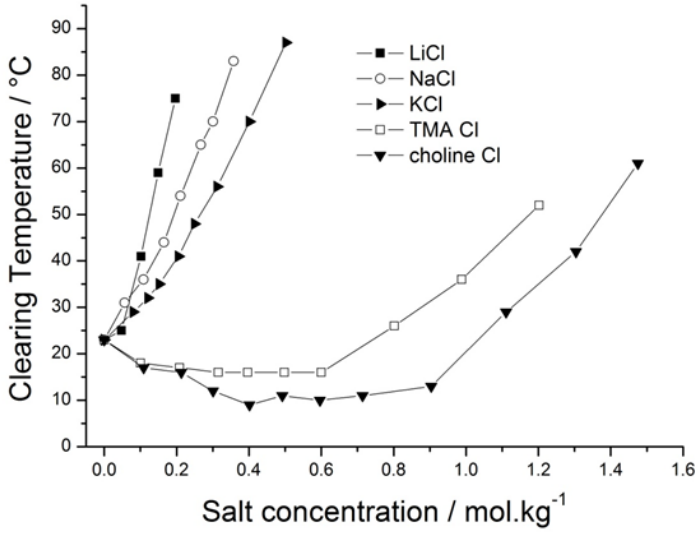

Figure 3.31. Clearing temperatures of the formulation B as function of the cation concentrations involved in the solution. The microemulsion areas are above the curves.

A different behaviour is observed for tetramethylammonium chloride (TMACl) and choline chloride (ChCl). Their curves are not straight lines but can be described with parabolas. Until a concentration of 0.4 mol.kg^{-1} of ChCl and 0.6 mol.kg^{-1} of TMACl these salts are salting-in. With a

certain amount of salt the microemulsion is more stable and forms even at temperatures lower than without added salt. With higher concentrations both salts become salting-out and the formulation has to be warmed up to turn into a microemulsion. For the same salt concentration the microemulsion with ChCl forms at lower temperature than the one with TMACl.

These results are analogous to the ones found by Lin *et al.* for the dissolution of a soap in water.[229] They studied the influence of cations on a micellar solution by using the ternary system water/salt/sodium myristate. They observed that the clearing temperature of the solution increased or decreased by increasing respectively the concentration of NaCl and $NaClO_4$ or different ammonium salts. Klein *et al.* also found that long-chain carboxylates become water soluble at room temperature with choline as counterion.[230, 231] The results are also in agreement with the well-known fact that beyond a certain concentration all salts become salting-out.

Table 4. pH and volume of added 1 wt% citric acid solution, for which a cloudy solution was obtained for the system corresponding to point B with different quantities of choline chloride, at 30 °C.

Quantity of choline chloride		pH	Volume of 1 wt% citric acid
mol.kg^{-1}	*wt%*	-	*ml*
0	0	9.05	3.6
0.13	1.9	8.9	2.4
0.5	7	8.8	2.2
1.05	14.7	9.2	1.2

The same apK_A study was carried out for the formulation B with different percentages of ChCl. The different formulations were warmed up to 30 °C to allow the solutions to be clear and homogeneous when the titration started. However, with high salt concentrations, it was difficult to study the obtained neutralisation curves due to the high viscosity of the solution. To overcome these difficulties, the pH was recorded and the volume of 1 wt% citric acid solution for which a cloudy solution was first obtained was noted to study the ChCl effect on the apK_A of the surfactant (see **Table 4**). A continuous and important decrease of the volume of citric acid necessary to obtain the cloudy solution was observed. This decrease indicates that less ionic forms are present at the beginning of the titration. We may suppose that the decrease of Tα, which was observed for low ChCl concentrations, is not caused by an increase of the ionisation of the surfactant, but by another phenomenon, which remains to be determined.

All anions behave alike, whereas cations have different influences on the microemulsion. This was already observed for salt influences on the pH of buffers, polyelectrolytes, and proteins.[232] At

this point two observations can be made. First, it is interesting to note that for the studied system the classic Hofmeister series for cations is inversed. As explained in the introduction, Li^+, Na^+ and K^+ have a salting-in effect regarding proteins. In our work, these cations have a salting-out effect. These observations can be explained by the fact that Li^+ can exchange more easily on the carboxylate than Na^+ and K^+ in the bulk. It was shown that Li^+ has a higher affinity than Na^+ and that Na^+ has a higher affinity than K^+ for carboxylate groups.[105, 233, 234] The more the cation is bound to the surfactant molecules, the more the surfactants increase their Krafft temperature and lose their solubility. The strong interaction between carboxylate groups and small ions of high density such as Li^+ or Na^+ is also observed in proteins.[234] However, the consequences are different. In micellar systems these strong interactions lead to a dehydration of the micelles and consequently to a salting-out phenomenon, whereas in protein systems these strong interactions lead to a denaturation of the protein, which is a salting-in phenomenon.

At low concentrations, ChCl and TMACl have a salting-in effect and above respectively 0.4 and 0.6 $mol.kg^{-1}$ a salting-out effect. At low concentration, these results are in agreement with the observations of Klein *et al.*,[230, 231] who showed that ChCl and TMACl are weakly associated to carboxylate, in contrast to Li^+, Na^+ and K^+, which show a stronger association. This fact, associated with an unsymmetrical or bulky structure[235] leads to a better solubility of alkyl carboxylates with quaternary ammonium counterions, which is reflected by lower Krafft temperatures and lower clearing temperatures. At higher ChCl and TMACl concentrations these salts may act as cosurfactants and get incorporated in the interfacial film resulting in a decrease in curvature. Further, at high salt concentrations, all salts become salting-out, because of prevailing strong ion-water interactions and a resulting dehydration of the surfactant headgroups.

Comparison of the Tα curves obtained adding ChCl and TMACl shows that the main evolution of the curves is due to the ammonium group and only minor modifications are due to the alcoholic function of the choline cation.

3.2.1.4.4. Effect of polyols

The same investigations were also carried out with glycerol and sorbitol. The latter were chosen, because they are two strongly hydrophilic nonionic molecules. They were added to the microemulsion having a composition corresponding to point B. As shown in **Figure 3.32** both molecules have a salting-in effect on the formulation. The clearing temperature decreases from 23 °C to 15 °C with 1.3 $mol.kg^{-1}$ of glycerol in the formulation and from 23 °C to 1 °C with 1.2 $mol.kg^{-1}$ of sorbitol. Sorbitol is more effective than glycerol and microemulsions can form even at 1 °C. Apparently, this result is in disagreement with the work of Copolovici *et al.* who found a salting-out effect of sorbitol studying the partition coefficient of limonene and linalool (isomer of

citronellol) between water/octanol and water/gas phases.[236] However, the systems are not really compatible, due to presence of the co-solvent ethanol in our case. This makes the difference.

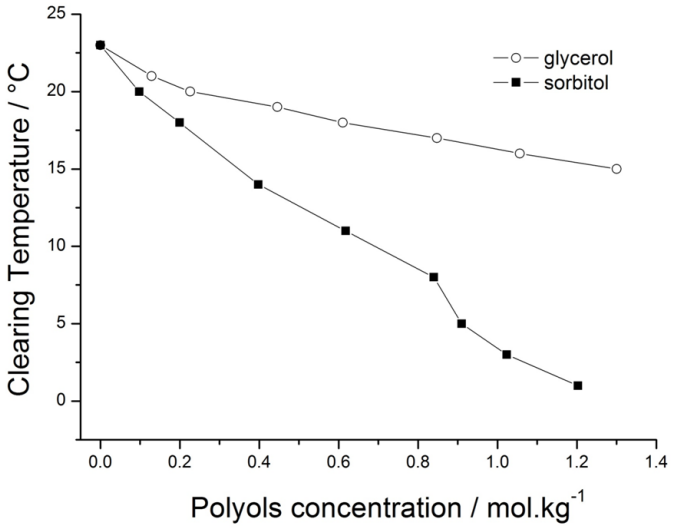

Figure 3.32. Clearing temperature of the formulation B as function of the polyol concentration in the solution. The microemulsion areas are above the curves.

An apK_A study was also carried out for the system water/Na-Oleate/sorbitol, where 10 wt% of Na-Oleate was used in the solution to mimic the conditions in the microemulsion B (see **Figure 3.25**). The percentage of sorbitol in the solution was varied from 0 to 30 wt%. As shown in **Figure 3.33**.a (curve 1) the surfactant apK_A has almost the same value whatever the quantity of sorbitol dissolved in water and is between 9.6 and 9.7. The percentage of sorbitol was also varied from 0 to 60 wt% in the formulation B (see **Figure 3.33**.a, curve 2 and **Figure 3.33**.b). As shown in **Figure 3.33**.a (curve 2), the apK_A decreases from 9.15 to 8.2, when 60 wt% of sorbitol is solubilised in the microemulsion. Curve 3 in **Figure 3.33**.a is similar to the decrease of the apK_A for the micellar system water/Na-Oleate/ethanol.

These investigations lead to the conclusion that the action of sorbitol on the apK_A depends on the presence or not of ethanol. When no ethanol is involved in the solution the sorbitol has almost no influence on the apK_A. As expected, without ethanol the sorbitol molecules stay in the aqueous bulk and do not interfere with the surfactant molecules at the interface.

In presence of ethanol, two different hypotheses can be drawn. On the one hand, the sorbitol can increase the cosurfactant power of ethanol by pushing it towards the micelles, like in the case of sodium sulphate in presence of sodium xylene sulfonate and an extended surfactant.[142] The ethanol molecules can then insert between the Na-Oleate molecules. The repulsions between the headgroups of the latter decrease, so does the apK_A. On the other hand, ethanol molecules can distort the micelles. This enables the sorbitol to go between the headgroups and to have an action comparable to ethanol. However, this second hypothesis is much less probable.

As a consequence and as already mentioned, the disagreement with Copolovici *et al.* stems from the presence of ethanol in our formulation.

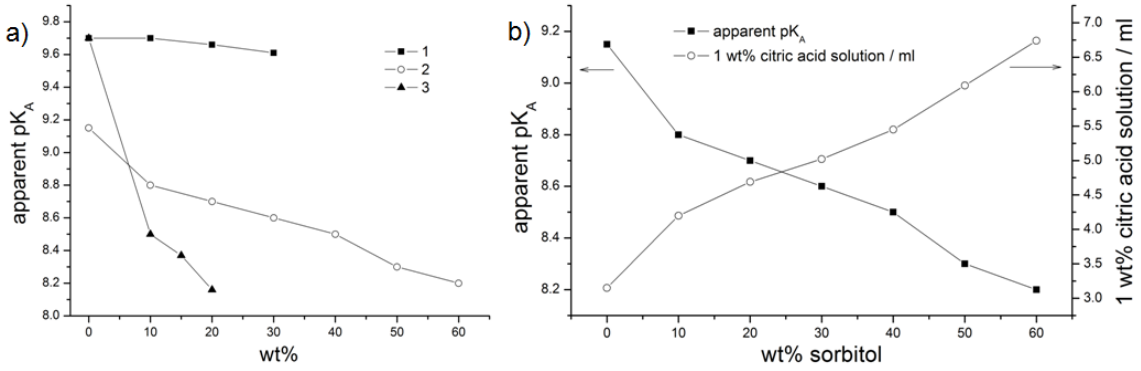

Figure 3.33. a) apparent pK_A of the surfactant as function of the mass percentage of sorbitol or ethanol in the system 1) water/Na-Oleate (10 wt%)/*sorbitol*; 2) water+*sorbitol*/Na-Oleate (10 wt%)/ethanol (9.25 wt%) – citronellol (0.75 wt%)/limonene (5 wt%); 3) water/Na-Oleate (10 wt%)/*ethanol* at 25 °C. The compound for which the mass percentage was varied is in italics; b) apparent pK_A (left scale and black squares) and volume of 1 wt% citric acid solution added to the formulation (right scale and open circles) plotted against the mass percentage of sorbitol involved in the formulation corresponding to point B, at 25 °C.

3.2.1.5. Conclusion

This work deals with the influence of ethanol, citronellol, limonene, salts, and polyols on the temperature stability of an oil-in-water formulation (water 75 wt%, sodium oleate 10 wt%, ethanol 9.25 wt%, citronellol 0.75 wt%, and limonene 5 wt%) and on the apK_A of its surfactant. It was shown that the apK_A decreases for the micellar system water/Na-Oleate with an increase of temperature. By adding ethanol to this mixture, a decrease of the apK_A was also observed. It may be argued that ethanol molecules insert in the interfacial film, separate the soap headgroups and thus decrease the unfavourable repulsive electrostatic interactions of the headgroups. Using a small amount of citronellol as second cosurfactant does not influence the apK_A or the volume necessary to reach the equivalence point. When limonene is used as oil to form the microemulsion water/Na-Oleate (10 wt%)/ethanol (9.25 wt%)/citronellol (0.75 wt%)/limonene, an increase of the apK_A is observed due to the solubilisation of uncharged oleic acid in the organic (limonene) core of the microemulsion droplets. At high concentrations, citronellol has probably the same effect as limonene.

The study of the influence of sodium and chloride salts on the microemulsion system showed that the anions have no specific influence. The evolution of Tα as function of the salt concentrations simply follows electrostatic interactions. The specificity of the cations is linked to the possibility for cations to exchange with the original surfactant counterion. The temperature stability of the microemulsion as well as the Krafft temperature are strongly dependent on the headgroup-

counterion association and hydration of the surfactant headgroup. The order of ion association to carboxylate is $Li^+ > Na^+ > K^+ >$ ChCl, exactly as in proteins, but the consequences are different. Micelles are salted-out whereas proteins are salted-in.[106]

Glycerol and sorbitol are salting-in in our formulation, only in the presence of ethanol in the microemulsion.

Previous studies concerning the influence of salts on the apK_A of organic acids allow us to understand the salt specificities beyond the Debye-Hückel result. The observations obtained with non-structured media can be transferred to media where organic acids (soaps) are self-associating.[227, 232]

We further studied the influence of ethanol which is also used for the manufacturing of soaps and beverages, and many formulations involve glycerol and sorbitol in both cases.[237-240] The study of the interactions of these compounds with soap molecules is crucial to better understand these formulations. The studied microemulsions are interesting because they are highly water dilutable, and thus can be useful as perfume or aroma carriers. The dilution or the neutralisation to pH smaller than 7 of the microemulsion may lead to emulsions with enough stability for a good dispersion in a process. The incorporation of artificial and natural sweeteners in this highly water dilutable microemulsion is also investigated in the next section.

3.2.2. Influence of high intensity sweeteners and sugar alcohols on a beverage microemulsion

3.2.2.1. Abstract

The present work shows the effects of added sugars and sweeteners on the clearing temperature of a highly water dilutable fatty acid salt microemulsion (the same that the one investigated in section 3.2.1) used as a model of a beverage concentrate. There is a twofold interest in this work. The first one is practical and relates to the fact that many fatty acid salt surfactants can be used in food without major regulatory restrictions. As is shown here, they allow making highly stable microemulsions even at neutral and acidic pH. The second one is more of scientific interest. The model system can be used to study the effect of sugars and sweeteners on the formulation stability depending on their charges, amphiphilic properties, and localisation in the microemulsion interfacial film. An important practical result is the discovery of the possibility to formulate highly dilutable microemulsions at neutral or slightly acid pH with a good taste in presence of sucralose. Further, a significant decrease of the pK_A of the fatty acid is observed in presence of stevia, thus allowing transparent, fairly stable systems at neutral pH.

3.2.2.2. Introduction

Microemulsions are mixtures of polar and non-polar liquids. They are optically homogeneous, translucid and thermodynamically stable solutions.[3, 11] Contrary to the well-known emulsions, which are kinetically stable[1, 241] and can be stabilised by a single surfactant, the action of a cosurfactant is often required for a microemulsion to form.[157] Microemulsions can be in equilibrium with the oil phase, the water phase or both phases of the studied system. Such systems are respectively referred to Winsor I, II, or III. Microemulsions can also be the only phase of the studied system (Winsor IV).[12] Depending on the composition, three different microemulsion types can be observed: water-in-oil (w/o), bicontinuous, and oil-in-water (o/w), and spherical, non-spherical, and rode-like structures can be found on the nanoscopic scale.[9, 210, 242, 243] As microemulsions enable organic and hydrophobic compounds to be integrated into an aqueous phase, they are interesting for many applications. They are used in cosmetic products, in pharmaceutical and lacquer fields, as well as for enhanced oil recoveries and food industries.[29, 161, 167, 244]

The first objective of the present work is to study the effect of sweeteners on the realms-of existence of a highly water dilutable fatty acid salt microemulsion used as a concentrated beverage model. The system used in this work is the same as in section 3.2.1 and was first reported by Klossek *et al.*[157] The authors investigated the system water/sodium

oleate/ethanol/citronellol/limonene and found the existence of highly water dilutable microemulsions. High stabilities of the emulsions after titration with citric acid were also observed. The pH of these emulsions are compatible with the pH of a beverage. However, the taste was too bitter due to the presence of the surfactant. In our model oil-in-water microemulsion, sodium oleate was used as the fatty acid salt surfactant because of its low Krafft temperature, citronellol and ethanol as cosurfactants and limonene as the oil phase. Sodium oleate is classified by the Food and Drug Administration as food additive under the code E470. It is not limited in use.[157, 245]

Natural and artificial sweeteners are very often used in modern beverages. Two different types of sweeteners can be identified regarding their sweetness power in comparison to sucrose: the *high intensity sweeteners* and the *sugar alcohols* are respectively sweeter and less sweet than sucrose.

In the present work, we investigate the effect of artificial and natural high intensity sweeteners and sugar alcohols on the microemulsion's clearing temperature and on the apparent pK_A of sodium oleate. Saccharin, cyclamate, acesulfame K, aspartame, neotame, sucralose, isomalt, neohesperidin DC, and naringin DC were used as artificial sweeteners. Sorbitol, sucrose, and stevia RA95 (at least 95% of Rebaudioside A) were used as natural sweeteners. It can be noted that saccharin, cyclamate, and aspartame were discovered by chance and that sucralose was discovered using the AH (hydrogen bond donator),B (hydrogen bond acceptor) theory of hydrogen bonding of the sweetener to the receptor site, developed by Shallenberger *et al.* in 1967 and completed by Kier *et al.* in 1972.[246, 247]

In the following, we propose a short presentation of the artificial and natural high intensity sweeteners and sugar alcohols used.

3.2.2.2.1. Artificial and natural high intensity sweeteners

- *Saccharin* (**Figure 3.34**.a) has the food additive code E954. It is about 300-400 times sweeter than sucrose.[248, 249] Saccharin was found in 1879 by Ira Remsen and Constantin Fahlberg, when the latter went to lunch without washing his hands.[250, 251] This sweetener became popular only when sugar was rationed during World War I.

- *Cyclamate* (**Figure 3.34**.b) was accidentally discovered by Michael Sveda in 1937 when he placed his cigarette on the bench.[252] It is about 30-40 times sweeter than sucrose and has the food additive code E952.[248, 249] Cyclamate can be used in over 50 countries around the world but is banned in the United States.[253]

- *Acesulfame K* (**Figure 3.34**.c) is about 200 times sweeter than sucrose and has the food additive code E950.[248] It was discovered by German chemists Karl Clauss and Harald Jensen at Hoechst AG in 1967.[249]

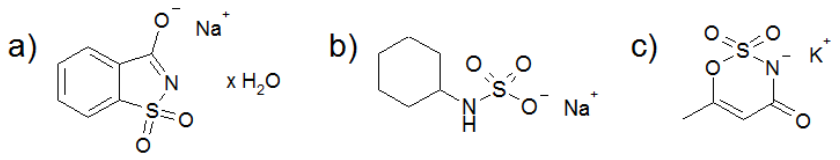

Figure 3.34. Molecular structures of a) saccharin; b) cyclamate; c) acesulfame K.

- *Aspartame* (**Figure 3.35**.a) was discovered in 1965 by James M. Schlatter at G. D. Searle & Company when he licked his finger to grab a piece of paper.[254, 255] Aspartame is a dipeptide composed of two natural amino acids, which is also about 200 times sweeter than sucrose.[256] Having the food additive code E951, aspartame is authorised in many countries and used in numerous food products.[248, 257-259] After a lot of political and medical controversies, the European Food Safety Authority and the Food and Drug Administration (FDA) finally confirmed its inoffensive effect, as long as its level of consumption does not exceed a defined daily intake.[256, 260]

- *Neotame* (**Figure 3.35**.b) was developed by Monsanto. The discovery of neotame is due to the academic work of C. Nofre and J. M. Tinti.[261] Neotame is allowed in Australia since August 2001, and it was authorised in the United States by the FDA in 2002.[262] It is an artificial sweetener derived from aspartic acid and has a structure similar to aspartame. However, neotame is 7000-13000 times sweeter than sucrose.[262]

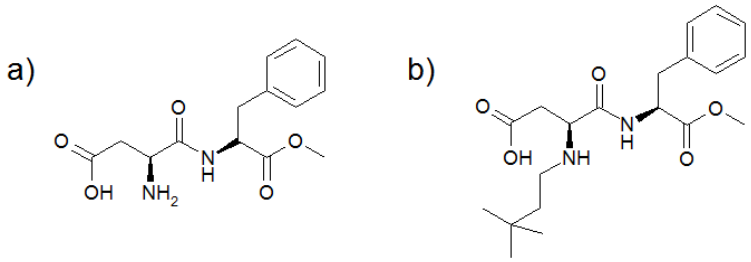

Figure 3.35. Molecular structure of a) aspartame; and b) neotame.

- *Sucralose* (**Figure 3.36**.b) was discovered in 1976 by scientists working at Tate & Lyle PLC together with researchers from the Queen Elizabeth College of London.[263, 264] According to the theory of Shallenberger *et al.*[246] they replaced three hydroxyl groups with chlorine atoms in the structure of sucrose, increasing the lipophilic character of sucrose to facilitate the absorption into the receptor site. Sucralose is about 500-600 times sweeter than sucrose, and is used under the food additive code E955.[248, 265]

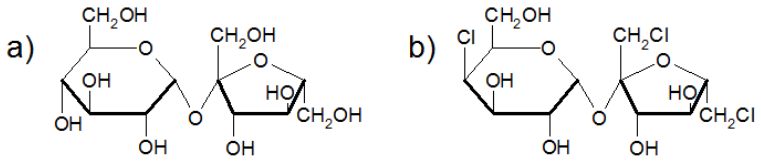

Figure 3.36. Molecular structure of a) sucrose compared to the molecular structure of b) sucralose.

- *Neohesperidin DC* is an intense sweetener, known under the food additive code E959, it is 1000-1500 times sweeter than sucrose.[266] It was first prepared in 1963 by Horowitz and Gentili by hydrogenation of neohesperidin, present in citrus peel, to reduce the bitterness of citrus juices.[267] As it can be seen in **Figure 3.37**.a, two glycosyl units give an amphiphilic character to neohesperidin DC coupled with a hydrophobic chalcone skeleton.

- *Naringin DC* (**Figure 3.37**.b) is 300-1800 times sweeter than sucrose and was discovered at the same time as neohesperidin DC as part of the same research.[268, 269]

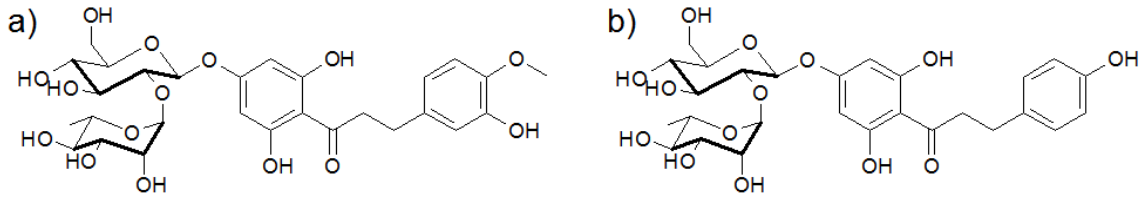

Figure 3.37. Molecular structure of a) neohesperidin dihydrochalcone; and b) naringin dihydrochalcone.

- *Stevia* is a general term used to refer to the plant of *Stevia rebaudiana*. The sweet tasting compounds are found in leaves of the stevia plant and named steviol glycosides. A leaf contains at least 10 unique steviol glycosides, such as stevioside (see **Figure 3.38**.a) or rebaudioside A (see **Figure 3.38**.b). The latter is the predominant steviol glycoside and provides a sweet taste without bitter notes.[270, 271] Stevia is about 300 times sweeter than sucrose and has the advantage of being a low-sugar sweetener.[272]

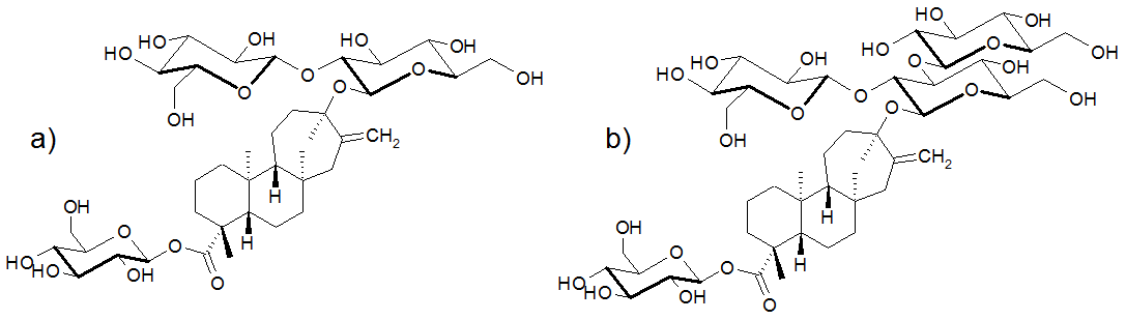

Figure 3.38. Molecular structure of a) stevioside; b) rebaudioside A.

3.2.2.2.2. Artificial and natural sugar alcohols

- *Sucrose*, the common table sugar, is used as a reference and represented in **Figure 3.36**.a .

- *Isomalt* is an artificial sweetener having the food additive code E953.[248] Isomalt is an approximately equimolar mixture of two sugar derivatives obtained after chemical transformations, 1,6-glucopyranosyl-D-sorbitol (**Figure 3.39**.a) and 1,1-glucopyranosyl-D-mannitol (**Figure 3.39**.b).[273] The mixture has a sweetness power of 0.5 and is therefore less sweet than sucrose.

- *Sorbitol* (**Figure 3.39**.c) is a naturally occurring sugar alcohol being two times less sweet than sucrose and having the food additive code E420.[248, 274] Sorbitol occurs naturally in apples, pears, peaches, and berries from trees of the genus *Sorbus*. Besides its application as sweetener, sorbitol is also used in cosmetic products as humectant and thickener.[275]

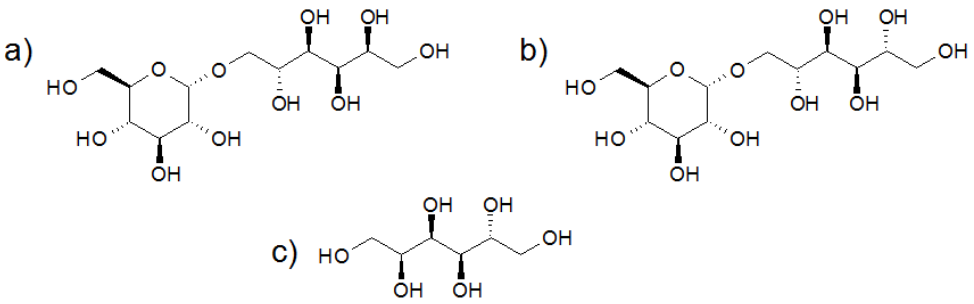

Figure 3.39. Molecular structure of a) 1,6-glucopyranosyl-D-sorbitol; b) 1,1-glucopyranosyl-D-mannitol; and c) sorbitol.

3.2.2.2.3. The studied microemulsion

The effects of different sweeteners on a oil-in-water highly water dilutable microemulsion were investigated, where the microemulsion corresponded to the system water/sodium oleate/ethanol (92.5 wt%)-citronellol (7.5 wt%)/limonene, where sodium oleate was used as surfactant, the mixture ethanol/citronellol as cosurfactant and limonene as the oil phase, see **Figure 3.25**. The surfactant-to-cosurfactant weight ratio was equal to one. The highly water dilutable formulation studied here is the same as in section 3.2.1 and had the composition indicated by point B in the pseudo-ternary phase diagram in **Figure 3.25**. Klossek *et al.* already described this reference system in details.[157]

3.2.2.3. Results and discussion

The influences of high intensity sweeteners and sugar alcohols were investigated on the clearing temperature T_α, defined as the temperature at which the samples change from turbid to clear, of the oil-in-water microemulsion corresponding to point B (**Figure 3.25**) and on the apparent pK_A (apK_A) of its surfactant, i.e. sodium oleate. The clearing temperature T_α for the microemulsion without additives was 23 °C. The apK_A of sodium oleate in the microemulsion without additives was equal to 9.2 at 20 °C and to 9.0 at 25 °C. When it was difficult to determine the apK_A from the titration curves, especially with stevia and cyclamate (in italics in the legends of the respective figures), the apK_A was equated with the pH for which these solutions became cloudy. The results are organised following the sweeteners which exhibit similar behaviours.

3.2.2.3.1. Electrolyte (saccharin, acesulfame K)

The high intensity sweeteners saccharin and acesulfame K have a very similar influence on the clearing temperature of the microemulsion (see **Figure 3.40**). Both T_α curves increase with more or less the same slope until a concentration of 0.4 $mol.kg^{-1}$. At that given concentration, both slopes decrease in the same way while remaining positive. T_α reaches 80 °C for respectively 0.5 and 0.6 $mol.kg^{-1}$ of saccharin and acesulfame K.

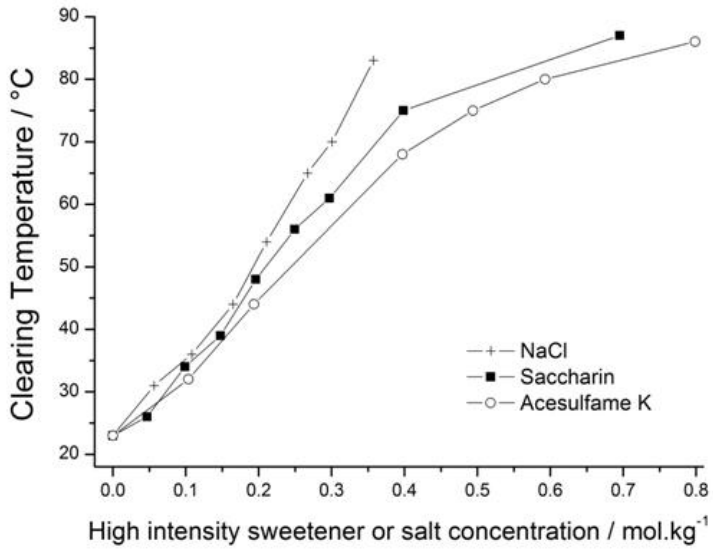

Figure 3.40. Clearing temperature in °C for the formulation B as a function of the high intensity sweetener or NaCl concentration in $mol.kg^{-1}$. The microemulsion area is above the curves.

The T_α curves of the negatively charged high intensity sweeteners saccharin and acesulfame K are similar to the one obtained with NaCl for the same microemulsion (see **Figure 3.40** or section 3.2.1). A salting-out effect can thus be postulated for saccharin and acesulfame K.

3.2.2.3.2. Surface active agents (cyclamate, sucralose)

The high intensity sweetener cyclamate behaves like saccharin and acesulfame K at low concentrations. As it can be seen in **Figure 3.41**.a, T_α increases with the same slope and reaches 35 °C with 0.15 mol.kg^{-1} of cyclamate. At higher concentrations, the slope decreases while remaining positive and reaches 46 °C with 1.2 mol.kg^{-1} of cyclamate in the formulation. The T_α curve obtained using sucralose has a negative slope until 0.3 mol.kg^{-1} (see **Figure 3.41**.a). At higher sucralose concentration, the slope becomes even more negative and T_α is smaller than 0 °C for 0.4 mol.kg^{-1}. Then, the slope becomes positive again and T_α is equal to 45 °C with 1 mol.kg^{-1} of sucralose in the formulation. Following the results of the clearing temperature study, the solutions with cyclamate were warmed to 40 °C to obtain the microemulsions and to investigate the influence on the apK_A with a larger range of concentrations. It should also be noted that the formulations with cyclamate were titrated with a 0.5 wt% (instead of 1 wt%) citric acid solution. The addition of cyclamate from 0 to 0.3 mol.kg^{-1} leads to an increase of apK_A. The slope of the cyclamate curve becomes negative for concentrations higher than 0.3 mol.kg^{-1} and the apK_A of the surfactant reaches 8.6 with 0.5 mol.kg^{-1} of cyclamate in the microemulsion. The addition of sucralose leads to a curve with a negative slope, associated with a continuous decrease of the apK_A. An apK_A of 7.4 is reached with 0.6 mol.kg^{-1} of sucralose in the formulation.

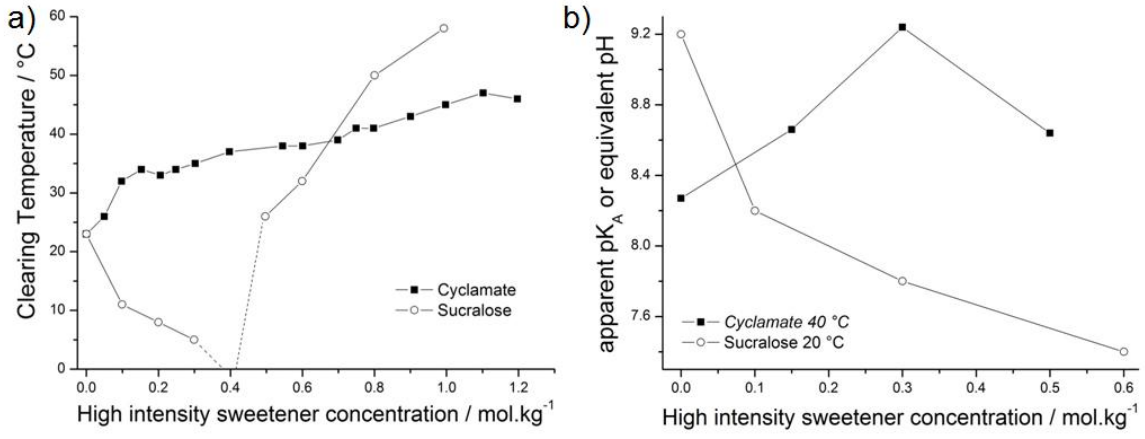

Figure 3.41. a) Clearing temperature in °C for the formulation B as a function of the high intensity sweetener concentration in mol.kg^{-1}. The microemulsion area is above the curves; b) apparent pK_A or equivalent pH (in italics, for cyclamate) of the surfactant sodium oleate as a function of the high intensity sweetener concentration for the formulation corresponding to point B.

At low concentrations, the T_α curve of the negatively charged high intensity sweetener cyclamate is also similar to the one obtained with NaCl for the same microemulsion (see **Figure 3.40** and section 3.2.1). A salting-out effect can thus be also postulated for cyclamate until a concentration of 0.15 mol.kg^{-1}. However, the cyclamate T_α curve increases very slowly after 0.15 mol.kg^{-1} and

has a much smaller slope than saccharin and acesulfame K. At higher concentrations, cyclamate may have a very slight cosurfactant (hydrotropic) behaviour that attenuates its salting-out effect. The different behaviours of saccharin and cyclamate are also described by Hianik *et al.* who studied their interaction with large unilamellar liposomes and with planar bilayer lipid membranes.[276] They found that both sweeteners interact with the surface of lipid bilayers and can modify the physical properties of lipid membranes. Saccharin induced aggregation of liposomes, whereas cyclamate caused increase of the hydration of the liposome surface. As the surface of liposomes can be compared to the surface of micelles, we may suppose that saccharin molecules cause an aggregation of the micelles and a dehydration of the surfactant. This is in agreement with the mainly ionic behaviour of saccharin that we mentioned before. Thus, the temperature has to be increased to break these aggregates and compensate the dehydration as an increase of the temperature favors the ionisation of the surfactant (see section 3.2.1). As a consequence, a clear and homogeneous microemulsion is formed again. It may also be the case for acesulfame K, as both of the curves have the same tendency. The clearing temperature is much lower for cyclamate due to the slight cosurfactant behaviour previously described.

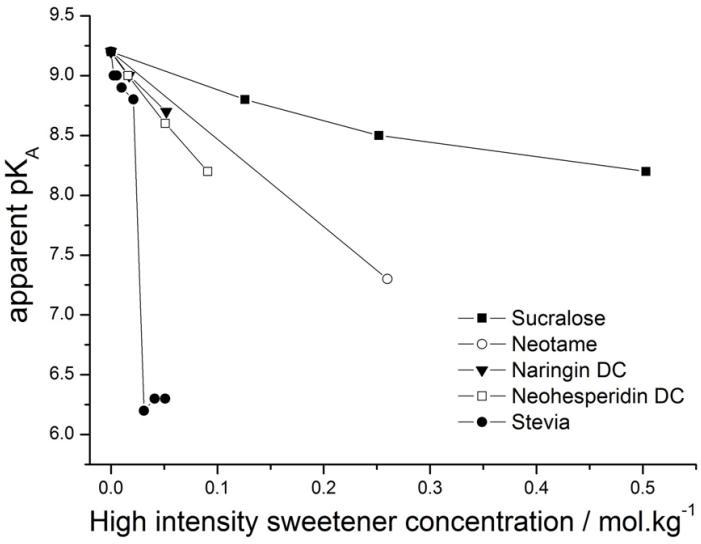

Figure 3.42. Apparent pK$_A$ of the surfactant sodium oleate as a function of the sucralose, neotame, naringin DC, neohesperidin DC, and stevia concentration for the system water/sodium oleate (10 wt%), at 25 °C.

In order to discuss the non-continuous behaviour of T_α of sucralose, its effect on the apK$_A$ of sodium oleate was studied for the system water/sodium oleate (10 wt%)/sucralose only, without cosurfactants and limonene. The obtained results are reported in **Figure 3.42**. A continuous and slight decrease of the sodium oleate apK$_A$ can be observed adding sucralose. The decrease must be due to slight or important interactions of the sweetener with the surfactant. The slight negative slope of the apK$_A$ curve with sucralose in the water/sodium oleate (10 wt%)/sucralose system

contrasts with the sharply decreasing apK_A curve in the microemulsion, see **Figure 3.41**.b. Obviously, sucralose is strongly hydrated and has a strong salting-out effect on the ethanol present in the aqueous pseudo-phase of the microemulsion. In other words, sucralose both accumulates at the surface of the micelles and pushes ethanol into the interfacial film of the microemulsion, without penetrating deeply into it. The increase of the temperature curve, observed at concentration higher than 0.4 $mol.kg^{-1}$ of sucralose, can be explained by the fact that the sucralose solubility in water increases with temperature, as found by Li *et al.*[265] It should be underlined that clear microemulsions can be formulated at pH around 7.5 with 0.6 $mol.kg^{-1}$ of sucralose. This pH is near the one of human blood (pH = 7.3) and compatible with a beverage pH. To our knowledge this is the first time that a beverage microemulsion is formulated with a fatty acid salt as surfactant at nearly neutral pH.

3.2.2.3.3. Precipitation (aspartame)

The T_α curve of aspartame in the microemulsion increases very sharply and reaches 80 °C for less than 0.1 $mol.kg^{-1}$ of sweetener, see **Figure 3.43**.

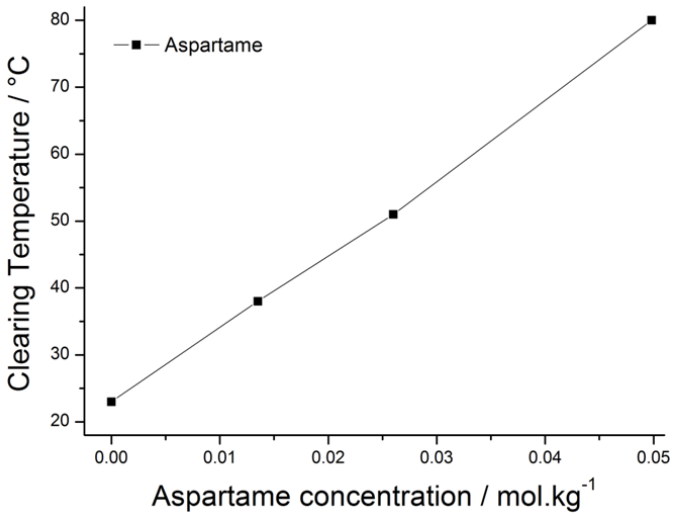

Figure 3.43. Clearing temperature in °C for the formulation B as a function of the aspartame concentration in $mol.kg^{-1}$. The microemulsion area is above the curves.

The pH of the microemulsions in the aspartame concentration range should be around 9. The amine groups in aspartame are then positively charged as the pK_A^1(COOH) of aspartame is equal to 3.1 and the pK_A^2(NH) to 7.9. The double positive charged sweetener is thus expected to show a very strong salting-out effect or a strong precipitation behaviour, which is indeed found as the clearing temperature sharply rises with aspartame concentration.

3.2.2.3.4. Surfactant (stevia, neotame, neohesperidin DC, naringin DC)

The curves obtained using stevia and neohesperidin DC show a similar negative slope until 0.07 mol.kg^{-1} (see **Figure 3.44**.a). Then, the clearing temperature T_α decreases further until 3 °C for 0.14 mol.kg^{-1} of stevia. It is interesting to note the particular behaviour of stevia at higher concentrations. The clearing temperature increases sharply to reach 100 °C for only 0.4 mol.kg^{-1} of stevia in the solution. The clearing temperature decreases until 15 °C with 0.07 mol.kg^{-1} of neohesperidin DC in the microemulsion. At higher concentrations, T_α increases sharply and reaches 53°C with 0.4 mol.kg^{-1}. Similar experiments were carried out with naringin DC. However, the latter was not at all soluble in the microemulsion, although its structure is close to the one of neohesperidin DC. As it can be seen in **Figure 3.44**.a, T_α increases for neotame and reaches 35°C at 0.1 mol.kg^{-1}. The slope of the curve becomes negative for concentrations higher than 0.1 mol.kg^{-1} and positive again from 0.3 mol.kg^{-1}. Following the results of the clearing temperature study, the solutions with neohesperidin DC and neotame were warmed to respectively 35 and 40 °C to investigate the influences on the apK_A with a larger range of concentrations. The addition of stevia and neotame, from 0.1 mol.kg^{-1}, leads to a curve with a negative slope, associated with a continuous decrease of the apK_A (see **Figure 3.44**.b). An apK_A of 7.1 is reached with respectively 0.2 and 0.4 mol.kg^{-1} of stevia and neotame in the formulation.

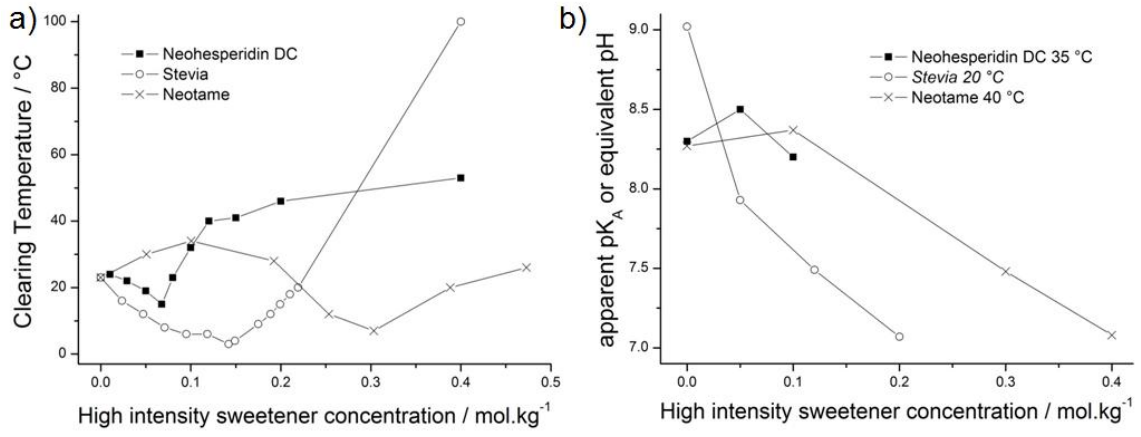

Figure 3.44. a) Clearing temperature in °C for the formulation B as a function of the high intensity sweetener concentration in mol.kg^{-1}. The microemulsion area is above the curves; b) apparent pK_A or equivalent pH (in italics, for stevia) of the surfactant sodium oleate as a function of the high intensity sweetener concentration for the formulation corresponding to point B. Regarding stevia, the molar mass used was the one of stevioside (M = 804.87 g.mol^{-1}).

Neotame should show electrostatic effects similar to aspartame, but in addition it has a hydrophobic part which may act as a cosurfactant (see **Figure 3.35**.b). Indeed, the surface tension values reported in the literature are 65 mN/m at 4.10^{-5} mol/l neotame concentration in water and

35 mN/m at 10^{-2} mol/l, indicating that neotame can be considered as a true surfactant.[261] This together with the solubility limit of neotame in pure water (0.03 mol.kg^{-1} at 20 °C)[277] causes a more complex behaviour of the corresponding T_α curve in the microemulsion. At very low neotame concentration, the T_α curve increases in a way that is very similar to the one caused by the addition of NaCl, see **Figure 3.40**. Above the solubility limit in water, neotame partitions preferably into the interfacial oleate film until a 1:1 molecular ratio of neotame-to-sodium oleate is reached. Accordingly, when neotame takes part in the interfacial film, the clearing temperature goes down. For even more neotame molecules, the interfacial film is saturated and more thermal energy is needed to get all the molecules in solutions and consequently to obtain a clear microemulsion. The onset of the strong surfactant-cosurfactant interactions between oleate and neotame is supported by the decrease of the apK_A of oleate above about 0.1 mol.kg^{-1} of neotame (see **Figure 3.44**.b). The decrease of the pK_A of oleate in the system water/sodium oleate (10 wt%)/neotame, without cosurfactants and limonene (see **Figure 3.42**), as a function of the neotame concentration confirms the cosurfactant behaviour. The penetration of neotame in the interfacial film is certainly deeper than the one of sucralose because the pK_A of oleate in the system water/sodium oleate (10 wt%)/sucralose stays nearly constant.

Again, in order to discuss the non-continuous behaviour of the T_α curves, the effect of stevia, neohesperidin DC, and naringin DC on the apK_A of sodium oleate was studied for the system water/sodium oleate (10 wt%)/sweetener only, without cosurfactants and limonene. The obtained results are reported in **Figure 3.42**. Contrary to sucralose, stevia and neohesperidin DC lead to a more important decrease of the apK_A of the surfactant in the sodium oleate aqueous solution. This leads to the conclusion that stevia and neohesperidin DC are stronger cosurfactants than sucralose and get considerably inserted into the sodium oleate interfacial films, both in the micelles and in the microemulsions. This contribution is consistent with the amphiphilic properties of stevia and neohesperidin DC, well established by their capacity to form micelles in water.[278-282] The amphiphilic properties of stevia are strongly supported by the important capacity of this sweetener to solubilise a hydrophobic dye like Disperse Red 13 at very low molar concentrations (data not shown here). This is compatible with a surfactant behaviour.[283]

At low concentrations, stevia, neohesperdin DC, or naringin DC seem to considerably partition into the interfacial film and form a co-micelle with sodium oleate. The association sodium oleate/stevia leads to the decrease of the unfavorable electrostatic interactions between the surfactant heads, as the apK_A decreases sharply in the microemulsion. However, neohesperidin DC has no real influence on the apK_A of the surfactant in the microemulsion (see **Figure 3.44**.b), which means that the molecules partition more into the nano-droplets core and do not interact with the charged surfactant heads. At higher concentrations, stevia and neohesperidin DC are no longer soluble in the formulation, most probably because of their high hydrophobicity and also very low solubility in citronellol and limonene.

Again, regarding the results obtained with stevia, it is to our knowledge the first time that an important decrease of the pH was observed by combining sodium oleate and stevia. The microemulsions were stable over a few days at a pH value of around and even slightly below 7. It is also the first time that a neutral or even slightly acidic pH is reported for an aqueous concentrated solution of sodium oleate using a natural high intensity sweetener. The same observation was already reported using cationic surfactant or nonionic ones.[284]

3.2.2.3.5. Osmolytes (sucrose, sorbitol, isomalt)

The clearing temperature curves obtained by addition of sucrose, sorbitol, and isomalt have nearly the same decreasing slopes for concentrations between 0 and 0.2 mol.kg^{-1} (see **Figure 3.45**.a). At this concentration, T_α is about 20 °C for the three sweeteners. T_α keeps decreasing for sucrose and sorbitol at higher concentration. The reached T_α is equal to 8 and 1 °C for 1.2 mol.kg^{-1} of respectively sucrose and sorbitol. Adding more isomalt in the formulation, T_α still decreases and reaches 13 °C with 0.4 mol.kg^{-1}. Then, the slope of the curve becomes positive and T_α is equal to 50 °C with 1 mol.kg^{-1} in the formulation. Following the results of the clearing temperature study, the solutions with sucrose and isomalt were warmed to 25 °C to investigate the influence on the apK_A with a larger range of concentrations. The curves obtained with sucrose and sorbitol have negative slopes at any concentration (see **Figure 3.45**.b). The apK_A decreases approximately by one unit with 3.3 mol.kg^{-1} of sorbitol in the formulation. A small decrease is also observed with sucrose. The apK_A varies from 9.0 to 8.5 with 1.2 mol.kg^{-1} of sucrose in the formulation. Note that the apK_A value decreases with increasing temperature, as shown in section 3.2.1. For example, it is equal to 9.2 at 20 °C and 9.0 at 25 °C.

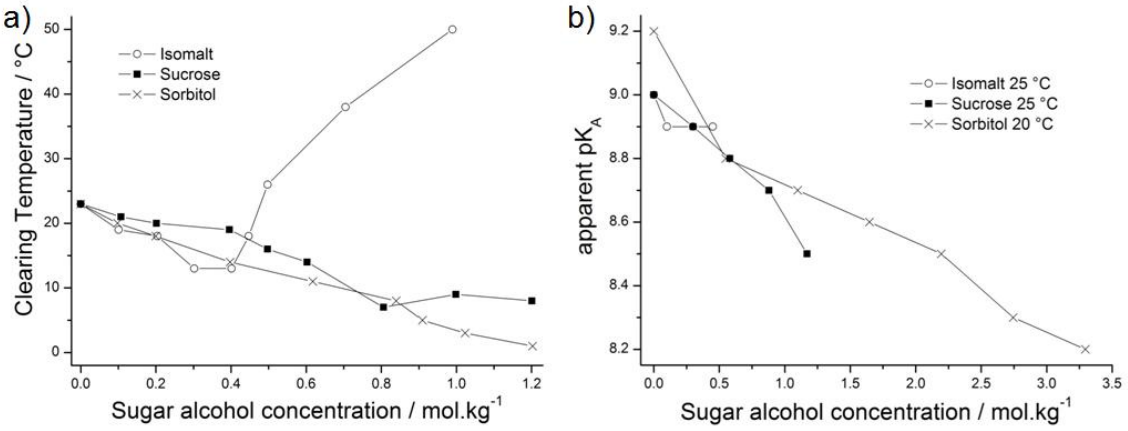

Figure 3.45. a) Clearing temperature in °C for the formulation B as a function of the sugar alcohol concentration in mol.kg^{-1}. The microemulsion area is above the curves. b) Apparent pK_A of the surfactant sodium oleate as a function of the sugar alcohol concentration for the formulation corresponding to point B.

The continuous decrease of T_α observed in presence of increasing sorbitol and sucrose concentrations, just as the one reported for low isomalt concentrations, can be explained by the fact that sorbitol, sucrose, and isomalt can push the ethanol into the micelles by a salting-out effect.[285] This is in agreement with the osmolyte properties of these molecules.[286] They improve indirectly the solubility of sodium oleate and the stability of the microemulsion nano-droplets by decreasing the sodium oleate apK_A. It was shown in section 3.2.1 that no shift of the pK_A of sodium oleate was observed without ethanol. The increase of the slope for the T_α curve of isomalt starts at the limit of its solubility in water.[287] An increase of the temperature is then probably necessary for the microemulsion to form by increasing the solubility of isomalt in the aqueous pseudo-phase.

3.2.2.4. Conclusion

Studies concerning the influences of additives on the nano-structures of microemulsions are recurrent in the literature, for example influences of cosurfactant or cosolvents,[16] of mixed surfactants[288] or of electrolytes.[289-291] However, studies of the effects of such additives on the pK_A of a fatty acid salt used as a surfactant in microemulsions are rare. Fatty acid salts are good candidates as surfactants in the food industry as they are green and can be used without limitation according to the legislation. However, their use is difficult to implement because of their high pK_A. So any additive that can help using fatty acids at moderate pH is very welcome. Another issue of soaps is of course their unpleasant taste. To a certain extent, it can be attenuated by adding sweeteners. In the ideal case, the sweetener would also favorably influence the pK_A of the fatty acid. This consideration was the starting point of the present work.

Here, we investigated the influences of artificial and natural high intensity sweeteners and sugar alcohols on the clearing temperature of a microemulsion and on the apK_A of its surfactant, i.e. sodium oleate. The results can be summarized in the form of an Euler diagram represented in **Figure 3.46**. High intensity sweeteners can be classified according to their localisation in the microemulsion. While the artificial charged high intensity sweeteners saccharin and acesulfame K behave like electrolytes and dehydrate the interfacial film of the microemulsion nano-droplets, the high intensity sweeteners neotame, stevia and neohesperidin DC act like (co)surfactants. Their amphiphilic structure allows them to form a co-micelle with sodium oleate. Due to the strong interactions of stevia with the sodium oleate head groups, an important shift of its pK_A is observed. Aspartame exhibits a strong precipitation behaviour, whereas cyclamate and sucralose interact with the surface of the sodium oleate micelles or with the interfacial film of the microemulsion nano-droplets without penetrating them. The artificial and natural sugar alcohols

sucrose, sorbitol and isomalt seem to play indirectly on the interfacial film of the microemulsion nano-droplets by pushing the ethanol molecules towards them.

The most important result of this work is the fact that homogeneous and clear microemulsions with a fatty acid salt as surfactant can be formulated at nearly neutral pH using appropriate sweeteners. An important decrease of the apK_A of sodium oleate was observed by combining it either with sucralose or stevia or even neotame. Thus, formulations of beverages with those sweeteners and a fatty acid salt are now possible. The next step will be the development and improvement of such beverages.

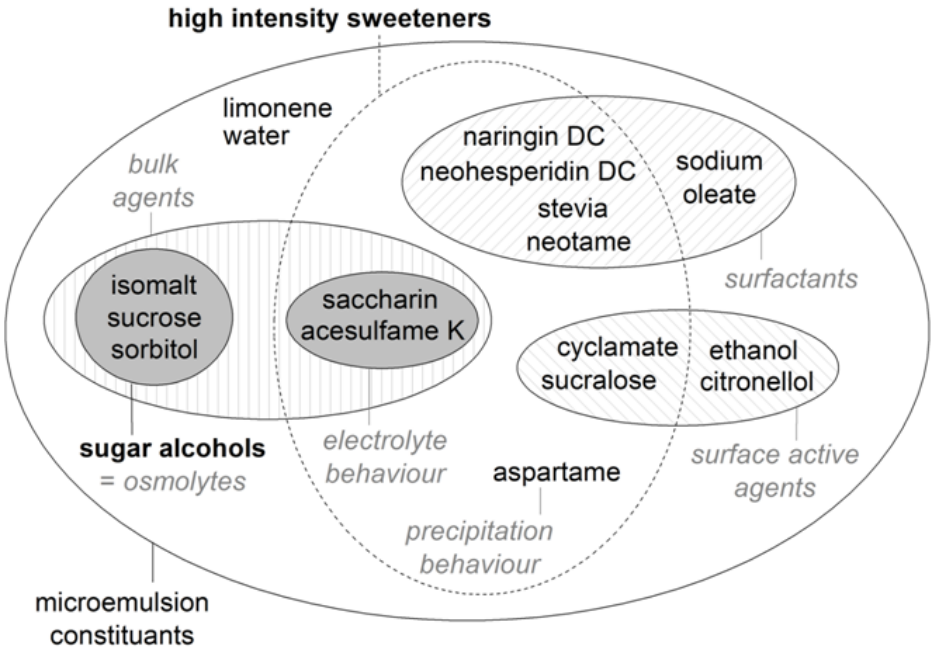

Figure 3.46. Euler diagram proposing a sub-classification of sweeteners in regards to their properties.

CHAPTER 4 CONCLUSIONS

The work of this thesis was divided into two major parts. Surfactant-free microemulsions and surfactant-based microemulsions were respectively investigated in the first and second part.

After the first investigations on the occurrence and nano-structures of **surfactant-free microemulsions**, we investigated the influences of different salts and surfactants on the system water/ethanol/1-octanol (see section 3.1.1). The latter consists of fluctuating oil-rich aggregates surrounded by a water-rich bulk phase with a slight accumulation of ethanol at the interface. Upon addition of electrolytes, either a salting-out effect toward ethanol is observed, or a charge separation via the antagonistic ion effect described by Onuki *et al.* Surfactants such as SDS or NaDEHP induce a gradual transition towards monodisperse ionic micelles, where ethanol acts as cosurfactant. It can be noted that both fluctuations of aggregate concentration and of ethanol between both pseudo-phases have to be taken into account to understand the DLS results.

In section 3.1.2, water-free and surfactant-free microemulsions were investigated with the systems glycerol/ethanol/1-octanol, and deep eutectic solvent (DES)/tetrahydrofurfuryl alcohol/diethyl adipate, where the DESs were either ethylene glycol-choline chloride or urea-choline chloride. It was shown that fluctuating nano-structures also occur in surfactant-free microemulsions without water and that their size increases when approaching the demixing boundary. Further, one important result was the fact that the amphiphilic behaviour of 1-octanol was not responsible for these fluctuations. Also, it was definitely proven that these fluctuations are not due to critical molecular fluctuations near a critical point.

Two examples of surfactant-free microemulsions were then presented. The systems water/ethanol/fragrance were studied, where the fragrance molecules were citronellol, citral, geranyl acetate, and limonene (see section 3.1.3). The latter can be found in numerous perfumes.

According to our model formulations, such nano-structures can be predicted in Eau de Toilette and Eau de Parfum or in perfume, in presence of very hydrophobic fragrance molecules, and affect considerably the performance of the perfume. A strong evaporation of ethanol in the pre-Ouzo zone was observed, as well as a noticeable auto-encapsulation of the fragrance in the Ouzo domain, when the water evaporates. As also shown in section 3.1.4, fluctuating nano-structures can also appear in mosquito repellents. This study was performed in the systems water/ethanol or isopropanol/mosquito repellent, where the mosquito repellents used were the ones available on the market, i.e. citriodiol, PMD, 2-undecanone, DEET, KBR 3023, and IR 3535. Such a nano-structuring may have an impact on the behaviour of such products on the skin or have an influence on the outer pseudo-phase or on the mosquito receptors. However, the last assumptions have to be further investigated.

⟶ In this thesis we completed the knowledge of surfactant-free microemulsions. It cannot be stressed enough that the observed fluctuations are not due to critical molecular fluctuations near a critical point. That point was definitely checked. As explained in the *Fundamentals* part, salts exhibit different behaviours depending on the studied system. Those behaviours can be completed with those observed in the surfactant-free microemulsion. The fact that antagonistic ions behave like surfactants in presence of ethanol in such systems could be useful for applications involving a surfactant that must be ultimately removed from the system. Further, surfactant-free microemulsions only exhibit an Ornstein-Zernike pattern in SAXS, in contrast to typical surfactant-based microemulsions which are characterised by a liquid order peak. It was interesting to observe the transition between both upon addition of antagonistic salts. This thesis aims at proving that the pre-Ouzo effect, i.e. the presence of fluctuating nano-structures near the demixing boundary, is general and occurs with or without water. It seems that it is independent of the oil type, as we investigated systems involving a primary alcohol, an aldehyde, an ester, a terpene, a diol, a ketone, an amide, and more complex structures with nitrogen groups. The main and perhaps only criterion is that two immiscible solvents are rendered mutually soluble by a third one. In this thesis, the latter was ethanol, isopropanol or tetrahydrofurfuryl alcohol.

However, the fact that these surfactant-free microemulsions are stable is quite remarkable. In a recent article, Zemb *et al.* explained how such mixtures form.[148] They used a DLVO-like theory and found that the electrostatics versus van der Waals balance, valid for all classical micellar systems, has to be replaced by a hydration versus entropy balance, corrected by a weak bending energy term for surfactant-free microemulsions. As for the DLVO theory, a free energy minimum is obtained for droplet sizes around 2 nm in radius. They explained that the entropy of dispersion drives the system toward smaller domains. As the molecules are not randomly dispersed close to the demixing boundary, the free energy minimum is obtained for an optimum size of the aggregates. Further, the hydration force is significant near the interface. A net repulsion of the

droplets is observed due to the structured adsorbed layer of water and the slight excess of ethanol at the interface.

The investigations of **surfactant-based microemulsions** were performed using one particular oil-in-water microemulsion composed of 75 wt% water, 10 wt% sodium oleate, 9.25 wt% ethanol, 0.75 wt% citronellol, and 5 wt% limonene. Sodium oleate is a fatty acid salt and was used as surfactant, the mixture ethanol/citronellol as cosurfactant and limonene as oil. Further, this microemulsion is highly water dilutable.

In a first work presented in section 3.2.1, the influences of ethanol, citronellol, limonene, salts, and polyols were investigated on the temperature stability of that formulation and on the apparent pK_A (apK_A) of its soap surfactant. The apK_A decreases for the aqueous solution of sodium oleate with an increase of temperature. A decrease of apK_A was also observed upon addition of ethanol, which participates in the interfacial film and separates the surfactant headgroups, thus decreasing the unfavourable repulsive electrostatic interactions. No influence on the apKA was observed with a small amount of citronellol. However, the apK_A increases when limonene is added as oil to form the investigated formulation. This increase can be explained with the solubilisation of uncharged oleic acid in the organic core of the microemulsion droplets. Citronellol may have the same effect at high concentrations. The anions have no specific influence on the microemulsion system and the evolution of the clearing temperature follows electrostatic interactions. However, the specificity of the cations is linked to the possibility for cations to exchange with the original surfactant counterion. Further, glycerol and sorbitol are salting-in in our microemulsion, but only in the presence of ethanol.

The influences of artificial and natural high intensity sweeteners and sugar alcohols on the clearing temperature and on the apK_A of the same oil-in-water highly dilutable microemulsion were investigated in the second work presented in section 3.2.2. These two investigation methods allowed us to classify those artificial and natural sweeteners according to their localisation in the microemulsion. Saccharin and acesulfame K behave like electrolytes and dehydrate the interfacial film of the microemulsion droplets. The high intensity sweeteners neotame, stevia, and neohesperidin DC act like (co)surfactants due to their amphiphilic structure, which allows them to form a co-micelle with sodium oleate. An important decrease of the apK_A is observed upon addition of stevia. Aspartame tends to precipitate, whereas cyclamate and sucralose interact with the surface of the surfactant micelles or with the interfacial film of the microemulsion droplets. The sugar alcohols sucrose, sorbitol and isomalt behave like osmolytes and push the ethanol molecules toward the microemulsion droplets.

→ Fatty acid salts are good candidates as surfactants in the food industry as they are green and can be used without limitation according to the legislation. However, their use is difficult to

implement because of their high pK_A and their unpleasant soapy taste. That may be why studies of the effects of additives, such as salts or sweeteners, on the pK_A of a fatty acid salt or on a microemulsion system involving a soap as surfactant are rare. Such studies are crucial to better understand their roles in these formulations. This thesis allows us to better understand i) the influence of each component of our model formulation on the apK_A of the surfactant, and ii) the influences of salts on a soap in systems where they are self-associating. Such highly water dilutable microemulsions can be used as perfume or aroma carriers. Their dilution or neutralisation to pH smaller than 7 leads to emulsions with enough stability for a good dispersion in a process. The influences of sweeteners on such soap molecules are also important to investigate as they can decrease their apK_A and attenuate their unpleasant taste. We succeeded in formulating homogeneous, clear, and thermodynamically stable microemulsions with a fatty acid salt as surfactant at nearly neutral pH, upon addition of stevia, sucralose, or neotame. Formulations of beverages with such sweeteners and a fatty acid salt are now possible and have to be further developed.

List of figures

List of tables

Literature

1. T. P. Hoar and J. H. Schulman, *Nature*, **1943**, *152*, 102-103.
2. J. H. Schulman, W. Stoeckenius and L. M. Prince, *J. Phys. Chem.*, **1959**, *63*, 1677-1680.
3. B. Lindman and H. Wennerström, *Top. Curr. Chem.*, **1980**, *87*, 1-83.
4. H. F. Eicke, *Top. Curr. Chem.*, **1980**, *87*, 85-145.
5. P. G. De Gennes and C. Taupin, *J. Phys. Chem.*, **1982**, *86*, 2294-2304.
6. J. H. Schulman and T. S. McRoberts, *T. Faraday Soc.*, **1946**, *42B*, 165-170.
7. A. Goebel and K. Lunkenheimer, *Langmuir*, **1997**, *13*, 369-372.
8. D. Touraud, Thesis, Université de Compiègne, **1991**.
9. L. E. Scriven, *Nature*, **1976**, *263*, 123-125.
10. D. Langevin, *Annu. Rev. Phys. Chem.*, **1992**, *43*, 341-369.
11. M. Clausse, J. Peyrelasse, J. Heil, C. Boned and B. Lagourette, *Nature*, **1981**, *293*, 636-638.
12. P. A. Winsor, *T. Faraday Soc.*, **1948**, *44*, 376-382.
13. V. K. Bansal, K. Chinnaswamy, C. Ramachandran and D. O. Shah, *J. Colloid Interface Sci.*, **1979**, *72*, 524-537.
14. E. Sjöblom and S. Friberg, *J. Colloid Interface Sci.*, **1978**, *67*, 16-30.
15. E. Caponetti, A. Lizzio, R. Triolo, W. L. Griffith and J. J. S. Johnson, *Langmuir*, **1992**, *8*, 1554-1562.
16. R. Zana, *Adv. Colloid Interface Sci.*, **1995**, *57*, 1-64.
17. M. Fanun, *Microemulsions. Properties and applications*, CRC Press, **2008**.
18. R. Strey and M. Jonströmer, *J. Phys. Chem.*, **1992**, *96*, 4537-4542.
19. B. Lindman, P. Stilbs and K. Rapacki, *J. Colloid Interface Sci.*, **1983**, *95*, 583-585.
20. J. Peyrelasse, C. Boned, J. Heil and M. Clausse, *J. Phys. C. Solid State*, **1982**, *15*, 7099-7118.
21. J. L. Salager, R. Antón and J.-M. Aubry, *Techniques de l'Ingénieur J2*, **2006**, *158*, 1-15.
22. A. Pizzino, V. Molinier, M. Catté, J.-L. Salager and J.-M. Aubry, *J. Phys. Chem. B*, **2009**, *113*, 16142-16150.
23. B. Lagourette, J. Peyrelasse, C. Boned and M. Clausse, *Nature*, **1979**, *281*, 60-62.
24. M. Lagues, R. Ober and C. Taupin, *J. Phys. Lett.*, **1978**, *39*, 487-491.
25. M. Lagues, *J. Phys. Lett.*, **1979**, *40*, 331-333.
26. A. Ponton, T. K. Bose and G. Delbos, *J. Chem. Phys.*, **1991**, *94*, 6879.
27. M. Lagues and C. Sauterey, *J. Phys. Chem.*, **1980**, *84*, 3503-3508.
28. M. L. Klossek, J. Marcus, D. Touraud and W. Kunz, *Colloids Surf., A*, **2013**, *427*, 95-100.
29. M. L. Klossek, D. Touraud and W. Kunz, *Green Chem.*, **2012**, *14*, 2017.
30. J. Fang and R. L. Venable, *J. Colloid Interface Sci.*, **1987**, *116*, 269-277.

31. M. Giustini, G. Palazzo, G. Colafemmina, M. D. Monica, M. Giomini and A. Ceglie, *J. Phys. Chem.*, **1996**, *100*, 3190-3198.
32. A. Bumajdad and J. Eastoe, *J. Colloid Interface Sci.*, **2004**, *274*, 268-276.
33. Y. Gao, S. Wang, L. Zheng, S. Han, X. Zhang, D. Lu, L. Yu, Y. Ji and G. Zhang, *J. Colloid Interface Sci.*, **2006**, *301*, 612-616.
34. C. Mathew, P. K. Patanjali, A. Nabi and A. Maitra, *Colloids Surf.*, **1988**, *30*, 253-263.
35. P. Lindner and T. Zemb, *Neutrons, X-Rays and Light scattering methods applied to soft condensed matter*, Elsevier, **2002**.
36. A. M. Cazabat and D. Langevin, *J. Chem. Phys.*, **1981**, *74*, 3148.
37. J. Rouch, A. Safouane, P. Tartaglia and S. H. Chen, *J. Chem. Phys.*, **1989**, *90*, 3756.
38. C. A. T. Laia, P. López-Cornejo, S. M. B. Costa, J. d'Oliveira and J. M. G. Martinho, *Langmuir*, **1998**, *14*, 3531-3537.
39. T. Blochowicz, C. Gögelein, T. Spehr, M. Müller and B. Stühn, *Phys. Rev. E*, **2007**, *76*, 1-9.
40. M. L. Klossek, D. Touraud and W. Kunz, *ACS Sustainable Chem. Eng.*, **2013**, *1*, 603-610.
41. Malvern, 2013.
42. P. J. Wyatt, *Anal. Chim. Acta*, **1993**, *272*, 1-40.
43. B. H. Zimm, *J. Chem. Phys.*, **1948**, *16*, 1093-1099.
44. M. J. Hou, M. Kim and D. O. Shah, *J. Colloid Interface Sci.*, **1988**, *123*, 398-412.
45. U. Menge, P. Lang and G. H. Findenegg, *J. Phys. Chem. B*, **1999**, *103*, 5768-5774.
46. A. Shioi, M. Harada and M. Tanabe, *J. Phys. Chem.*, **1995**, *99*, 4750-4756.
47. Commissariat à l'énergie atomique, What is measured in a small angle x-ray scattering, http://iramis.cea.fr/Phocea/Vie_des_labos/Ast/ast_sstechnique.php?id_ast=1065, **2015**.
48. B. R. Pauw, *J. Phys.: Condens. Matter*, **2013**, *25*, 1-24.
49. H. Schnablegger and Y. Singh, Anton Paar GmbH, 2011.
50. O. Glatter and O. Kratky, *Small Angle X-ray scattering*, Academic Press, London, **1982**.
51. A. Guinier and G. Fournet, *Small-angle scattering of X-Rays*, Wiley, New York, **1955**.
52. G. Porod, *Kolloid-Zeitschrift*, **1951**, *124*, 83-114.
53. J. W. Shield, H. D. Ferguson, A. S. Bommarius and T. A. Hatton, *Ind. Eng. Chem. Fundam.*, **1986**, *25*, 603-612.
54. C. Solans and H. Kunieda, *Industrial applications of microemulsions*, Marcel Dekker, New York, **1997**.
55. V. Papadimitriou, A. Xenakis and A. E. Evangelopoulos, *Colloids Surf., B*, **1993**, *1*, 295-303.
56. D. Han and J. S. Rhee, *Biotechnol. Bioeng.*, **1986**, *28*, 1250-1255.
57. M. E. Kraeling and W. A. Ritschel, *Method. Find. Exp. Clin.*, **1992**, *14*, 199-209.
58. P. Kumar and K. L. Mittal, *Handbook of microemulsion science and technology*, Marcel Dekker, New York, **1999**.
59. C. Fox, *Cosmet. Toiletries*, **1995**, *110*, 59-62.
60. D. H. Britwistle, patent EP 468721 A1 19920129, **1992**.
61. D. J. Halloran, patent EP 514934 A1 19921125, **1992**.

62. R. J. Miller and Y. S. You, patent US5047084 A, **1990**.
63. E. R. Washburn, V. Hnizda and R. Vold, *J. Am. Chem. Soc.*, **1931**, *53*, 3237-3244.
64. R. D. Vold and E. R. Washburn, *J. Am. Chem. Soc.*, **1932**, *54*, 4217-4225.
65. E. R. Washburn and H. C. Spencer, *J. Am. Chem. Soc.*, **1934**, *56*, 361-364.
66. A. L. Olsen and E. R. Washburn, *J. Am. Chem. Soc.*, **1935**, *57*, 303-305.
67. E. R. Washburn, A. E. Beguin and O. C. Beckord, *J. Am. Chem. Soc.*, **1939**, *61*, 1694-1695.
68. G. D. Smith, C. E. Donelan and R. E. Barden, *J. Colloid Interface Sci.*, **1977**, *60*, 488-496.
69. B. A. Keiser, D. Varie, R. E. Barden and S. L. Holt, *J. Phys. Chem.*, **1979**, *83*, 1276-1280.
70. N. F. Borys, S. L. Holt and R. E. Barden, *J. Colloid Interface Sci.*, **1979**, *71*, 526-532.
71. G. Lund and S. L. Holt, *J. Am. Oil Chem. Soc.*, **1980**, *57*, 264-267.
72. C. J. O'Connor and D. R. Cleverly, *Biocatal. Biotransform.*, **1995**, *12*, 193-204.
73. Y. L. Khmelnitsky, A. K. Gladilin, I. N. Neverova, A. V. Levashov and K. Martinek, *Collect. Czech. Chem. Commun.*, **1990**, *55*, 555-563.
74. M. Zoumpanioti, M. Karali, A. Xenakis and H. Stamatis, *Enzyme Microb. Technol.*, **2006**, *39*, 531-539.
75. M. Zoumpanioti, H. Stamatis, V. Papadimitriou and A. Xenakis, *Colloids Surf., B*, **2006**, *47*, 1-9.
76. N. L. Sitnikova, R. Sprik and G. Wegdam, *Langmuir*, **2005**, *21*, 7083-7089.
77. S. A. Vitale and J. L. Katz, *Langmuir*, **2003**, *19*, 4105-4110.
78. D. Carteau, I. Pianet, P. Brunerie, B. Guillemat and D. M. Bassani, *Langmuir*, **2007**, *23*, 3561-3565.
79. R. Botet, *J. Phys.: Conf. Ser.*, **2012**, *352*, 012047.
80. I. Grillo, *Colloids Surf., A*, **2003**, *225*, 153-160.
81. E. Aschenbrenner, K. Bley, K. Koynov, M. Makowski, M. Kappl, K. Landfester and C. K. Weiss, *Langmuir*, **2013**, *29*, 8845-8855.
82. X. Yan, M. Delgado, A. Fu, P. Alcouffe, S. G. Gouin, E. Fleury, J. L. Katz, F. Ganachaud and J. Bernard, *Angew. Chem. Int. Ed.*, **2014**, *53*, 6910-6913.
83. J. Aubry, F. Ganachaud, J.-P. Cohen Addad and B. Cabane, *Langmuir*, **2009**, *25*, 1970-1979.
84. F. Ganachaud and J. L. Katz, *ChemPhysChem*, **2005**, *6*, 209-216.
85. S. Peng, C. Xu, T. C. Hughes and X. Zhang, *Langmuir*, **2014**, *30*, 12270-12277.
86. D. Horn, *Angew. Makromol. Chem.*, **1989**, *166/167*, 139-153.
87. E. Lepeltier, C. Bourgaux and P. Couvreur, *Adv. Drug Deliver. Rev.*, **2014**, *71*, 86-97.
88. M. L. Klossek, D. Touraud, T. Zemb and W. Kunz, *ChemPhysChem*, **2012**, *13*, 4116-4119.
89. M. L. Klossek, D. Touraud and W. Kunz, *Phys. Chem. Chem. Phys.*, **2013**, *15*, 10971-10977.
90. O. Diat, M. L. Klossek, D. Touraud, B. Deme, I. Grillo, W. Kunz and T. Zemb, *J. Appl. Crystallogr.*, **2013**, *46*, 1665-1669.

91. S. Schöttl, J. Marcus, O. Diat, D. Touraud, W. Kunz, T. Zemb and D. Horinek, *Chem. Sci.*, **2014**, *5*, 2949.

92. D. Subramanian, C. T. Boughter, J. B. Klauda, B. Hammouda and M. A. Anisimov, *Faraday Discuss.*, **2013**, *167*, 217-238.

93. D. Subramanian and M. A. Anisimov, *Fluid Phase Equilib.*, **2014**, *362*, 170-176.

94. V. Tchakalova, T. Zemb and D. Benczédi, *Colloids Surf., A*, **2014**, *460*, 414-421.

95. R. F. Hankel, P. E. Rojas, M. Cano-Sarabia, S. Sala, J. Veciana, A. Braeuer and N. Ventosa, *Chem. Commun.*, **2014**, *50*, 8215-8218.

96. J. Lang, C. Tondre, R. Zana, R. Bauer, H. Hoffmann and W. Ulbricht, *J. Phys. Chem.*, **1975**, *79*, 276-283.

97. E. A. G. Aniansson, S. N. Wall, M. Almgren, H. Hoffmann, I. Kielmann, W. Ulbricht, R. Zana, J. Lang and C. Tondre, *J. Phys. Chem.*, **1976**, *80*, 905-922.

98. D. A. Ivanov and J. Winkelmann, *Phys. Chem. Chem. Phys.*, **2004**, *6*, 3490-3499.

99. A. Heller, J. Chen, M. S. H. Fleys, G. P. van der Laan, M. H. Rausch and A. P. Fröba, presented in part at the Nineteenth Symposium on Thermophysical Properties, Boulder, CO, USA, June 21-26, **2015**.

100. A. Arce, A. Blanco, A. Soto and I. Vidal, *J. Chem. Eng. Data*, **1993**, *38*, 336-340.

101. F. Hofmeister, *Arch. Exp. Pathol. Pharmakol.*, **1888**, *24*, 247-260.

102. W. Kunz, *Specific ion effects*, World Scientific Publishing, **2010**.

103. K. D. Collins, *Methods*, **2004**, *34*, 300-311.

104. W. Kunz, *Curr. Opin. Colloid Interface Sci.*, **2010**, *15*, 34-39.

105. N. Vlachy, M. Drechsler, J. M. Verbavatz, D. Touraud and W. Kunz, *J. Colloid Interface Sci.*, **2008**, *319*, 542-548.

106. N. Vlachy, B. Jagoda-Cwiklik, R. Vacha, D. Touraud, P. Jungwirth and W. Kunz, *Adv. Colloid Interface Sci.*, **2009**, *146*, 42-47.

107. N. Schwierz, D. Horinek and R. R. Netz, *Langmuir*, **2010**, *26*, 7370-7379.

108. N. Schwierz, D. Horinek and R. R. Netz, *Langmuir*, **2013**, *29*, 2602-2614.

109. K. Sadakane, A. Onuki, S. Koizumi and H. Seto, *Phys. Rev. Lett.*, **2009**, *103*.

110. K. Sadakane, N. Iguchi, M. Nagao, H. Endo, Y. B. Melnichenko and H. Seto, *Soft Matter*, **2011**, *7*, 1334.

111. K. Sadakane, H. Seto, H. Endo and M. Shibayama, *J. Phys. Soc. Jpn.*, **2007**, *76*, 113602/113601-113602/113603.

112. K. Sadakane, M. Nagao, H. Endo and H. Seto, *J. Chem. Phys.*, **2013**, *139*, 234905.

113. F. Pousaneh and A. Ciach, *Soft Matter*, **2014**, *10*, 8188-8201.

114. K. Sadakane, Y. Horikawa, M. Nagao and H. Seto, *Chem. Lett.*, **2012**, *41*, 1075-1077.

115. D. Michler, N. Shahidzadeh, M. Westbroek, R. van Roij and D. Bonn, *Langmuir*, **2015**, *31*, 906-911.

116. A. Onuki, R. Okamoto and T. Araki, *Bull. Chem. Soc. Jpn.*, **2011**, *84*, 569-587.

117. A. Onuki, *J. Chem. Phys.*, **2008**, *128*, 224704.

118. A. Onuki, T. Araki and R. Okamoto, *J. Phys.: Condens. Matter*, **2011**, *23*, 284113.

119. T. Araki and A. Onuki, *J. Phys.: Condens. Matter*, **2009**, *21*, 424116.

120. K. Holmberg, *Handbook of applied surface and colloid chemistry*, Wiley, **2002**.

121. D. M. Small, *Handbook of lipid research*, Plenum Press, **1986**.

122. J. J. Janke, W. F. Bennett and D. P. Tieleman, *Langmuir*, **2014**, *30*, 10661-10667.

123. J. R. Kanicky, A. F. Poniatowski, N. R. Mehta and D. O. Shah, *Langmuir*, **2000**, *16*, 172-177.

124. J. R. Kanicky and D. O. Shah, *Langmuir*, **2003**, *19*, 2034-2038.

125. A. Psurek and G. K. E. Scriba, *Electrophoresis*, **2003**, *24*, 765-773.

126. S. E. Creager and J. Clarke, *Langmuir*, **1994**, *10*, 3675-3683.

127. M. Egret-Charlier, A. Sanson, M. Ptak and O. Bouloussa, *FEBS Lett.*, **1978**, *89*, 313-316.

128. E. D. Goddard, *Adv. Colloid Interface Sci.*, **1974**, *4*, 45-78.

129. R. G. Bates, *Solute-solvent interactions*, Marcel Dekker, New York, **1969**.

130. J. R. Kanicky and D. O. Shah, *J. Colloid Interface Sci.*, **2002**, *256*, 201-207.

131. D. P. Cistola, J. A. Hamilton, D. Jackson and D. M. Small, *Biochemistry*, **1988**, *27*, 1881-1888.

132. S. V. Pande and J. F. Mead, *J. Biol. Chem.*, **1968**, *243*, 6180-6185.

133. A. M. Katz and F. C. Messineo, *Circ. Res.*, **1981**, *48*, 1-16.

134. A. A. Spector, *Lipid Res.*, **1975**, *16*, 165-179.

135. M. Clausse, L. Nicolas-Morgantini, A. Zrabda and D. Touraud, *Microemulsion Systems*, Dekker, New York, **1987**.

136. H. Preu, C. Schirmer, M. Tomsic, M. Bester Rogac, A. Jamnik, L. Belloni and W. Kunz, *J. Phys. Chem. B*, **2003**, *107*, 13862-13870.

137. Y. Einaga, F. Abe and H. Yamakawa, *J. Phys. Chem.*, **1992**, *96*, 3948-3953.

138. Y. Niebel, M. D. Buschmann, M. Lavertu and G. De Crescenzo, *Biomacromolecules*, **2014**, *15*, 940-947.

139. J. B. Hayter and J. Penfold, *Colloid Polym. Sci.*, **1983**, *261*, 1022-1030.

140. M. Duvail, L. Arleth, T. Zemb and J.-F. Dufreche, *J. Chem. Phys.*, **2014**, *140*, 164711/164711-164711/164711.

141. P. Bauduin, F. Testard and T. Zemb, *J. Phys. Chem. B*, **2008**, *112*, 12354-12360.

142. W. Kunz, P. Lo Nostro and B. W. Ninham, *Curr. Opin. Colloid Interface Sci.*, **2004**, *9*, 1-18.

143. Y. Marcus, *Ion properties*, Marcel Dekker, Inc., New York, **1997**.

144. C. J. Rizzo, *J. Org. Chem.*, **1992**, *57*, 6382-6384.

145. A. Onuki and H. Kitamura, *J. Chem. Phys.*, **2004**, *121*, 3143-3151.

146. E. Leontidis, M. Christoforou, C. Georgiou and T. Delclos, *Curr. Opin. Colloid Interface Sci.*, **2014**, *19*, 2-8.

147. C. Tanford, *The hydrophobic effect: formation of micelles and biological membranes*, John Wiley & Sons Inc., New York, **1973**.

148. T. Zemb, M. L. Klossek, T. Lopian, J. Marcus, D. Horinek, S. Schöttl, S. Prevost, D. Touraud, O. Diat, S. Marčelja and W. Kunz, *PNAS*, **2015**, submitted.

149. J. B. Hayter, *Langmuir*, **1992**, *8*, 2873-2876.

150. T. Zemb, *Colloids Surf., A*, **1997**, *129-130*, 435-454.

151. B. W. Ninham and V. A. Parsegian, *J. Theor. Biol.*, **1971**, *31*, 405-428.

152. K. V. Schubert and R. Strey, *J. Chem. Phys.*, **1991**, *95*, 8532-8545.

153. K. V. Schubert, R. Strey, S. R. Kline and E. W. Kaler, *J. Chem. Phys.*, **1994**, *101*, 5343-5355.

154. S. Marčelja, *Nature*, **1997**, *385*, 689-690.

155. S. Schöttl and D. Horinek, *in preparation*, **2015**.

156. R. Okamoto and A. Onuki, *Phys. Rev. E*, **2010**, *82*, 1-20.

157. M. L. Klossek, J. Marcus, D. Touraud and W. Kunz, *Colloids Surf., A*, **2014**, *442*, 105-110.

158. A. Kogan and N. Garti, *Adv. Colloid Interface Sci.*, **2006**, *123*, 369-385.

159. M. F. Nazar, S. S. Shah and M. A. Khosa, *Pet. Sci. Technol.*, **2011**, *29*, 1353-1365.

160. M. Hloucha, H.-M. Haake and G. Pellon, *Cosmet. Toiletries*, **2009**, *124*, 58-69.

161. C. Solans, *Microemulsions in cosmetics, in: Industrial Applications of microemulsions*, Marcel Dekker, New York, **1997**.

162. F. Comelles, *J. Dispersion Sci. Technol.*, **1999**, *20*, 491-511.

163. N. Garti, *Curr. Opin. Colloid Interface Sci.*, **2003**, *8*, 197-211.

164. J. Flanagan and H. Singh, *Crit. Rev. Food Sci.*, **2006**, *46*, 221-237.

165. M. J. Lawrence and G. D. Rees, *Adv. Drug Deliver. Rev.*, **2000**, *45*, 89-121.

166. B. K. Paul and S. P. Moulik, *Curr. Sci.*, **2001**, *80*, 990-1001.

167. M. Fanun, *Curr. Opin. Colloid Interface Sci.*, **2012**, *17*, 306-313.

168. W. von Rybinski, M. Hloucha and I. Johansson, *Microemulsions in cosmetics and detergents, from Microemulsions*, Blackwell Publishing Ltd., **2009**.

169. H. D. Doerfler, A. Grosse and H. Kruessmann, *Tenside Surfact. Det.*, **1996**, *33*, 432-440.

170. I. Rico and A. Lattes, *Nouv. J. Chim.*, **1984**, *8*, 429-431.

171. I. Rico and A. Lattes, *J. Colloid Interface Sci.*, **1984**, *102*, 285-287.

172. A. Ahamd-Zadeh Samii, A. de Savignac, I. Rico and A. Lattes, *Tetrahedron*, **1985**, *41*, 3683-3688.

173. M. Gautier, I. Rico, A. Ahmad-Zadeh Samii, A. de Savignac and A. Lattes, *J. Colloid Interface Sci.*, **1986**, *112*, 484-487.

174. A. Harrar, O. Zech, A. Klaus, P. Bauduin and W. Kunz, *J. Colloid Interface Sci.*, **2011**, *362*, 423-429.

175. S. Hamdan, F. B. H. Ahmad, Y. Y. Dai, K. Dzulkefly and K. H. Ku Bulat, *J. Disper. Sci. Technol.*, **1999**, *20*, 415-423.

176. S. E. Friberg and W. M. Sun, *Colloid. Polym. Sci.*, **1990**, *268*, 755-759.

177. H.-L. Cai, X.-Q. An, B. Liu, Q.-A. Qiao and W.-G. Shen, *J. Solution Chem.*, **2010**, *39*, 718-726.

178. J. Peyrelasse, C. Boned and Z. Saidi, *Phys. Rev. E*, **1993**, *47*, 3412-3417.

179. N. M. Correa, J. J. Silber, R. E. Riter and N. E. Levinger, *Chem. Rev.*, **2012**, *112*, 4569-4602.

180. M. B. Oliveira, S. Barbedo, J. I. Soletti, S. H. V. Carvalho, A. J. Queimada and J. A. P. Coutinho, *Fuel*, **2011**, *90*, 2738-2745.

181. F. M. R. Mesquita, A. M. M. Bessa, D. D. de Lima, H. B. de Sant'Ana and R. S. de Santiago-Aguiar, *Fluid Phase Equilib.*, **2012**, *318*, 51-55.

182. A. B. Machado, Y. C. Ardila, L. H. de Oliveira, M. Aznar and M. R. Wolf Maciel, *J. Chem. Eng. Data*, **2012**, *57*, 1417-1422.

183. F. M. R. Mesquita, N. S. Evangelista, H. B. de Sant'Ana and R. S. de Santiago-Aguiar, *J. Chem. Eng. Data*, **2012**, *57*, 3557-3562.

184. F. M. R. Mesquita, F. X. Feitosa, N. E. Sombra, R. S. de Santiago-Aguiar and H. B. de Sant'Ana, *J. Chem. Eng. Data*, **2011**, *56*, 4061-4067.

185. N. Arpornpong, C. Attaphong, A. Charoensaeng, D. A. Sabatini and S. Khaodhiar, *Fuel*, **2014**, *132*, 101-106.

186. E. J. Silva, M. E. D. Zaniquelli and W. Loh, *Energy Fuels*, **2007**, *21*, 222-226.

187. A. P. Abbott, G. Capper, D. L. Davies, R. K. Rasheed and V. Tambyrajah, *Chem. Commun.*, **2003**, 70-71.

188. A. P. Abbott, D. Boothby, G. Capper, D. L. Davies and R. K. Rasheed, *J. Am. Chem. Soc.*, **2004**, *126*, 9142-9147.

189. International Programme on chemical safety, http://www.inchem.org/, **2015**.

190. Pennakem, Tetrahydrofurfuryl alcohol (THFA), http://www.pennakem.com/pdfs/thfa_tds02.pdf, **2015**.

191. J. Marcus, M. Müller, J. Nistler, D. Touraud and W. Kunz, *Colloids Surf., A*, **2014**, *458*, 3-9.

192. J. Marcus, M. L. Klossek, D. Touraud and W. Kunz, *Flavour Frag. J.*, **2013**, *28*, 294-299.

193. F. Gyger, P. Bockstaller, D. Gerthsen and C. Feldmann, *Angew. Chem. Int. Ed.*, **2013**, *52*, 12443-12447.

194. A. Arce, A. Marchiaro, J. M. Martínez-Ageitos and A. Soto, *Can. J. Chem. Eng.*, **2005**, *83*, 366-370.

195. N. E. Tajidin, *Afr. J. Biotechnol.*, **2012**, *11*, 2685-2693.

196. T. A. Misharina, M. B. Terenina, N. I. Krikunova and M. A. Kalinichenko, *Russ. J. Bioorg. Chem.*, **2011**, *37*, 883-887.

197. S. Bourgou, F. Z. Rahali, I. Ourghemmi and M. Saidani Tounsi, *ScientificWorldJournal*, **2012**, *2012*, 528593.

198. N. Manika, P. Mishra, N. Kumar, C. S. Chanotiya and G. D. Bagchi, *J. Med. Plants Res.*, **2012**, *6*, 2875-2879.

199. R. Garcia-Domenech, J. Aguilera, A. E. Moncef, S. Pocovi and J. Galvez, *Mol. Divers.*, **2010**, *14*, 321-329.

200. J. Drapeau, M. Verdier, D. Touraud, U. Kröckel, M. Geier, A. Rose and W. Kunz, *Chem. Biodivers.*, **2009**, *6*, 934-947.

201. K. E. Tsitsanou, T. Thireou, C. E. Drakou, K. Koussis, M. V. Keramioti, D. D. Leonidas, E. Eliopoulos, K. Iatrou and S. E. Zographos, *Cell. Mol. Life Sci.*, **2012**, *69*, 283-297.

202. E. K. Patel, A. Gupta and R. J. Oswal, *IJPCBS*, **2012**, *2*, 310-317.

203. A. R. Katritzky, Z. Wang, S. Slavov, M. Tsikolia, D. Dobchev, N. G. Akhmedov, C. D. Hall, U. R. Bernier, G. G. Clark and K. J. Linthicum, *PNAS*, **2008**, *105*, 7359-7364.

204. H. O. Lawal, G. O. Adewuyi, A. B. Fawehinmi, A. O. Adeogun and S. O. Etatuvie, *J. Nat. Prod.*, **2012**, *5*, 109-115.

205. Citrefine International Ltd., What is Citriodiol?, http://www.citrefine.com/citriodiol.html, **2015**.

206. V. De Feo, F. De Simone and F. Senatore, *Phytochemistry*, **2002**, *61*, 573-578.

207. J. Boeckh, H. Breer, M. Geier, F.-P. Hoever, B.-W. Krüger, G. Nentwig and H. Sass, *Pestic. Sci.*, **1996**, *48*, 359-373.

208. M. S. Fradin and J. F. Day, *N. Engl. J. Med.*, **2002**, *347*, 13-18.

209. A. Klaus, G. J. Tiddy, R. Rachel, A. P. Trinh, E. Maurer, D. Touraud and W. Kunz, *Langmuir*, **2011**, *27*, 4403-4411.

210. J. L. Anderson, J. Ding, T. Welton and D. W. Armstrong, *J. Am. Chem. Soc.*, **2002**, *124*, 14247-14254.

211. A. Kabalnov, U. Olsson and H. Wennerström, *J. Phys. Chem.*, **1995**, *99*, 6220-6230.

212. L. S. Romsted, *Langmuir*, **2007**, *23*, 414-424.

213. C. Bauer, P. Bauduin, O. Diat and T. Zemb, *Langmuir*, **2011**, *27*, 1653-1661.

214. S. Murgia, M. Monduzzi and B. W. Ninham, *Curr. Opin. Colloid Interface Sci.*, **2004**, *9*, 102-106.

215. M. Nydén, O. Söderman and P. Hansson, *Langmuir*, **2001**, *17*, 6794-6803.

216. G. Gillberg, H. Lehtinen and S. Friberg, *J. Colloid Interface Sci.*, **1970**, *33*, 40-53.

217. A. S. Kertes, B. Jernstrom and S. Friberg, *J. Colloid Interface Sci.*, **1975**, *52*, 122-128.

218. V. K. Bansal, D. O. Shah and J. P. O'Connell, *J. Colloid Interface Sci.*, **1980**, *75*, 462-475.

219. C. Boned, M. Clausse, B. Lagourette and J. Peyrelasse, *J. Phys. Chem.*, **1980**, *84*, 1520-1525.

220. E. Sjöblom and U. Henriksson, *J. Phys. Chem.*, **1982**, *86*, 4451-4456.

221. B. Jönsson and H. Wennerström, *J. Phys. Chem.*, **1987**, *91*, 338-352.

222. R. Leung and D. O. Shah, *J. Colloid Interface Sci.*, **1987**, *120*, 330-344.

223. E. Caponetti, A. Lizzio and R. Triolo, *Langmuir*, **1990**, *6*, 1628-1634.

224. M. Antonietti, R. Basten and F. Gröhn, *Langmuir*, **1994**, *10*, 2498-2500.

225. J. K. Weil, C. A. Schollenberger and W. M. Linfield, *J. Am. Oil Chem. Soc.*, **1977**, *54*, 1-3.

226. V. Tchakalova and W. Fieber, *J. Surfact. Deterg.*, **2012**, *15*, 167-177.

227. P. Bauduin, F. Nohmie, D. Touraud, R. Neueder, W. Kunz and B. W. Ninham, *J. Mol. Liq.*, **2006**, *123*, 14-19.

228. R. A. Robinson and R. H. Stokes, *Electrolyte Solutions, 2nd edition*, Butterworths, London, **1959**.

229. B. Lin, A. V. McCormick, H. T. Davis and R. Strey, *J. Colloid Interface Sci.*, **2005**, *291*, 543-549.

230. R. Klein, D. Touraud and W. Kunz, *Green Chem.*, **2008**, *10*, 433.

231. R. Klein, M. Kellermeier, M. Drechsler, D. Touraud and W. Kunz, *Colloids Surf., A*, **2009**, *338*, 129-134.

232. A. E. Voinescu, P. Bauduin, M. Cristina Pinna, D. Touraud, B. W. Ninham and W. Kunz, *J. Phys. Chem. B*, **2006**, *110*, 8870-8876.

233. S. Dengler, A. Klaus, G. J. T. Tiddy and W. Kunz, *Faraday Discuss.*, **2013**, *160*, 121.

234. L. Vrbka, J. Vondrasek, B. Jagoda-Cwiklik, R. Vacha and P. Jungwirth, *PNAS*, **2006**, *103*, 15440-15444.

235. R. Klein, M. Kellermeier, D. Touraud, E. Muller and W. Kunz, *J. Colloid Interface Sci.*, **2013**, *392*, 274-280.

236. L. Copolovici and U. Niinemets, *Chemosphere*, **2007**, *69*, 621-629.

237. H. Brueckel and M. Hood, patent GB 2247463 A 19920304, **1992**.

238. X. Wang, patent CN 103114008 A 20130522, **2013**.

239. G. D. Najafpour and L. C. Wee, *J. Phys. Sci.*, **2000**, *11*, 9-16.

240. X. Wang and D. Li, *Shipin Kexue*, **1988**, *97*, 30-31.

241. J. Israelachvili, *Colloids Surf., A*, **1994**, *91*, 1-8.

242. K. Shinoda and S. Friberg, *Adv. Colloid Interface Sci.*, **1975**, *4*, 281-300.

243. Y. Talmon and S. Prager, *J. Chem. Phys.*, **1978**, *69*, 2984.

244. N. Garti, A. Yaghmur, M. E. Leser, V. Clement and H. J. Watzke, *J. Agric. Food Chem.*, **2001**, *49*, 2552-2562.

245. M. Awad, Thesis, Universität Bonn, **2002**.

246. R. S. Shallenberger and T. E. Acree, *Nature*, **1967**, *216*, 480-482.

247. L. B. Kier, *J. Pharm. Sci.*, **1972**, *61*, 1394-1397.

248. Parlement européen, *Directive 94/35/CE du parlement européen et du conseil du 30 juin 1994 concernant les édulcorants destinés à être employés dans les denrées alimentaires*, Journal Officiel n° L237, **1994**.

249. K. Clauss and H. Jensen, *Angew. Chem. Int. Ed.*, **1973**, *12*, 869-876.

250. *The inventor of saccharine*, Scientific American (July 17, 1886), **1886**.

251. C. Fahlberg and I. Remsen, *Chem. Ber.*, **1879**, *12*, 469-473.

252. J. Emsley, *The consumers's good chemical guide*, Odile Jacob, Paris, **1996**.

253. D. E. Newton, *Food chemistry*, Facts on file Inc., **2007**.

254. R. Lewis, *Discovery: windows on the life sciences*, Oxford: Blackwell Science, **2001**.

255. R. H. Mazur, *Aspartame: Physiology and Biochemistry*, Marcel Dekker, New York, **1984**.

256. B. A. Magnuson, G. A. Burdock, J. Doull, R. M. Kroes, G. M. Marsh, M. W. Pariza, P. S. Spencer, W. J. Waddell, R. Walker and G. M. Williams, *Crit. Rev. Toxicol.*, **2007**, *37*, 629-727.

257. S. Arora, H. Gawande, K. Narendra, S. Yarrakula, V. P. Singh, V. Sharma, B. K. Wadhwa, S. K. Tomer and G. S. Sharma, *J. Food Sci. Tech.*, **2008**, *45*, 263-266.

258. Y. A. Verkholantsev and G. V. Kuranov, patent RU 2311800 C2 20071210, **2007**.

259. Z. Wang and X. Ye, patent CN 1911089 A 20070214, **2007**.

260. E. F. S. Authority, *EFSA Journal*, **2006**, *356*, 1-44.

261. C. Nofre and J.-M. Tinti, *Food Chem.*, **2000**, *69*, 245-257.

262. Beneo-Palatinit GmbH, Further sweeteners, http://www.intense-sweeteners.com/en/Products/Further_sweeteners/, **2015**.

263. L. Hough and S. P. Phadnis, *Nature*, **1976**, *263*, 800.

264. L. Hough and R. Khan, *TIBS*, **1978**, 61-63.

265. X. Li, Z. Du, X. Huang, W. Yuan and H. Ying, *J. Chem. Eng. Data*, **2010**, *55*, 2600-2602.

266. G. Cordes, U. Vollmer and D. Mertin, patent DE 19843027 A1 20000323, **2000**.

267. R. M. Horowitz and B. Gentili, patent US 3087821 19630430, **1963**.

268. R. Ikan, *1-flavonoides, E. synthesis of naringin dihydrochalcone - a sweetening agent, in: Natural products: a laboratory guide*, Academic Press, **1991**.

269. P. Tomasik, *Chemical and functional properties of food saccharides*, CRC Press, **2003**.

270. Cargill, What is stevia?, http://www.cargillfoods.com/na/en/products/sweeteners/specialty-sweeteners/truvia/about-stevia/index.jsp, **2015**.

271. C. Gardana, M. Scaglianti and P. Simonetti, *J. Chromatogr. A*, **2010**, *1217*, 1463-1470.

272. R. A. Adbullateef, N. H. Zakaria, N. H. Hasali and M. Osman, *IJB*, **2012**, *4*, 72-79.

273. H. K. Cammenga and B. Zielasko, *Thermochim. Acta*, **1996**, *271*, 149-153.

274. K. Ulrich, *Zucker*, **1952**, *5*, 236-239.

275. P. R. Jamieson, *Sorbitol and mannitol, in: Alternative Sweeteners (4th edition)*, Lyn O'Brien Nabors, **2012**.

276. T. Hianik, P. Rybár, L. Svobodová, S. Kresák and D. P. Nikolelis, *Pharmazie*, **2001**, *56*, 633-635.

277. Neotame, http://www.neotame-sweetener.com/neotame-solubility.html#anchor-top, **2015**.

278. Z. L. Wan, J. M. Wang, L. Y. Wang, X. Q. Yang and Y. Yuan, *J. Agric. Food Chem.*, **2013**, *61*, 4433-4440.

279. H. Uchiyama, Y. Tozuka, M. Nishikawa and H. Takeuchi, *Int. J. Pharm.*, **2012**, *428*, 183-186.

280. H. Uchiyama, Y. Tozuka, M. Imono and H. Takeuchi, *Eur. J. Pharm. Biopharm.*, **2010**, *76*, 238-244.

281. H. Uchiyama, Y. Tozuka, F. Asamoto and H. Takeuchi, *Eur. J. Pharm. Sci.*, **2011**, *43*, 71-77.

282. J. Zhang, Y. Tozuka, H. Uchiyama, K. Higashi, K. Moribe, H. Takeuchi and K. Yamamoto, *J. Pharm. Sci.*, **2011**, *100*, 4421-4431.

283. P. Bauduin, A. Renoncourt, A. Kopf, D. Touraud and W. Kunz, *Langmuir*, **2005**, *21*, 6769-6775.

284. F. L. B. da Silva, D. Bogren, O. Söderman, T. Akesson and B. Jönsson, *J. Phys. Chem. B*, **2002**, *106*, 3315-3522.

285. M. Müller, D. Touraud and W. Kunz, *in preparation*, **2015**.

286. P. H. Yancey, M. E. Clark, S. C. Hand, R. D. Bowlus and G. N. Somero, *Science*, **1982**, *217*, 1214-1222.

287. P. Wang, J. Jiang, L. He, H. Li, J. Li, J. Liu, X. Liu, M. Luo, Z. Ma, S. Qiu, H. Wu and Y. Zhao, *J. Chem. Eng. Data*, **2013**, *58*, 364-369.

288. S. Mahiuddin, A. Renoncourt, P. Bauduin, D. Touraud and W. Kunz, *Langmuir*, **2005**, *21*, 5259-5262.

289. G. B. Thurston, J. L. Salager and R. S. Schechter, *J. Colloid Interface Sci.*, **1979**, *70*, 517-523.

290. P. Ayyub, A. Maitra and D. O. Shah, *J. Chem. Soc. Faraday Trans. ,* **1993**, *89*, 3585-3589.

291. B. Bedwell and E. Gulari, *J. Colloid Interface Sci.*, **1984**, *102*, 88-100.

Publications

As already indicated, parts of this work have already been published or accepted. My papers as first author are summed up below.

1. J. Marcus, M. L. Klossek, D. Touraud, W. Kunz, **Nano-droplet formation in fragrance tinctures**, *Flav. Fragr. Journal*, **2013**, *28*, 294-299

2. J. Marcus, D. Touraud, W. Kunz, **Formulation and stability of a soap microemulsion and the apparent pK_A herein**, *J. Colloid Interface Sci.*, **2013**, *407*, 382-389

3. J. Marcus, M. Müller, J. Nistler, D. Touraud, W. Kunz, **Nano-droplet formation in water/ethanol or isopropanol/mosquito repellent formulations**, *Colloids Surf. A*, **2014**, *458*, 3-9

4. J. Marcus, V. Fischer, D. Touraud, O. Diat, W. Kunz, **Toward surfactant-free and water-free microemulsions**, *J. Colloid Interface Sci.*, **2015**, *453*, 186-193

5. J. Marcus, D. Touraud, W. Kunz, **Influence of high intensity sweeteners and sugar alcohols on a beverage microemulsion**, *J. Colloid Interface Sci.*, **2015**, doi:10.1016/j.jcis.2015.08.036

The other papers as co-author are listed below.

1. M. L. Klossek, J. Marcus, D. Touraud, W. Kunz, **The extension of microemulsion regions by combining ethanol with other cosurfactants**, *Colloids Surf. A*, **2013**, *427*, 95-100

2. M. L. Klossek, J. Marcus, D. Touraud, W. Kunz, **Highly water dilutable green microemulsions**, *Colloids Surf. A*, **2014**, *442*, 105-110

3. S. Schöttl, J. Marcus, O. Diat, D. Touraud, W. Kunz, T. Zemb, D. Horinek, **Emergence of surfactant-free micelles from ternary solutions**, *Chem. Sci.*, **2014**, *5*, 2949-2954

4. T. Zemb, M. Klossek, T. Lopian, J. Marcus, D. Horinek, S. Schöttl, S. Prevost, D. Touraud, O. Diat, S. Marčelja, W. Kunz, **How to explain the occurrence of microemulsions formed by solvent mixtures without surfactants**, *PNAS*, **2015**, submitted

Declaration

Herewith I declare that I have made this existing work single-handed. I have only used the stated utilities.

Julien Marcus

Regensburg, September 16, 2015